A STUDY OF PHOTOCURRENT AND BAND STRUCTURE FROM THE SEMICONDUCTING MATERIALS

By

Aldrin Malsawmtluanga

Registration No. MZU/ Ph. D/ 179 of 13. 06. 2008

Submitted

in fulfillment for the requirements of the

Degree of Doctor of Philosophy in Physics of

Mizoram University

Department of Physics

School of Physical Sciences

Mizoram University, Aizawl

Mizoram, India

January 2015

Mizoram University (A Central University)
Tanhril-796 004, Aizawl, Mizoram
Department of Physics

Prof. Zaithanzauva Pachuau
Head
Ph.: +91-9862770341

Post Box No. 190
Gram: MZU
Phone: 0389-2330435, 230522
Email: zpc21@yahoo.com

Dated : 28th January, 2015

Certificate

Certify that Mr. Aldrin Malsawmtluanga has carried out research work under my Supervision and guidance in the Department of Physics, Mizoram University. The results of research work by Mr. Aldrin Malsawmtluanga have been presented in this thesis entitled ***'A Study of Photocurrent and Band Structure from the Semiconducting Materials'*** *and the same has been submitted to the Mizoram University, Aizawl, Mizoram, for the degree of Doctor of Philosophy.*

Mr. Aldrin Malsawmtluanga has fulfilled all the requirements under the Ph.D. regulations of the Mizoram University. To the best of my knowledge, this thesis as a whole or any part thereof has not been submitted to this University or any other institution for any degree.

(Prof. ZAITHANZAUVA PACHUAU)
Supervisor

Department of Physics
Mizoram University
Aizawl : Mizoram

Declaration of the candidate

I, Aldrin Malsawmtluanga do hereby declare that the subject matter of this thesis is the record of the works done by me, that the contents of this thesis did not form basis of the award of any previous degree to me or to the best of my knowledge to anybody else, and that the thesis has not been submitted by me to any other University or Institute for any other degree.

I also declare that the present investigation relates to bonafide research and the title of the thesis is ***"A STUDY OF PHOTOCURRENT AND BAND STRUCTURE FROM THE SEMICONDUCTING MATERIALS"***

(Prof. ZAITHANZAUVA PACHUAU)
Supervisor

(ALDRIN MALSAWMTLUANGA)
Candidate

Head

Acknowledgement

Throughout the work of this thesis, I have been blessed with help and support from a number of people in many different aspects. I will be failing in my duty if I do not acknowledge some of those whose contributions are highly significant in my research works. First of all, I want to express my heartfelt gratitude to Prof. Zaithanzauva Pachuau, Supervisor and Head, Department of Physics, Mizoram University who is always there to guide and support me. In fact, it was him who initiated the topic of the research investigation for this thesis. Without his constant help and encouragements, not to mention his endless patience, this work would not have been possible. I would also like to thank the Faculty and Staff of the Department of Physics, Mizoram University, for their kind help and cooperation during the course of this research work.

Thanks are due to other research scholars Mr. Lalnunpuia, Lawrence Zonunmawia Chhangte, Ricky L. Ralte and Dr. Lalmuanpuia for their help and encouragements. The discussions we had regarding our research works have been tremendous help to me.

I would like to give a very special thanks to my beloved wife C. Lalrinzuali and three of my kids Brenda, Timothy and Mary as well as my father Mr. R. Lalkhawhluna and my mother Mrs. Ngurchhuanthangi for their unending love and encouragements. They are my constant source of support and they are the ones who are always pushing me to go one step further ahead. I would also like to thank all my friends for their constant prayers and support. Once again I thank God for all the blessings bestowed upon me and giving all these wonderful people in my life.

Dated Aizawl,
The 28th January, 2015 (ALDRIN MALSAWMTLUANGA)

CONTENTS

LIST OF FIGURES

LIST OF TABLES

CHAPTER – 1

Introduction

Semiconductors are substances which, like metals, are electronic conductors. In contrast to metals, however, the density of freely mobile charge carriers in semiconductors is, under normal conditions, smaller by orders of magnitude than it is in metals. In semiconductors, a small change in the absolute value of the charge carrier density can induce a large relative change in this carrier density and in the electrical conductivity. In metals, on the other hand, the carrier density is so high from the beginning that it is practically impossible to produce a reasonable relative change by small changes of the absolute value of the carrier density. Thus we can say that in semiconductors, and only in semiconductors, is it possible to manipulate the electronic conduction by small changes of the carrier density. Such changes can be effected by a number of techniques, for instance by chemical doping, by temperature changes, by the application of an electric field, or by light. The electronic conductivity of a semiconductor can be changed intentionally by these techniques by orders of magnitude; some techniques allow stationary changes, and some techniques also allow time-dependent changes on a very short timescale.

Compound semiconductors have been a subject of semiconductor research for nearly as long as elemental semiconductors. Initial discoveries of the late 1940's and early 1950's, discoveries that began the use of semiconductors in our everyday life, were in germanium. With time, it has been supplanted by silicon—a more robust, reliable, and technologically well-behaved material with a stable oxide. Compound semiconductors, whose merit of superior transport was recognized as early as 1952, have continued to be of interest since these early days although their success has been narrower in scope (Welker, 1952).

There are many types of compound semiconductors being produced commercially. The main categories, which will be the subject of exhaustive analysis in

this report, include a binary compounds between one element from the third group of the Periodic Table, namely Al, Ga and In, and one element from the fifth group of the Periodic Table, P, As and Sb, the so-called III–V semiconductors; and binary compounds between one element from the second group of the Periodic Table, namely Be and Zn, and one element from the sixth group of the Periodic Table S, Se, and Te, the so-called II–VI semiconductors. In fact, these major groups form a kind of basic set for the physical understanding of semiconductor phenomena and for the wide field of semiconductor applications.

In the last century, considerable advances have been realized in the research and applications of semiconductors. During this time, semiconductor technology laid the foundations for the development of data processing and of communication technology and, more generally, for the establishment of the information society. Today, semiconductor technology is a basic technology of our economy, business practice, and daily life 0 with its modern comforts (Martienssen and Warlimont, 2005).

The wide-bandgap II–VI semiconductors offer new exciting possibilities for their scientific and technology interests. A revolutionary breakthrough in overhead illumination, in picture transmission and in visualization techniques is expected through the introduction of short-wavelength emitting laser diodes (LD) and light-emitting diodes (LEDs). Blue-violet color light sources are based on nitrides, but green color presents few difficulties. There are some hopes that ZnSe-based structures will be good for such applications. Beryllium chalcogenide BeX (X = S, Se, Te) semiconductor alloys have recently been proposed for improving the performance of ZnSe-based blue-green lasers. BeX have much higher bonding energy, hardness, and thus exhibit unusual electronic, elastic, and vibrational properties. These unique properties make them potentially useful for various technological applications including laser diodes, high efficiency p-i-n photo-

detectors. The incorporation of transition metal ions of the iron group into II–VIs compounds has also resulted in dilute magnetic semiconductors commonly used in spintronics applications. (Ameri *et al*., 2008; Laref and Laref, 2012; Hacini *et al*., 2012; Hassan and Akbarzadeh, 2006; Al-Douri *et al*., 2012). Zinc chalcogenides ZnX (X = S, Se, Te) are a primary candidate for optical device technology such as visual displays, high-density optical memories, optical switching devices, fabrication of visible light emitting devices and modulated hetero-structures, solid-state laser devices, photodetectors, solar cells, etc. (Erdiven and Ufuktepe, 2011; Karazhanov *et al*., 2007; Bang *et al.*, 2001; Reshak and Auluck, 2007).

Long-distance fibre-optic communications, laser printers and compact disk players all depend on the same material and device technology – the semiconductor laser. These highly efficient sources are based on gallium arsenide (GaAs) and related III–V compounds. They operate at infrared, and sometimes at red wavelengths, but since the 1960s, physicists, materials scientists and electrical engineers have tried to extend these devices to shorter visible wavelengths. There are many potential applications for compact lasers and light-emitting diodes (LEDs) at blue and green wavelengths. Recent proposals include high-density optical memories and display devices, medical diagnostics, and communications through sea water and ice. (Gunshor *et al.*, 1992). In recent years, III-Antimonides have attracted more interest due to their potential applications in rechargeable lithium batteries as anode materials. GaSb is a good candidate for thermo-photovoltaic cells for systems with low radiator temperature, as its cell technology is rather straightforward resulting in higher efficiency than Si thermo-photovoltaic cells. GaAs and GaInP are used for Solar cell of high-efficiency ground and satellite device, GaN and GaP for LEDs of white light illumination, flat panel display backlighting, signs, indicators etc. GaAs, GaN and InP are used for Lasers like Optical storage, data

communications, telecom switches whereas GaAs, InP and GaN for Wireless Mobile communication, base stations, etc. (Mastro, 2011). Because of direct band gap and high reliability, III-V semiconductors (GaAs and in particular, InGaP) are ideal candidates for the realisation of high efficiency solar cells. In the past years, they have been successfully used as power sources for satellites in space, where they are able to produce electricity from sunlight with an overall efficiency of around 30%. Nowadays, the use of arsenides and phosphides as photovoltaic (PV) devices is confined only to space applications since their price is much higher than conventional Si flat panel modules, the leading PV market technology. But with the introduction of multi-junction solar cells capable of operating in high concentration solar light, the area and, therefore, the cost of these cells can be reduced and will eventually find an application and market also on Earth (Bosi and Pelosi, 2007).

In view of their importance as "base material" for many state of the art devices, it is important to know different properties of these semiconductor compounds. To understand the physical properties of semiconductors, we need to understand how electrons behave inside semiconductors and how they response to external stimuli.

To study both the surface and the bulk electronic properties of solids like compound semiconductors, a method of Photoelectron spectroscopy has been extensively used. Photoemission is basically a process in which electrons are emitted when electromagnetic radiation, typically in the visible or ultraviolet region is incident on the surface (Feuerbacher *et al.*, 1978). The process of photoemission is complicated from the viewpoint of quantum physics, and it's a single-step quantum mechanism event. To develop a formal description and due to the complexity of the one-step model (Mahan, 1970; Schaich and Ashcroft, 1971; Caroli *et al*., 1973; Feibelman and Eastman, 1974), a phenomenological three-step model is introduced to describe the process of

photoemission. In Ultraviolet Photoemission Spectroscopy (UPS), the source of radiation is ultraviolet lamp. The ultraviolet radiation in the range of 10 - 300 eV brings the excitation of electrons within a small value of escape depth which can come out of a solid and make photoemission a useful technique for the study of properties of surface of solids. Also, the variation of photon energy leads to a variation in escape depth of the electrons by means of which its relative importance to the surface and the bulk effects can be varied. In X-ray Photoelectron Spectroscopy (XPS), the source of radiation is an X-ray tube. An X-ray in the range of 1000 eV or more is also used to study the inner core level of the solid due to its highly penetrating characteristic. The high absorption coefficient of ultra-violet radiation and small escape depth of the electron emitted from solids gives the UPS a greater advantage over other methods of investigating the electronic states of solids. Von Niessen (1991) has demonstrated the usefulness of Green's functions in the calculation and interpretation of photoelectron spectra (PES). The complexities of electronic and vibrational processes which find their expression in PES require powerful computational tools and both theoretical and numerical developments.

Photoemission techniques can be classified according to the manner in which the energy and momentum of the incident photon and the ejected photoelectron are controlled. In Angle-integrated Ultraviolet Photoemission, all emitted electrons are collected by a hemispherical detector while in angle-resolved photoemission the emitted electrons are collected for a specified angle. Angle integrated photoemission gives a joint density of states while, the angle-resolved photoemission gives a detailed information of band structure, surface sensitiveness etc. In Angle-Resolved Ultraviolet Photoelectron Spectroscopy (ARUPS), the energy of the electrons emitted at a fixed angle is analysed and this gives rise to energy distribution curve. By determining the momentum of electrons which shows a maximum on the curve and by measuring the change in energy

position of the maximum on the energy distribution curve with the change of momentum, one can determine the energy-wave vector relationship. The method of ARUPS is shown in Fig. (1.1) where θ_i is the angle of incidence of the incoming UV radiation, θ is the angle of the energy analyser with respect to the normal which can be varied from 0^o to 90^o. As these experimental techniques allows measuring the dispersion of occupied bands as well the unoccupied bands in and around Fermi level, they have become an important tool for investigating the electronic properties of clean and adsorbate-covered surfaces and thin films. The detailed interpretation of photoemission data obtained from experiments requires the use of theory which should be able to incorporate appropriately the initial and final state wavefunctions of the electrons as well as the spatial form of the electromagnetic field which is responsible for photoexcitation in the first place. More detailed information about the ARUPS can be obtained from various literatures (Feuerbacher *et al*., 1978; Williams *et al*., 1980; Inglesfield, 1982; Plummer and Eberhardt, 1982; Braun, 1996; Dose, 1983; Schattke, 1997).

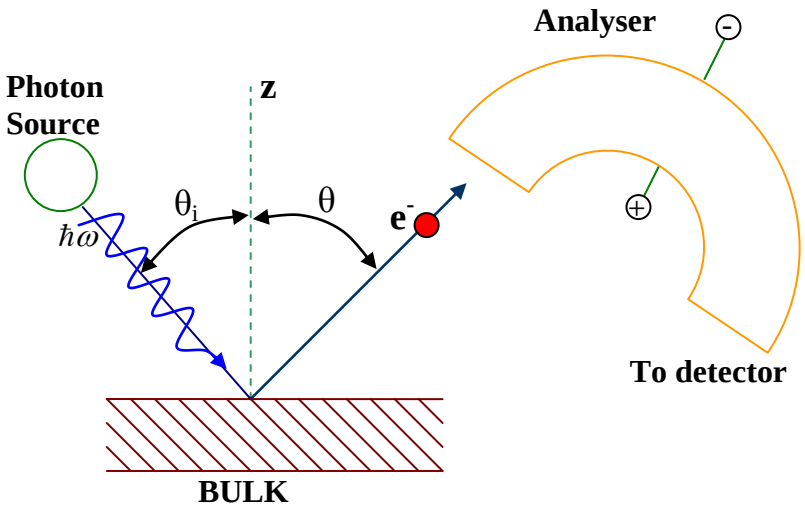

Figure (1.1): Schematic diagram of Angle-Resolved Ultraviolet Photoelectron Spectroscopy (ARUPS).

The photocurrent density formula may be written with the help of Golden Rule formula (Penn, 1972) as

$$\frac{dj(E)}{d\Omega} = \frac{2\pi}{\hbar}\sum|<\psi_f \mid H' \mid \psi_i>|^2 \ \delta(E-E_f)\delta(E_f - E_i - \hbar\omega) f_o(E-\hbar\omega)[1- f_o(E)] \tag{1.1}$$

where E_i and E_f are the initial and final state of energy, ψ_i and ψ_f are the initial and final state wavefunction, f_o denotes the Fermi occupation function and δ - function establish the energy selection rule. The perturbation in the Hamiltonian responsible for the photoexcitation of the electron is given by

$$H' = \frac{e}{2mc}(\boldsymbol{p}.\boldsymbol{A} + \boldsymbol{A}.\boldsymbol{p}) \tag{1.2}$$

where $\boldsymbol{p}$ is the one electron momentum vector and $\boldsymbol{A}$ is the vector potential.

Now, the formula for photoemission cross-section can be written as

$$\frac{d\sigma}{d\Omega} = \frac{k^2}{\omega}\left|\left\langle\psi_f \left|H'\right|\psi_i\right\rangle\right|^2 \tag{1.3}$$

Thus, we see that the calculation photocurrent density is based on the evaluation of matrix element $\left\langle\psi_f \left|H'\right|\psi_i\right\rangle$.

The calculation of the matrix element in Eq. (1.3) involves the knowledge of ψ_i and ψ_f . Pendry (1976) and others have recognised that the calculation of ψ_i and ψ_f was in principle, similar to LEED calculation. They considered the solid to be a stack of identical layers terminated at the surface. The final state was shown to be a time-reversed LEED state. As for example, Pendry has given a detailed method of calculation using this method and developed a detailed program for application to real system with notable success. In his calculations, the initial and final states are computed quite accurately but however, the vector potential is taken to be a constant. Pendry has recognised that the

vector potential would vary in the surface region but taking the exact account of spatial variation was a complex problem. Also by taking **A** to be a constant, it has simplified the calculation of the matrix element. This method of calculation has been successful in different cases. However, for the case of photocurrent against photon energy from a constant initial state, the method did not give a good result especially near the plasmon energy.

In photoemission theory of solids, the essential ingredient is the proper treatment of the electromagnetic fields within the solid. Mukhopadhyay and Lundqvist (1978) calculated electromagnetic field near a semi infinite jellium surface. The vector potential in the bulk and vacuum region are of asymptotic form and in the surface region, it is modified due to the potential. The model was used to study the semi classical infinite barrier (SCIB) model of the metal surface and the long wavelength limit for the electromagnetic wave incident on a diffuse metal surface. Maniv and Metiu (1980) were concerned with the fields in the immediate vicinity of the interface and developed a scheme for a general solution of Feibelman's model (Feibelman, 1975). They determined a dielectric function which is continuous across the interface. They found their model to be valid for photon energy greater than the plasmon energy and are applicable only to free electron type of solids. Haneman (1987) reviews the knowledge of the structure and surface states of several clean low-index faces of silicon. Ishii and Aisaka (1991) presented a theoretical analysis of angle resolved photoemission spectrum by using dynamical multiple scattering formalism for photoelectrons. Angle-resolved photoemission spectra have been calculated by Strasser *et al.* (2005) with the one-step model for S adsorption on GaAs and compared with experimental distributions. Makinistian and Albanesi (2007) have used an *ab initio* FP-LAPW method to assess the electronic structure and optical properties of the semiconductor GeSe. From their

calculated conduction band and DOS, they have obtained very good agreement with the experimental core excitation spectra.

Photoemission spectroscopy (PES) has been established as one of the most important methods to study the electronic structure of molecules, solids and surfaces (Cardona and Ley 1978, Hüfner 2003). In direct PES, ultraviolet or X-ray photons irradiate a sample surface and eject photoelectrons from the occupied electronic states, and thus provides information of the occupied density of states (DOS). Inverse photoemission (IPES) utilizes electrons (with predefined, known energies) aimed at the sample surface which relax into unoccupied electronic states and emit photons, and thus provides the unoccupied DOS (Schattke and Van Hove, 2003). Ultraviolet PES (or UPS) and IPES can be combined to provide the electronic structure of a material such as the energy band gap (Eg). Angle-resolved photoemission spectroscopy (ARPES) is one of the most direct methods of studying the electronic structure of solids. By measuring the kinetic energy and angular distribution of the electrons photoemitted from a sample illuminated with sufficiently high-energy radiation, one can gain information on both the energy and momentum of the electrons propagating inside a material. This is of vital importance in interpreting the connection between electronic, magnetic and chemical structure of solids, in particular for those complex systems (Damascelli, 2004). ARPES has now become a powerful imaging technique providing very direct **k**-space images of band dispersions as well as of constant energy surfaces. Moreover, in combination with synchrotron radiation as a tuneable photon source the experimental restrictions of ARPES regarding full **k**-space accessibility are strongly relaxed and it is possible to study three-dimensional electronic structures in great detail (Schattke and Van Hove, 2003).

Physically, the photoemission uses incident photons with energy hν to excite and eject electrons from occupied electronic states. The intensity of the photoelectrons is

proportional to the transition probability given by Fermi's golden rule (Krasovskii and Schattke, 1995). Ultraviolet Photoelectron Spectroscopy (UPS) is more suited for studying the filled electronic states in the valence band. XPS could be used, but the electrons from the valence band have a low photoelectron cross section and the kinetic energies of these valence electrons are high. Any photon energies between 4 – 150 eV could be used for UPS. At the low photon energies most often used in ARPES experiments $\hbar\omega$ < 100 eV, as it is much smaller than the typical Brillouin-zone dimension $\frac{2\pi}{a}$ of a solid.

Within the three-step model description (Hüfner, 2003), the optical transition between the bulk initial and final states can be described by a vertical transition in the reduced-zone scheme ($\mathbf{k}_f$ - $\mathbf{k}_i$ = 0), or equivalently by a transition between momentum-space points connected by a reciprocal-lattice vector **G** in the extended-zone scheme ($\mathbf{k}_f$ - $\mathbf{k}_i$ = **G**) (Mahan, 1970). In the three-step model (Hüfner, 2003), the transmission through the sample surface is obtained by matching the bulk Bloch eigenstates inside the sample to free-electron plane waves in vacuum. Because of the translational symmetry in the x–y plane across the surface, from these matching conditions it follows that the parallel component of the electron momentum is actually conserved in the process i.e.

$$\boldsymbol{k} = \boldsymbol{K} = \frac{1}{\hbar}\sqrt{2mE_k}\,\sin\theta \qquad (1.4)$$

Where $\boldsymbol{k}$ is the component parallel to the surface of the electron crystal momentum in the extended-zone scheme and $\boldsymbol{E_k}$ is the kinetic energy of electron. As for the determination of $\boldsymbol{k}$, which is not conserved but is also needed in order to map the electronic dispersion E($\boldsymbol{k}$) vs the total crystal wave vector $\boldsymbol{k}$; a different complex approach is required (Hüfner, 2003; Strocov *et al.,* 1997; Strocov *et al.,* 1998). Alternatively, the value of $\boldsymbol{k}$ can be determined if some a priori assumption is made for the dispersion of the electron final

states involved in the photoemission process; in particular, one can either use the results of band structure calculations, or adopt a nearly-free-electron description for the final bulk Bloch states as given by

$$\boldsymbol{E}_f(\boldsymbol{k}) = \frac{\hbar^2 \boldsymbol{k}^2}{2\boldsymbol{m}} - |\boldsymbol{E}_0| \tag{1.5}$$

Where once again the electron momenta are defined in the extended-zone scheme, and E_0 corresponds to the bottom of the valence band (note that both E_0 and E_f are referred to the Fermi energy E_F; while E_k is referred to the vacuum level E_v). Because $E_f = E_k + \boldsymbol{\phi}$ and $\frac{\hbar^2 \boldsymbol{k}^2}{2\boldsymbol{m}} = \boldsymbol{E}_k \sin^2 \boldsymbol{\theta}$, we can write

$$\boldsymbol{k} = \frac{1}{\hbar}\sqrt{2\boldsymbol{m}(\boldsymbol{E}_k \cos^2 \boldsymbol{\theta} + \boldsymbol{V}_0}} \tag{1.6}$$

Here $V_0 = |E_0| + \boldsymbol{\phi}$ is the inner potential, which corresponds to the energy of the bottom of the valence band referred to vacuum level E_v.

If the measured values of E_k, $\boldsymbol{\theta}$ and V_0 is known, one can then obtain the corresponding value of **k**. The most convenient method for determination of V_0 is to infer V_0 from the experimentally observed periodicity of the dispersion E(**k**) as the experiment can be realized by simply detecting the photoelectrons emitted along the surface normal (i.e. **K**= 0) while varying the incident photon energy and, in turn, the energy E_k of the photoelectrons.

Within this approach, the photoemission process is subdivided into three independent and sequential steps (Feibelman and Eastman 1974, Berglund and Spicer 1964): (i) Optical excitation of the electron in the bulk. (ii) Travel of the excited electron to the surface. (iii) Escape of the photoelectron into vacuum. The total photoemission intensity is then given by the product of three independent terms: the total probability for the optical transition, the scattering probability for the travelling electrons, and the

transmission probability through the surface potential barrier. Step (i) contains all the information about the intrinsic electronic structure of the material. Step (ii) can be described in terms of an effective mean free path, proportional to the probability that the excited electron will reach the surface without scattering (i.e, with no change in energy and momentum). Step (iii) is described by a transmission probability through the surface, which depends on the energy of the excited electron and the material work function ϕ (in order to have any finite escape probability the condition $\frac{\hbar^2 k^2}{2m} \geq |E_0| + \phi$ must be satisfied).

Bagchi and Kar (1978) developed a frequency-dependent dielectric model which is chosen to be a local one, which interpolates linearly between the bulk value inside the metal and the vacuum value (unity) outside. They showed that even with simple model, consideration of variation of field near the surface gave a reasonable qualitative agreement with experimental results for the photocurrent from the tungsten surface as a function of photon energy. Using the dielectric model developed by Bagchi and Kar, Thapa (1993) studied the variation of electromagnetic field from various metals and showed that the results were in good agreement with experimental results. Using the same dielectric model and by considering the crystal potential to be Kronig-Penny potential (Kronig and Penney, 1931), Thapa *et al*. (1995) also calculated the photocurrent in the case of a number of metals and semiconductors. Pachuau and others (2000, 2002) have calculated photoemission using Mathieu potential model as described by Davison and Steslicka (1992) to various metals and semiconductor which reproduces qualitatively the behaviour of the experimental results as reported by Bartynski *et al.* (1985). Zoliana and others (2003) have used projection operator method of group theory to develop the initial state wavefunction which is used for the evaluation of photocurrent.

Electronic and optical properties have been calculated by using various methods like empirical pseudopotential method (Kohn *et al*., 1973), Tight-Binding method (Slater and Kosker, 1954) etc. Hohenberg and Kohn (1964) have used Density Functional Theory (DFT) for the calculation of electronic properties of solids. They have shown that the electron density uniquely defines the total energy of a system and is a functional of the density. For solving the DFT equation, the full potential linearized augmented plane wave (FP-LAPW) method was developed (Madsen *et al*. 2001). They solved the Kohn-Sham equations for studying the band structure, density of states, optical properties etc. by writing several FORTRAN programs. This in the form of a standard program is known as WIEN2k code (Blaha *et al.*, 2008).

We have used the full potential linearized augmented plane wave (FPLAPW) method to determine the electronic properties of the investigated compounds. Development in linear methods for solving the band structure problem during the last two decades has totally erased the limitations that were present in other contemporary band structure techniques. The linear methods have been used to calculate a wide range of electronic properties, and linear optical properties. In the LAPW (linearized augmented plane wave) method, the unit cell is partitioned into non-overlapping atomic spheres centered on atomic sites and an interstitial region. For the construction of the basis function, the muffin-tin approximation (MTA) is used. In the interstitial region, plane waves form the complete basis set and inside the atomic sphere, the solutions for a spherically symmetric potential are atomic basis functions. The LAPW's form the basis for expanding the crystalline orbitals (Bloch states). The MTA works reasonably well in highly coordinated systems, such as fcc metals. For covalently bonded solids or layered structures, the MTA is a poor approximation and leads to discrepancies with experiments. The more general treatment of the potential, such as provided by a full potential (FP)

method has advantages over the atomic sphere approximation (ASA) and MTA based methods. In full potential methods, the potential and charge density are expanded into lattice harmonics inside each atomic sphere and as a Fourier series in the interstitial region. The FPLAPW calculations have proven to be one of the most accurate methods for the computation of the electronic structure of solids within density functional theory (DFT). The foundation of the DFT was laid by Hohenberg and Kohn(1964). They showed that the total energies are a functional of the electron density. As a result one does not need to know the complicated many electron wave function, but only the electron density, in order to determine the total energy of the system and other ground state properties. In DFT, the exchange correlation (XC) energy is needed. This requires the use of approximations which can limit the accuracy of the calculated ground state properties. In DFT, the local density approximation (LDA) or the improved generalized gradient approximation (GGA) can be used. Existing literature shows that GGA works well for calculating electronic and optical properties. Hence we have used GGA for our calculations.

In this thesis, we will present a simple method of calculating the initial state wavefunction by using Mathieu Potential which will be used in photocurrent calculations. It was Pachuau and others (2000, 2002) who has used the Mathieu potential for the first time in photoemission studies. This was done by writing a FORTRAN code which will be used in this thesis also for study of surface photoemission. For the surface photocurrent, the dielectric function generated from the optical data are used which is mentioned in Chapter 5. Photocurrent from different compound semiconductors will be calculated. Further, electronic and optical structures will be calculated by using the full-potential linearized (FP-LAPW) method which is implemented in WIEN2k code.

The topics in this thesis are arranged as follows: In Chapter 2, the basic theory involved in the calculation of the vector potential $\tilde{A}_{\omega}(\omega, z)$ will be briefly discussed. This vector potential is spatially dependent and is defined separately for the bulk, surface and vacuum regions. For different compound semiconductors, the variation of the vector potential $\tilde{A}_{\omega}(\omega, z)$ against the incident photon energy $\hbar\omega$ will be calculated.

In Chapter 3, we will first present the formulation of the initial state wave function by using Mathieu Potential followed by its application for photocurrent calculations. Results of surface photocurrent calculations from different compound semiconductors will be presented and discussed.

In Chapter 4, we briefly describe the method that is used to perform electronic structure calculations. An outline of DFT within LDA and GGA is included along with the methodology of FPLAPW in the chapter. This chapter also includes a discussion of the optical properties with special reference to the frequency-dependent dielectric function.

In Chapter 5, we present studies on the II-VI semiconductors of BeX and ZnX (X = S, Se, Te) as well as III-V semiconductors of AlX, GaX and InX (X = P, As, Sb). The results for the density of states, band structure and the frequency-dependent linear optical response are presented.

In Chapter 6, we will present the conclusion of the thesis, which will be followed by references and appendices.

CHAPTER 2

Calculation of Electromagnetic Fields using Dielectric Model

In this chapter, we shall discuss the dielectric model used and the calculation of electromagnetic fields in a solid when electromagnetic radiation is incident on it. In angle-resolved photoemission, when an electromagnetic radiation is incident on the surface of a solid, plays an important role. The calculation of the fields near a surface is a complex problem and *ab initio* calculations have been done only for jellium (Kiejna, 1999). However, these calculations have not been extended to other metals where the jellium model is not applicable. For calculations of electromagnetic fields on metals, one requires to start with simpler model. Such a model was proposed by Bagchi and Kar (1978) and they showed that consideration of variation of field near the surface gave a reasonable qualitative agreement with experimental results for the photocurrent from the tungsten surface as a function of photon energy. In their model, they used experimentally measured optical data as input and hence can be extended to the case of semiconductors as well. Thapa *et al*. (1993, 1995) have also used this model and applied it successfully to aluminium and other metals and semiconductors. We have also used this model in our photocurrent calculations and therefore, we shall give a brief description of the modified form of dielectric model as used by Bagchi and Kar to derive the electromagnetic field. In Bagchi and Kar model (1978), the surface width was defined by $-\frac{a}{2} \le z \le \frac{a}{2}$, and $z = 0$ was the nominal surface plane. But in our calculations, we consider $-d \le z \le 0$ as the realistic surface region with $z = 0$ as the true surface plane as shown in Fig. (2.1). We shall then discuss the application of the derived electromagnetic field to compound semiconductors.

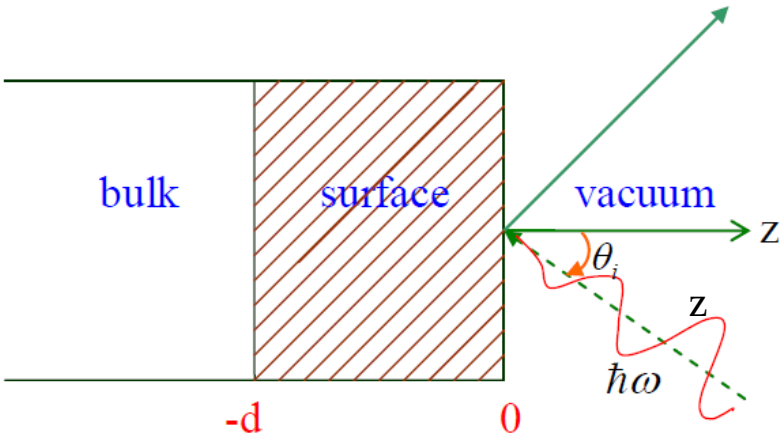

Figure (2.1): Dielectric model used for the calculation of vector potential. Here d is the width of the surface, $\hbar\omega$ is the incident photon energy and θ_i is the angle of incidence.

2.1 Dielectric Model and Electromagnetic Field Calculations:

For calculation of electromagnetic field, the dielectric model (Bagchi and Kar 1978) is shown in Figure (2.1). The solid is assumed to occupy the space to the left of z = 0 plane. The dielectric constant varies linearly over the region $-d \le z \le 0$, where it is a local function interpolating between the bulk value inside the solid and the vacuum value (unity) outside. The frequency-dependent dielectric model is given by:

$$\varepsilon(\omega,z)=\begin{cases}=\varepsilon(\omega)\cong\varepsilon_1(\omega)+i\varepsilon_2(\omega), & for \quad z\le -d \ (bulk).\\ 1+[1-\varepsilon(\omega)]\dfrac{z}{d}, & for \quad -d\le z\le 0 (surface).\\ 1, & for \quad z\ge 0 (vacuum).\end{cases} \quad \ldots \quad (2.1)$$

Where d is the width of the surface, and $\varepsilon(\omega)$ is a complex dielectric function. The refractive index of the bulk metal $\hat{n}$ is also a complex one such that $\hat{n}=\sqrt{\varepsilon_1+i\varepsilon_2}$ = n+ik. The real part $\varepsilon_1(\omega)$ and imaginary part $\varepsilon_2(\omega)$ are defined in the following way to simplify the calculation,

$$\alpha_1 = 1\ ; \qquad \beta_1 = \frac{(1-\varepsilon_1)}{d}$$

$$\alpha_2 = 0; \qquad \beta_2 = \frac{-\varepsilon_2}{d}$$

such that $\varepsilon_1(z) = \alpha_1 + \beta_1 z$ … (2.2a)

$\varepsilon_2(z) = \alpha_2 + \beta_2 z$ … (2.2b)

The incident radiation is considered to be a light of angular frequency ω with θ_i as the angle of incidence on the metal surface defined by the x-y plane. A gauge was chosen in which the scalar potential is set equal to zero i.e. $\varphi(\vec{r}, t) = 0$, such that the electromagnetic field $\boldsymbol{E}(\boldsymbol{K}, \omega, z)$ can be expressed in terms of the vector potential as

$$\boldsymbol{E}(\boldsymbol{K}, \omega, z) = -\frac{i\omega}{c}\boldsymbol{A}(\boldsymbol{K}, \omega, z), \quad \text{… (2.3a)}$$

where $\boldsymbol{K} = \frac{\omega}{c}\sin\theta_i$ is the parallel component of wave vector.

The magnetic field is related to vector potential by the formula

$$\mathbf{B} = \nabla \times \mathbf{A} \quad \text{… (2.3b)}$$

Let $\mathbf{A}(\mathbf{r}, t) = \mathbf{A}(z).e^{i(\mathbf{K}.\boldsymbol{\rho} - \omega t)}$, where $\boldsymbol{\rho} = x\hat{x} + y\hat{y}$ and $\mathbf{K} = K\hat{x} = \hat{x}(\frac{\omega}{c}\sin\theta_i)$

Therefore, $\frac{\partial}{\partial t}\mathbf{A}(\mathbf{r}, t) = \mathbf{A}(z).e^{i(\mathbf{K}.\boldsymbol{\rho} - \omega t)}(-i\omega) = -i\omega\mathbf{A}(\mathbf{r}, t)$

i.e $\frac{\partial}{\partial t} \leftrightarrow -i\omega$ … (2.4a)

Also, $\nabla\ \mathbf{A}(\mathbf{r}, t) = \nabla\ \mathbf{A}(z)e^{i[K\hat{x}.(x\hat{x}+y\hat{y})-\omega t]}$

$$= \left(\hat{x}\frac{\partial}{\partial x} + \hat{y}\frac{\partial}{\partial y} + \hat{z}\frac{\partial}{\partial z}\right)\left[\mathbf{A}(z)e^{i(Kx-\omega t)}\right]$$

$$= \left(iK\hat{x} + \hat{z}\frac{\partial}{\partial z}\right)\mathbf{A}(\mathbf{r}, t)$$

Therefore, $\nabla \leftrightarrow \left(iK\hat{x} + \hat{z}\frac{\partial}{\partial z}\right)$. … (2.4b)

From Maxwell's equations

$$\left.\begin{aligned} &\nabla.\mathbf{D}=0, \qquad\qquad \nabla.\mathbf{B}=0 \\ &\nabla\times\mathbf{E}=-\frac{1}{c}\frac{\partial\mathbf{B}}{\partial t} \\ &\nabla\times\mathbf{B}=\frac{1}{c}\frac{\partial\mathbf{E}}{\partial t}+\frac{4\pi}{c}\mathbf{J} \end{aligned}\right\} \quad \ldots \quad (2.5)$$

we assume $\mu=1 \Rightarrow \mathbf{B}=\mathbf{H}$. Also, $\mathbf{J}_{ext}$ = 0, i.e. there are no external currents and charges.

Since $\mathbf{J} = \mathbf{J}_{ind} = \sigma\mathbf{E}$, the last of Maxwell's equations gives

$$\nabla\times\mathbf{B}=\frac{1}{c}\frac{\partial\mathbf{E}}{\partial t}+\frac{4\pi\sigma}{c}\mathbf{E}$$

$$= \frac{1}{c}\frac{\partial\mathbf{E}}{\partial t}+\frac{4\pi\sigma}{c}\frac{1}{(-i\omega)}\frac{\partial\mathbf{E}}{\partial t}, \qquad \left(\because \quad \frac{\partial\mathbf{E}}{\partial t}=-i\omega\mathbf{E}\right)$$

$$= \frac{1}{c}(1+\frac{4\pi\sigma\, i}{\omega})\frac{\partial\mathbf{E}}{\partial t}= \frac{\varepsilon}{c}\frac{\partial\mathbf{E}}{\partial t} \quad \ldots \quad (2.6)$$

where $\varepsilon = 1+\frac{4\pi i\,\sigma}{\omega}$.

In terms of the vector potential, Eq. (1.3b) can be written as

$$\nabla \text{ x} \nabla \text{ x}\, \mathbf{A} = \nabla\ (\nabla.\mathbf{A}) - \nabla^2\mathbf{A} = -\frac{\varepsilon}{c^2}\frac{\partial^2\mathbf{A}}{\partial t^2} \quad \ldots \quad (2.7)$$

Substituting (1.4a) and (1.4b) in (1.7) we have,

$$(-\mathbf{K}^2+\frac{\partial^2}{\partial z^2})\ \mathbf{A}(z)+\frac{\varepsilon\omega^2}{c^2}\mathbf{A}(z)-(i\mathbf{K}+\hat{z}\frac{\partial}{\partial z})\ [(i\mathbf{K}+\hat{z}\frac{\partial}{\partial z}).\mathbf{A}(z)]=0 \quad \ldots \quad (2.8)$$

Now we consider the case of *p*-polarisation. In this case, $\mathbf{A}$ is in the xz-plane and $\mathbf{B}\|\mathbf{y}$. Hence, the x-and z- components of $\mathbf{A}$ can be deduced from Eq. (2.8).

Firstly taking the x-component of $\mathbf{A}$:

$$(-\mathbf{K}^2+\frac{\partial^2}{\partial z^2})\ A^x(z)\hat{x}+\frac{\varepsilon\omega^2}{c^2}A^x(z)\hat{x}-(iK\hat{x}+\hat{z}\frac{\partial}{\partial z})\ [(iK\hat{x}+\hat{z}\frac{\partial}{\partial z}).A^x(z)\hat{x}]=0$$

or $$\frac{d^2A^x(z)\hat{x}}{dz^2}+\frac{\varepsilon\omega^2}{c^2}A^x(z)\hat{x}=iK\frac{dA^x(z)\hat{z}}{dz}$$

i.e. $$\frac{d^2A_x}{dz^2}+\frac{\varepsilon\omega^2}{c^2}A_x=iK\frac{dA_z}{dz} \quad \ldots \quad (2.9a)$$

where $A_x = A^x(z)\hat{x}, \quad A_z = A^x(z)\hat{z}$

Now the z-component of **A** will give,

$$(-\mathbf{K}^2 + \frac{\partial^2}{\partial z^2})\, A^z(z)\hat{z} + \frac{\varepsilon\omega^2}{c^2} A^z(z)\hat{z} - (iK\hat{x} + \hat{z}\frac{\partial}{\partial z})\,[(iK\hat{x} + \hat{z}\frac{\partial}{\partial z}).A^z(z)\hat{z}] = 0$$

or $$-\mathbf{K}^2 A^z(z)\hat{z} + \frac{d^2A^z(z)\hat{z}}{dz^2} + \frac{\varepsilon\omega^2}{c^2} A^z(z)\hat{z} - iK\frac{dA^z(z)\hat{x}}{dz} - \frac{d^2A^z(z)\hat{z}}{dz^2} = 0$$

i.e. $$\left(\frac{\varepsilon\omega^2}{c^2} - \mathbf{K}^2\right)A_z = iK\frac{dA_x}{dz} \qquad \ldots \quad (2.9b)$$

We also note that from Eq. (2.3b) that

$$\mathbf{B} = \nabla \times \mathbf{A} \;=\; \left(i\,K\hat{x} + \hat{z}\frac{\partial}{\partial z}\right) \times \left(A^x\hat{x} + A^z\hat{z}\right)$$

$$= \frac{\partial A_x}{\partial z} - iKA_z$$

where $A_x = A^x\hat{x}$ and $A_z = A^z\hat{z}$

Dividing Eq. (2.9a) by ε and differentiating with respect to z, we have

$$\frac{1}{\varepsilon}\frac{d^3A_x}{dz^3} - \frac{iK}{\varepsilon}\frac{d^2A_z}{dz^2} + \frac{\omega^2}{c^2}\frac{dA_x}{dz} = 0 \qquad \ldots \quad (2.9c)$$

Also Eq. (2.9b) gives $$iK\left(\frac{\varepsilon\omega^2}{c^2} - \mathbf{K}^2\right)A_z + \frac{dA_x}{dz} = 0 \qquad \ldots \quad (2.9d)$$

Equating Eqs. (2.9c) and (2.9d) results in Landau and Lifshitz (1984) equation, viz.

$$\frac{\partial}{\partial z}(\frac{1}{\varepsilon}\frac{\partial B}{\partial z}) + (\frac{\omega^2}{c^2} - \frac{K^2}{\varepsilon})B = 0 \qquad \ldots \quad (2.10)$$

We must solve this equation under the boundary condition that both B and $\frac{\partial B}{\partial z}$ are continuous. Once B is known, the electric field components can be found by using Maxwell's equation, i.e.

$$-i\omega\mathbf{E} = \frac{c}{\varepsilon}(\nabla \times \mathbf{B})$$

$$= \frac{c}{\varepsilon}\left\{\left(iK\hat{x} + \hat{z}\frac{\partial}{\partial z}\right) \times \left(B\hat{y}\right)\right\}$$

In terms of Cartesian components,

$$\left.\begin{aligned} E_x &= \frac{1}{ik\varepsilon}\frac{\partial B}{\partial z} \\ E_z &= -\frac{K}{k\varepsilon}B = -\frac{\sin\theta_i}{\varepsilon}B \end{aligned}\right\} \qquad \ldots \quad (2.11)$$

To solve Eq. (2.10), we follow the prescription of Landau and Lifshitz (1984) and use the substitution B(z) = u(z) $\sqrt{\varepsilon(z)}$ and by substituting $\frac{\omega^2}{c^2} = k^2$ and K = $k \sin\theta_i$, we obtain

$$\frac{\partial}{\partial z}(\frac{1}{\varepsilon})(\frac{\partial B}{\partial z}) + \frac{\partial^2 B}{\partial z^2}\frac{1}{\varepsilon} + \frac{k^2}{\varepsilon}(\varepsilon - \sin^2\theta_i)B = 0$$

or $$-\frac{1}{\varepsilon}\frac{\partial \varepsilon}{\partial z}\frac{\partial}{\partial z}(u\sqrt{\varepsilon}) + \frac{\partial}{\partial z}(\frac{\partial u\sqrt{\varepsilon}}{\partial z}) + k^2(\varepsilon - \sin^2\theta_i)u\sqrt{\varepsilon} = 0$$

The final result gives

$$\frac{d^2u}{dz^2} + k^2(\varepsilon - \sin^2\theta_i)u + [\frac{1}{2\varepsilon}\frac{d^2\varepsilon}{dz^2} - \frac{3}{4}\frac{1}{\varepsilon^2}(\frac{d\varepsilon}{dz})^2]u = 0 \qquad \ldots \quad (2.12)$$

In Eq.(2.12), clearly $\frac{d^2\varepsilon}{dz^2} = 0$ everywhere except for $z = -d$ and 0, where it vanishes.

Now, substituting the values of dielectric for each region in Eq. (2.12), we can obtain the expression for the magnetic field for the three regions of the solid.

In the first region, $z \geq 0$ (vacuum), where ε =1, we have

$$\frac{d^2u}{dz^2} + k^2\cos^2\theta_i u = 0 \qquad \ldots (2.13a)$$

whose solution is B = $B_0 e^{-ik_z z} + B_0'' e^{ik_z z}$ $\ldots$ (2.13b)

In the second region, $z \leq -d$ and $\varepsilon = \varepsilon_1 + i\varepsilon_2 = \hat{n}$

$$\frac{d^2u}{dz^2} + k^2\hat{n}^2\cos^2\gamma u = 0 \qquad \ldots (2.14a)$$

The solution is (absorbing $\hat{n}$ into the constant coefficient)

$$B = B_o' e^{-ik(\hat{n}\cos\gamma)z} \qquad \ldots (2.14b)$$

For the third region, $-d \leq z \leq 0$ (surface),

$$\frac{d^2u}{dz^2} + k^2(\varepsilon - \sin^2\theta_i)u - \frac{3}{4}\frac{1}{\varepsilon^2}(\frac{d\varepsilon}{dz})^2]u = 0 \qquad \ldots (2.15a)$$

Recalling Eqs. (2.2a) and (2.2b), Eq.(2.15a) becomes

$$\frac{d^2u}{dz^2} + k^2(b + cz)u - \frac{3}{4}\frac{1}{(b' + cz)^2}c^2u = 0 \qquad \ldots (2.15b)$$

where $b' = \alpha_1 + i\alpha_2 = b + \sin^2\theta_i$ is a short hand notation introduced purely for convenience.

Eq. (2.15b) has the solution u(z) = $Az'^{3/2} + Bz'^{-1/2}$

But $\varepsilon(z) = b' + cz = cz'$ .Therefore, B(z) = C z'^2 +D

$$= C[z + \frac{(\alpha_1 + i\alpha_2)}{\beta_1 + i\beta_2}]^2 + D,$$

i.e. $$B(z) = C[z + \frac{b'}{c}]^2 + D, \quad -d \le z \le 0 \qquad \ldots (2.15c)$$

The constants C and D are determined by matching the boundary conditions at z = -*d* and z = 0.

At z = 0, from Eqs. (2.13b) and (2.15c) we have,

$$\left.\begin{aligned} B_0 + B_0'' &= C(\frac{b'}{c})^2 + D \\ ik\cos\theta_i[-B_0 + B_0''] &= 2C(\frac{b'}{c}) \end{aligned}\right\} \qquad \ldots (2.16a)$$

At z = -*d*, from Eqs. (2.14b) and (2.15c) we have,

$$\left.\begin{aligned} C(-d + \frac{b'}{c})^2 + D &= B_0' e^{ik(\alpha+i\beta)d} \\ 2C(-d + \frac{b'}{c}) &= -ik(\alpha+i\beta)B_0' e^{-ik(\alpha+i\beta)(-d)} \end{aligned}\right\} \qquad \ldots (2.16b)$$

Calculations from Eqs. (2.16a) and (2.16b) shows the results as:

$$\frac{B_0''}{B_o} = \frac{-1 + \cos\theta_i\{\frac{\varepsilon}{\alpha+i\beta} - \frac{ikd}{2}(1+\varepsilon)\}}{1 + \cos\theta_i\{\frac{\varepsilon}{\alpha+i\beta} - \frac{ikd}{2}(1+\varepsilon)\}} \qquad \ldots (2.17a)$$

$$\frac{C}{B_0} = \frac{ik\cos\theta_i}{d}(1-\varepsilon)\frac{1}{1 + \cos\theta_i\{\frac{\varepsilon}{\alpha+i\beta} - \frac{ikd}{2}(1-\varepsilon)\}} \qquad \ldots (2.17b)$$

$$\frac{D}{B_0} = \varepsilon\cos\theta_i \frac{[\frac{2}{(\alpha+i\beta)} + ikd(\frac{\varepsilon}{1-\varepsilon})]}{1 + \cos\theta_i\{\frac{\varepsilon}{\alpha+i\beta} - \frac{ikd}{2}(1+\varepsilon)\}} \qquad \ldots (2.17c)$$

$$\& \quad \frac{B_0'}{B_0} = \frac{2\varepsilon\cos\theta_i}{\alpha+i\beta}\frac{e^{-ikd(\alpha+i\beta)/2}}{1 + \cos\theta_i\left\{\frac{\varepsilon}{\alpha+i\beta} - \frac{ikd}{2}(1+\varepsilon)\right\}} \qquad \ldots (2.17d)$$

Therefore, the expression for magnetic field can be obtained as

$$\frac{B(z)}{B_0} = e^{-ik\cos\theta_i z} + \frac{B_0''}{B_0} e^{ik\cos\theta_i z}, \qquad z \ge 0 \qquad \ldots (2.18a)$$

$$= \left(\frac{C}{B_0}\right)\left[z+\frac{d}{1-\varepsilon}\right]^2 + \frac{D}{B_0}, \qquad -d \le z \le 0 \qquad \ldots (2.18b)$$

$$= \frac{B_0'}{B_0} e^{-ik(\alpha+i\beta)z}, \qquad z \le -d \qquad \ldots (2.18c)$$

where B_o = amplitude of the magnetic field.

We now compute the electric field from Eq. (2.18) using Eq. (2.11). Recall that for the incident electromagnetic wave in vacuum, *the amplitude of the electric field is the same as the amplitude of the magnetic field, ie* $E_0 = B_0$. We also recall our model of linear dielectric variation,

$$\varepsilon(z) = 1, \qquad z \ge 0$$

$$= 1 + \frac{(1-\varepsilon)}{d} z, \qquad -d \le z \le 0$$

$$= \varepsilon \equiv \varepsilon_1 + i\varepsilon_2, \qquad z \le -d$$

Therefore, the x-component of electric field are given as

$$\frac{E_x(z)}{E_0} = \left[-e^{-ik\cos\theta_i(z)} + \left(\frac{B_0''}{B_0}\right) e^{ik\cos\theta_i(z)}\right]\cos\theta_i, \qquad z \ge 0 \qquad \ldots (2.19a)$$

$$= \frac{1}{ik\left[1+\frac{(1-\varepsilon)}{d}z\right]} \left(\frac{C}{B_0}\right) \cdot 2\left[z+\frac{d}{1-\varepsilon}\right]$$

$$= \frac{-2\cos\theta_i}{1+\cos\theta_i\left\{\frac{\varepsilon}{\alpha+i\beta} - \frac{dki}{2}(1+\varepsilon)\right\}}, \qquad -d \le z \le 0 \qquad \ldots (2.19b)$$

$$= -ik\left(\frac{\alpha+i\beta}{\varepsilon}\right)\left(\frac{B'}{B_0}\right) e^{-ik(\alpha+i\beta)z}, \qquad z \le -d \qquad \ldots (2.19c)$$

It is to be noted that the x component of the electric field in the interface region $(-d \le z \le 0)$ is a constant quantity and is independent of z. On the other hand, for the z-component of the electric field, we obtain electric field for different regions as follows:

For vacuum region, i.e. $z \ge 0$,

$$\frac{E_z(z)}{E_0} = -\sin\theta_i\left[e^{-ik\cos\theta_i(z)} + \frac{B_0''}{B_0} e^{ik\cos\theta_i(z)}\right],$$

$$= -\sin\theta_i\left[e^{-ik\cos\theta_i(z)} + e^{ik\cos\theta_i(z)} \frac{-1+\cos\theta_i\left\{\frac{\varepsilon}{\alpha+i\beta} - \frac{dki(1+\varepsilon)}{2}\right\}}{1+\cos\theta_i\left\{\frac{\varepsilon}{\alpha+i\beta} - \frac{dki(1+\varepsilon)}{2}\right\}}\right]$$

In the long wavelength limit, kd<<1, and $z \geq 0$,

$$\frac{E_z(z)}{E_0} = -\sin\theta_i \left[1+\frac{-1+\dfrac{\varepsilon\cos\theta_i}{\alpha+i\beta}}{1+\dfrac{\varepsilon\cos\theta_i}{\alpha+i\beta}}\right]$$

$$= -\frac{\varepsilon\sin 2\theta_i}{\left[\varepsilon-\sin^2\theta_i\right]^{\frac{1}{2}}+\varepsilon\cos\theta_i}, \qquad \text{for } z \geq 0 \qquad \ldots \quad (2.20a)$$

For the surface region, i.e. $-d \leq z \leq 0$,

$$\frac{E_z(z)}{E_0} = \frac{-\sin\theta_i}{1+(1-\varepsilon)\dfrac{z}{d}}\left[\frac{C}{B_0}\left(z+\frac{d}{1-\varepsilon}\right)^2+\frac{D}{B_0}\right],$$

$$= \frac{-\sin\theta_i d}{1+(1-\varepsilon)\dfrac{z}{d}}\left\{-\frac{ik\cos\theta_i}{d}\frac{(1-\varepsilon)[z+\dfrac{d}{2}(\dfrac{1+\varepsilon}{1-\varepsilon})]^2}{1+\cos\theta_i\{\dfrac{\varepsilon}{\alpha+i\beta}-\dfrac{ikd}{2}(1+\varepsilon)\}}+\varepsilon\cos\theta_i\right.$$

$$\left.\times\left\{\frac{[\dfrac{2}{\alpha+i\beta}+ikd(\dfrac{\varepsilon}{1-\varepsilon})]}{1+\cos\theta_i\{\dfrac{\varepsilon}{\alpha+i\beta}-\dfrac{ikd}{2}(1+\varepsilon)}\right\}\right.$$

Let us consider when the wavelength of light is much larger than d, then kd <<1,

$$\frac{E_z(z)}{E_0} \underset{kd\to 0}{\cong} \frac{-d}{1+(1-\varepsilon)\dfrac{z}{d}}\frac{2\sin\theta_i\cos\theta_i}{1+\cos\theta_i\dfrac{\varepsilon}{\alpha+i\beta}}\frac{\dfrac{\varepsilon}{\alpha+i\beta}}{}$$

$$= -\frac{\sin 2\theta_i}{(\alpha+i\beta)+\varepsilon\cos\theta_i}\frac{\varepsilon d}{d+(1-\varepsilon)z}$$

Noting that $\alpha+i\beta = \hat{n}\cos\gamma = \sqrt{\varepsilon-\sin^2\theta_i}$, we obtain

$$\frac{E_z(z)}{E_0} \underset{k\,d\to 0}{\cong} -\frac{\sin 2\theta_i}{\left[\varepsilon-\sin^2\theta_i\right]^{\frac{1}{2}}+\varepsilon\cos\theta_i}\frac{\varepsilon d}{d+(1-\varepsilon)z}, \quad \text{for } -d \leq z \leq 0 \qquad \ldots \quad (2.20b)$$

Again in the bulk region, i.e. $z \leq -d$,

$$\frac{E_z(z)}{E_0} = \frac{-\sin\theta_i}{\varepsilon}\left[\left(\frac{B_0'}{B_0}\right)e^{-ik(\alpha+i\beta)z}\right]$$

$$= \frac{\sin\theta_i}{\varepsilon}\left[\frac{2\varepsilon\cos\theta_i}{(\alpha+i\beta)}\frac{e^{-ik(\alpha+i\beta)d}\,e^{-ik(\alpha+i\beta)z}}{1+\cos\theta_i\left\{\dfrac{\varepsilon}{\alpha+i\beta}-\dfrac{dki(1+\varepsilon)}{2}\right\}}\right]$$

In the long wavelength limit, k d<<1 and for z ≤ $-d$

$$\therefore \quad \frac{E_z(z)}{E_0} = \frac{-\sin 2\theta_i}{(\alpha+i\beta)}\frac{1}{1+\dfrac{\varepsilon\cos\theta_i}{(\alpha+i\beta)}}$$

$$= -\frac{\sin 2\theta_i}{\left[\varepsilon-\sin^2\theta_i\right]^{\frac{1}{2}}+\varepsilon\cos\theta_i}, \qquad \text{for} \quad z \le -d \qquad \ldots \quad (2.20c)$$

Thus the normal component of the electric field vector potential in the long wavelength limit can be collectively taken as:

$$\tilde{A}_\omega(z) = \frac{E_z(z)}{E_0} = \begin{cases} -\dfrac{\varepsilon.\sin 2\theta_i}{\left[\varepsilon-\sin^2\theta_i\right]^{\frac{1}{2}}+\varepsilon.\cos\theta_i} & z \ge 0 \\ -\dfrac{\sin 2\theta_i}{\left[\varepsilon-\sin^2\theta_i\right]^{\frac{1}{2}}+\varepsilon.\cos\theta_i}\;\dfrac{\varepsilon.d}{d+(1-\varepsilon)z}, & -d \le z \le 0 \\ -\dfrac{\sin 2\theta_i}{\left[\varepsilon-\sin^2\theta_i\right]^{\frac{1}{2}}+\varepsilon.\cos\theta_i}, & z \le -d \end{cases}$$

$$\ldots \quad (2.21)$$

2.2 Evaluation of Electromagnetic Fields:

By using Eq. (2.21), electromagnetic fields as a function of incident photon energy are calculated for different solids like binary compounds between one element from the second group of the Periodic Table, namely Be and Zn, and one element from the sixth group of the Periodic Table like S, Se, and Te, the so-called II–VI semiconductors; binary compounds between one element from the third group of the Periodic Table, namely Al, Ga and In, and one element from the fifth group of the Periodic Table like P, As and Sb, the so-called III–V semiconductors.

We have also calculated the electromagnetic fields as a function of the distance *z* from the surface of solids. The value of the dielectric constant $\varepsilon(\omega)$ is unity for vacuum region. For the bulk and the surface region, we have used our generated data for $\varepsilon(\omega)$. However, it has been found by Appelbaum (1975) that for most metals, the surface width d~15 $\overset{0}{\text{A}}$ with respect to the last plane of the atoms beyond which the electronic properties are independent of the presence of the surface and hence we have taken the value of *d*~ 10 $\overset{0}{\text{A}}$.

(i) Beryllium chalcogenides:

In Figure 2.2(a), a graph of $\left|\tilde{A}_{\omega}(z)\right|^2$ against the incident photon energy ($\hbar\omega$) is plotted for the surface plane located at *z* = 0 (vacuum), *z* = - *0.5 d* (surface) and *z* = *-d* (bulk) for BeX (X= S, Se, Te) where *d is* the width of the surface. We find that for the surface region *z* = - *0.5d*, $\left|\tilde{A}_{\omega}(z)\right|^2$ increases with the increase in the incident photon energy and a peak occurs at photon energy $\hbar\omega$ = 15.39 eV, 14.41 eV, 12.64 eV after which it starts decreasing with further increase in the photon energy and becomes minimum at $\hbar\omega$ = 21.84 eV, 20.99 eV, 17.40 eV for BeS, BeSe, BeTe respectively. The

calculated plasmon energies ($\hbar\omega_p$) of BeS, BeSe, BeTe are 19.52 eV, 18.39 eV, 16.12 eV (Kumar *et al*. 2013; Yadav and Kumar, 2013). For further increase in photon energy a secondary peak occurs at photon energy $\hbar\omega$ = 28 eV for BeS and BeSe while $\hbar\omega$ = 25 eV for BeTe. For the location of the surface plane at *z = 0*, which is the vacuum region, we find that with the increase in the photon energy, $\left|\tilde{A}_\omega(z)\right|^2$ decreases slightly and we do not observe a proper peak below the plasmon energy but a minimum is observed near the plasmon energy. For the other locations of the surface plane at *z = -d*, which is the bulk region, $\left|\tilde{A}_\omega(z)\right|^2$ increases slightly with the increase in the photon energy and a hump is observed at around $\hbar\omega$ = 27 eV for BeS and BeSe while $\hbar\omega$ = 25 eV for BeTe.

Figure 2.2(b) shows the plot of spatial variation of electromagnetic field ($\frac{d\tilde{A}_\omega}{dz}$) against the location of the surface plane (z) for different values of photon energy. It is seen that $\frac{d\tilde{A}_\omega}{dz}$ is maximum in the middle of surface region for $\hbar\omega$ = 15.39 eV, 14.41 eV, 12.64 eV for BeS, BeSe, BeTe respectively, whereas for other photon energies, peak values in $\frac{d\tilde{A}_\omega}{dz}$ shifts either towards the bulk or the vacuum side. The fact that the peak is localised at the surface (Fig. 2.2(b)) means that photoemission is a surface related phenomena.

(ii) Zinc chalcogenides:

In Figure 2.3(a), a graph of $\left|\tilde{A}_\omega(z)\right|^2$ against the incident photon energy ($\hbar\omega$) is plotted for the surface plane located at *z* = 0 (vacuum), *z = - 0.5 d* (surface) and *z = -d* (bulk) for ZnX (X= S, Se, Te) where *d is* the width of the surface. We find that for the

surface region z = - *0.5d*, $\left|\tilde{A}_{\omega}(z)\right|^2$ increases with the increase in the incident photon energy and a peak occurs at photon energy $\hbar\omega$ = 14.3 eV, 13.6 eV, 11.7 eV after which it starts decreasing with further increase in the photon energy and becomes minimum at $\hbar\omega$ = 20.0 eV, 18.0 eV, 16.15 eV for ZnS, ZnSe, ZnTe respectively. The calculated plasmon energies ($\hbar\omega_p$) of ZnS, ZnSe, ZnTe are 16.71 eV, 15.78 eV, 14.76 eV (Kumar *et al*. 2013; Yadav and Kumar, 2013; Kumar, 2013). Reddy *et al.* (2003) have calculated the values for ZnS, ZnSe, ZnTe as 14.73 eV, 14.33 eV, 13.66 eV respectively. For the location of the surface plane at z = *0*, which is the vacuum region, we find that with the increase in the photon energy, $\left|\tilde{A}_{\omega}(z)\right|^2$ decreases slightly and we do not observe a proper peak below the plasmon energy but a minimum is observed near the plasmon energy. For the other locations of the surface plane at z = - *d*, which is the bulk region, $\left|\tilde{A}_{\omega}(z)\right|^2$ increases slightly with the increase in the photon energy and a hump is observed at around $\hbar\omega$ = 27 eV for ZnS and ZnSe while $\hbar\omega$ = 25 eV for ZnTe.

Figure 2.3(b) shows the plot of spatial variation of electromagnetic field ($\frac{d\tilde{A}_{\omega}}{dz}$) against the location of the surface plane (z) for different values of photon energy. It is seen that $\frac{d\tilde{A}_{\omega}}{dz}$ is maximum in the middle of surface region for $\hbar\omega$ = 14.3 eV, 13.6 eV, 11.7 eV for ZnS, ZnSe, ZnTe respectively, whereas for other photon energies, peak values in $\frac{d\tilde{A}_{\omega}}{dz}$ shifts either towards the bulk or the vacuum side. The fact that the peak is localised at the surface (Fig. 2.3(b)) means that photoemission is a surface related phenomena.

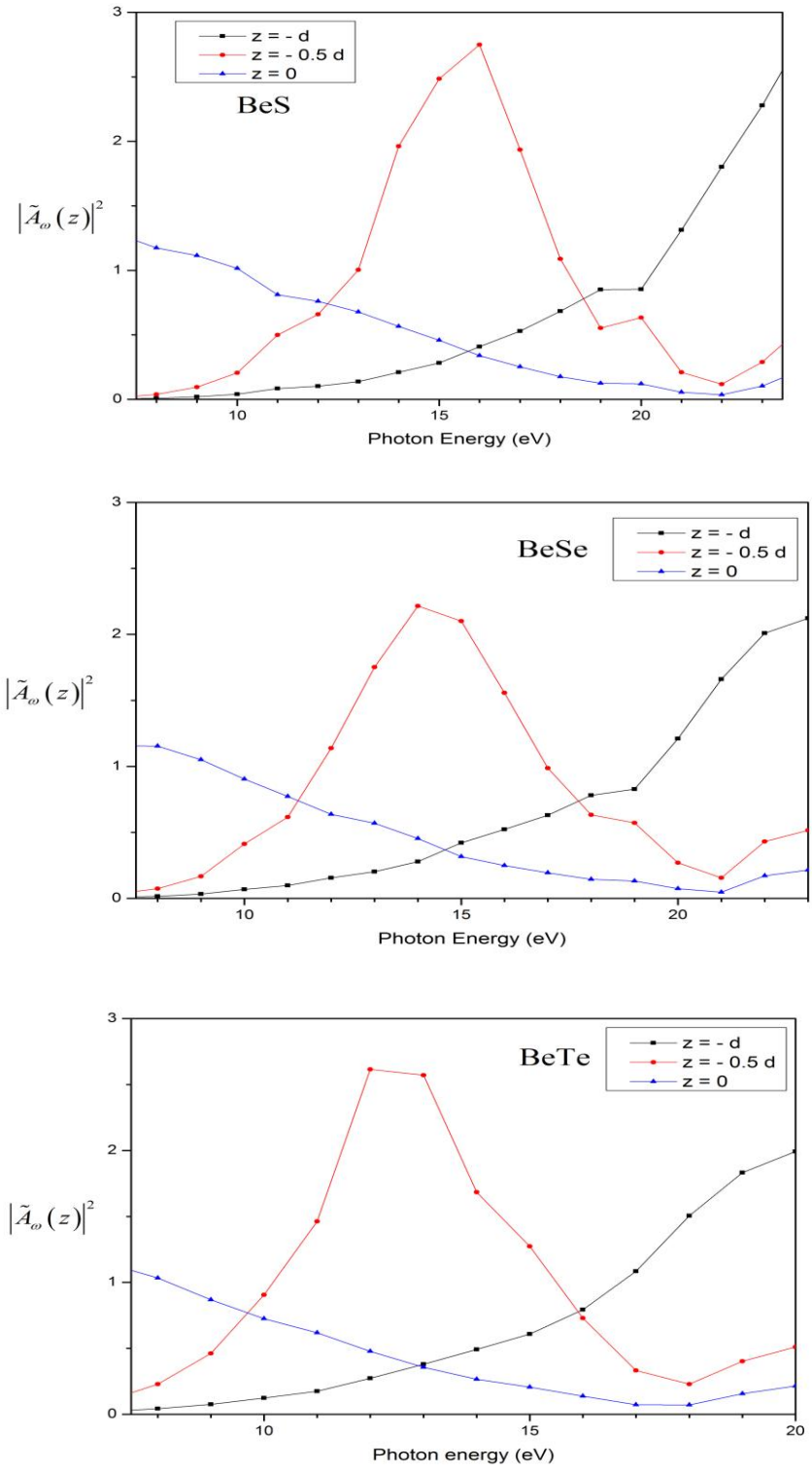

Figure 2.2 (a): Plot of variation of $\left|\tilde{A}_\omega(z)\right|^2$ against photon energy for location of surface planes at z = -d, -0.5d and 0 for BeX (X= S, Se, Te) using calculated data.

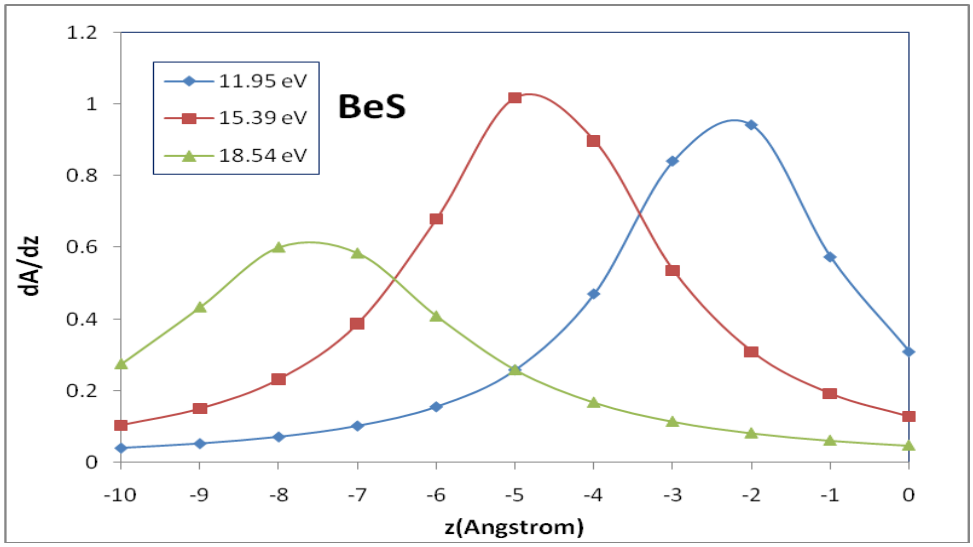

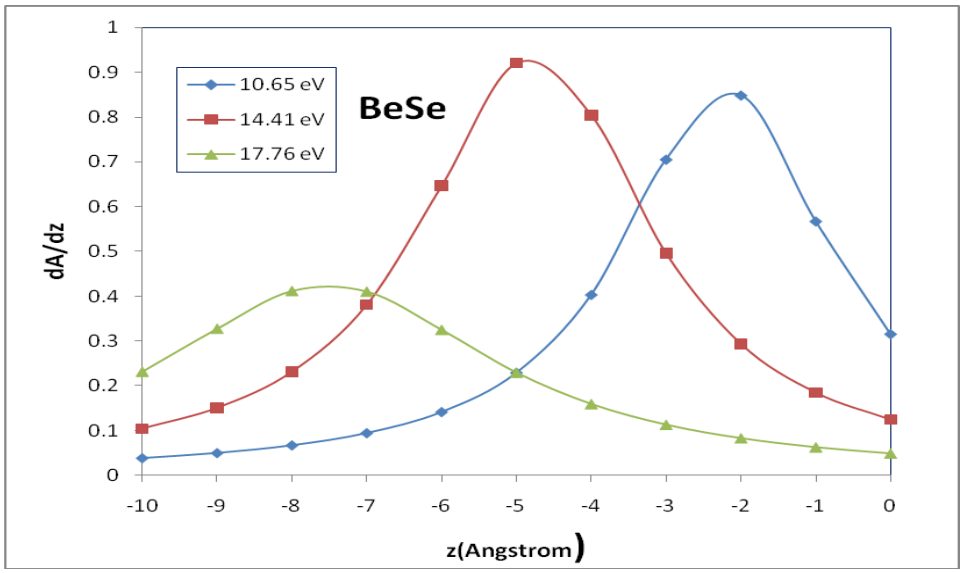

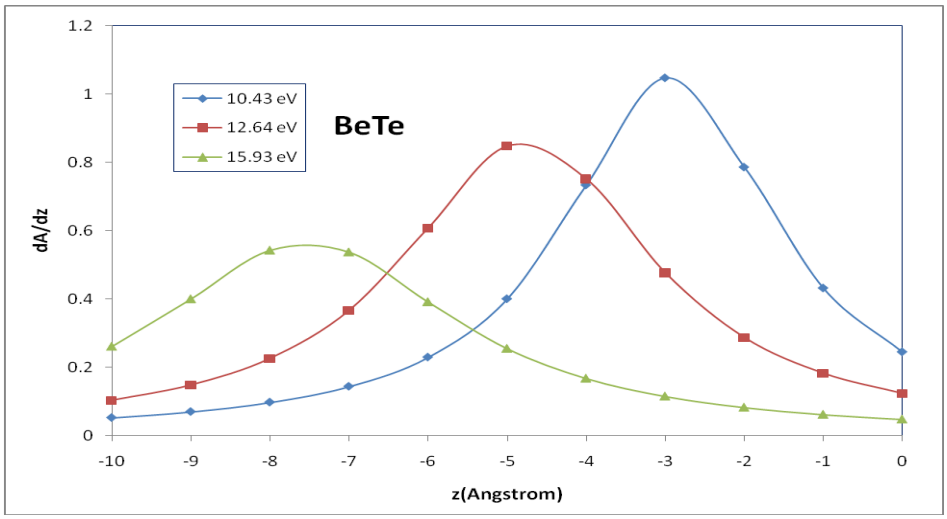

Figure 2.2 (b): Plot of $\frac{d\tilde{A}_{\omega}}{dz}$ against distance from the surface for various photon energies in BeX (X= S, Se, Te) using calculated data.

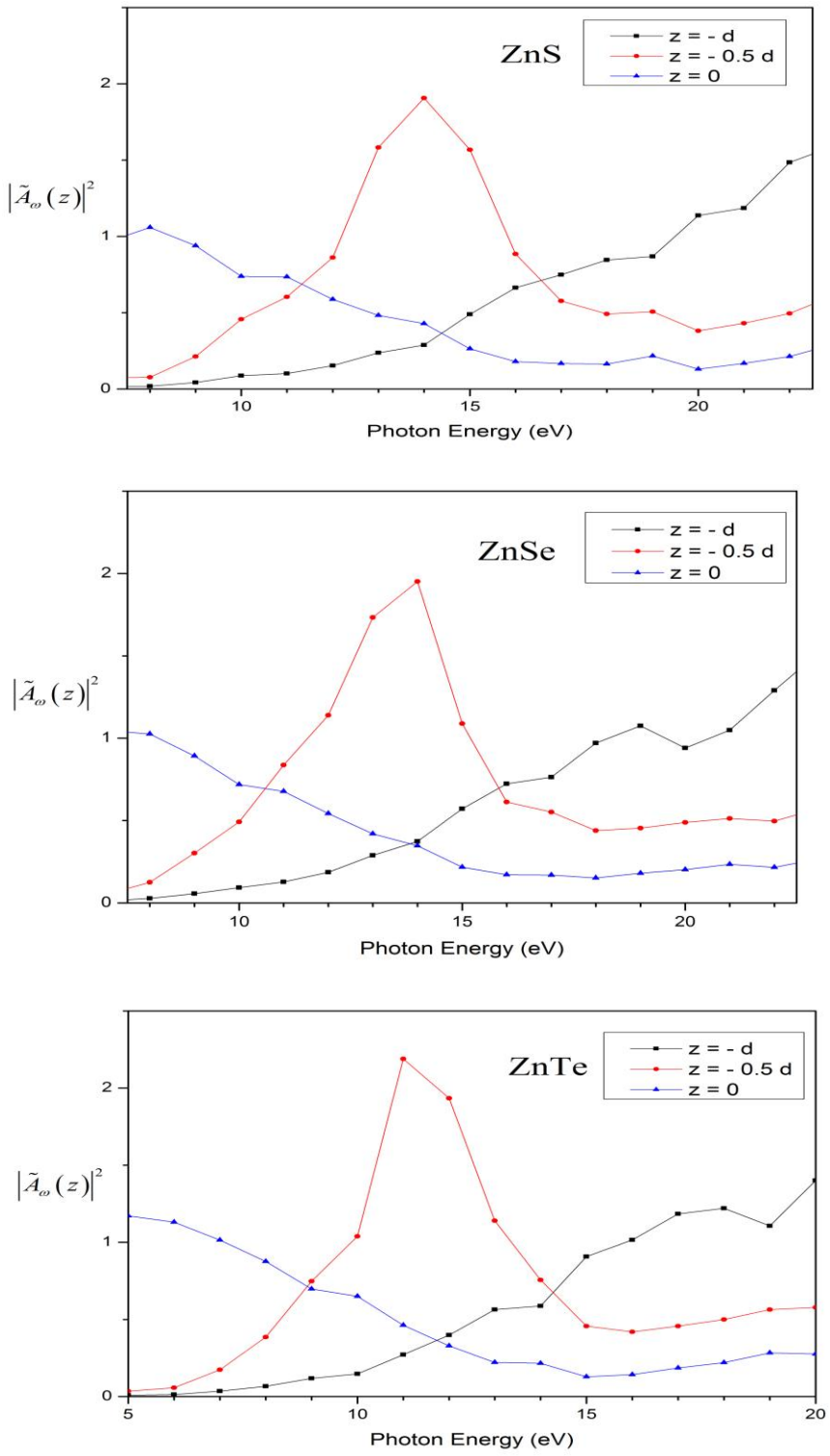

Figure 2.3(a): Plot of variation of $|\tilde{A}_\omega(z)|^2$ against photon energy for location of surface planes at *z* = -d, -0.5d and 0 for ZnX (X= S, Se, Te) using calculated data.

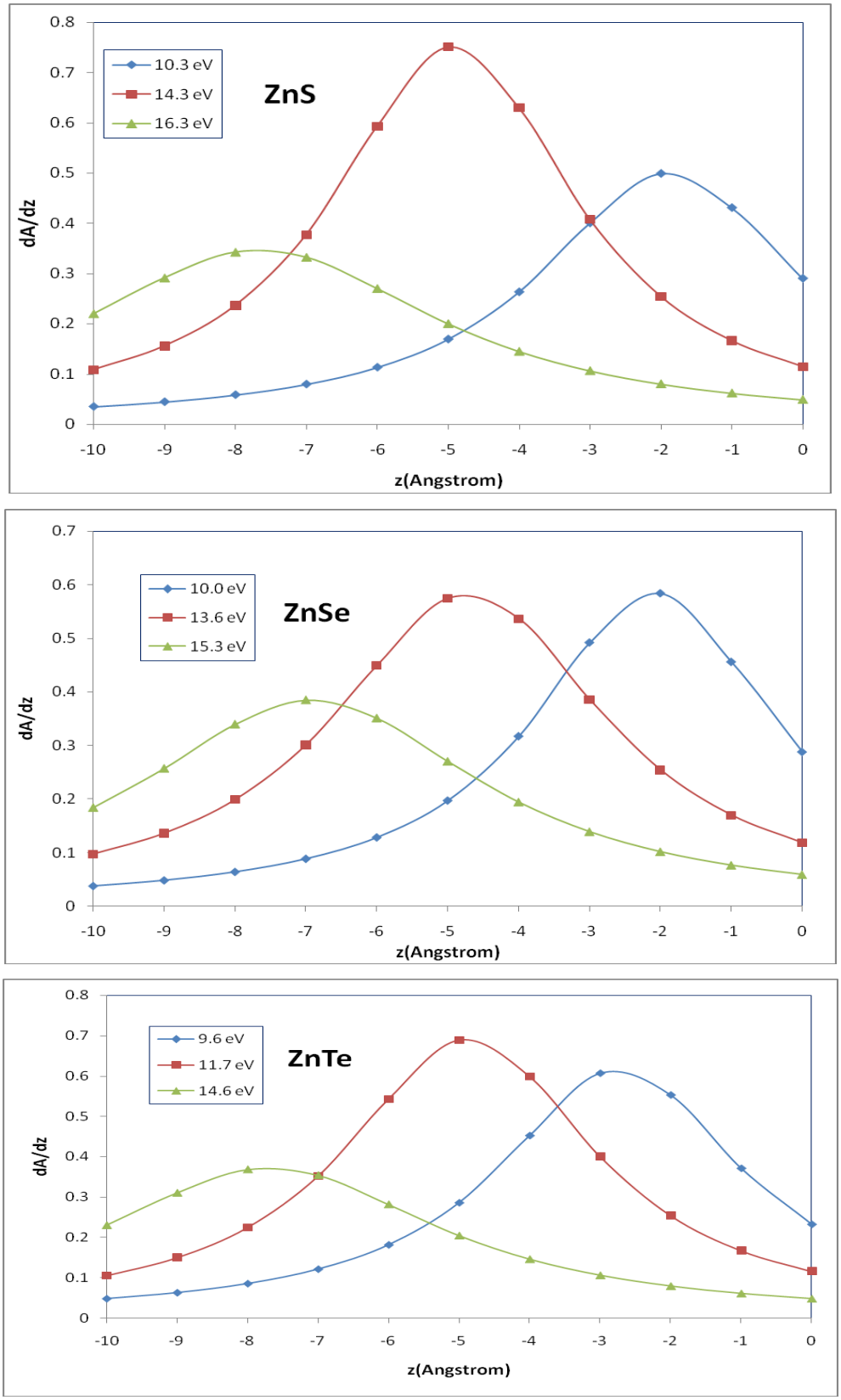

Figure 2.3(b): Plot of $\frac{d\tilde{A}_{\omega}}{dz}$ against distance from the surface for various photon energies in ZnX (X= S, Se, Te) using calculated data.

(iii) Aluminium pnictides:

In Figure 2.4, a graph of $\left|\tilde{A}_{\omega}(z)\right|^2$ against the incident photon energy ($\hbar\omega$) is plotted for the surface plane located at *z* = 0 (vacuum), *z* = - *0.5 d* (surface) and *z* = *-d* (bulk) for AlX (X= P, AS, Sb) where *d is* the width of the surface. We find that for the surface region *z* = - *0.5d*, $\left|\tilde{A}_{\omega}(z)\right|^2$ increases with the increase in the incident photon energy and a peak occurs at photon energy $\hbar\omega$ = 12.3 eV, 12.0 eV, 10.9 eV after which it starts decreasing with further increase in the photon energy and becomes minimum at $\hbar\omega$ = 17.43 eV, 16.75 eV, 15.28 for AlP, AlAs, AlSb respectively. The calculated plasmon energies ($\hbar\omega_p$) of AlP, AlAs, AlSb are 16.65 eV, 15.75 eV, 13.72 eV (Kumar *et al*. 2013; Yadav and Kumar, 2013; Yadav and Singh, 2010; Kumar, 2013). Reddy *et al.* (2003) have calculated the values of AlP, AlAs, AlSb as 18.1 eV, 16.5 eV, 15.5 eV respectively. For further increase in photon energy, a secondary peaks occurs at around photon energy $\hbar\omega$ = 23 eV for AlP and AlAs while $\hbar\omega$ = 20 eV for AlSb. For the location of the surface plane at *z = 0*, which is the vacuum region, we find that with the increase in the photon energy, $\left|\tilde{A}_{\omega}(z)\right|^2$ decreases slightly and we do not observe a proper peak below the plasmon energy but a minimum is observed near the plasmon energy. For the other locations of the surface plane at *z* = - *d*, which is the bulk region, $\left|\tilde{A}_{\omega}(z)\right|^2$ increases slightly with the increase in the photon energy and a peak is observed at around $\hbar\omega$ = 23 eV, 22 eV, 19 eV for AlP, AlAs, AlSb respectively.

(iv) Gallium pnictides:

In Figure 2.5, a graph of $\left|\tilde{A}_{\omega}(z)\right|^2$ against the incident photon energy ($\hbar\omega$) is plotted for the surface plane located at z = 0 (vacuum), z = - *0.5 d* (surface) and z = *-d* (bulk) for GaX (X= P, AS, Sb) where *d is* the width of the surface. We find that for the surface region z = - *0.5d*, $\left|\tilde{A}_{\omega}(z)\right|^2$ increases with the increase in the incident photon energy and a peak occurs at photon energy $\hbar\omega$ = 12.8 eV, 12.0 eV, 10.7 eV after which it starts decreasing with further increase in the photon energy and becomes minimum at $\hbar\omega$ = 16.07 eV, 16.31 eV, 15.14 eV for GaP, GaAs, GaSb respectively. The calculated plasmon energies ($\hbar\omega_p$) of GaP, GaAs, GaSb are 16.50 eV, 15.35 eV, 13.38 eV (Kumar *et al*. 2013; Yadav and Kumar, 2013; Yadav and Singh, 2010; Kumar, 2013) but Reddy *et al.* (2003) have calculated to be 17.14 eV, 14.87 eV, 12.5 eV respectively. For further increase in photon energy, an insignificant humps occurs at around photon energy $\hbar\omega$ = 23 eV for GaP and GaAs while $\hbar\omega$ = 22 eV for GaSb. For the location of the surface plane at z = *0,* which is the vacuum region, we find that with the increase in the photon energy, $\left|\tilde{A}_{\omega}(z)\right|^2$ decreases slightly and we do not observe a proper peak below the plasmon energy but a minimum is observed near the plasmon energy. For the other locations of the surface plane at z = - *d,* which is the bulk region, $\left|\tilde{A}_{\omega}(z)\right|^2$ increases slightly with the increase in the photon energy and a number of humps and suppressions are observed at around $\hbar\omega$ = 23 eV for GaP, GaAs where $\hbar\omega$ = 17 eV for GaSb.

(iv) Indium pnictides:

In Figure 2.6, a graph of $\left|\tilde{A}_{\omega}(z)\right|^2$ against the incident photon energy ($\hbar\omega$) is plotted for the surface plane located at $z = 0$ (vacuum), $z = -0.5\,d$ (surface) and $z = -d$ (bulk) for InX (X= P, AS, Sb) where *d is* the width of the surface. We find that for the surface region $z = -0.5d$, $\left|\tilde{A}_{\omega}(z)\right|^2$ increases with the increase in the incident photon energy and a peak occurs at photon energy $\hbar\omega$ = 11.0 eV, 10.8 eV, 9.9 eV after which it starts decreasing with further increase in the photon energy and becomes minimum at $\hbar\omega$ = 14.76 eV, 14.73 eV, 13.46 eV for InP, InAs, InSb respectively. The calculated plasmon energies ($\hbar\omega_p$) of InP, InAs, InSb are 14.76 eV, 14.07 eV, 12.73 eV (Kumar *et al*. 2013; Yadav and Kumar, 2013; Yadav and Singh, 2010; Kumar, 2013) but Reddy *et al.* (2003) have calculated to be 15.96 eV, 13.85 eV, 11.81 eV respectively. For the location of the surface plane at $z = 0$, which is the vacuum region, we find that with the increase in the photon energy, $\left|\tilde{A}_{\omega}(z)\right|^2$ decreases slightly and we do not observe a proper peak below the plasmon energy but a minimum is observed near the plasmon energy. For the other locations of the surface plane at $z = -d$, which is the bulk region, $\left|\tilde{A}_{\omega}(z)\right|^2$ increases slightly with the increase in the photon energy and a number of humps and suppressions are observed at around $\hbar\omega$ = 15 eV for InP, InAs, InSb.

In all the plots shown above showing the variation of the electromagnetic field as a function of the incident photon energy ($\hbar\omega$), for the location of the surface plane at the surface region, we have observed a maximum in the electromagnetic field below the plasmon energy and a suppression near the plasmon energy. The plasmon energy is chosen to be defined as the energy at which the real value of $\varepsilon_1(\omega)$ disappears. The peak

value in $\left|\tilde{A}_{\omega}(z)\right|^2$ at incident photon energy below the plasmon energy is due to the excitations of the surface plasmon. The suppression of the electromagnetic field in the neighbourhood of the plasmon energy for the surface region indicates that the behaviour of the electromagnetic field in the surface region is very similar to its behaviour outside the surface. For other locations of the surface plane, that is, at the vacuum and at the bulk region, peak in electromagnetic field below the plasmon energy and minimum near the plasmon energy were not observed. This shows the importance of the surface region in compound semiconductors.

Hence we can conclude that the origin of a peak in the field calculation is a surface feature. From the results shown above, we can also conclude that the electromagnetic fields we have calculated which is deduced using a local dielectric model can be used for surface photocurrent calculations for compound semiconductors.

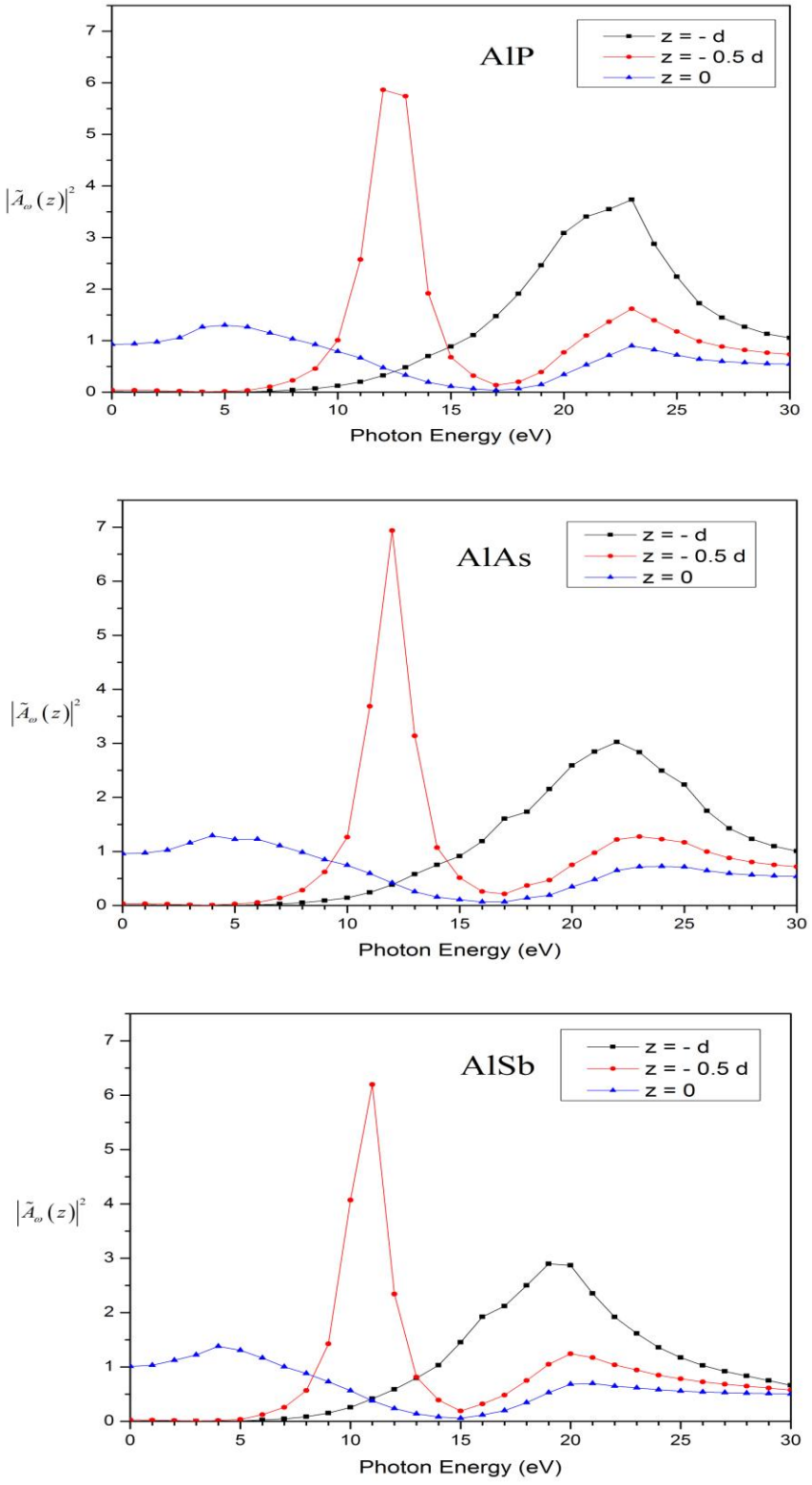

Figure 2.4: Plot of variation of $\left|\tilde{A}_\omega(z)\right|^2$ against photon energy for location of surface planes at *z* = -d, -0.5d and 0 for AlX (X= P, AS, Sb) using calculated data.

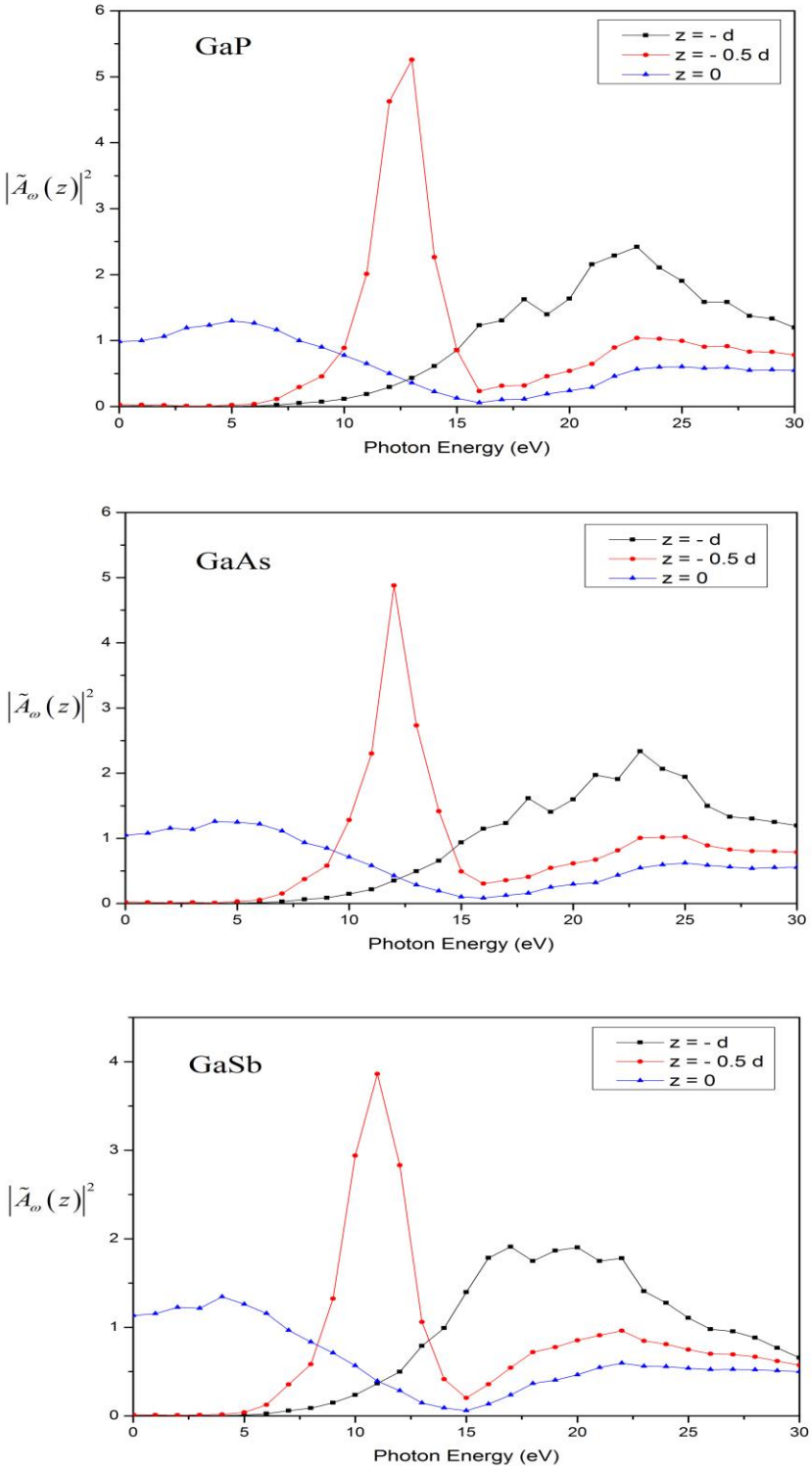

Figure 2.5: Plot of variation of $|\tilde{A}_\omega(z)|^2$ against photon energy for location of surface planes at *z* = -d, -0.5d and 0 for GaX (X= P, AS, Sb) using calculated data.

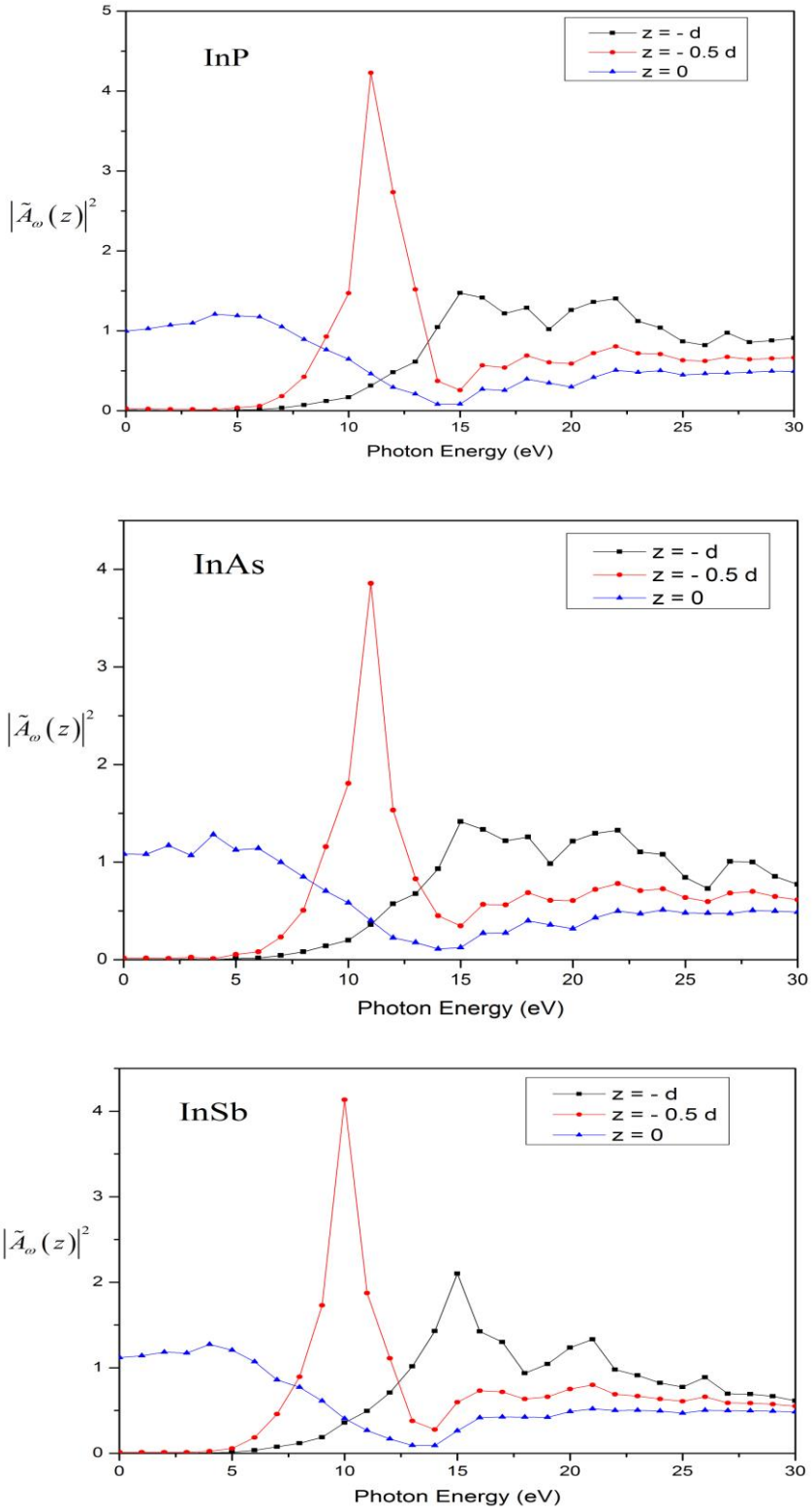

Figure 2.6: Plot of variation of $|\tilde{A}_\omega(z)|^2$ against photon energy for location of surface planes at z = -d, -0.5d and 0 for InX (X= P, AS, Sb) using calculated data.

CHAPTER - 3

Photocurrent Calculations using the Mathieu Potential Model

In this chapter, we present the calculations of photocurrent from compound semiconductors by using the Mathieu potential for the crystal. In this model, the potential is represented by a periodic sinusoidal wave in one-dimensional crystal. For such a potential, the Schrödinger equation reduces to the *Mathieu equation* whose solutions have been discussed in detail by McLachlan (1951). Brillouin (1953) had used this model as an appropriate model for developing the energy band theory of solids, while Morse used it in his study of electron diffraction. Slater (1952) used the Mathieu potential problem in one, two and three dimensions to describe the energy bands in a realistic crystal. Then Carver (1971) has discussed the symmetries of Mathieu functions, and the relations between the functions and the electron wave functions at the centres and edges of the crystal bands. The Mathieu potential has been at first used by Statz (1950) for surface state calculation. Levine has used Mathieu potential for calculating the condition for arbitrary surface termination. In this chapter, we will discuss a formalism developed for photoemission calculations in which the electron states are derived by using the Mathieu potential (Levine, 1968). Two cases will be discussed namely, the effects of the empty lattice and strong periodic lattice potential on the electronic states for deriving the initial state wave functions as described by Davison and Steslicka (1992).

It was Pachuau *et al.* (2001, 2002) who had used this approach of Davison and Steslicka for deriving the initial state wavefunctions for evaluation of the matrix element $\left\langle \psi_f \left| H' \right| \psi_i \right\rangle$ for calculating photocurrent. The calculated photocurrent results as obtained by Pachuau *et al.* (2000) in the case of free electron metals like Al and Be showed satisfactory behaviour especially for photon energy below and above the plasmon energies. They have developed also formulae for initial state wavefunction which is applicable to other metals than free electron metals. This was applied to calculate photocurrent by using Eqn. (1.1) of Chapter 1 from *d*-band metals like W, Mo, Cu and

semiconductor Si. The photocurrent data in the UV photon energy range showed interesting features comparable to experimental results especially in the case of W and Mo. With this motivation, we have applied Mathieu potential model to evaluate the initial state wave function to calculate the matrix element in photocurrent by using the same dielectric model as used in the earlier chapters.

3.1 Formulation of initial state wavefunction by Mathieu Potential Model

3.1.1 Empty Potential with Finite Surface:

Let us consider a one - dimensional crystal whose potential is represented by a sinusoidal potential given by

$$V(x)=V_0 \cos\left(\frac{2\pi x}{a}\right) \tag{3.1}$$

where *'a'* is the period of the potential having a maximum value V_0 at x = 0. The one-dimensional Schrödinger equation can be written as

$$\frac{d^2\psi(z)}{dz^2}+(\alpha-2q\cos 2z)\psi(z)=0 \tag{3.2}$$

where $2q=\frac{V_0}{a}$, $z=\frac{\pi x}{a}$, $T=\left(\frac{\pi}{a}\right)^2$, $\alpha=\frac{E}{T}$

Here q is the amplitude of the potential which measures its strength. Equation (3.2) can be solved for obtaining initial state wavefunction $\psi_i(x)$ for the bulk and surface regions $(x\le 0)$, and also for the vacuum regions $(x>0)$. Equation (3.2) is the Mathieu equation and its solution is derived for free electron or empty potential (q ~ 0) when the crystal potential is flat as shown in Figure (3.1). To determine the initial state wave function ψ_i(x) in Equation (3.2), we have included a surface of width (d) in the crystal potential.

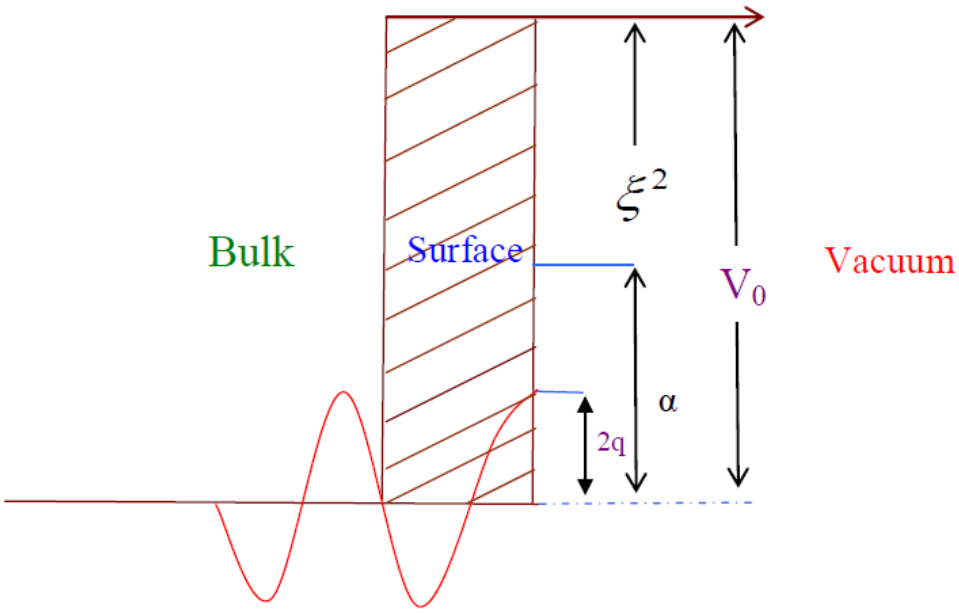

Figure 3.1: Model diagram of sinusoidal Mathieu Potential used for calculating the initial state wave function.

The initial state wave function for the bulk and surface and for the vacuum regions is given by

$$\psi_i(x,q)=\begin{cases}\left(\frac{1}{4\pi k_i}\right)^{\frac{1}{2}}\varphi(x_0,q)e^{-\mu(x_0-x)}, & (\ for\ \mu>0), \quad x\le 0\\ (2\xi)^{\frac{1}{2}}e^{-\xi(x-x_0)}, & (\ for\ \xi>0), \quad x\ge 0\end{cases} \tag{3.3}$$

where $x_0=\frac{\pi}{a}z_0$, and x_0 is the location of the crystal surface plane. In Eq. (3.3), ξ is related to work function of the metal and μ the wave vector. In Eq. (3.3) above, we have $k_i=\sqrt{2E_i}$ and

$$\phi(x_0,q)=\lambda\cos m'x-\sin m'x$$

$$\lambda=\tan m'(x_0-\xi^{-1})$$

such that $m'=\frac{m\pi}{a}$, m being the band gap index, ξ is the height of step potential and λ is the hybridization parameter.

3.1.2 Strong Periodic Potential with Finite Surface :

The case of empty lattice potential is not applicable to the strongly bonded metals like *d*-band metals or semiconductors. Hence one needs to develop the initial state wave functions by solving the Mathieu equation in Eq. (3.1) by incorporating the sine and cosine elliptic functions. We have considered the same model as in the case of empty lattice potential model which is given in Fig. (3.1), but used for strong periodic lattice (i.e. $q > 0$).

It is therefore, necessary to find an explicit form of atomic orbital $\phi(x'_0, q)$ to derive the initial state wave function $\psi_i(z)$. The most general form is a linear combination of all the bulk standing states $se_m(x'_0, q)$ and $ce_m(x'_0, q)$ for all the Fermi energy gap *m*. Thus, the surface states will be largely a hybrid of sine and cosine elliptic functions which is given by the expression

$$\phi(x'_0, q) = \lambda_m ce_m(x'_0, q) - se_m(x'_0, q) \tag{3.4}$$

where λ_m is the hybridization parameter which can be written as

$$\lambda_m = \frac{se_m(x'_0, q) - (\xi + \mu)^{-1} se'_m(x'_0, q)}{ce_m(x'_0, q) - (\xi + \mu)^{-1} ce'_m(x'_0, q)} \tag{3.5}$$

Here $se_m(x'_0, q)$ and $ce_m(x'_0, q)$ are the sine and cosine elliptic functions in Eq. (3.4). These functions in expanded form can be written as

$$se_m(x'_0, q) = \sin m x'_0 - \frac{q}{4}\left[\frac{\sin(m+2)x'_0}{m+1} - \frac{\sin(m-2)x'_0}{m-1}\right]$$

$$+ \frac{q}{3}\left[\frac{\sin(m+4)x'_0}{(m+1)(m+2)} + \frac{\sin(m-4)x'_0}{(m-1)(m-2)}\right] + \ldots\ldots\ldots \tag{3.6}$$

and $$ce_m(x'_0, q) = \cos m x'_0 - \frac{q}{4}\left[\frac{\cos(m+2)x'_0}{m+1} - \frac{\cos(m-2)x'_0}{m-1}\right]$$

$$+ \frac{q}{3}\left[\frac{\cos(m+2)x'_0}{(m+1)(m+2)} + \frac{\cos(m-4)x'_0}{(m-1)(m-2)}\right] + \ldots\ldots\ldots \tag{3.7}$$

For finite surface potential, surface state existence condition implies that

$$x_0 = \frac{a}{2},\ \xi = \frac{12}{a},\quad \lambda > 0 \quad \text{and} \quad m = 3, 5\ldots \tag{3.8}$$

We are considering surface state occurring for *m* = 3 and hence from Eqs. (3.6), (3.7) and (3.8), we can write,

$$ce_3(x'_0,q)=0 \quad , \qquad ce'_3(x'_0,q)=3\left(1+\frac{q}{16}-\frac{q^2}{640}\right)$$

$$se_3(x'_0,q)=-1+\frac{q}{16}-\frac{11}{640}q^2 \quad , \quad se'_3(x'_0,q)=0 \tag{3.9}$$

Hence, we may obtain the value of λ_3 as:

$$\lambda_3=\frac{(\xi+\mu)\left[1-\frac{q}{16}+\frac{11}{640}q^2\right]}{3\left(1+\frac{q}{16}-\frac{q^2}{640}\right)} \tag{3.10}$$

Using Eqs. (3.8) and (3.9) into Eq. (3.4), the initial state wave function in the case of strong periodic potential becomes

$$\psi_i(x,q)=\begin{cases}\left(\frac{1}{4\pi k_i}\right)^{\frac{1}{2}}\left(1-\frac{q}{16}+\frac{11}{640}q^2\right)e^{-\mu(x'_0-x)}, & x\le 0\\ (2\xi)^{\frac{1}{2}}e^{-\xi(x-x'_0)}, & x\ge 0\end{cases} \tag{3.11}$$

Here,

$$q=1, k_i^2=2E_i \text{ , } \xi=2, \; x_0^{'}=\frac{\pi}{a}.z_0$$

z_0 is the location of the surface state wavefunction and *a* is the lattice constant. We have calculated photocurrent for two locations of the initial state wavefunctions in the surface region z_0. The derivation of $\psi_i(x,q)$ is discussed in detailed by Pachuau (2001).

The final state wave function ψ_f as the scattering state of the step potential which is encountered by the electron (Bagchi and Kar 1978). Step potential is defined by

$$V(x) = -V_0\theta(x)$$

where $\theta(x)$ is unit function such that $\theta(x) = 1$ (0) for $x > 0$ ($x < 0$).

The final state wave function which is the solution of the step potential can be written as (in atomic units):

$$\psi_f(z)=\begin{cases}\left(\frac{1}{2\pi q_f}\right)^{\frac{1}{2}}\frac{2q_f}{q_f+k_f}e^{ik_f z}e^{-\alpha|z|} & z\le 0\\ \left(\frac{1}{2\pi q_f}\right)^{\frac{1}{2}}\left(e^{iq_f z}+\frac{q_f-k_f}{q_f+k_f}\right)e^{-iq_f z} & z\ge 0\end{cases} \tag{3.12}$$

where $k_f^2 = 2E_f$, $q_f^2 = 2(E_f - V_0)$ and $E_f = E_i + \hbar\omega$. In Eq. (3.12), the factor $e^{-\alpha|z|}$ is included on the surface and bulk side to take into accounts the inelastic scattering of the electrons.

The photocurrent density formula may be written with the help of Golden Rule formula (Penn, 1972) as

$$\frac{dj(E)}{d\Omega} = \frac{2\pi}{\hbar}\sum|<\psi_f \mid H' \mid \psi_i>|^2\ \delta(E-E_f)\delta(E_f - E_i - \hbar\omega)\, f_o(E-\hbar\omega)[1- f_o(E)] \tag{3.13}$$

where E_i and E_f are the initial and final state of energy, ψ_i and ψ_f are the initial and final state wavefunction, f_o denotes the Fermi occupation function and δ - function establish the energy selection rule. The perturbation in the Hamiltonian responsible for the photoexcitation of the electron is given by

$$H' = \frac{e}{2m_e c}(\boldsymbol{p}.\boldsymbol{A} + \boldsymbol{A}.\boldsymbol{p}) \tag{3.14}$$

where m_e is the mass of the elcetron, $\boldsymbol{p}$ is the one electron momentum vector and $\boldsymbol{A}$ is the vector potential of the incident photon field.

To compute the photon field, we have used the local dielectric model of Bagchi and Kar (1978) which has been used in Chapter 2. With simple modifications, the photon field used in our calculations for three regions can be written as

$$\tilde{A}_\omega(\omega, x) = \begin{cases} A_1, & x < -d \\ \dfrac{A_1 \varepsilon(\omega) d}{[1-\varepsilon(\omega)]x + d}, & -d \le x \le 0 \\ A_1 \varepsilon(\omega), & x > 0 \end{cases} \tag{3.15}$$

where A_1 is a constant depending on dielectric function $\varepsilon(\omega)$, photon energy $\hbar\omega$ and angle of incidence θ_i.

The matrix element $<\psi_f | H' | \psi_i>$ involved in scattering cross-section can be expanded as follows:

$$I = <\psi_f | H' | \psi_i>$$

$$= \int_{-\infty}^{\infty} \psi_f^*(z) \tilde{A}_\omega(z) \psi_i dz$$

$$= \int_{-\infty}^{-d} \psi_f^* \tilde{A}_\omega \psi_i \, dz + \int_{-d}^{0} \psi_f^* \tilde{A}_\omega \frac{d}{dz}\psi_i \, dz + \frac{1}{2}\int_{-d}^{0} \psi_f^* \frac{d\tilde{A}_\omega}{dz}\psi_i \, dz + \int_0^\infty \psi_f^* \tilde{A}_\omega \varepsilon(\omega) \frac{d}{dz}\psi_i dz \tag{3.16}$$

We will discuss here the contribution of the surface region $(-d \le z \le 0)$ only to evaluate matrix element in Eqn. (3.16) for calculating photocurrent. The matrix element in Eqn. (3.16) can now be represented by

$$I = \int_{-d}^{0} \psi_f^* \tilde{A}_\omega(z) \frac{d\psi_i}{dz} dz + \frac{1}{2}\int_{-d}^{0} \psi_f^* \frac{d\tilde{A}_\omega(z)}{dz}\psi_i \, dz \tag{3.17}$$

Photocurrent was calculated as a function of photon energy ($\hbar\omega$) in the case of compound semiconductors. For each of these compounds semiconductors, we used our generated dielectric function.

The detailed expansion of Eq. (3.16) is shown in APPENDIX-I and the FORTRAN programme for calculating photocurrent is given in APPENDIX-II.

3.2 Calculation of photocurrent by using Mathieu Potential Model with Strong Periodic Potential with Finite Surface

We discuss here the photocurrent results in the case of compound semiconductors like Beryllium chalcogenides, Zinc chalcogenides, Aluminium pnictides, Gallium pnictides and Indium pnictides. For each of these compound semiconductors, we have used our generated dielectric constant. Choice of parameter like initial state energy (E_i), magnitude of potential (V_0), Fermi level (E_F), were those pertaining to respective semiconductors. However, angle of incidence was $\theta_i = 45^0$ for *p*-polarised light under consideration in all the cases. Photocurrent had been calculated for values of z_0 = -2 a.u. and z_0 = -8 a.u. As the width of the surface is 10 a.u. in all the cases, z_0 = - 2 a.u. is near the surface-vacuum interface and z_0 = -8 a.u. is towards the surface-bulk interface. We have shown in all the cases the plot of photocurrent has been converted to normalized values. This has been done in order to avoid the large difference in numerical magnitude of the calculated photocurrent data which could not be reflected as graph plots especially for the case of z_0 = -8 a.u., as it was too small to be plotted on the same unit scale.

(i) Beryllium chalcogenides:

The plot of photocurrent as a function of photon energy ($\hbar\omega$) for BeS, BeSe, BeTe is shown in Figure (3.2). We have plotted the results in normalised unit for two locations of surface states. For location of ψ_i near the surface-vacuum interface, i.e., in the surface region (z_0 = - 2 a.u.), we find that photocurrent showed a peak at $\hbar\omega$ = 6.29 eV in the three compounds. With the increase in photon energy, it decreases and attained a minimum value at $\hbar\omega$ = 16.65 eV, 15.91 eV, 15.17 eV for BeS, BeSe, BeTe respectively. Measured value of plasmon energies ($\hbar\omega_p$) of BeS, BeSe, BeTe are 19.52 eV, 18.39 eV, 16.12 eV (Kumar *et al*. 2013; Yadav and Kumar, 2013). Hence, we find that photocurrent decreased to minimum near about the bulk plasmon energy. For further increase in photon energy beyond $\hbar\omega_p$, photocurrent attained another maxima at $\hbar\omega$ = 27.02 eV for BeS, $\hbar\omega$ = 26.28 eV for BeSe and BeTe but of smaller height than the first peaks. However, in the case of z_0 = -8 a.u. in which the surface state is located closer towards the bulk, the behaviour of the photocurrent is somewhat different. There is no proper peak in photocurrent like the case of z_0 = - 2 a.u. for values of photon energy below and above $\hbar\omega_p$ but minimum at $\hbar\omega$ =17.39 eV, 15.91 eV, 15.17 eV for BeS, BeSe and BeTe.

(ii) Zinc chalcogenides:

The plot of photocurrent as a function of photon energy ($\hbar\omega$) for ZnS, ZnSe, ZnTe is shown in Figure (3.3). We have plotted the results in normalised unit for two locations of surface states. For location of ψ_i near the surface-vacuum interface, i.e., in the surface region (z_0 = - 2 a.u.), we find that photocurrent showed a peak at $\hbar\omega$ =5.55 eV for ZnS, $\hbar\omega$ = 6.29 eV for ZnSe and ZnTe. With the increase in photon energy, it

decreases and attained a minimum value at $\hbar\omega$ = 16.65 eV, 15.17 eV, 14.43 eV. Measured value of plasmon energies ($\hbar\omega_p$) of ZnS, ZnSe, ZnTe are 16.71 eV, 15.78 eV, 14.76 eV (Kumar *et al*. 2013; Yadav and Kumar, 2013; Kumar 2013) and Reddy *et al.* (2003) have calculated 14.73 eV, 14.33 eV, 13.66 eV respectively. Hence, we find that photocurrent decreased to minimum near about the bulk plasmon energy. For further increase in photon energy beyond $\hbar\omega_p$, photocurrent attained another maxima at $\hbar\omega$ = 26.27eV for all compounds but of smaller height than the first peaks. However, in the case of z_0 = -8 a.u. in which the surface state wavefunction is located closer towards the bulk, the behaviour of the photocurrent is somewhat different. There is no proper peak in photocurrent like the case of z_0 = - 2 a.u. for values of photon energy below and above $\hbar\omega_p$ but minimum at $\hbar\omega$ =15.91 eV, 15.17 eV, 14.43 eV for ZnS, ZnSe and ZnTe.

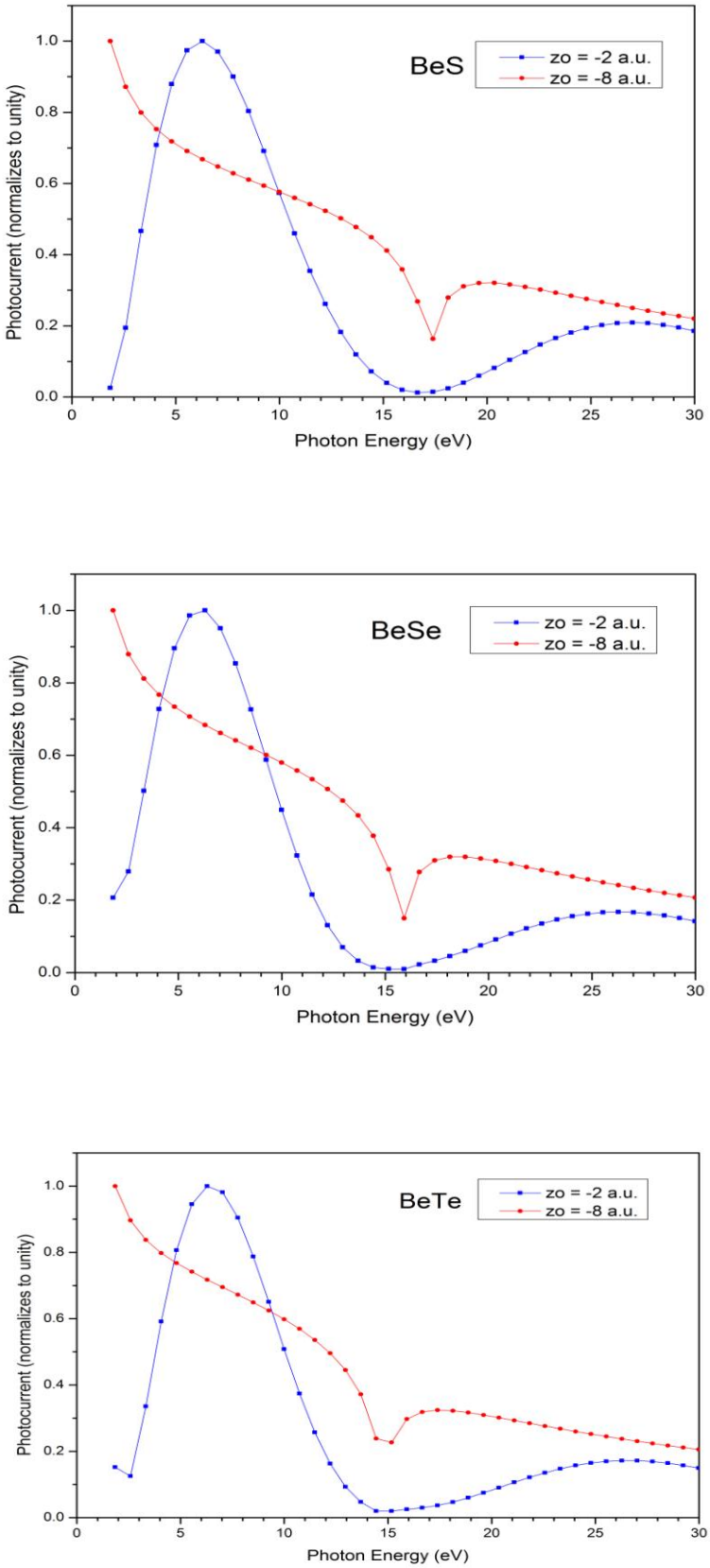

Figure 3.2: Plot of photocurrent against photon energy $\hbar\omega$ with ψ_i defined by Mathieu model for strong potential in the case of BeX (X= S, Se, Te) using calculated data.

.

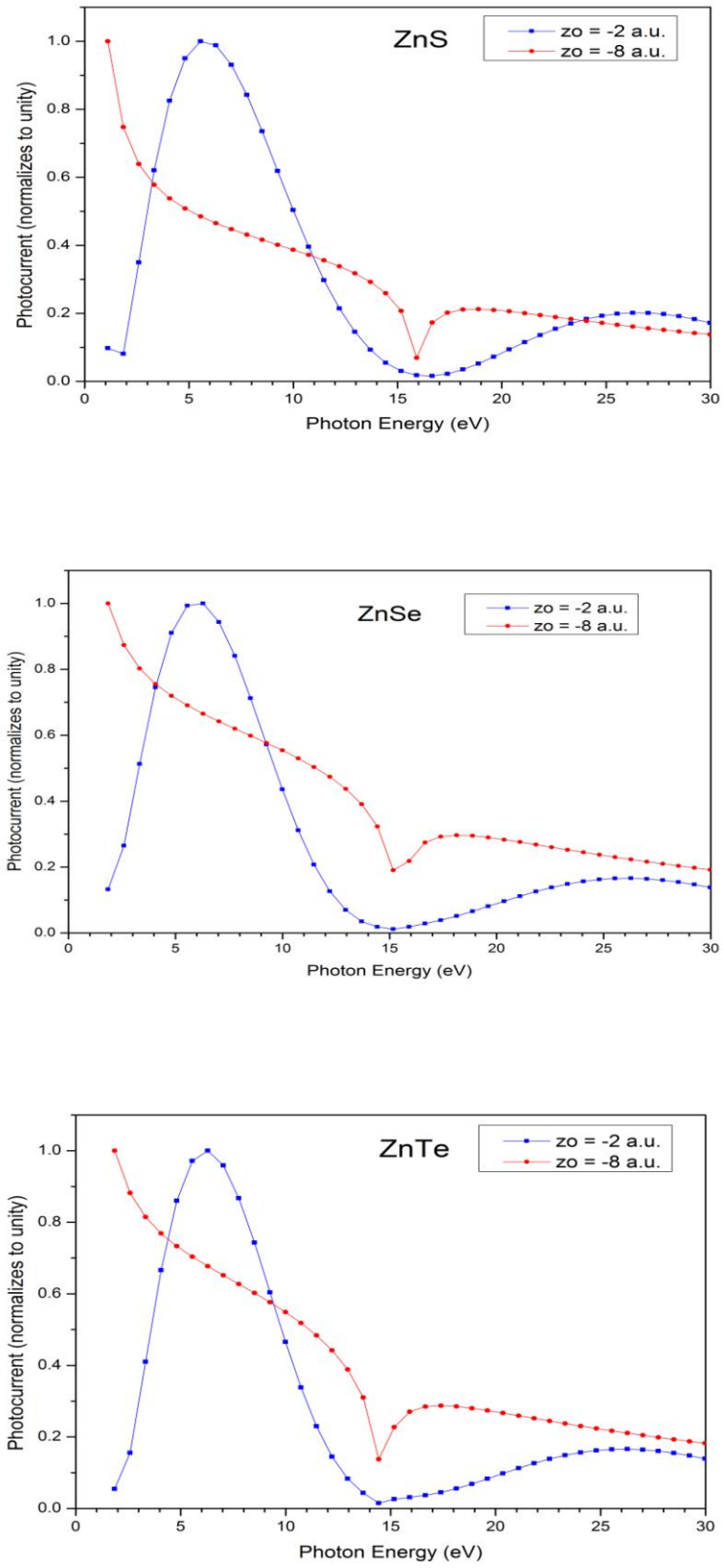

Figure 3.3: Plot of photocurrent against photon energy $\hbar\omega$ with ψ_i defined by Mathieu model for strong potential in the case of ZnX (X= S, Se, Te) using calculated data.

(iii) Aluminium pnictides:

The plot of photocurrent as a function of photon energy ($\hbar\omega$) for AlP, AlAs, AlSb is shown in Figure (3.4). We have plotted the results in normalised unit for two locations of surface states. For location of ψ_i near the surface-vacuum interface, i.e., in the surface region (z_0 = - 2 a.u.), we find that photocurrent showed a peak at $\hbar\omega$ = 4.81 for AlP and AlAs, $\hbar\omega$ = 5.55 eV for AlSb. With the increase in photon energy, it decreases and attained a minimum value at $\hbar\omega$ = 15.91 eV, 15.17 eV, 14.43 eV. The calculated plasmon energies ($\hbar\omega_p$) of AlP, AlAs, AlSb are 16.65 eV, 15.75 eV, 13.72 eV (Kumar *et al*. 2013; Yadav and Kumar, 2013; Yadav and Singh, 2010; Kumar, 2013) and Reddy *et al.* (2003) have calculated 18.1 eV, 16.5 eV, 15.5 eV respectively. Hence, we find that photocurrent decreased to minimum near about the bulk plasmon energy. For further increase in photon energy beyond $\hbar\omega_p$, photocurrent attained another maxima at $\hbar\omega$ = 25.54 eV, 24.80 eV, 25.54 eV, but of smaller height than the first peaks. However, in the case of z_0 = -8 a.u. in which the surface state is located closer towards the bulk, the behaviour of the photocurrent is somewhat different. There is no proper peak in photocurrent like the case of z_0 = - 2 a.u. for values of photon energy below and above $\hbar\omega_p$ but minimum at $\hbar\omega$ =15.91 eV, 15.17 eV, 14.43 eV for AlP, AlAs and AlSb.

(iv) Gallium pnictides:

The plot of photocurrent as a function of photon energy ($\hbar\omega$) for GaP, GaAs, GaSb is shown in Figure (3.5). We have plotted the results in normalised unit for two locations of surface states. For location of ψ_i near the surface-vacuum interface, i.e., in the surface region (z_0 = - 2 a.u.), we find that photocurrent showed a peak at $\hbar\omega$ = 6.29 eV for GaP and GaAs, $\hbar\omega$ = 7.03 eV for GaSb. With the increase in photon energy, it

decreases and attained a minimum value at $\hbar\omega$ = 16.65 eV, 15.17 eV, 14.43 eV. The calculated plasmon energies ($\hbar\omega_p$) of GaP, GaAs, GaSb are 16.50 eV, 15.35 eV, 13.38 eV (Kumar *et al*. 2013; Yadav and Kumar, 2013; Yadav and Singh, 2010; Kumar, 2013) and Reddy *et al.* (2003) have calculated 17.14 eV, 14.87 eV, 12.5 eV respectively. Hence, we find that photocurrent decreased to minimum near about the bulk plasmon energy. For further increase in photon energy beyond $\hbar\omega_p$, photocurrent attained another maxima at $\hbar\omega$ = 25.54 eV for GaS, $\hbar\omega$ = 26.28 eV for GaAs and GaSb, but of smaller height than the first peaks. However, in the case of z_0 = -8 a.u. in which the surface state wavefunction is located closer towards the bulk, the behaviour of the photocurrent is somewhat different. There is no proper peak in photocurrent like the case of z_0 = - 2 a.u. for values of photon energy below and above $\hbar\omega_p$ but minimum at $\hbar\omega$ =16.65 eV, 15.17 eV, 14.43 eV for GaP, GaAs and GaSb.

(v) Indium pnictides:

The plot of photocurrent as a function of photon energy ($\hbar\omega$) for InP, InAs, InSb is shown in Figure (3.6). We have plotted the results in normalised unit for two locations of surface states. For location of ψ_i near the surface-vacuum interface, i.e., in the surface region (z_0 = - 2 a.u.), we find that photocurrent showed a peak at $\hbar\omega$ = 6.29 eV for InP, $\hbar\omega$ = 7.03 eV for InAs and InSb. With the increase in photon energy, it decreases and attained a minimum value at $\hbar\omega$ = 16.65 eV, 15.91 eV, 14.43 eV. The calculated plasmon energies ($\hbar\omega_p$) of InP, InAs, InSb are 14.76 eV, 14.07 eV, 12.73 eV (Kumar *et al*. 2013; Yadav and Kumar, 2013; Yadav and Singh, 2010; Kumar, 2013) and Reddy *et al.* (2003) have calculated 15.96 eV, 13.85 eV, 11.81 eV respectively. hence we find that photocurrent decreased to minimum near about the bulk plasmon energy. For further

increase in photon energy beyond $\hbar\omega_p$, photocurrent attained another maxima at $\hbar\omega$ = 25.54 eV for InP and InAs, $\hbar\omega$ = 27.02 eV for InSb, but of smaller height than the first peaks. However, in the case of z_0 = -8 a.u. in which the surface state is located closer towards the bulk, the behaviour of the photocurrent is somewhat different. There is no proper peak in photocurrent like the case of z_0 = - 2 a.u. for values of photon energy below and above $\hbar\omega_p$ but minimum at $\hbar\omega$ =16.65 eV, 15.91 eV, 14.43 eV for InP, InAs and InSb.

We find that almost in all the case of compounds semiconductors, photocurrent showed similar trends. For example, as photon energy increased, photocurrent reached a minimum at around the values of photon energy equal to measured value of plasmon energy. Beyond the plasmon energy, a second peak in photocurrent was obtained whose height is smaller in magnitude than the first one at $\hbar\omega < \hbar\omega_p$. The reason for the occurrence of peak in photocurrent at $\hbar\omega < \hbar\omega_p$ is due to surface refraction effect where the z-component of electromagnetic field becomes maximum at $\hbar\omega_s = \hbar\omega_p / \sqrt{2}$.

We, therefore, concluded that the model used here for photoemission calculations is applicable to the case of compound semiconductors. However, it can be shown that one can also make use of Mathieu type of potential in photoemission calculations. Though the model used is simple, however, the inclusion of initial state wave function into the matrix element appears to produce the qualitative features as observed earlier in the measured data of photocurrent. The main drawback of the model used is that the same initial state wave function ψ_i is used to describe both the surface and bulk regions of the solids under study.

However, there are two drawbacks in the method of calculation of photoemission as discussed by Pachuau *et al.* (2000, 2002). It had been found out by numerical analysis that the first and the last integrands in the above equation do not converge due to choice of values of scattering factor α and μ. It is required that $\alpha < \mu$ for these integrals to converge. Secondly, as discussed above, contributions from the bulk as well as from the vacuum regions to matrix element is considered. This is essentially the case of surface resonance where one considers photoemission to be due to surface and bulk effects.

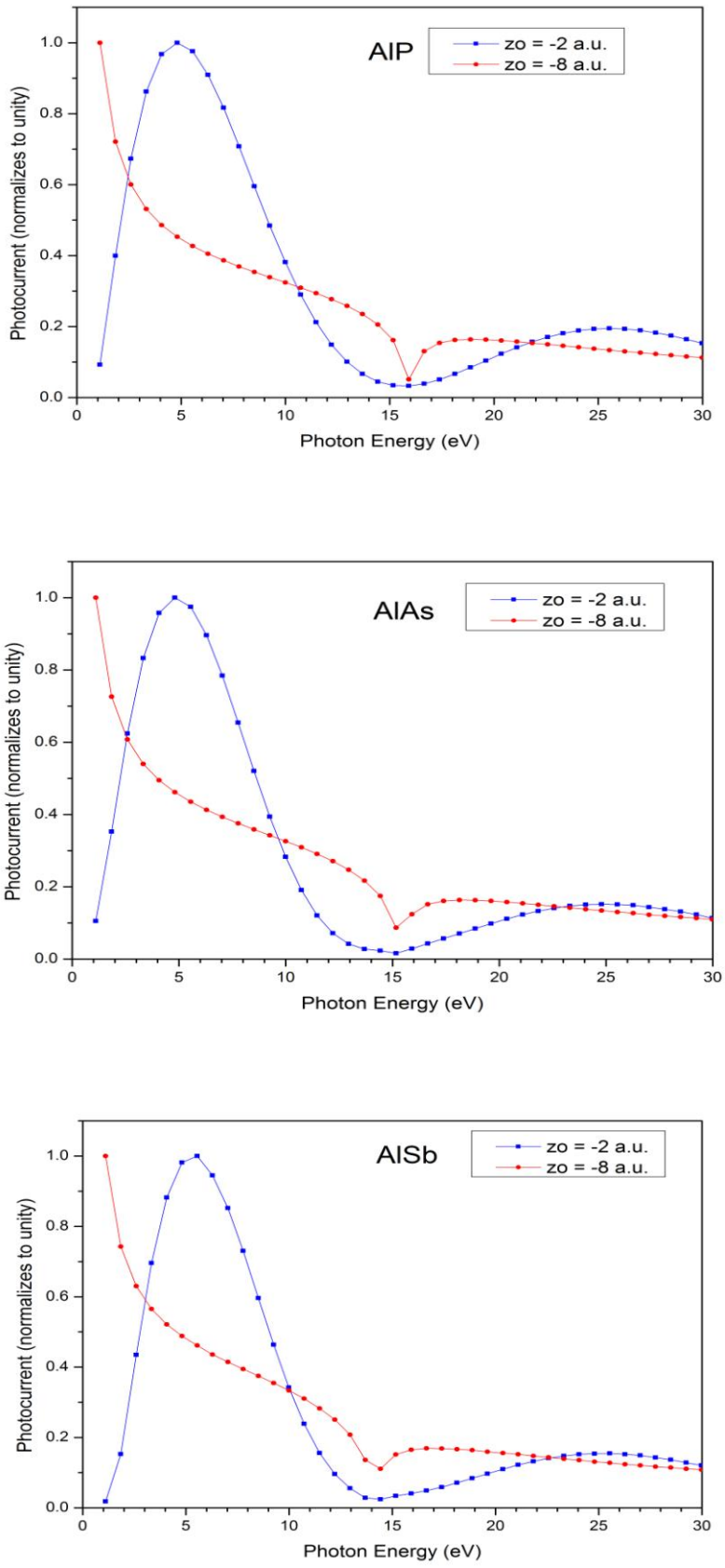

Figure 3.4: Plot of photocurrent against photon energy $\hbar\omega$ with ψ_i defined by Mathieu model for strong potential in the case of AlX (X= P, AS, Sb) using calculated data.

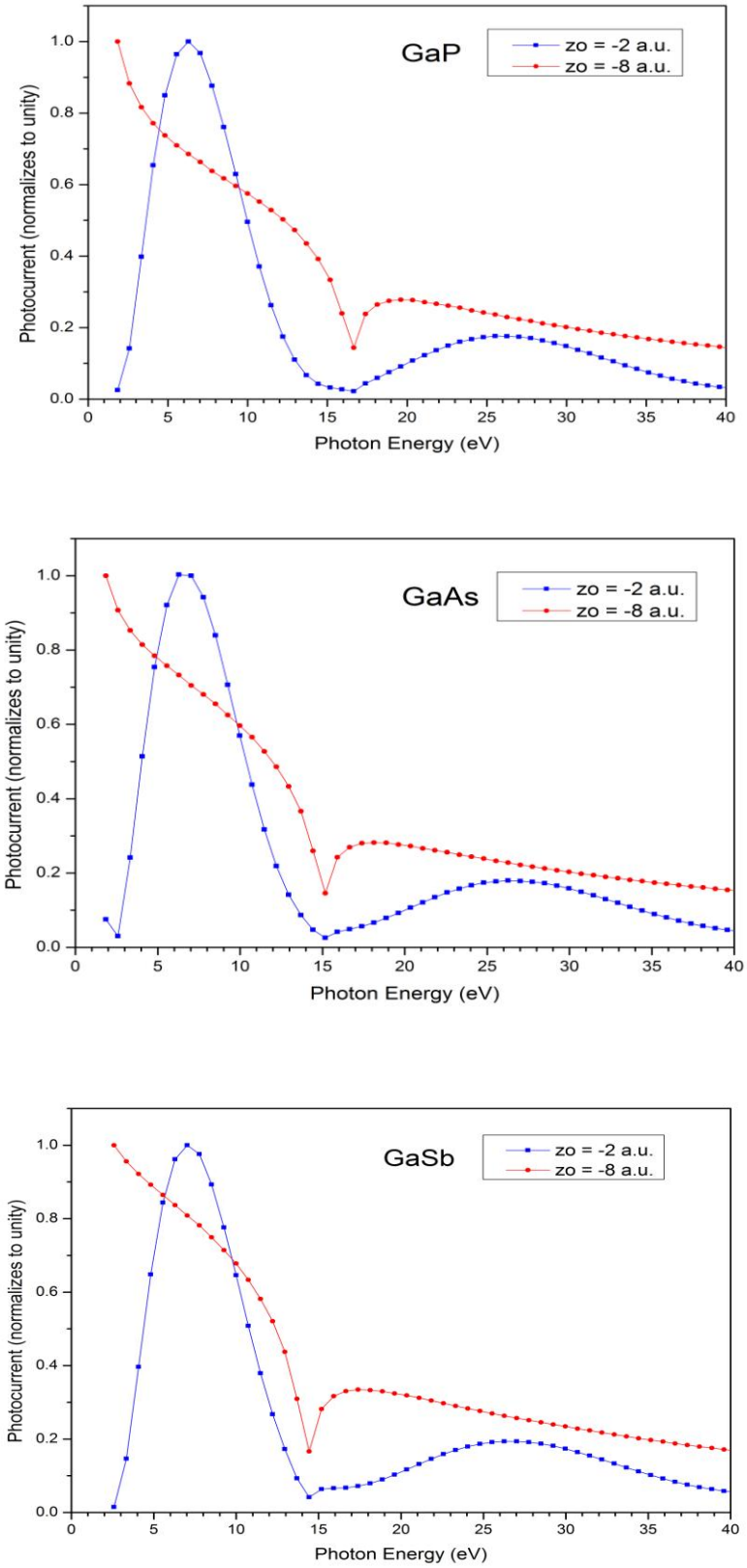

Figure 3.5: Plot of photocurrent against photon energy $\hbar\omega$ with ψ_i defined by Mathieu model for strong potential in the case of GaX(X= P, AS, Sb) using calculated data.

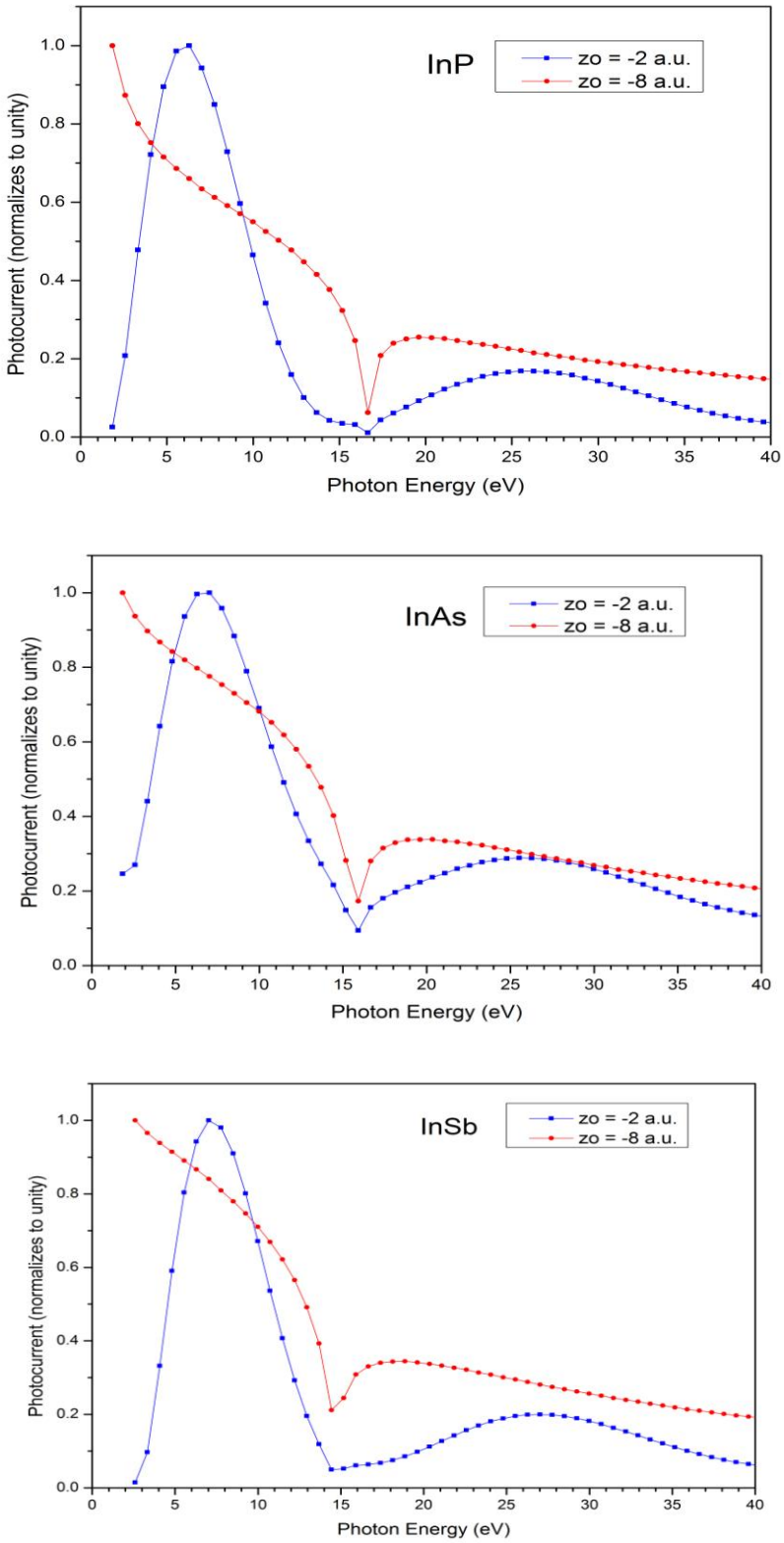

Figure 3.6: Plot of photocurrent against photon energy $\hbar\omega$ with ψ_i defined by Mathieu model for strong potential in the case of InX (X= P, AS, Sb) using calculated data.

CHAPTER 4

Methodology for

Electronic and Optical Properties

4.1 Density Functional Theory (DFT):

DFT is an extremely successful approach for the description of ground state properties of metals, semiconductors, and insulators. The full-potential linearized augmented plane wave (FPLAPW) method employs density-functional theory (DFT), introduced by Hohenbergand Kohn (1964) and Kohn and Sham (1965). The underlying theorem (Hohenberg-Kohn-Sham theorem) on which this theory rests is that the total energy, *E*, of an atomistic system can be expresses as a functional of its electron density, ρ, namely $E = E[\rho]$, that *E* is at its minimum for the ground-state density, and is stationary with respect to first-order variations in the density.

Typically, the Born-Oppenheimer approximation (Born and Oppenheimer, 1927) is employed which assumes that the motion of the nuclei are negligible with respect to that of electrons. This implies that the electronic structure is calculated for a given atomic geometry; the nuclei are then moved according to classical mechanics.

4.1.1 The Kohn-Sham equations

To obtain the ground-state density, the variational principle is applied with respect to the one-particle wave functions:

$$\left[-\frac{\hbar^2}{2m}\vec{\nabla}^2 + V_{eff}(\vec{r})\right]\psi_i(\vec{r}) = \varepsilon_i\psi_i(\vec{r}) \tag{4.1}$$

where

$$V_{eff}(\vec{r}) = V_C(\vec{r}) + \mu_{xc}[\rho(\vec{r})] \tag{4.2}$$

is the effective potential and ε_i the effective one-electron eigenvalues. Equations (4.1) are the "Kohn-Sham equations" and the solutions, $\psi_i(\vec{r})$, form an orthonormal set,

i.e. $\int \psi_i^*(\vec{r})\ \psi_j(\vec{r})d\vec{r} = \delta_{ij}$

The Coulomb or electrostatic potential is given as:

$$V_C(\vec{r}) = -e^2 \sum_{\alpha} \frac{Z_\alpha}{\left|\vec{r} - \vec{R_\alpha}\right|} + e^2 \int \frac{\rho(\vec{r}')}{\left|\vec{r} - \vec{r}'\right|} d\vec{r}' \tag{3.3}$$

which can also be calculated using Poisson's equation, i.e.,

$$\nabla^2 V_C(\vec{r}) = -4\pi e^2 q(\vec{r}) \tag{4.4}$$

where $q(\vec{r})$ represents the electronic charge distribution and the positive point charges at position R_α.

The exchange-correlation potential is given by

$$\mu_{xc} = \partial E_{xc} \rho / \partial \rho \tag{4.5}$$

Because the exchange-correlation potential (and energy) are not known, approximations have to be made.

4.1.2 Local Density Approximation (LDA)

A very successful and widely used approximation for the exchange-correlation energy is the Local-density approximation (LDA). Here the exchange correlation energy is assumed to depend only on the local electron density of each volume element $d\vec{r}$:

$$E_{xc}\ [\rho] \approx \int \rho(\vec{r})\ \varepsilon_{xc}\ [\rho(\vec{r})]\ d\vec{r} \tag{4.6}$$

$\varepsilon_{xc}\ [\rho]$ is the exchange-correlation energy per electron of a homogeneous electron gas and is expressed as an analytic function of the electron density, as is the exchange-correlation potential, μ_{xc}. There are various forms of the LDA in the literature; we refer to those of Hedin and Lunqvist (1971) and Wigner (non-spin-polarized forms), and Barth

and Hedin (1972) (spin-polarized form) since they are the ones implemented in the PLAPW programme version.

4.1.3 Generalized Gradient Approximation (GGA)

Despite its simplicity, LDA calculations often yield results in close agreement with experimental but there are cases where they fail or show large discrepancies. In such case, it is quite natural to take the next step beyond the homogenous electron gas (the basis of LDA) and include gradient corrections, so that $E_{xc}^{GGA}[\rho]$ is a function of spin densities $n(r)$ and their gradients $\nabla\rho(\vec{r})$:

$$E_{xc}^{GGA}[\rho] = \int \rho(\vec{r})\ \varepsilon_{xc}^{GGA}\ [\rho(\vec{r}),\ \nabla\rho(\vec{r})]\ d\vec{r} \qquad (4.7)$$

By imposing certain conditions which, for example, the exchange (correlation) hole density must satisfy, GGA has been developed to improve the quality of LDA results. Many modern codes using DFT now use more advanced approximations to improve accuracy for certain physical properties. There are several different parameterizations of the GGA. As stated above, the LDA uses the exchange-correlation energy for the uniform electron gas at every point in the system regardless of the homogeneity of the real charge density. For non-uniform charge densities the exchange-correlation energy can deviate significantly from the uniform result. This deviation can be expressed in terms of the gradient and higher spatial derivatives of the total charge density. The GGA (Langreth and Perdew, 1980; Langreth and Mehl, 1983; Perdew, 1986; Perdew and Wang, 1986) used the gradient of the charge density to correct for this deviation. For systems where the charge density is slowly varying, the GGA has proved to be an improvement over LDA.

As a comparison between the LDA and GGA, the LDA has succeeded in structural properties of solids with slowly varying charge density. The GGA enable to expand a limitation of LDA to have dependence on the gradient of charge density. However, the superiority of the GGA with respect to LDA is not clear to clusters and solid. At the same time GGA are computationally as simple to use as the LDA. On the other hand, the result of many applications as well as formal analysis suggests (Zupan *et al.*, 1997; Moll *et al*,. 1995; Hammer *et al.*, 1999) that GGA functional are still too limited to yield a full consistent improvement over the LDA and to describe binding energies within the desired accuracy in general.

4.1.4 Full-Potential Linearized Augmented Plane Wave Method (FP-LAPW):

In this work, we used the full potential linearized augmented plane wave (FPLAPW) method. This method has proven to be one of the most accurate methods for performing electronic structure calculations for crystals. It is based on the DFT for the treatment of exchange correlation (XC) (Hohenberg and Kohn, 1964; Kohn and Sham, 1965) and uses e.g. the local spin density approximation (LSDA). Recent improvements using the GGA are available (Perdew *et al*. 1992, 1996). In LAPW method, a basis set is introduced which is especially adapted to the problem. This adaptation is achieved by dividing the unit cell into two regions, namely (i) non-overlapping atomic spheres (centered at the atomic sites) and (ii) an interstitial region (region II) as shown in Fig. (4.1). For the construction of basis functions, the muffin tin approximation (MTA) is used according to which the potential is assumed to be spherically symmetric within the atomic spheres in which an atomic-like function is used and constant outside in which plane waves are used.

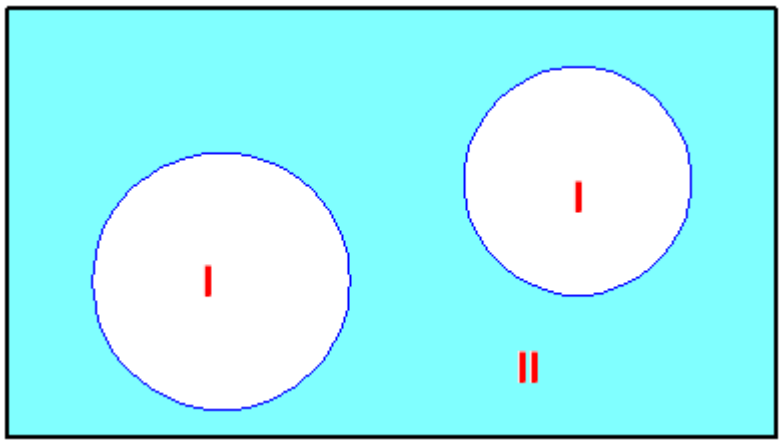

Figure (4.1): Partitioning of the unit cell into atomic spheres (I) and an interstitial region (II)

The basis functions for the two regions are:

(1) Inside atomic sphere **I**, of radius R_i, a linear combination of radial functions times spherical harmonics $Y_{lm}(r)$ is used

$$\phi_{kn} = \sum \left[A_{lm,k_n} u_l(\vec{r}, E_l) + B_{lm,k_n} \dot{u}_l(\vec{r}, E_l) \right] Y_{lm}(\hat{r}) \tag{4.8}$$

where $u_l(\vec{r}, E_l)$ is the regular solution of the radial Schrödinger equation for energy E_l and the spherical part of the potential inside sphere I; $\dot{u}_l(\vec{r}, E_l)$ is the energy derivative of u_l evaluated at the same energy E_l. A linear combination of these two functions constitutes the linearization of the radial function. The coefficients A_{lm} and B_{lm} are functions of k_n determined by requiring that this basis function matches each plane wave (PW) the corresponding basis function of the interstitial region. u_l and $\dot{u}_l$ are obtained by numerical integration of the radial Schrödinger equation on a radial mesh inside the sphere.

(2) In the interstitial region a plane wave expansion is used

$$\phi_{k_n} = \frac{1}{\sqrt{\omega}} e^{i\vec{k}_n \cdot \vec{r}} \tag{4.9}$$

where $\vec{k}_n = \vec{k} + \vec{K}_n$; $\vec{K}_n$ are the reciprocal lattice vectors and $\vec{k}$ is the wave vector inside the first Brillouin zone. Each plane wave is augmented by an atomic-like function in every atomic sphere.

The solutions to the Kohn-Sham equations are expanded in this combined basis set of LAPW's according to the linear variation method

$$\psi_k = \sum_n c_n \phi_{k_n} \tag{4.10}$$

and the coefficients c_n are determined by the Rayleigh-Ritz variational principle.

In order to improve upon the linearization and to make possible a consistent treatment of semicore and valence states in one energy window, adding additional basis functions called 'local orbitals (LO)' was suggested by Singh (1991). Local orbitals consists of a linear combination of 2 radial functions at 2 different energies and one energy derivative and is given as

$$\phi_{lm}^{LO} = \left[A_{lm}\, u_l(\vec{r}, E_{1,l}) + B_{lm}\, \dot{u}_l(\vec{r}, E_{1,l}) + C_{lm}\, u_l(\vec{r}, E_{1,l}) \right] Y_{lm}(\hat{r}) \tag{4.11}$$

In its general form, the FP-LAPW method expands both the potential and the charge density into the lattice harmonics inside each atomic sphere and as a Fourier series in the interstitial region. Thus we have

$$V(r) = \begin{cases} \sum_{LM} V_{LM}(\vec{r}) Y_{LM}(\hat{r}) & \text{inside sphere} \\ \sum_{K} V_K \exp\left(i\vec{k}.\vec{r}\right) & \text{outside sphere} \end{cases} \tag{4.12}$$

Thus their form is completely general so that such a scheme is termed full-potential calculation. In order to have a small number of LM values in the lattice harmonics expansion a local coordinate system for each atomic sphere is defined according to the point group symmetry of the corresponding atom. This specifies a rotation matrix that relates the local to the global coordinate system of the unit cell.

4.2 Linear Optics

Linear optics covers a variety of phenomena involving the interaction of light with matter. The constantly growing application of optics in technology, telecommunication, medicine, etc. demanding detailed theoretical modeling, has opened new fields for theoretical study. Understanding both the linear and nonlinear optical properties of solids

requires a detailed quantum mechanical picture of how electrons move in these materials. This is an important emerging area of theoretical condensed matter physics.

Despite the progress of modern theory, a profound understanding even of the well known optical processes is in many cases still far from satisfactory. A host of new and fundamental quantum interference effects in solids (so called "coherent control phenomena") recently predicted by J. E. Sipe's group (Deyirmenjian and Sipe, 1999) and confirmed experimentally, demonstrates that there is still a lot to be discovered in this field. Finally, the exciting and important theory of optical response in the fabricated semiconductor nanostructures, such as quantum wells, quantum dots, and super lattices, is still in its infancy. Besides important interest from the perspective of applied physics, these low-dimensional systems are a testing ground for fundamental concept in quantum mechanics itself.

4.2.1 Linear Optical Properties

The various ways in which light interacts with matter are of immense practical interest e.g. absorption, transmission, reflection, scattering or emission. These properties are energy dependent. The study of optical properties of solids has proven to be a powerful tool in our understanding of the electronic properties of materials. In particular structure, energy dependence of the properties mentioned above is in an intricate way related to the band structure. Information on energy eigenvalues and eigenfunction is needed to calculate the frequency / energy dependent optical properties.

When light of sufficient energy shines on a material, it induces transitions of electrons from occupied states (below E_F) to unoccupied states (above E_F). Clearly a quantitative study of these transitions must provide some understanding of the position of the initial and the final energy bands and symmetry of their associated wave functions.

The dielectric function $\varepsilon(\omega,q)$ of the electron gas, with its strong dependence on frequency and wave vector, has significant consequences for physical properties of solids. In one limit, $\varepsilon(\omega,0)$ describes the collective excitations of the Fermi sea such as the volume and surface plasmons. In another limit, $\varepsilon(0,q)$ describes the static screening of electron-electron, electron-lattice, and electron-impurity interactions in crystal. The dielectric function depends sensitively on the electronic band structure of a crystal, and studies of dielectric function by optical spectroscopy are very useful in determination of the overall band structure of the crystal. In the infrared, visible and ultraviolet spectral regions, the wave vector of the radiation is very small as compared with the shortest reciprocal lattice vector, and therefore it is taken to be zero. We are concerned with the real $\varepsilon_1(\omega)$ and imaginary $\varepsilon_2(\omega)$ parts of the dielectric function (Kittel, 1994; Dressel and Gruner, 2003)

$$\varepsilon(\omega)=\varepsilon_1(\omega)+i\varepsilon_2(\omega) \tag{4.13}$$

The $\varepsilon(\omega)$ has contributions from interband transitions.

4.2.1 Direct interband transitions

When the electromagnetic radiation falls on crystal, it interacts with the electrons of the crystal. We assume that the crystal is free of imperfections. The total Hamiltonian including the vector potential $\vec{A}$ of the electromagnetic field of the incident electromagnetic radiation is

$$H=\frac{1}{2m}\left(\vec{P}+e\vec{A}\right)^2+V(\vec{r}) \tag{4.14}$$

where $\vec{P}$ is the momentum and $V(\vec{r})$ is the periodic crystal potential.

The first order perturbation operator describing the interaction between the radiation and the electrons is the time-dependent linear term

$$H_o\left(\vec{r},t\right)=\frac{e}{m}\left(\vec{A}.\vec{p}\right) \tag{4.15}$$

For a plane wave, the vector potential can be written as

$$\vec{A}=\vec{A}_o\hat{e}\ \exp[i(\vec{k}.\vec{r}-\ \omega t)]+cc \tag{4.16}$$

where $\hat{e}$ the unit vector of polarization in the direction of the electric field and *cc* is the complex conjugate. Here only the first term is considered since it gives rise to absorption and the second term (emission) is neglected.

The transition probability (Chu and Sher, 2008) for an electron going from an occupied valence band state $E_v(\vec{k}_v)$ to an empty conduction band state $E_c(\vec{k}_c)$ is then

$$\mathrm{w}\left(\omega,t,\vec{k}_{\mathrm{v}},\vec{k}_{\mathrm{c}}\right)=\frac{e^2}{m^2\hbar^2}\left|\int_0^t dt'\int_v d\vec{r}\,\Psi_c\left(\vec{k}_c,\vec{r},t\right)\vec{A}.\vec{p}\ \Psi_v\left(\vec{k}_v,\vec{r},t\right)\right|^2 \tag{4.17}$$

Since Ψ_{v} and Ψ_{c} are Bloch type eigenfunctions belonging to E_v and E_c, respectively, we can write

$$\Psi_v\left(\vec{k}_v,\vec{r},t\right)=\exp\left[-i\hbar^{-1}E_v\left(\vec{k}_v\right)t\right]\exp\left(i\vec{k}_v.\vec{r}\right).\ u_v\left(\vec{k}_v,\vec{r}\right) \tag{4.18}$$

and correspondingly for Ψ_c. The term u_v and u_c contain periodicity of the lattice. From equations (4.16), (4.17), and (4.18) and using

$$\vec{E}=-\frac{\delta\vec{A}}{\delta t} \tag{4.19}$$

we obtain

$$\mathrm{w}\left(\omega,t,\vec{k}_{\mathrm{v}},\vec{k}_{\mathrm{c}}\right)=\frac{e^2E_o^2}{m^2\omega^2}\left|\int_0^t dt'\ exp\left[i\hbar^{-1}\left(E_c-E_v-\hbar\omega\right)t\right]\vec{e}.\vec{M}_{cv}\right|^2 \tag{4.20}$$

with the matrix element

$$\vec{e}.\overrightarrow{M}_{cv} = \int_V d\vec{r}\ exp\left[-i\left(\vec{k}_c - \vec{k}\right).\vec{r}\right] u_c^*\ \vec{e}.\vec{\nabla}\ \ \exp\left(i\vec{k}_v.\vec{r}\right)u_v \tag{4.21}$$

here the matrix element will vanish unless $\vec{k}_c - \vec{k} = \vec{k}_v - \vec{k}_n$ where $\vec{k}_n$ is the reciprocal lattice vector.

Since $\vec{k} = \frac{2\pi}{\lambda}$ is very small as compared to the linear dimensions of the BZ it can be neglected. This yields the first selection rule saying that only vertical transitions without a change of the wave vector are allowed. These are termed as direct transitions. After integrating over *t*′, equation (4.20) gives:

$$\mathrm{w}\left(\omega,t,\vec{k}_{\mathrm{v}},\vec{k}_{\mathrm{c}}\right) = \frac{e^2E_{\mathrm{o}}^2}{m^2\omega^2}\left|\frac{\exp\left[i\left(E_c - E_v - \hbar\omega\right)t/\hbar\right] - 1}{\left[i\left(E_c - E_v - \hbar\omega\right)/\hbar\right]}\vec{e}.\overrightarrow{M}_{cv}\right|^2 \tag{4.22}$$

This gives the transition probability per unit time (Chu and Sher, 2008)

$$\overrightarrow{W}_{cv} = \frac{\hbar e^2E_{\mathrm{o}}^2}{2\pi^2m^2\omega^2}\int d\vec{k}\left|\vec{e}.\overrightarrow{M}_{cv}\right|^2\delta\left(E_c - E_v - \hbar\omega\right) \tag{4.23}$$

The δ function contains the second selection rule. The transition probability is different from zero only if the energy difference between the final and initial states is equal to the photon energy.

We can now obtain the various optical constants as follows: The frequency dependent conductivity is given by

$$\sigma\left(\omega\right) = 2W_{cv}\hbar\omega/\vec{E}_{\mathrm{o}}^2 \tag{4.24}$$

The imaginary part of dielectric function is

$$\varepsilon_2\left(\omega\right) = \frac{4\hbar^2e^2}{\pi^2m^2\omega^2}\int d\vec{k}\left|\vec{e}.\overrightarrow{M}_{cv}\right|^2\delta\left(E_c - E_v - \hbar\omega\right) \tag{4.25}$$

$$\varepsilon_2\left(\omega\right) = \frac{4\hbar^2e^2}{\pi^2m^2\omega^2}\int_{\mathrm{c}} ds\frac{\left|\vec{e}.\overrightarrow{M}_{cv}\right|^2}{\left|\vec{\nabla}_k\left(E_c - E_v\right)\right|_{E_c - E_v\ =\ \hbar\omega}} \tag{4.26}$$

From $\varepsilon_2(\omega)$ the real part of the dielectric function can be calculated using the Kramers-Kronig relations (Dressel and Gruner, 2003),

$$\varepsilon_1(\omega) = 1 + \frac{2}{\pi} P \int_0^{\infty} \frac{\omega'}{(\omega')^2 - \omega^2} \varepsilon_2(\omega') d\omega' \tag{4.27}$$

$$\varepsilon_2(\omega) = -\frac{2\omega}{\pi} P \int_0^{\infty} \frac{1}{(\omega')^2 - \omega^2} \left[\varepsilon_1(\omega') - 1\right] d\omega' \tag{4.28}$$

where *P* denotes the principal part of the integral.

The results of optical constant obtained by using Equations (4.27) and (4.28) in case of Beryllium chalcogenides, Zinc chalcogenides, Aluminium pnictides, Gallium pnictides and Indium pnictides are given in details in Chapter 5.

CHAPTER – 5

Calculation of Electronic and Optical Properties by using FP-LAPW method

The full linearized augmented plane wave (FP-LAPW) method within the framework of density functional theory (DFT) (Hohenberg and Kohn, 1964), as implemented in the WIEN2k code (Blaha *et al.*, 2008), is used for computation of electronic structure, the density of state (DOS) and optical properties of Beryllium chalcogenides (BeS, BeSe and BeTe), Zinc chalcogenides (ZnS, ZnSe and ZnTe), Aluminium pnictides (AlP, AlAs and AlSb), Gallium pnictides (GaP, GaAs and GaSb) and Indium pnictides (InP, InAs and InSb). The fundamental space lattice is face-centered cubic in all binary compounds under studies. The first Brillioun zone of fcc crystal structure in k- space showing the high symmetry points and structure showing Zinc Blende (Sphalerite) are shown in Fig. (5.1). Equations (4.27) and (4.28) are used to find the real and imaginary part of dielectric function for all compound semiconductors under studies. The exchange-correlation potential was calculated with generalized gradient approximation (GGA) based on Perdew *et al.* (1996). Kohn-Sham wave functions (Kohn and Sham, 1965) were expanded in terms of spherical harmonic functions inside the non-overlapping muffin-tin spheres surrounding the atomic sites and in Fourier series in the interstitial region. We have used $R_{MT} \times K_{max} = 7$ to determine the matrix size, where K_{max} is the plane-wave cut off and R_{MT} is the muffin tin sphere radii. In the atomic region, the basis set consists of spherical harmonics with angular quantum number $l = 10$ and a non spherical contribution with $l = 4$. The self-consistent iterations are considered to be converged when the total energy of the system are stable within 10^{-5} Ry. A mesh point of 5000 *k*-points were used to obtain 111 special *k*-points in the irreducible wedge of the Brillouin zone for the compound semiconductors under study. The muffin-tin radius was varied to ensure total energy convergence.

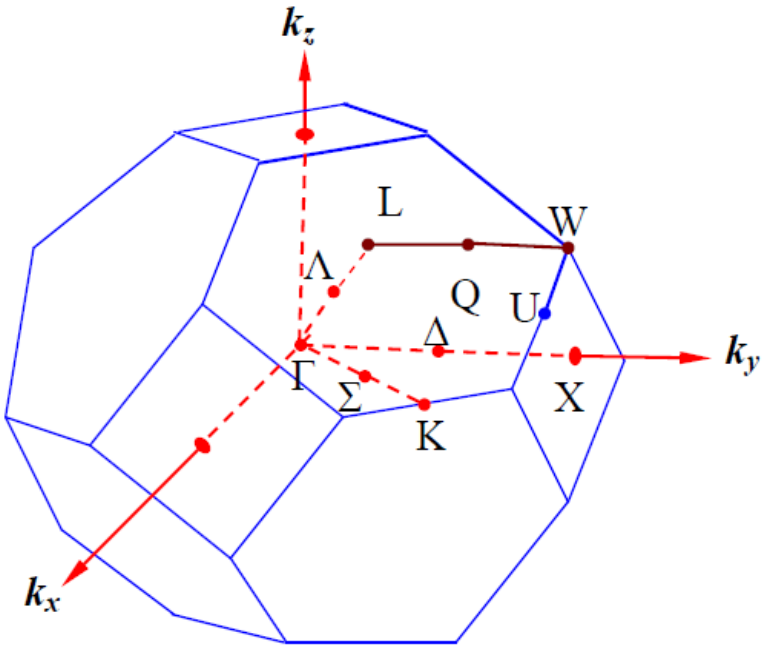

(a)

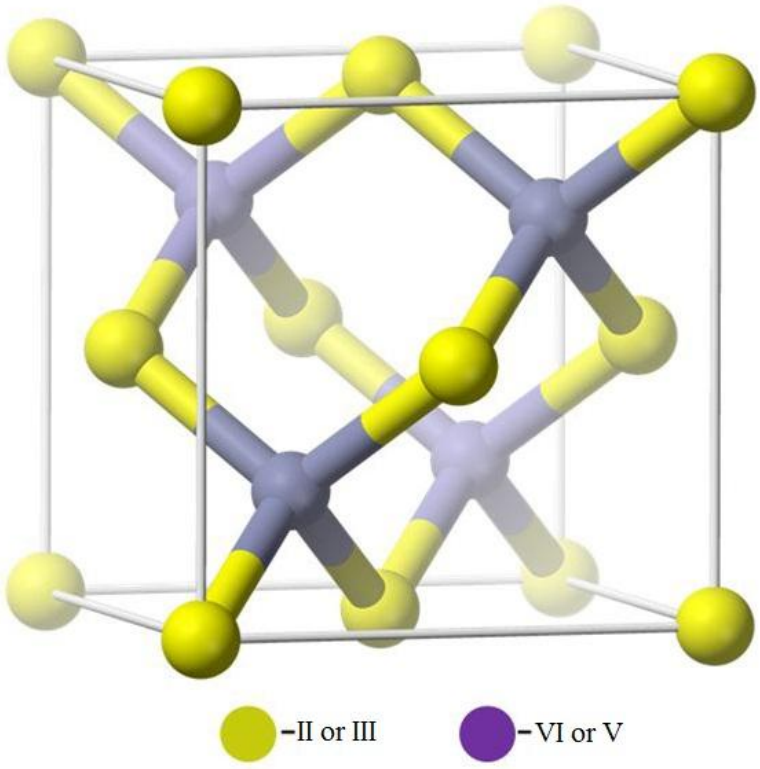

(b)

Figure 5.1: (a) First Brillouin zone of the face-centered cubic lattice showing symmetry points (Christensen and Gorczyca, 1994). (b) Structure showing Zinc Blende (Sphalerite)

5.1 Results and Discussion on Beryllium chalcogenides:

There is an intense investigation of the electronic and physical properties of BeS, BeSe and BeTe compounds. The lattice parameters of beryllium chalcogenides were initially measured by Zachariasen (1926). Yim *et al*., (1972) have confirmed the crystalline structure to be zinc-blende. Stukel (1970) studied the energy bands of beryllium chalcogenides using the first principle self-consistent orthogonalized-plane wave (OPW). The structural and electronic properties have also been theoretically investigated using the tight-binding linear muffin-tin orbital method within the framework of density functional theory in its local density approximation (LDA) by Kalpana *et al*. (1998). Fleszar and Hanke (2000) have calculated electronic excitations in BeX using the many-body Green's functions technique (GW) and have given a detailed discussion of LDA versus GW. A few non-relativistic local density approximation (LDA) calculations of the structural, electronic and optical properties for beryllium mono-chalcogenides have been performed by Okoye (2004). Hassan *et al.,* (2006) have present detail calculation of the band structure using more advanced Engel Vosko's GGA (EV-GGA) formalism. Imad Khan *et al.* (2013) have calculated electronic and optical properties of mixed Be-chalcogenides with the FP-LAPW method using a recently developed modified Beck and Johnson potential.

The electronic configurations of elements in beryllium chalcogenides are Be: [He] $2s^2$; S: [Ne] $3s^2$ $3p^4$; Se: [Ar] $3d^{10}$ $4s^2$ $4p^4$ and Te: [Kr] $4d^{10}$ $5s^2$ $5p^4$. We have chosen sphere radii of 1.8 Å for Be, 2.1 Å, 2.4 Å and 2.8 Å respectively for S, Se and Te. We used lattice parameter 4.8630 Å for BeS, 5.1520 Å for BeSe and 5.6270 Å for BeTe (Martienssen and Warlimont, 2005). At ambient temperature and pressure, the semiconducting beryllium chalcogenides crystallized in the zinc-blende structure. The

space group is F-43 m. The Be atom is located at the origin and the X atom is located at (1/4, 1/4, 1/4).

5.1.1 Density of States and Band Structure

The calculated total density of states, the partial density of states and band structures for Beryllium chalcogenides are shown in figures 5.2(a), 5.2(b) and 5.2(c). The valence band maximum (VBM) occurs at the **Γ** point and conduction band minimum (CBM) at the **X** point resulting in an indirect gap in agreement with experiment and previous theoretical work (Yim *et al.,* 1972; Martienssen and Warlimont, 2005; Stukel, 1970; Gonz´alez-Di´az *et al.,* 1997; Okoye, 2004; Fleszar and Hanke, 2000; Hassan and Akbarzadeh, 2006; Imad Khan *et al.,* 2013; Baaziz *et al.,* 2006; Al-Douri *et al.,* 2012; Hacini *et al.,* 2012; Ameri *et al.,* 2008; Kalpana *et al.,* 1998; Khenata *et al.,* 2006). The lowest-lying band shown in the graph arises mainly from the chalcogen valence *s* states and the upper valence bands arises from the chalcogen valence *p* states with the top occurring at the **Γ** point. The conduction band arises mainly from the beryllium *s* states and chalcogen *s, p* and *d* states with the minimum energy occurring at **X**-points.

The band gap of semiconductor BeX in the tetragonal phase as calculated by using the FP-LAPW method and using GGA approximation was found to be 3.12 eV, 2.64 eV and 1.98 eV for BeS, BeSe & BeTe respectively. The important features of the band structure for each compound are given in Table 5.1 which was reported by Malsawmtluanga *et al.* (2014) It is clearly seen that the band gap obtained by GGA are lower than the corresponding experimental values and results obtained from OPW and EV-GGA with the same exchange correlation approximation. This underestimation of the band gap is mainly due to the fact that the simple forms of GGA are not sufficiently

flexible to accurately reproduce both exchange correlation energy and its charge derivative.

5.1.2 Optical properties

The determination of the optical properties of a compound in the spectral range above its band gap plays an important role in the understanding of the nature of that material and also gives a clear picture of its applications in optoelectronic devices. The detailed variation of real, $\varepsilon_1(\omega)$ and imaginary $\varepsilon_2(\omega)$ parts of the dielectric function for BeX with photon energy are shown in Figure 5.2(d). The $\varepsilon_1(\omega)$ increases with an increase in photon energy in the energy range 0-5.8 eV, 0-5.18 eV, 0-4.1 eV respectively for BeS, BeSe and BeTe, and rises to a maximum value of 16.2 at 5.8 eV, 16.7 at 5.18 eV and 18.1 at 4.1 eV. The $\varepsilon_1(\omega)$ then decreases with increase in photon energy with a minimum value of -4.28 at 8.34 eV, -4.32 at 7.5 eV, -6.0 at 6.16eV for BeS, BeSe and BeTe. For the value of $\varepsilon_1(\omega) < 0$, the curve shows metallic reflectance characteristics. We have found that the three compounds have the same structure that is attributed to the fact that the band structures of these compounds are similar with minor differences causing insignificant changes in the structures of $\varepsilon_2(\omega)$. The decrease in the energy band gap moving from S to Se to Te causes to shift the whole structure $\varepsilon_2(\omega)$ to lower energies by around 1.0 eV, resulting in the edge of optical absorption (fundamental absorption edge) for $\varepsilon_2(\omega)$, which is located at 5.6 eV, 4.45 eV and 3.6 eV for BeS, BeSe and BeTe.

The peak of the imaginary part of the dielectric function is related to the electron excitation. It is clear from the figure that $\varepsilon_2(\omega)$ shows single peak at 6.9 eV, 6.2 eV, 5.1 eV for BeS, BeSe and BeTe respectively which was reported by Malsawmtluanga *et al.* (2014). The peaks are primarily due to the interband transition between the maximum of valence band at Γ - edge and the bottom most conduction band at X - edge. Moving from S to Se, the insignificant hump on the right shoulder of the main peak of BeS at 7.4 eV

clearly appears in the 7.0 eV at the $\varepsilon_2(\omega)$ structures of BeSe; this hump disappears again when we move from Se to Te. We compare our calculated $\varepsilon_2(\omega)$ with the previous theoretical calculations (Okoye, 2004; Al-Douri *et al*., 2012; Khenata *et al*., 2006) and agreement is found.

Table 5.1: Our calculated energy band gap values for BeS, BeSe and BeTe and the experimental and theoretical band gap (all values are in eV).

Comp-ounds	Expt. Band gap	Theoretical Band gap (E_g)				Present work GGA
		OPW	LDA	EVGGA	GGA	
BeS	>5.5[a]	4.17[b]	3.78[c], 2.828[g]	4.23[d], 4.26[f], 4.241[g], 4.247[h]	3.12[d], 4.20[e], 3.14[f], 3.141[g], 3.148[h], 2.911[i]	3.12
BeSe	4-4.5[a]	3.61[b]	3.12[c], 2.397[g]	3.61[d], 3.64[f], 3.655[g], 3.634[h]	2.66[d], 3.55[e], 2.67[f], 2.682[g], 2.672[h],	2.64
BeTe	~ 2.7[a]	2.94[b]	2.17[c], 1.796[g]	2.79[d], 2.81[f], 2.921[g]	1.98[d], 2.60[e], 2.03[f], 2.070[g],1.879[i]	1.98

[a]Yim *et al*. (1972), [b]Stukel (1970), [c]Kalpana *et al.* (1998), [d]Hassan and Akbarzadeh (2006), [e]Imad Khan *et al*. (2013), [f]Baaziz *et al*. (2006), [g]Al-Douri *et al*. (2012), [h]Hacini *et al*. (2012), [i]Ameri *et al*. (2008)

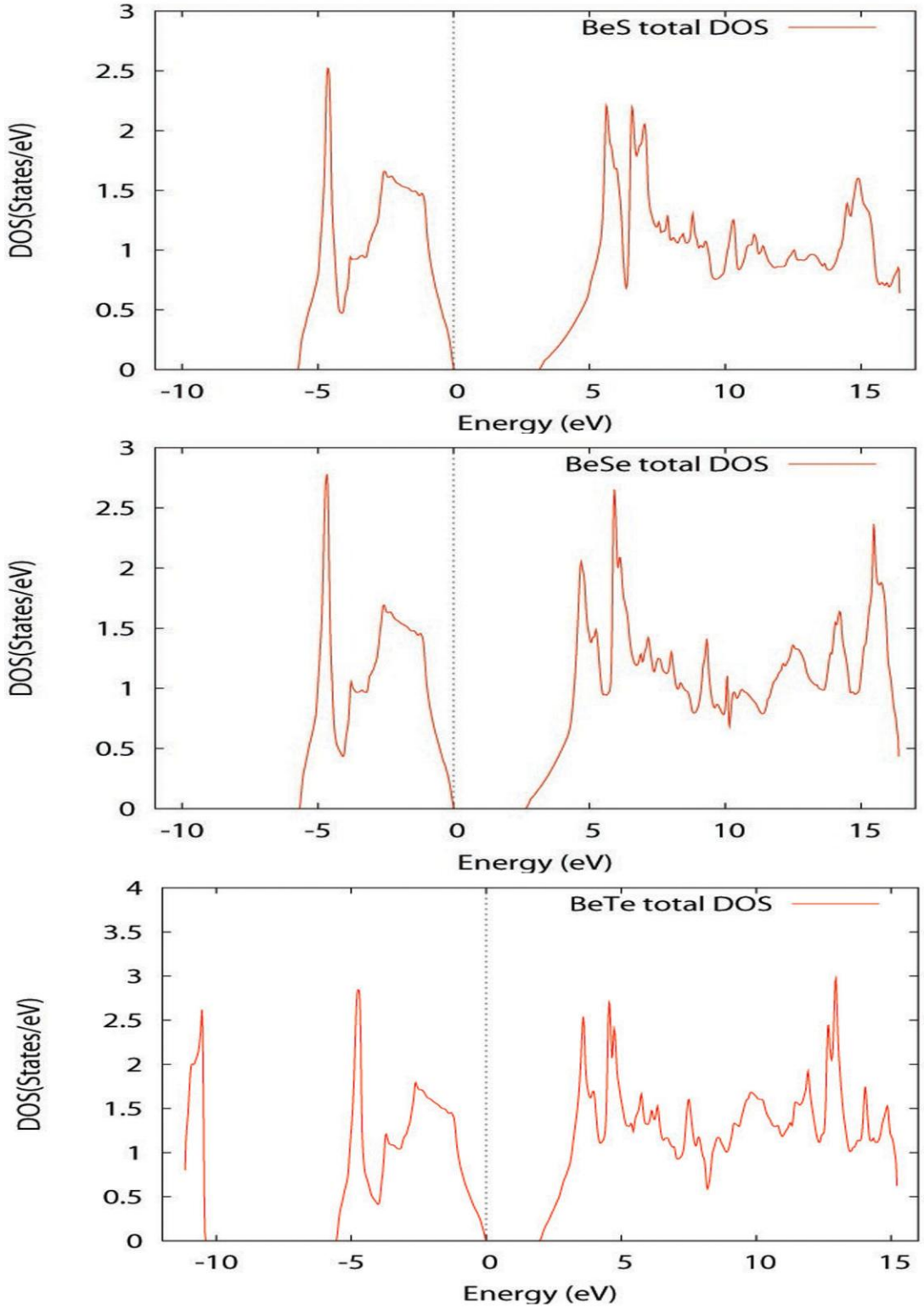

Figure 5.2(a). Total Density of States for BeS, BeSe and BeTe. The vertical dotted lines at E = 0 eV indicates the Fermi energy level.

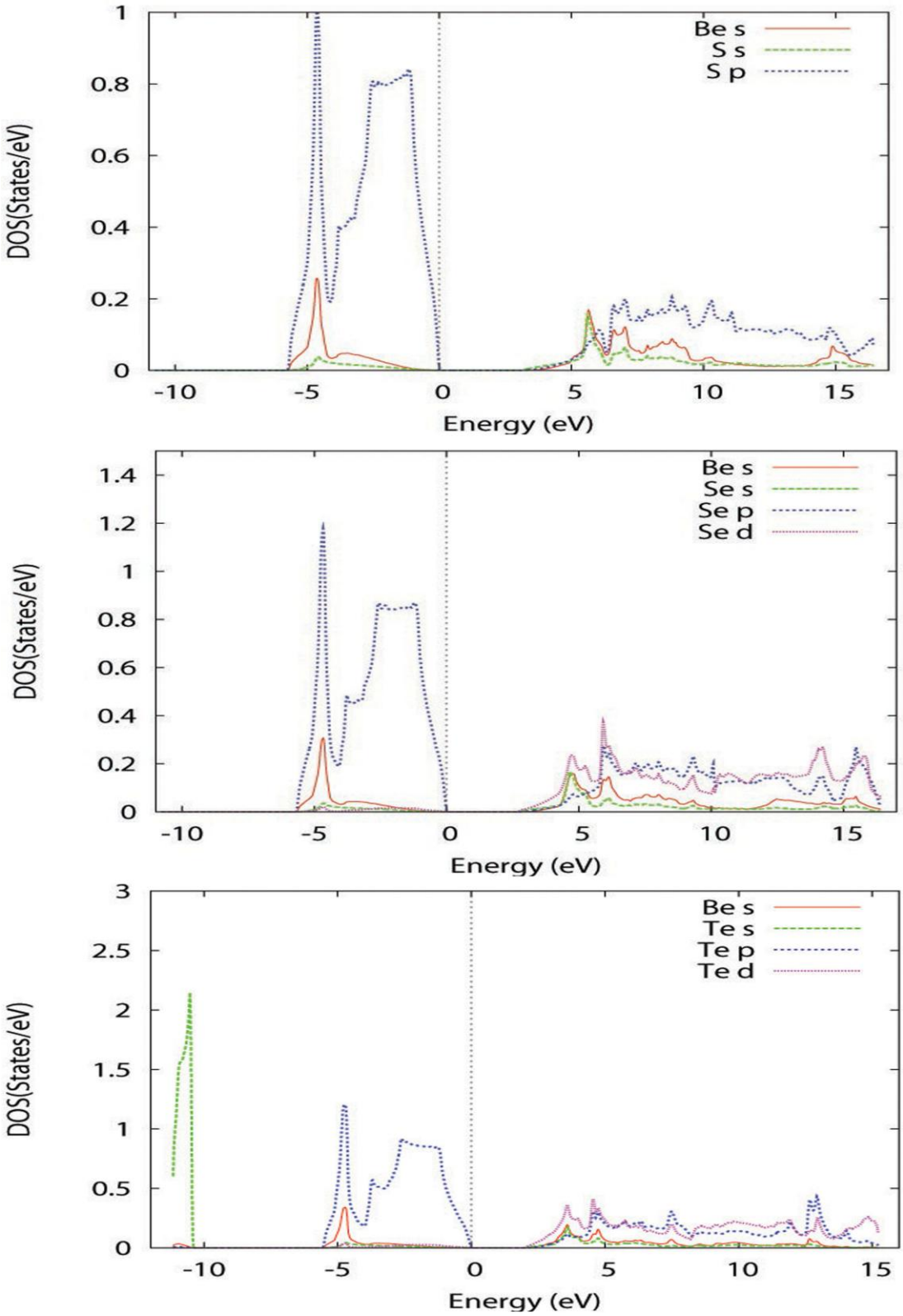

Figure 5.2(b). Partial Density of States for BeS, BeSe and BeTe. The vertical dotted lines at E = 0 eV indicates the Fermi energy level.

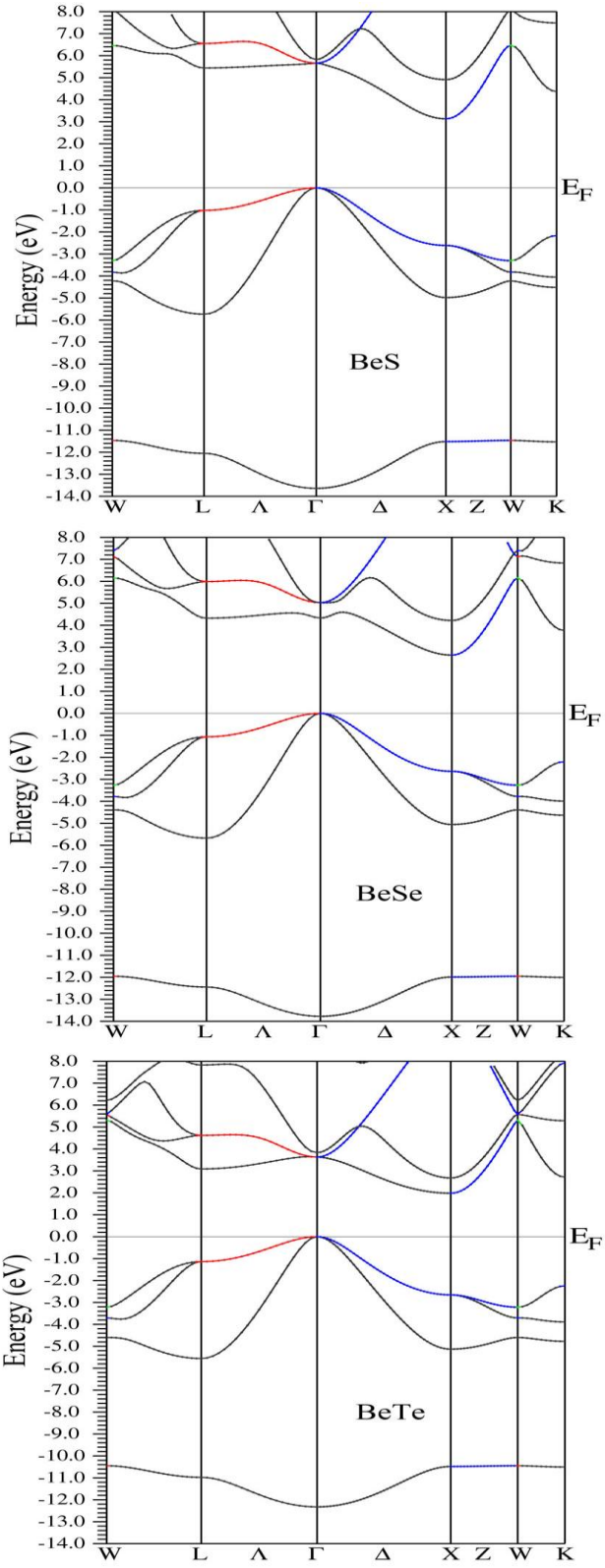

Figure 5.2(c). Band structure for BeS, BeSe and BeTe along the high symmetry directions. E_F = 0 eV corresponds to the Fermi level.

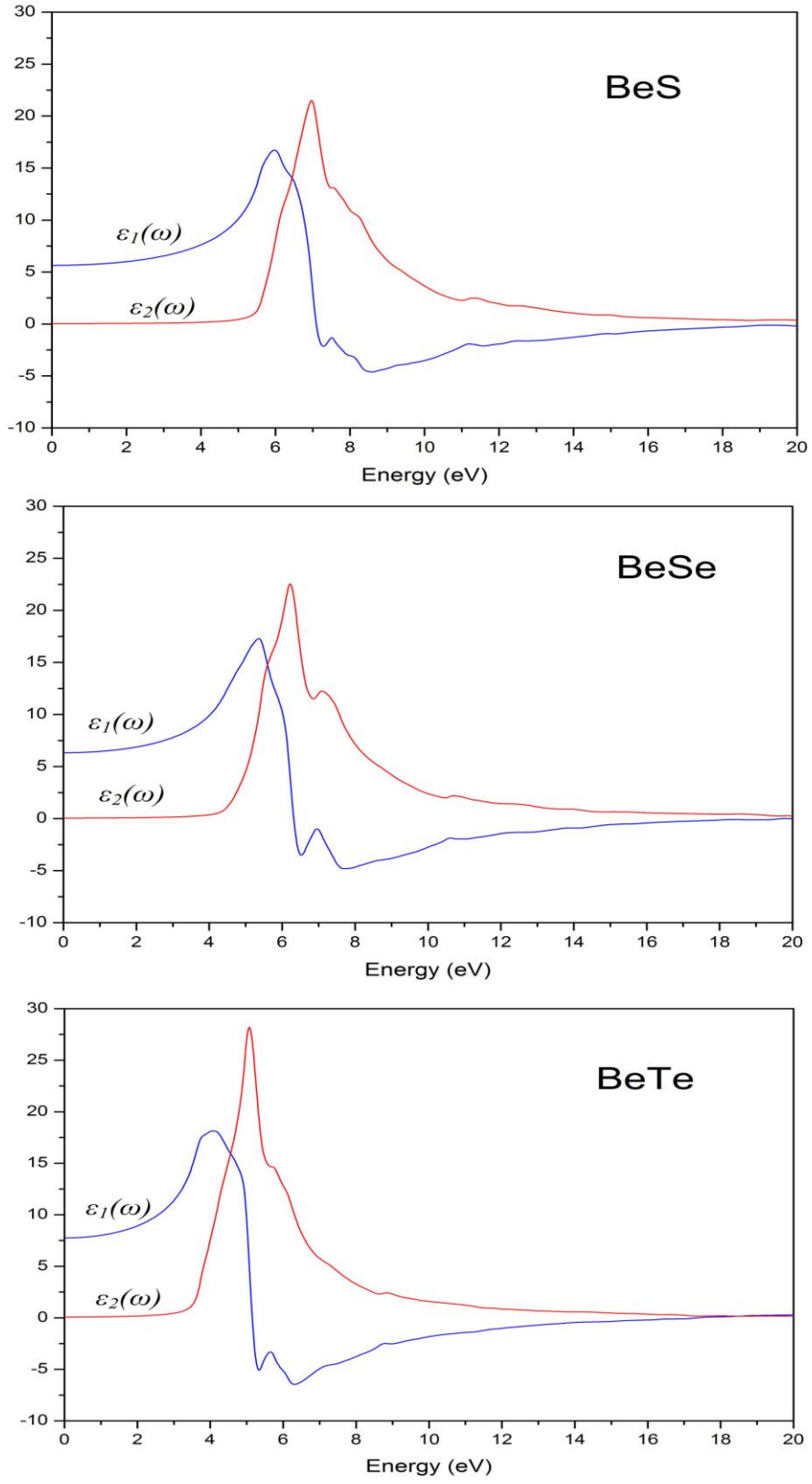

Figure 5.2(d). Real and Imaginary part of dielectric function for BeS, BeSe and BeTe.

5.2. Results and Discussion on Zinc chalcogenides.

Zinc chalcogenides have attracted much attention because they possess direct energy band gaps and are efficient light emitters even at room temperature. The electronic and optical properties have been extensively studies for many technological applications (Sapra *et al*., 2002; Walter *et al*., 1970; Tsuchiya *et al*., 2003; Huang and Ching, 1993; Erbarut, 2003; Ghahramani *et al*., 1991; Bang *et al*., 2001; Freeouf, 1973).

The electronic configurations of elements in Zinc chalcogenides are Zn: [Ar] $3d^{10}4s^2$; S: [Ne] $3s^2$ $3p^4$; Se: [Ar] $3d^{10}$ $4s^2$ $4p^4$ and Te: [Kr] $4d^{10}$ $5s^2$ $5p^4$. We have chosen sphere radii of 2.1 Å for Zn, 1.8 Å, 2.2 Å and 2.3 Å respectively for S, Se and Te. For our calculation, we used lattice parameters a = 5.4053 Å, 5.667 Å, and 6.0882 Å for ZnS, ZnSe, and ZnTe respectively (Martienssen and Warlimont, 2005). The semiconducting Zinc chalcogenides crystallized in the zinc-blende structure. The space group is F-43 m. The Zn atom is located at the origin and the X atom is located at (1/4, 1/4, 1/4).

5.2.1. Density of States and Band Structure

The calculated total density of states, the partial density of states and band structures for zinc chalcogenides are shown in figures 5.3(a),(b),(c) and (d). The valence band maximum (VBM) and conduction band minimum (CBM) are occurs at the Γ-point resulting in a direct gap of 2.1 eV, 1.5 eV and 1.3 eV for ZnS, ZnSe and ZnTe respectively in agreement with experiment and previous theoretical work (Martienssen and Warlimont, 2005; Huang and Ching, 1993; Reshak and Auluck, 2007; Corso *et al.*, 1996). It is clearly seen that the band gap are on the whole underestimated in comparison with experiments results as shown in Table 5.2 which was reported by Malsawmtluanga *et al.* (2012). This underestimation of the band gaps is mainly due to the fact that the simple form GGA do not take into account the quasiparticle self energy correctly

(Rashkeev and Lambrecht, 2001) which make it not sufficiently flexible to accurately reproduce both exchange correlation energy and its charge derivative.

From the PDOS, we are able to identify the angular momentum character of the various structures. The lowest energy group has mainly chalcogen *s* states. The second group between -7.0 to -6.0 eV and the third group from -5.0 eV up to the Fermi energy (E_F) is composed of Zn-*d* and chalcogen *p* states. The last group from 1 eV and above has contributions from Zn-*sd* and chalcogen *p* states. From the trends in the band structures (as we move from S to Se to Te), we can see that the first group in ZnSe is shifted towards lower energies by around 0.5 eV in comparison with ZnS, while in ZnTe it is shifted towards higher energies by around 1 eV. The bandwidth of the second group is reduced. This group is shifted towards lower energies by around 0.5 eV causing to increase the gap between the second and third groups. The bandwidth of the conduction band increases slightly by around 0.5 eV on going from S to Se to Te. From the PDOS, we note a strong hybridization between Zn-*d* and chalcogen *p* states. Following Yamasaki *et al*. (1987), we can define degree of hybridization by the ratio of Zn-*d* states and X-*p* states within the muffin tin sphere. Based on this, we can say that the hybridization between Zn-*d* and chalcogen-*p* states becomes stronger when moving from S to Se to Te.

5.2.2 Optical properties

The detailed variation of real, $\varepsilon_1(\omega)$ and imaginary $\varepsilon_2(\omega)$ parts of the dielectric function for ZnX with photon energy are shown in Figure 5.3 (e). The $\varepsilon_1(\omega)$ spectra appears at the same energy as a peak in the corresponding $\varepsilon_2(\omega)$ spectra. Since ZnX compounds have cubic symmetry, we need to calculate only the imaginary part of the frequency dependent dielectric function to completely characterize the linear optical properties. Our analysis of the $\varepsilon_2(\omega)$ curves show that the first critical points of the

dielectric function occurs at 1.9 eV, 0.9 eV and 0.7 eV for ZnS, ZnSe and ZnTe respectively. These critical points are followed by small structure located at 4.5 eV in ZnS, 3.7 eV in ZnSe and 2.9 eV in ZnTe related to direct transition (L - L). The main peaks in the spectra are situated at 6.0 eV, 5.5 eV and 4.5 eV respectively for ZnS, ZnSe and ZnTe. The main peak is followed by pronounced peak situated at 7.4 eV, 7.0 eV and 5.9 eV. These peaks are primarily due to direct transition between valence band and conduction band above the Fermi energy at L-edge. The experimental measurement localized the main peaks at 6.8 eV, 6.2 eV, and 5.3 eV for ZnS, ZnSe and ZnTe (Freeouff, 1973; Kim *et al.,* 1993). All the structures in $\mathcal{E}_2(\omega)$ are shifted towards the lower energies with increase in the peak height when S is replaced by Se and Se by Te, in agreement with the experimental data. In comparison with the experimental data, there is slight energy shift in the main peaks. This energy shifts mainly arise from the GGA, which give a smaller band gap in comparison with experiment which was reported by Malsawmtluanga *et al.* (2012).

Table 5.2: Our calculated energy band gap values for ZnS, ZnSe and ZnTe and the experimental and theoretical band gap (all values are in eV).

Comp-ounds	Expt. Band gap	Theoretical Band gap (E_g)			Present Work GGA
		LDA	GGA	EVGGA	
ZnS	3.87[a], 3.80[b]	2.34[b], 2.1[c], 2.4[d]	2.3[c], 1.96[e]	2.80[e]	2.1
ZnSe	2.67[a], 2.82[b]	1.65[b], 1.3[c], 1.6[d]	1.7[c], 1.11[e]	1.84[e]	1.5
ZnTe	2.25[a], 2.39[b]	2.24[b], 1.1[c], 1.6[d]	1.4[c], 1.01[e]	1.57[e]	1.3

[a]Strehlow and Cook (1973), [b]Huang and Ching (1993), [c]Reshak and Auluck (2007), [d]Corso *et al.* (1996), [e]Baaziz *et al.* (2006)

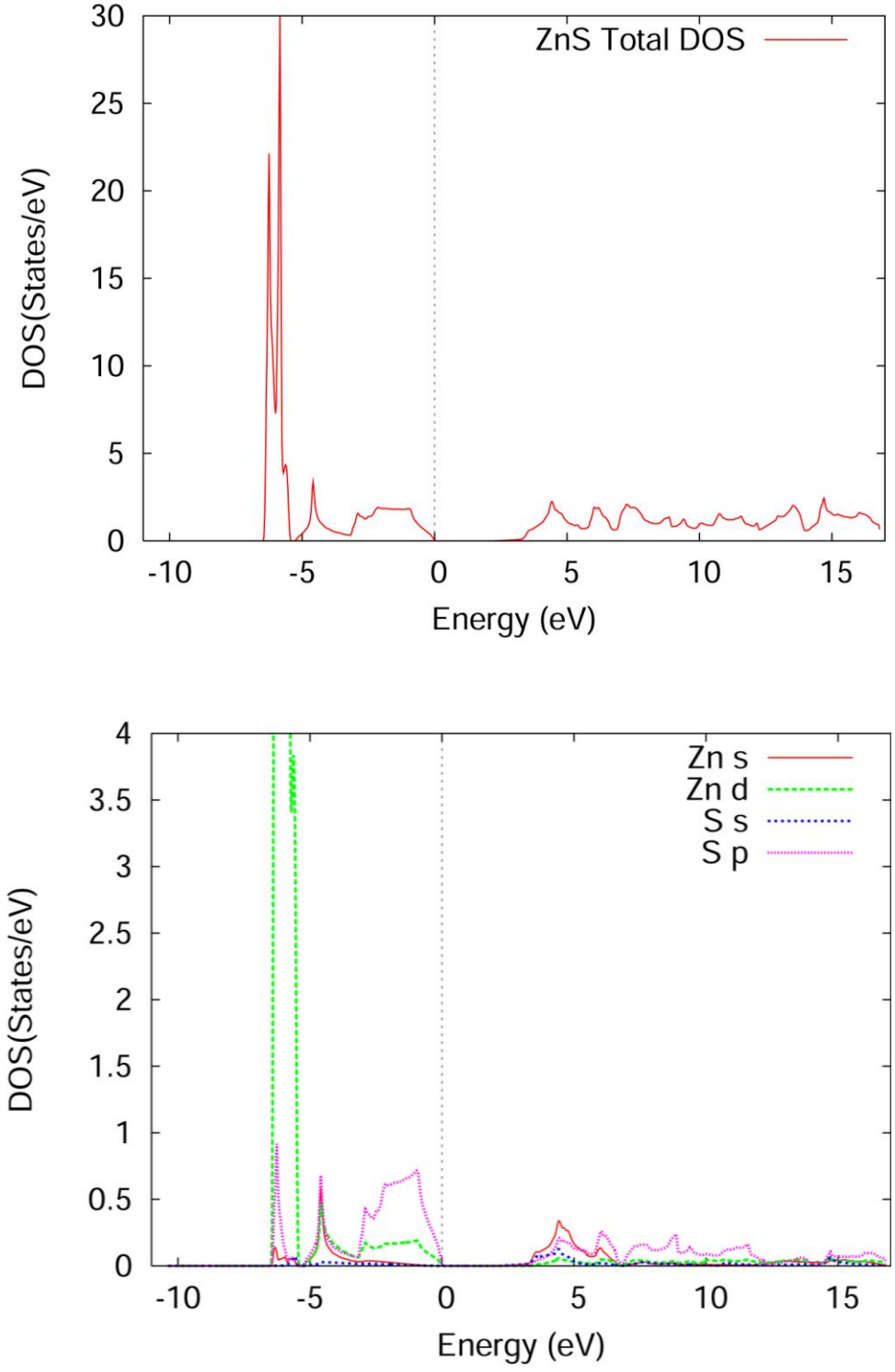

Figure 5.3(a). Total DOS and Partial DOS for ZnS. The vertical dotted lines at E = 0 eV indicates the Fermi energy level.

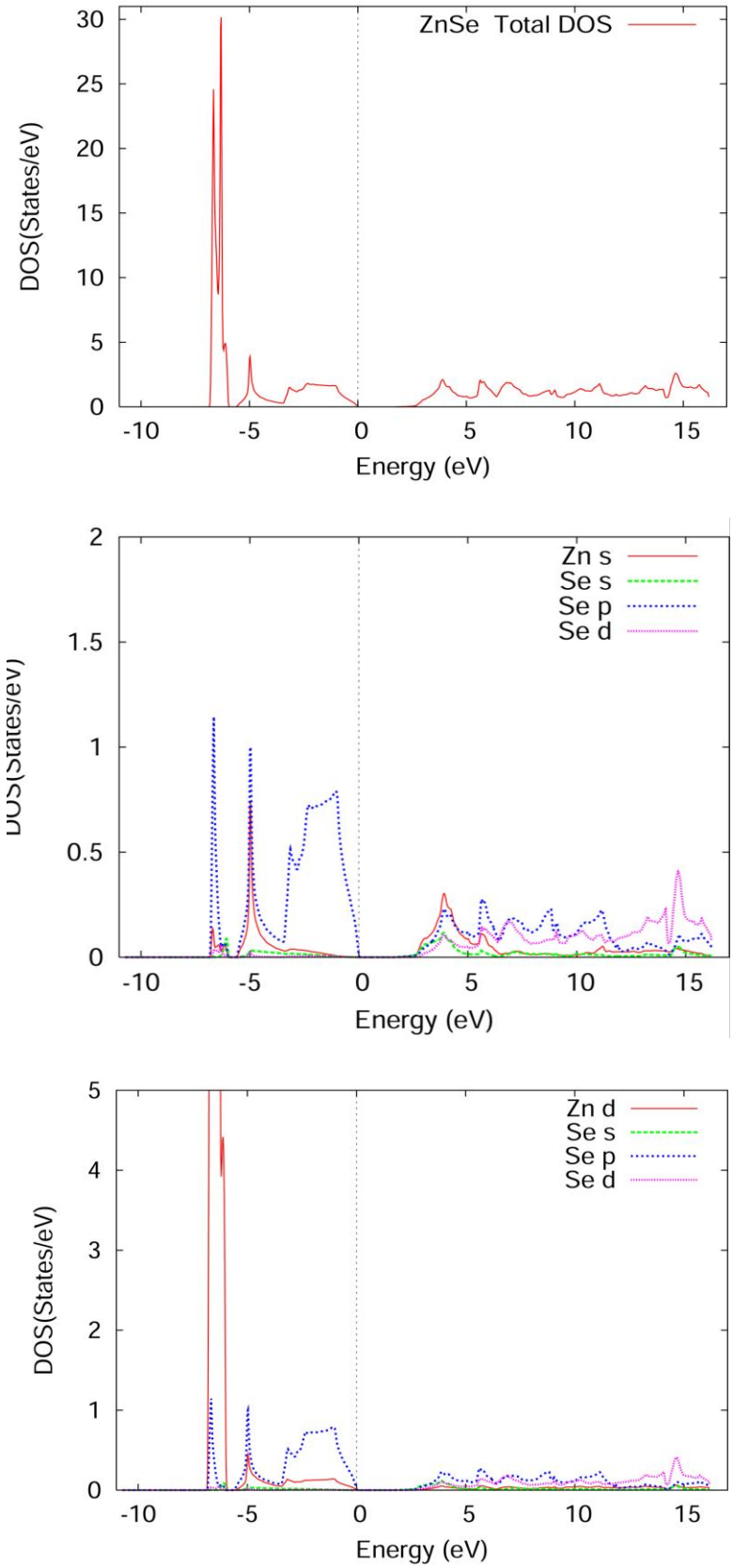

Figure 5.3(b). Total DOS and Partial DOS for ZnSe. The vertical dotted lines at E = 0 eV indicates the Fermi energy level.

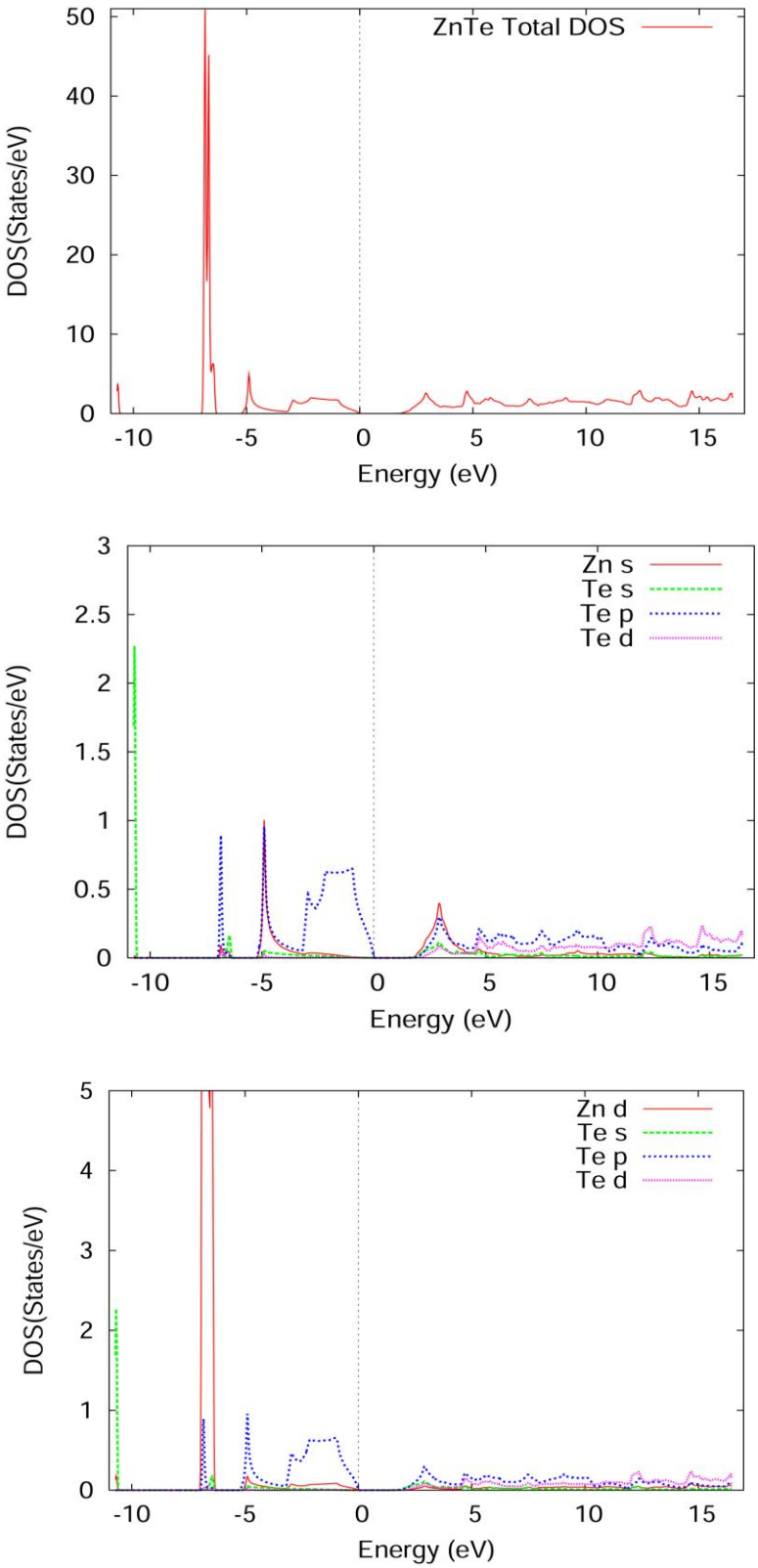

Figure 5.3(c). Total DOS and Partial DOS for ZnTe. The vertical dotted lines at E = 0 eV indicates the Fermi energy level.

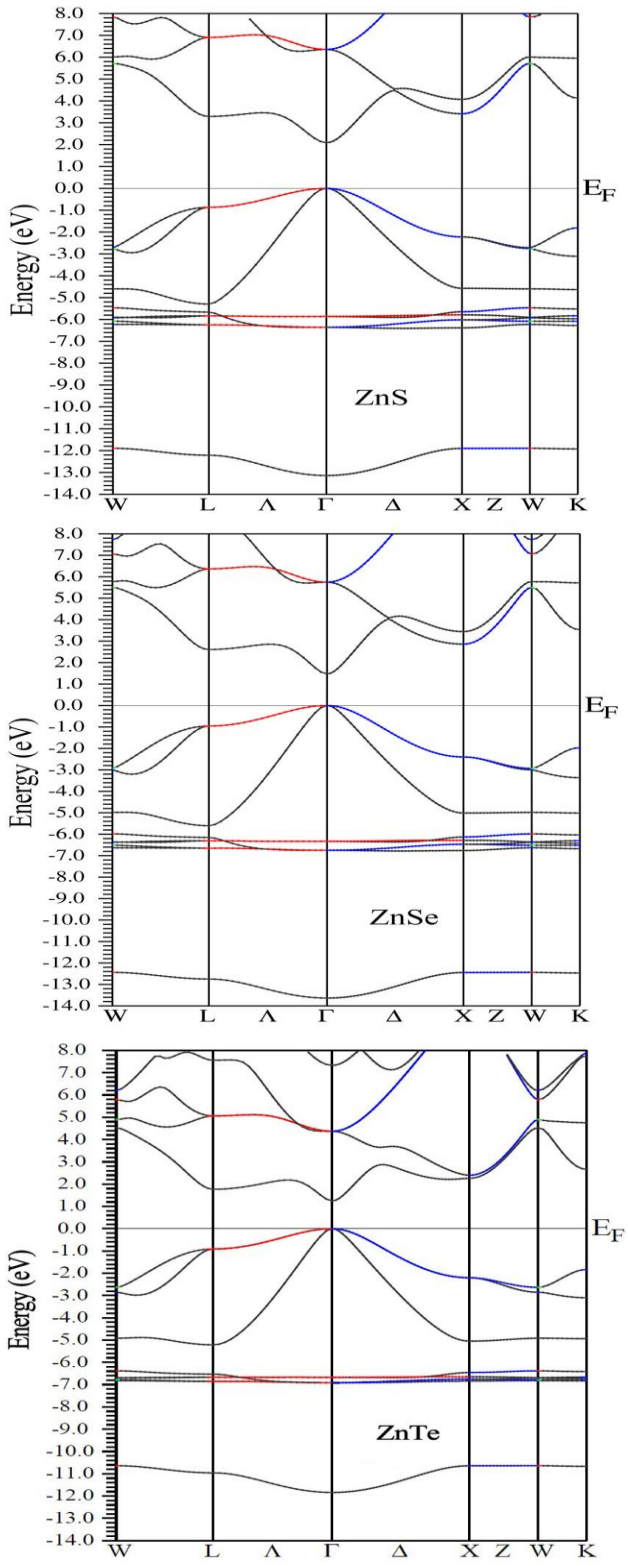

Figure 5.3(d). Band structure for ZnS, ZnSe and ZnTe along the high symmetry directions. E_F = 0 eV corresponds to the Fermi level.

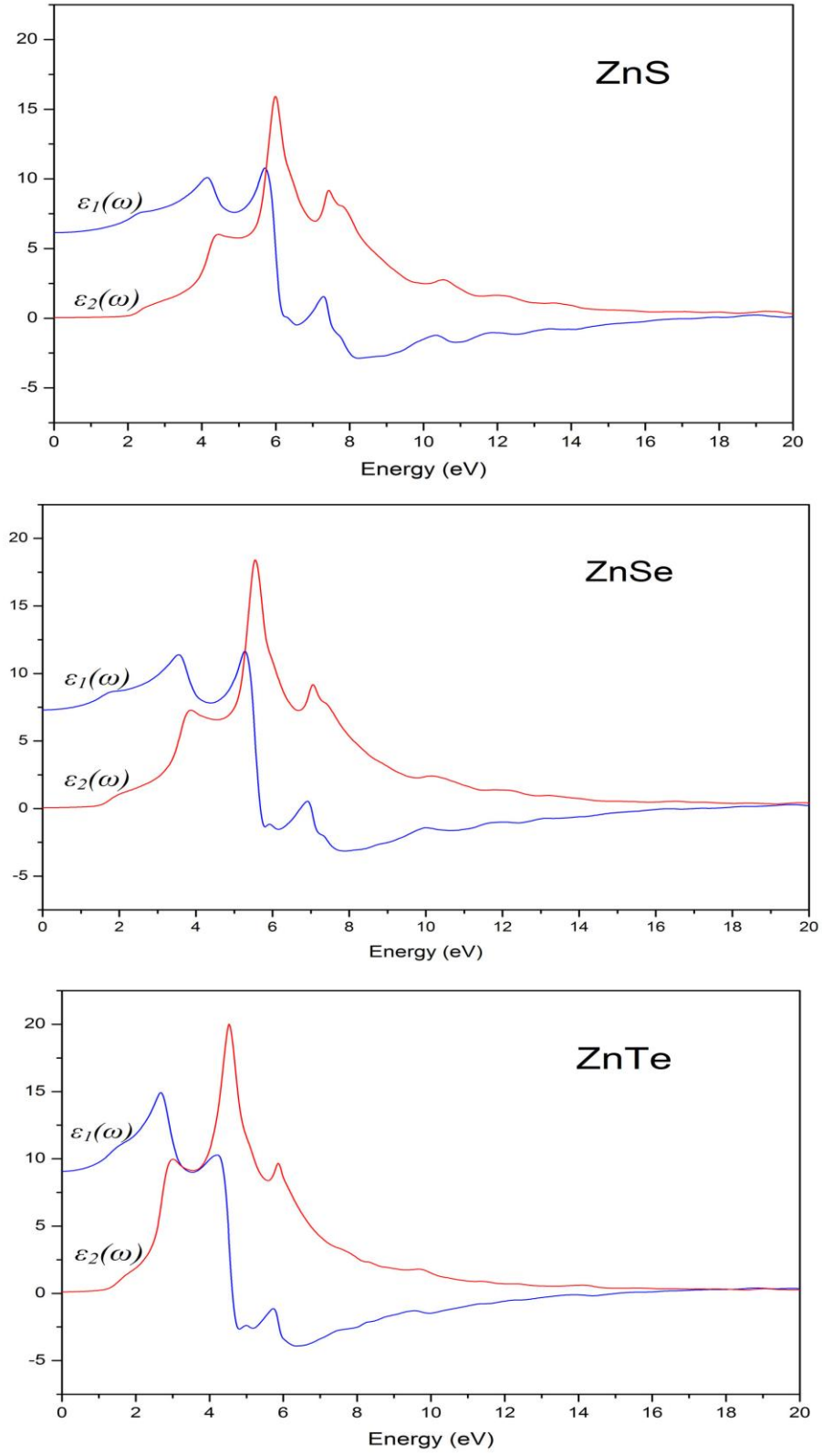

Figure 5.3(e). Real and Imaginary part of dielectric function for ZnS, ZnSe and ZnTe.

5.3 Results and Discussion on Aluminium pnictides:

The electronic configurations of elements in Gallium pnictides are Al: [Ne] $3s^2$ $3p^1$; P: [Ne] $3s^2$ $3p^3$; As: [Ar] $3d^{10}$ $4s^2$ $4p^3$ and Sb: [Kr] $4d^{10}$ $5s^2$ $5p^3$. We have chosen sphere radii of 2.1 Å for Al, 2.3 Å for P, 2.5 Å for As and 2.8 Å for Sb. For our calculation, we used lattice parameters a = 5.4635 Å, 5.66139 Å, and 6.09593 Å for AlP, AlAs and AlSb respectively (Martienssen and Warlimont, 2005). The compound AlX crystallized in the zinc-blende structure. The space group is F-43 m. The Al atom is located at the origin and the X atoms are located at (1/4, 1/4, 1/4).

5.3.1 Density of States and Band Structure

The calculated total density of states, the partial density of states and band structures for Aluminum pnictides are shown in figures 5.4(a),(b),(c) and (d). The band structure and DOS can be divided into three main groups. The lowest energy group has mainly pnictide *s* states. The second group is mainly Al-*s* and pnictide *p* states. The third group is mainly from *p* state of Al and pnictide. From the partial DOS, we note a strong hybridization between Al-*s* and pnictide *p* states below and above E_F. The valence band maximum (VBM) is located around Γ and the conduction band minimum (CBM) is located around X resulting in an indirect energy bad gap of 1.58 eV, 1.46 eV, 1.2 eV for AlP, AlAs and AlSb respectively. A comparison of the experimental and theoretical band gaps are given in Table 5.3 which was reported by Malsawmtluanga *et al.* (2014). It is clearly seen that the band gap obtained by GGA are lower than the corresponding experimental values and results obtained from Tight Binding method (Korti-Baghdadli *et al.*, 2013). Our results are in a good agreement with the other theoretical work with the same exchange correlation approximation of LDA (Huang and Ching, 1993; Reshak and

Auluck, 2007) and GGA (Bentouaf *et al.,* 2013; Ahmed *et al.,* 2009). We note that the energy gap decreases when P replaced by As and As by Sb in agreement with the previous theoretical calculations and experimental data.

5.3.2 Optical properties

The detailed variation of real, $\varepsilon_1(\omega)$ and imaginary $\varepsilon_2(\omega)$ parts of the dielectric function for AlX with photon energy are shown in Figure 5.4(e). Since the investigated compounds have cubic symmetry, we need to calculate only one dielectric tensor component to completely characterize the linear optical properties. This component is $\varepsilon_2(\omega)$ the imaginary part of the frequency dependent dielectric function. We note that $\varepsilon_2(\omega)$ shows a large peak located at 4.5 eV for AlP, 4.3 eV for AlAs, and 3.7 eV for AlSb which was reported by Malsawmtluanga *et al.* (2014). All the structures in $\varepsilon_2(\omega)$ are shifted towards the lower energies when P is replaced by As and As by Sb. This is attributed to the increases in the band width of the conduction bands when we move from P to As to Sb. We note that the peak heights are increases when we move from P to As to Sb. We compare our calculated $\varepsilon_2(\omega)$ with the most recent calculations of Huang and Ching (1993). Previous calculations (Huang and Ching, 1993) underestimate the magnitude of $\varepsilon_2(\omega)$ in the low energy regime. This could be due to an inaccurate representation of the wave functions.

Table 5.3: Our calculated energy band gap values for AlP, AlAs and AlSb and the experimental and theoretical band gap (all values are in eV).

Comp -ounds	Experimental Band gap	Theoretical Band gap (E_g)			Our Calculated Band-gaps GGA
		TB	LDA	GGA	
AlP	2.45[a], 2.50[b]	2.45[c]	2.17[b], 1.49[d]	1.638[e]	1.58
AlAs	2.153[a], 2.3[b]	2.153[c]	1.37[b], 1.39[d]	1.494[e]	1.46
AlSb	1.615[a], 1.87[b]	1.615[c]	1.23[b], 1.17[d]	1.214[f]	1.20

[a]Martienssen and Warlimont (2005), [b]Huang and Ching (1993); [c]Korti-Baghdadli *et al.* (2013); [d]Reshak and Auluck (2007); [e]Bentouaf *et al.* (2013); [f]Ahmed *et al.* (2009).

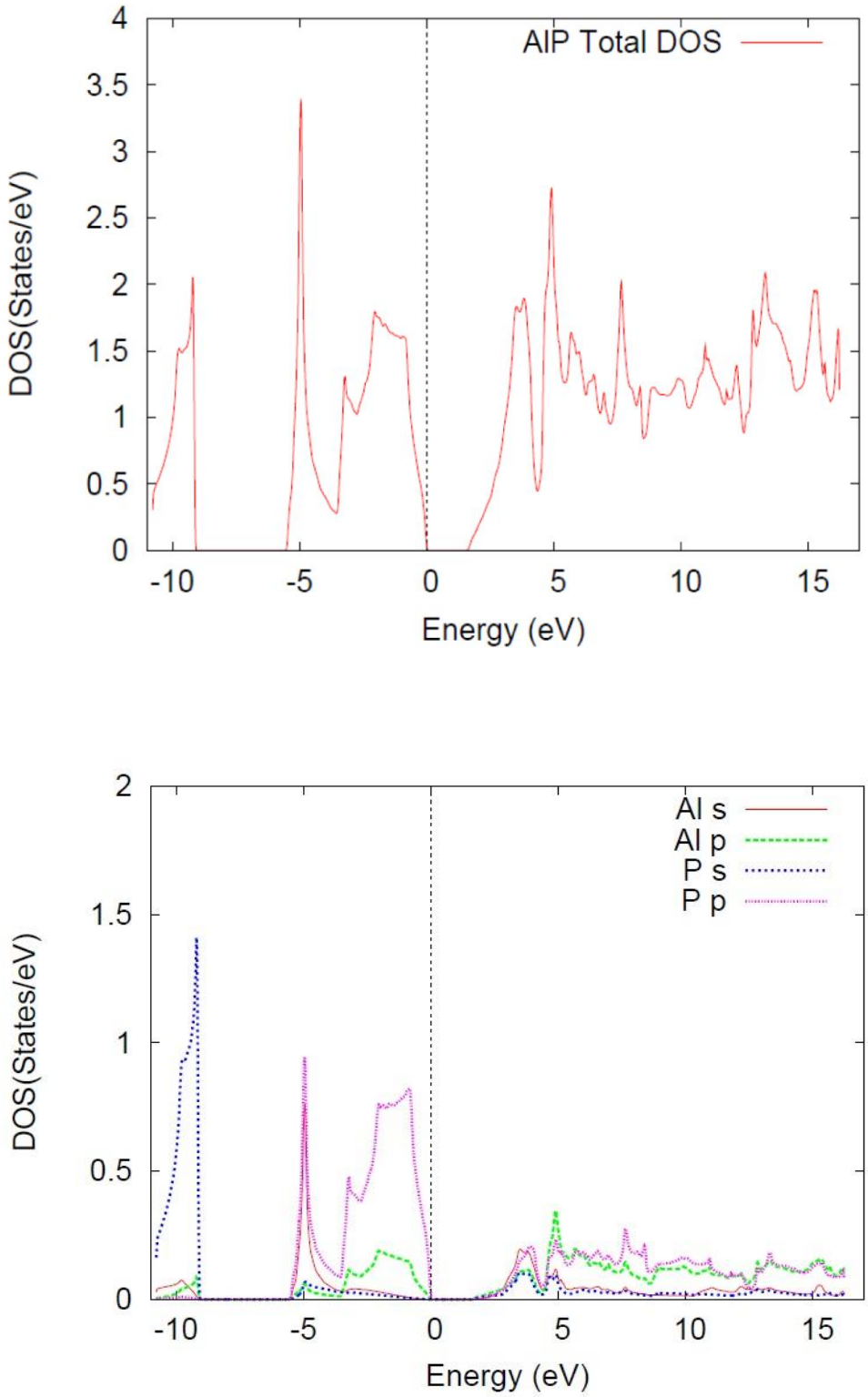

Figure 5.4(a). Total DOS and Partial DOS for AlP. The vertical dotted lines at E = 0 eV indicates the Fermi energy level.

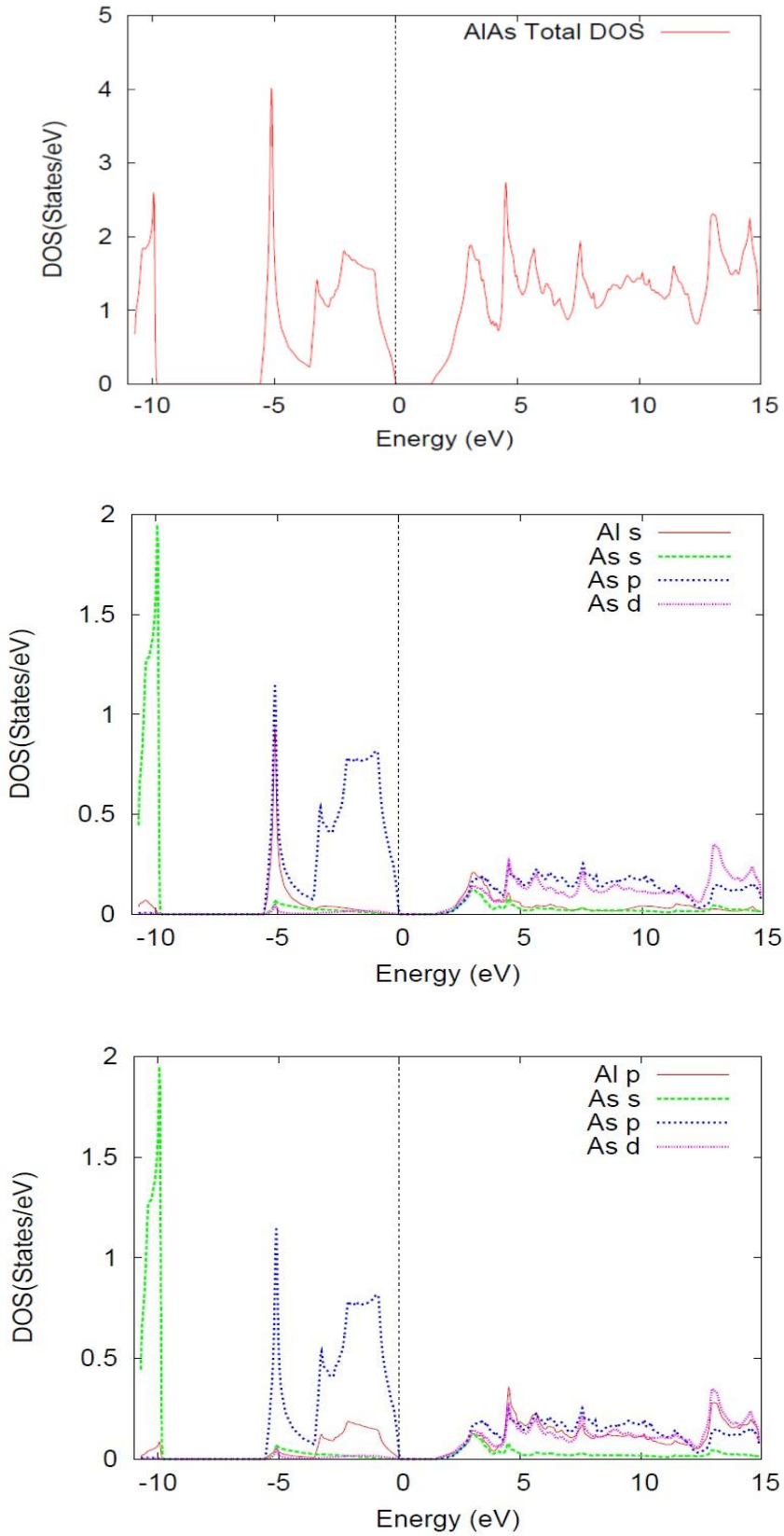

Figure 5.4(b). Total DOS and Partial DOS for AlAs. The vertical dotted lines at E = 0 eV indicates the Fermi energy level.

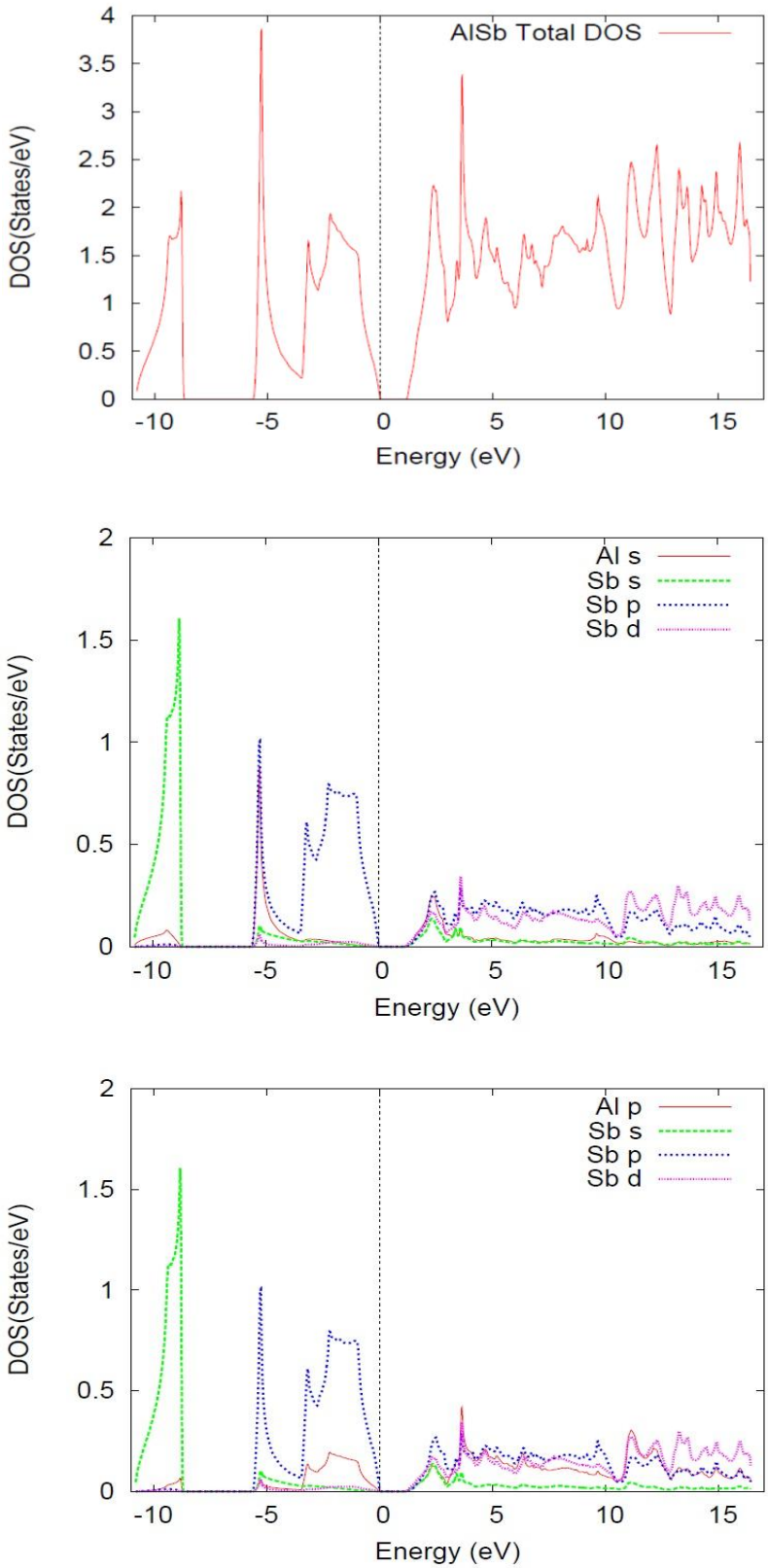

Figure 5.4(c). Total DOS and Partial DOS for AlSb. The vertical dotted lines at E = 0 eV indicates the Fermi energy level.

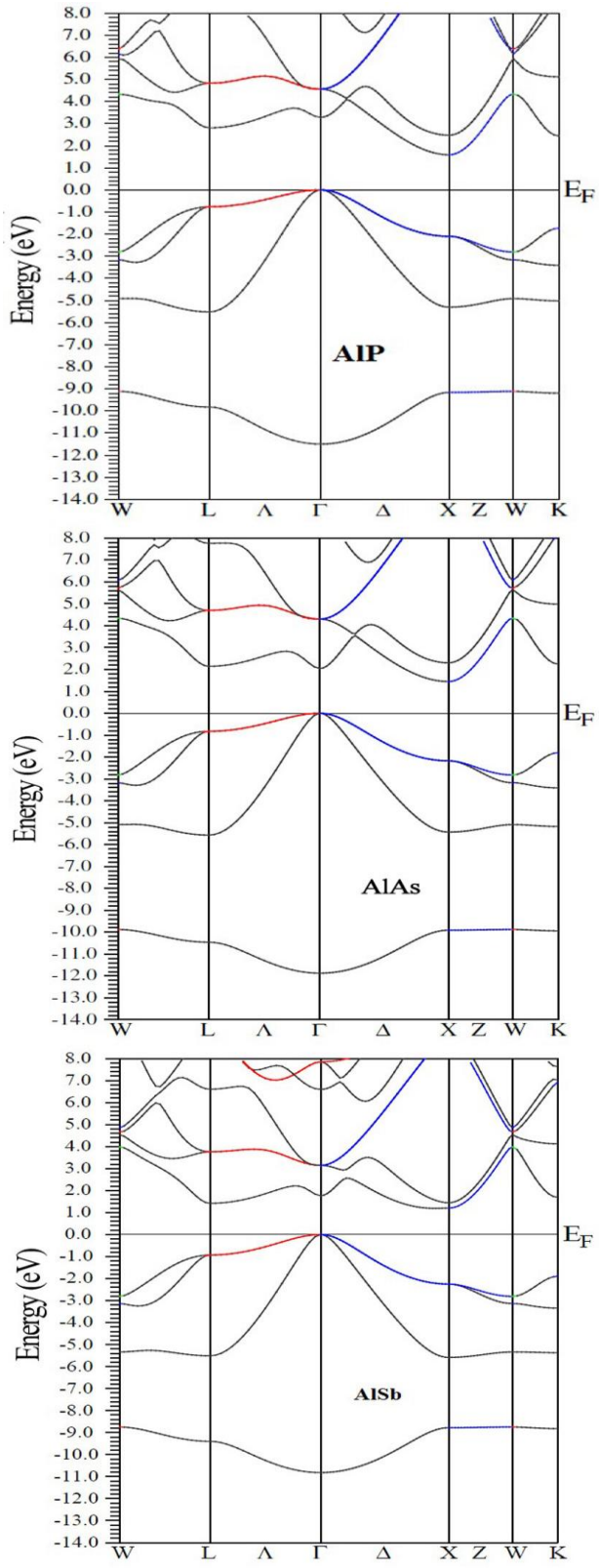

Figure 5.4(d). Band structure for AlP, AlAs and AlSb along the high symmetry directions. E_F = 0 eV corresponds to the Fermi level.

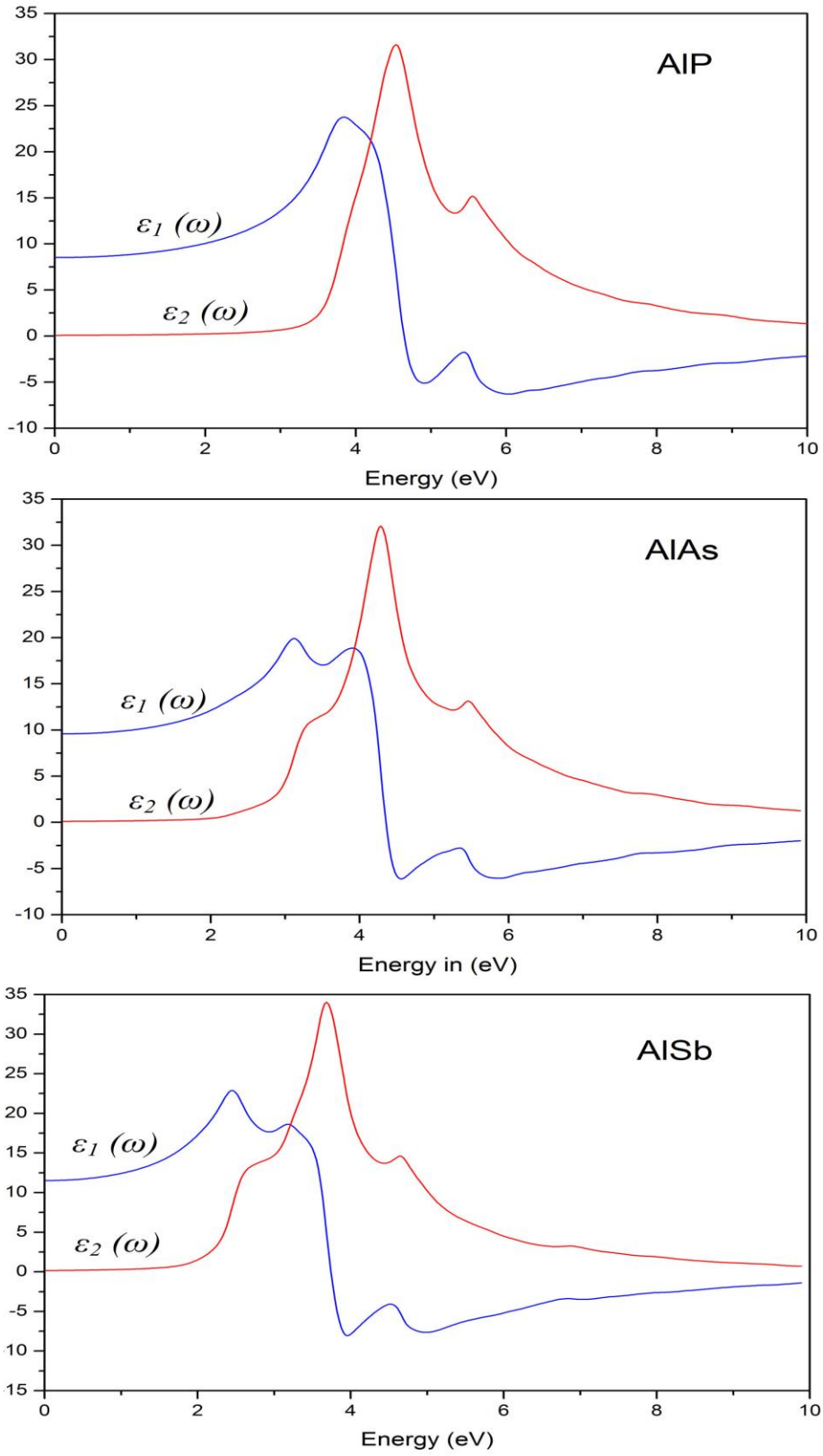

Figure 5.4(e). Real and Imaginary part of dielectric function for AlP, AlAs and AlSb.

5.4 Results and Discussion on Gallium Pnictides:

The semiconductor gallium pnictides are becoming of increasing importance in many emerging optoelectronic and electronic device applications. Among these applications are light emitting diodes, photovoltaic cells, photo detectors, lasers, modulators, integrated circuits, filters etc. (Jivani and Jani, 2012). In semiconductor GaX (X=P, As, Sb), there is a large variation in the energy gaps, suggesting that the energy band gap depends on the method of the band structure calculation (Al-Douri and Reshak, 2011; Reshak, 2005; Rabah *et al.*, 2003; Rahaman *et al.*, 2009).

The electronic configurations of elements in Gallium pnictides are Ga : [Ar] $3d^{10}$ $4s^2$ $4p^1$; P : [Ne] $3s^2$ $3p^3$; As : [Ar] $3d^{10}$ $4s^2$ $4p^3$ and Sb : [Kr] $4d^{10}$ $5s^2$ $5p^3$. We have chosen sphere radii of 2.2 Å for Ga, 2.1 Å, 2.3 Å and 2.7 Å respectively for P, As and Sb. The Gallium pnictides crystallize in the zinc-blende structure at ambient pressure and temperature with lattice parameter 5.4506 Å for GaP, 5.65359 Å for GaAs and 6.09593 Å for GaSb (Martienssen and Warlimont, 2005). The space group is F-43 m. The Ga atom is located at the origin and the X atom is located at (1/4, 1/4, 1/4).

5.4.1 Density of States and Band Structure

The calculated total density of states, the partial density of states and band structures for Gallium pnictides are shown in figures 5.5(a),(b),(c),(d) and (e). The band structure, partial and total DOS can be divided into three main groups. The lowest energy group has mainly pnictide *s* states. The second group between –7 eV to E_F is composed of Ga-*sp* and pnictide *p* states. The last group from 1.65 for GaP, 0.52 eV for GaAs, and 0.17 eV for GaSb and above has contributions from Ga-*spd* and pnictide *p* states. The valence band maximum (VBM) is located at Γ for all the three compounds. In GaP compound, the conduction band minimum (CBM) is located at X resulting in indirect

energy gap of about 1.65 eV. While in GaAs and GaSb compounds, the CBM located at Γ resulting in a direct energy gap of about 0.52 and 0.17 eV respectively. The location of the VBM and CBM is agreed with experiment (Martienssen and Warlimont, 2005; Postigo *et al.,* 1998; Kittel, 1994; Huang and Ching, 1993), and previous theoretical work (Reshak, 2005; Al-Douri and Reshak, 2011; Rahaman, 2009; Postigo *et al.,* 1998; Korti-Baghdadli, 2013). The trends in the band structures in moving from P to As to Sb shows that the first group in GaAs is shifted towards lower energies by around 0.5 eV in comparison with GaP, while in GaSb it is shifted towards higher energies by around 0.5 eV. The bandwidth of the second group is increased. The bandwidth of the conduction band slightly increases by around 0.5 eV towards Fermi energy (E_F) on going from P to As to Sb which causes to reduce the energy gap near Γ.

The important features of the band structure for each compound are given in Table 5.4 which was reported by Malsawmtluanga *et al.* (2014). It is clearly seen that the band gaps obtained by GGA are lower than the corresponding experimental values. This underestimation of the band gap is mainly due to the fact that the simple forms of GGA are not sufficiently flexible to accurately reproduce both ex-change correlation energy and its charge derivative. Whereas our results are in a good agreement with theoretical results obtained from GGA and LDA except Tight Binding method (Korti-Baghdadli *et al.,* 2013). We note that the reduction in the energy gap in agreement with the experimental data. GaAs and GaSb exhibit an overall reduction of the gap over the entire Brillouin zone.

5.4.2 Optical properties

The optical properties of solids can be described in terms of the optical dielectric function. The detailed variation of real, $\varepsilon_1(\omega)$ and imaginary $\varepsilon_2(\omega)$ parts of the dielectric

function for GaX with photon energy are shown in figure 5.5(f) which was reported by Malsawmtluanga *et al.* (2014). The $\varepsilon_1(\omega)$ spectra appears at the same energy as a peak in the corresponding $\varepsilon_2(\omega)$ spectra. For the value of $\varepsilon_1(\omega) < 0$, the curve shown metallic reflectance characteristics. Our analysis of the $\varepsilon_2(\omega)$ curves show that the first absorption edge of the dielectric function occurs at 1.65 eV, 0.52 eV and 0.17 eV for GaP, GaAs and GaSb respectively. These critical points are followed by small structure located at 3.03 eV in GaP, 2.4 eV in GaAs and 1.84 eV in GaSb. The main peaks in the spectra are situated at 4.48 eV, 4.23 eV and 3.61 eV respectively. The main peaks are followed by small hump situated at 5.70 eV, 5.59 eV and 4.83 eV respectively. The peak of the imaginary part of the dielectric function is related to the electron excitation.

We have found that the three compounds have the same structure that is attributed to the fact that the band structures of these compounds are similar with minor differences causing insignificant changes in the structures of $\varepsilon_2(\omega)$. All the structures in $\varepsilon_2(\omega)$ are shifted towards the lower energies with reduces in the peak heights when P is replaced by As and As by Sb, in agreement with the experimental data (Aspnes and Studna, 1983). This is attributed to the reduction in the band gaps. We have compared our calculated $\varepsilon_2(\omega)$ with the experimental data (Aspnes and Studna, 1983) and shows very good agreement in the case of the peak position and peak height.

Table 5.4: Our calculated energy band gap values for GaP, GaAs and GaSb and the experimental and theoretical band gap (all values are in eV).

Compo-unds	Experimental Band gap	Theoretical Band gap (E_g)			Our Calculated Band-gaps
		TB	LDA	GGA	
GaP	2.2[a], 2.26[b], 2.38[c], 2.22[d]	2.272[e]	1.22[c], 1.45[f], 1.62[g]	2.0[h]	1.65
GaAs	1.8[a], 1.43[b], 1.52[c],1.42[d]	1.419[e]	1.04[c], 0.4[f], 0.37[g]	0.49[h]	0.52
GaSb	1.2[a], 0.78[b], 0.81[c], 0.725[d]	0.725[e]	0.8[c], 0.2[f], 0.07[g]	0.4[h]	0.17

[a]Postigo *et al.* (1998), [b]Kittel (1994), [c]Huang and Ching (1993), [d]Strehlow and Cook (1973), [e]Korti-Baghdadli (2013), [f]Rabah (2003), [g] Rahaman (2009), [h]Al-Douri and Reshak (2011)

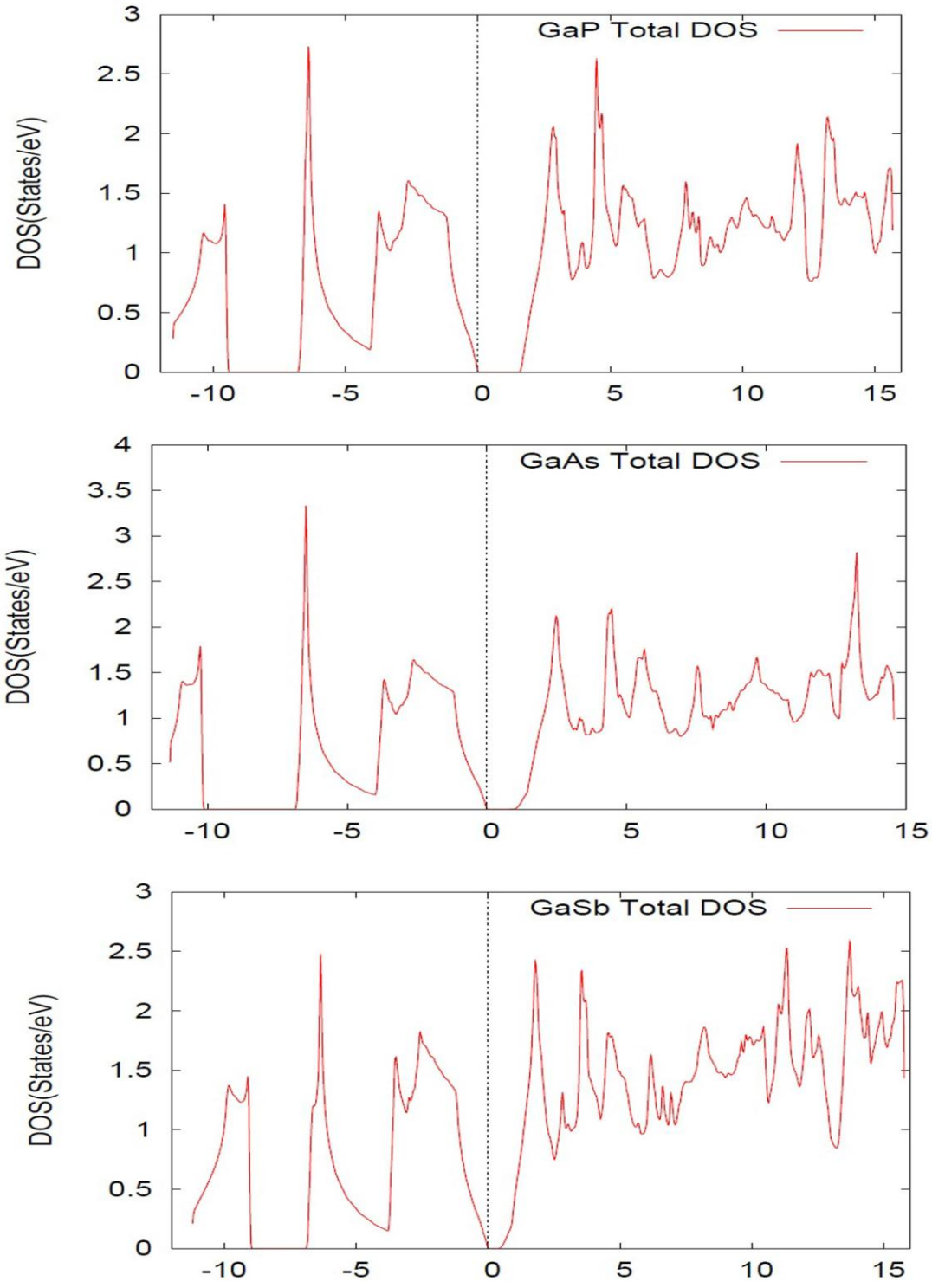

Figure 5.5(a). Total Density of States for GaP, GaAs and GaSb. The vertical dotted lines at E = 0 eV indicates the Fermi energy level

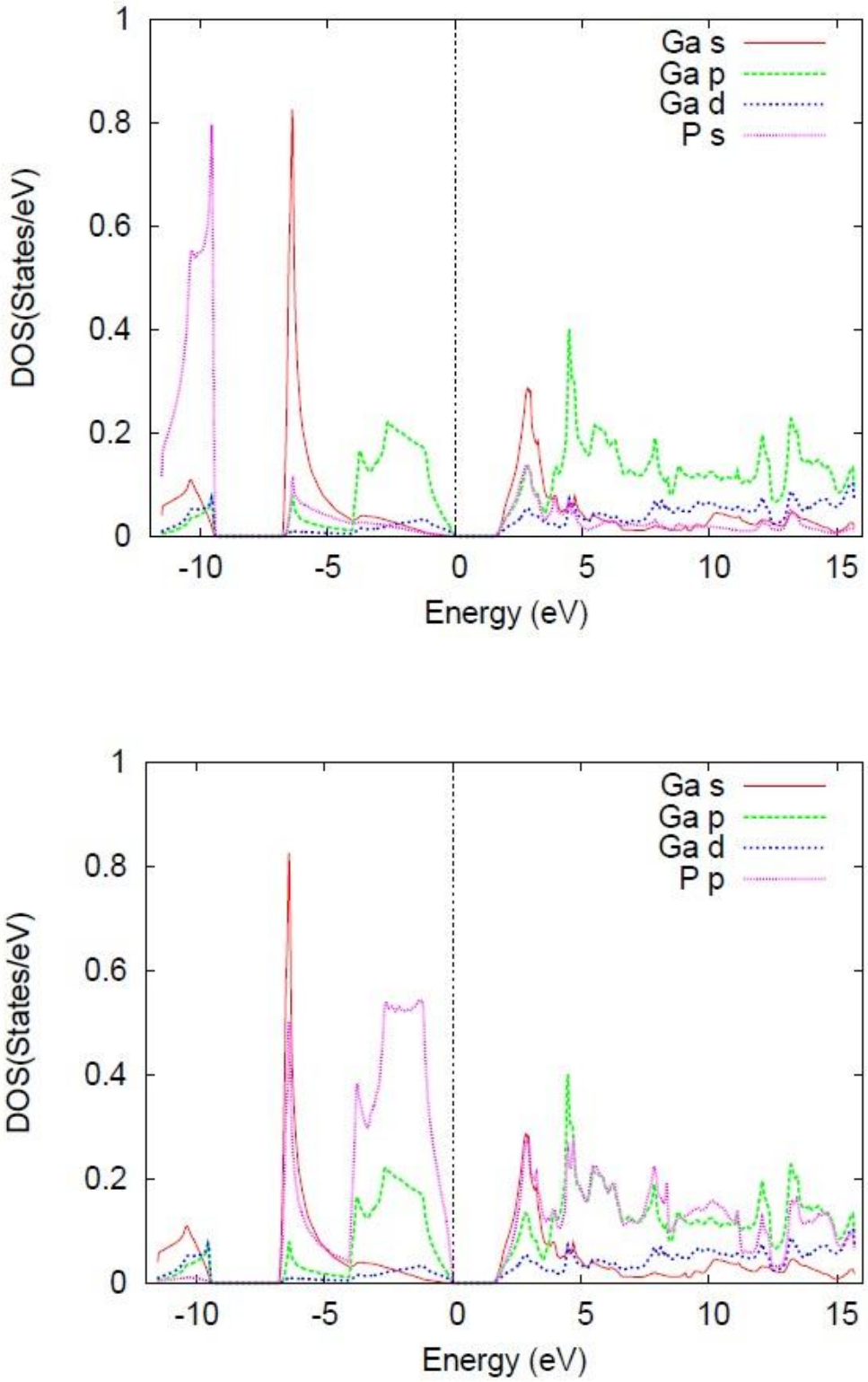

Figure 5.5(b). Partial Density of States for GaP. The vertical dotted lines at E = 0 eV indicates the Fermi energy level.

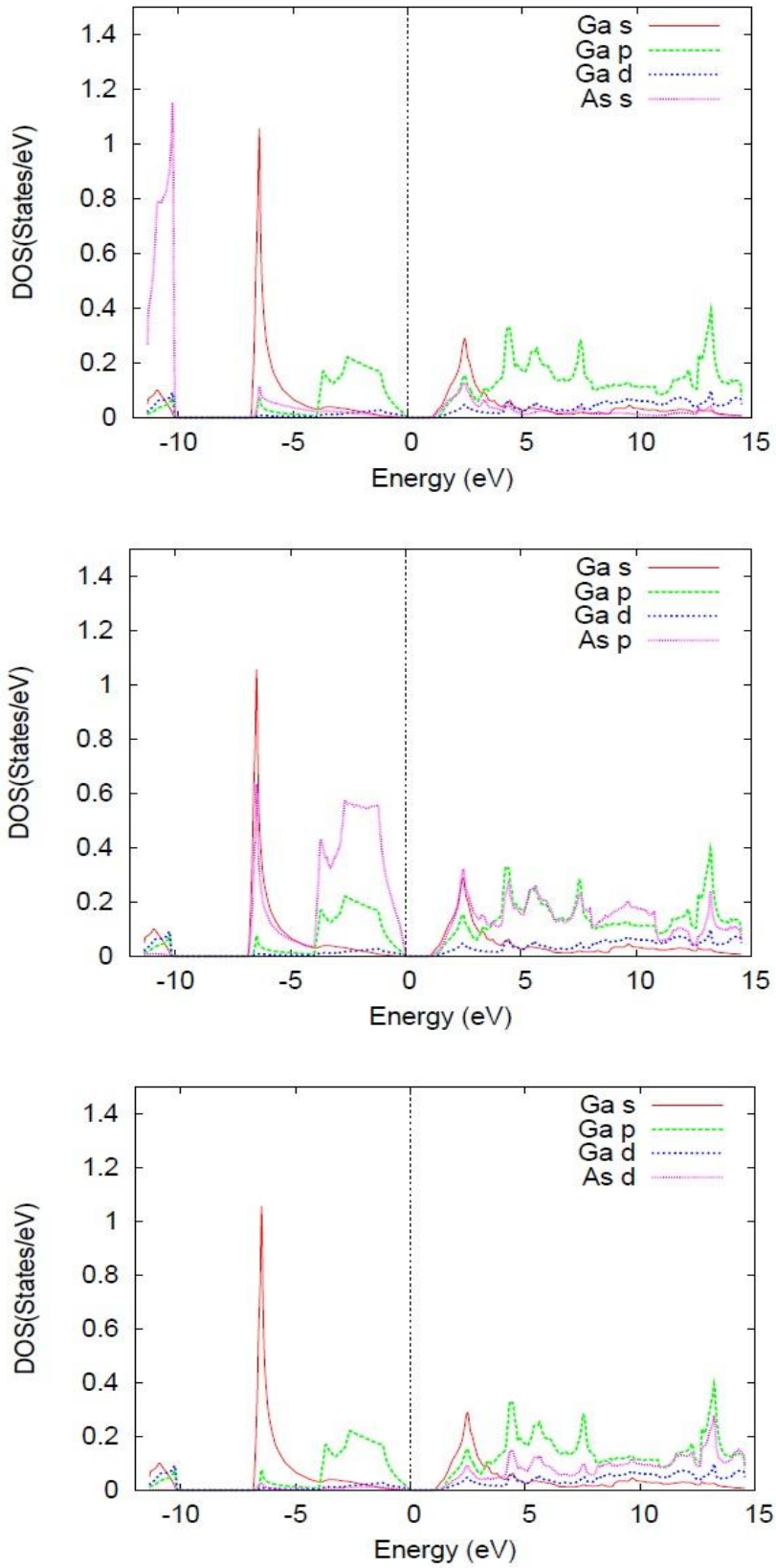

Figure 5.5(c). Partial Density of States for GaAs. The vertical dotted lines at E = 0 eV indicates the Fermi energy level.

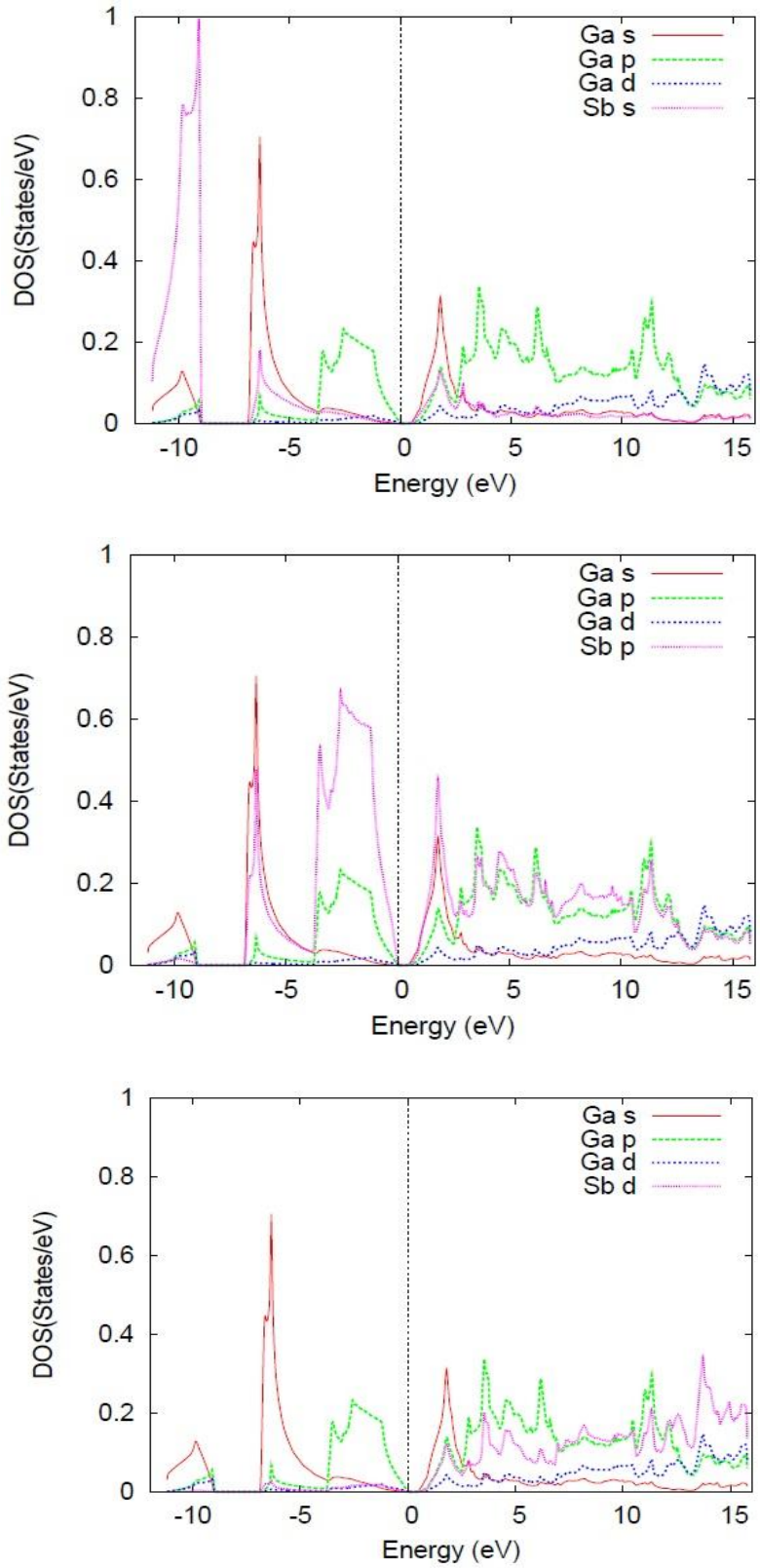

Figure 5.5(d). Partial Density of States for GaSb. The vertical dotted lines at E = 0 eV indicates the Fermi energy level.

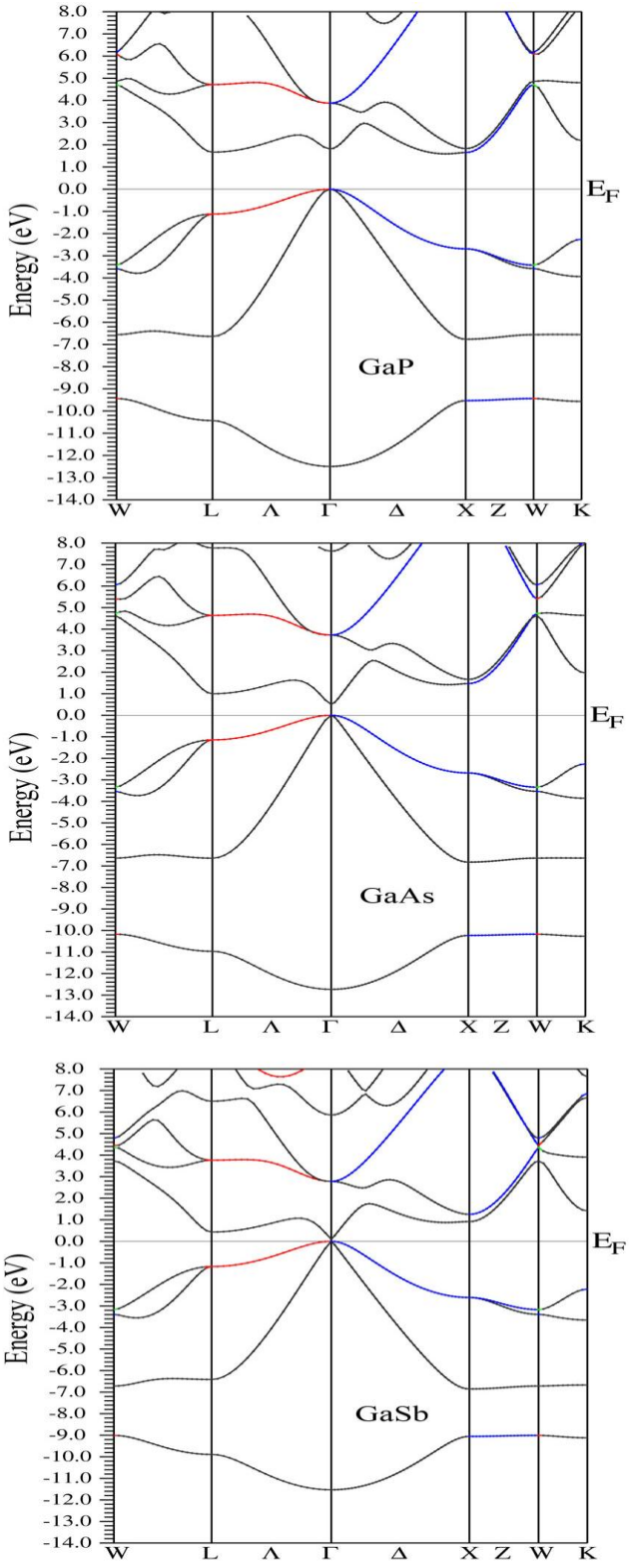

Figure 5.5(e). Band structure for GaP, GaAs and GaSb along the high symmetry directions. E_F = 0 eV corresponds to the Fermi level.

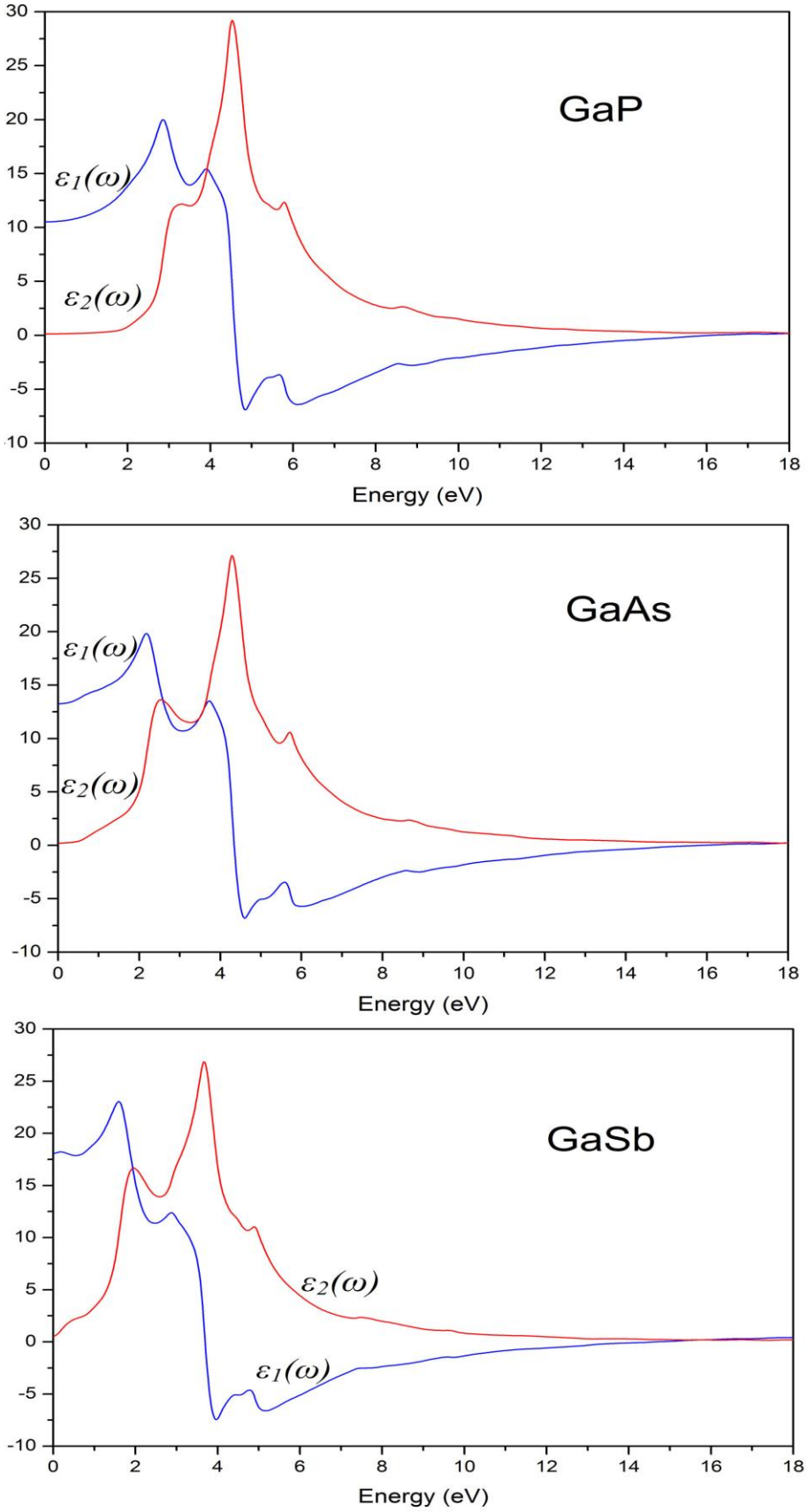

Figure 5.5(f). Real and Imaginary part of dielectric function for GaP, GaAs and GaSb.

5.5 Results and Discussion on Indium Pnictides:

The semiconductors Indium Pnictides InX (X=P, As, Sb) compounds have attracted much attention because they possess narrow band gaps and for their potential as new device materials. These compounds are important as solar cells for space applications due to its high efficiency conversion and good radiation resistance that its thinness provides, reducing the probability of radiation damage (Yamaguchi, 2001).

The electronic configurations of elements in Indium pnictides are In: [Kr] $4d^{10}$ $5s^2$ $5p^1$; P: [Ne] $3s^2$ $3p^3$; As: [Ar] $3d^{10}$ $4s^2$ $4p^3$ and Sb: [Kr] $4d^{10}$ $5s^2$ $5p^3$. We have chosen sphere radii of 2.3 Å for In, 2.1 Å, 2.5 Å and 2.8 Å respectively for P, As and Sb. The Indium pnictides crystallize in the zinc-blende structure at ambient pressure and temperature with lattice parameter 5.8687 Å for InP, 6.0583 Å for InAs and 6.47937 Å for InSb (Martienssen and Warlimont, 2005). The space group is F-43m. The In atom is located at the origin and the X atom is located at (1/4, 1/4, 1/4).

5.5.1 Density of States and Band Structure

Figures 5.6(a),(b),(c),(d) and (e) shows the calculated total density of states, the partial density of states and band structures for Indium pnictides InX (X=P, As, Sb). The band structure, partial and total DOS can be divided into three main groups. The lowest energy group has mainly pnictide *s* states. The second group between –7 eV to E_F is composed of In-*sp* and pnictide *p* states. The last group from 0.7 for InP, 0.031 eV for InAs, and 0.01 eV for InSb and above has contributions from In-*spd* and pnictide *pd* states. The valence band maximum (VBM) and the conduction band minimum (CBM) are located at Γ resulting in a direct gap in agreement with experiment and previous theoretical work (Martienssen and Warlimont, 2005; Huang and Ching 1993). The conduction bands shift towards Fermi energy (E_F) when moving from P to As to Sb.

A comparison of the experimental and theoretical band gaps are given in Table-I. It is clearly seen that the band gap obtained by GGA are lower than the corresponding experimental values and results obtained from Tight Binding method (Korti-Baghdadli *et al.,* 2013). We note that DOS does show a lager energy gaps than the band structures. This is attributed to the fact that the DOS near the conduction band minimum is very small because of the small effective mass. Our calculated value is lower than the value obtained by Reshak (2006) in the same exchange correlation potential which is attributed by the choice of parameters like lattice constant, *k*-points etc. Following Yamasaki *et al*. (1987), we can define degree of hybridization by the ratio of In-*d* states and pnictide *p* states within the muffin tin sphere. Based on this we can say that the hybridization between In-*d* and pnictide *p* states is very weak.

5.5.2 Optical properties

The detailed variation of real, $\varepsilon_1(\omega)$ and imaginary $\varepsilon_2(\omega)$ parts of the dielectric function for InX with photon energy are shown in figure 5.6(f). We note that $\varepsilon_2(\omega)$ shows a large peak located at 4.3 eV for InP, 4.0 eV for InAs, and 3.5 eV for InSb in between two small peaks. All the structures in $\varepsilon_2(\omega)$ are shifted towards the lower energies when P is replaced by As and As by Sb, in agreement with the experimental data (Aspnes and Studna, 1983). This is attributed to the reduction in the band gaps. We compare our calculated $\varepsilon_2(\omega)$ with the experimental data (Aspnes and Studna, 1983) and shows very good agreement in the case of the peak position and peak height.

Table 5.5: Our calculated energy band gap values for InP, InAs and InSb and the experimental and theoretical band gap (all values are in eV).

Compo-unds	Experimental Band gap	Theoretical Band gap (E_g)			Present work GGA
		TB	LDA	GGA	
InP	1.39[a], 1.351[b], 1.35[c]	1.34[d]	1.39[a], 1.804[e], 0.7[f], 0.71[g]	0.85[f]	0.7
InAs	0.42 [a], 0.356[b], 0.35[c]	0.35[d]	0.55[a], 0.259[e], 0.24[f], 0.03[g]	0.31[f]	0.031
InSb	0.24 [a] , 0.17[b], 0.18[c]	0.17[d]	0.24 [a], 0.00[e], 0.14[f], 0.01[g]	0.18[f]	0.01

[a]Huang and Ching (1993), [b]Strehlow and Cook (1973), [c]Kittel (1994), [d]Korti-Baghdadli *et al.* (2013), [e]Remediakis and Efthimios Kaxiras (1999), [f]Reshak (2006), [g]Rahaman *et al.* (2009)

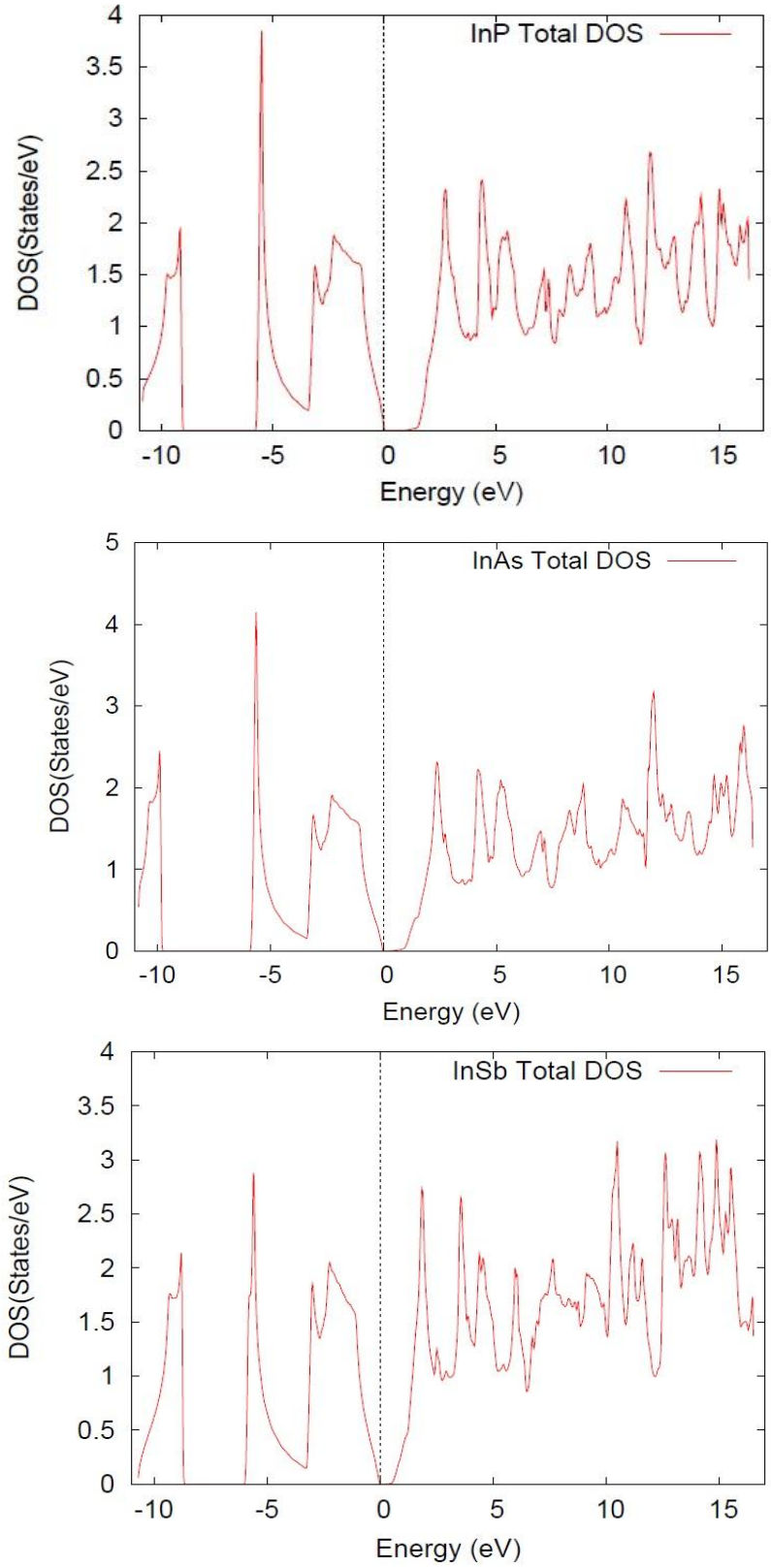

Figure 5.6(a). Total Density of States for InP, InAs and InSb. The vertical dotted lines at E = 0 eV indicates the Fermi energy level.

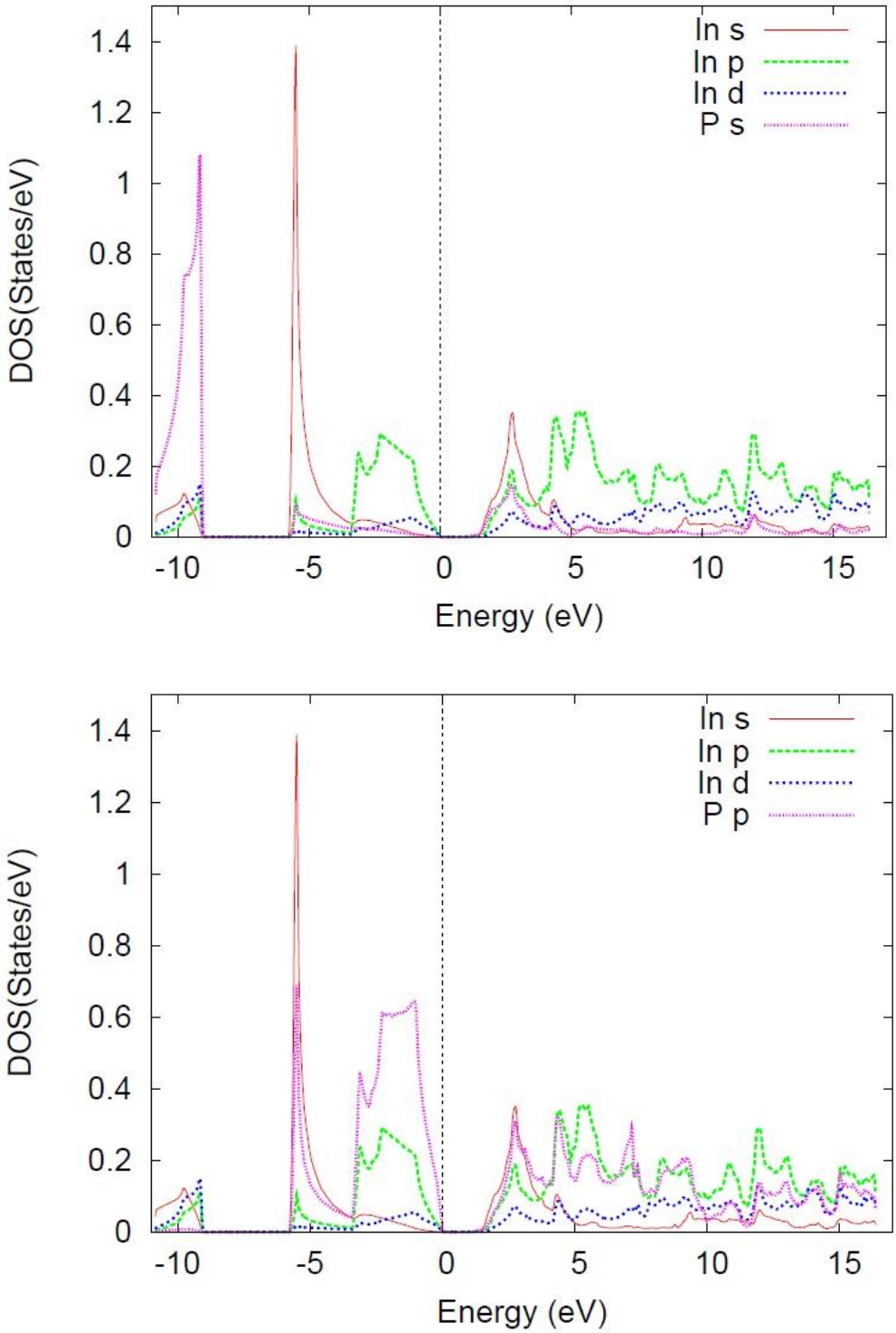

Figure 5.6(b). Partial Density of States for InP. The vertical dotted lines at E = 0 eV indicates the Fermi energy level.

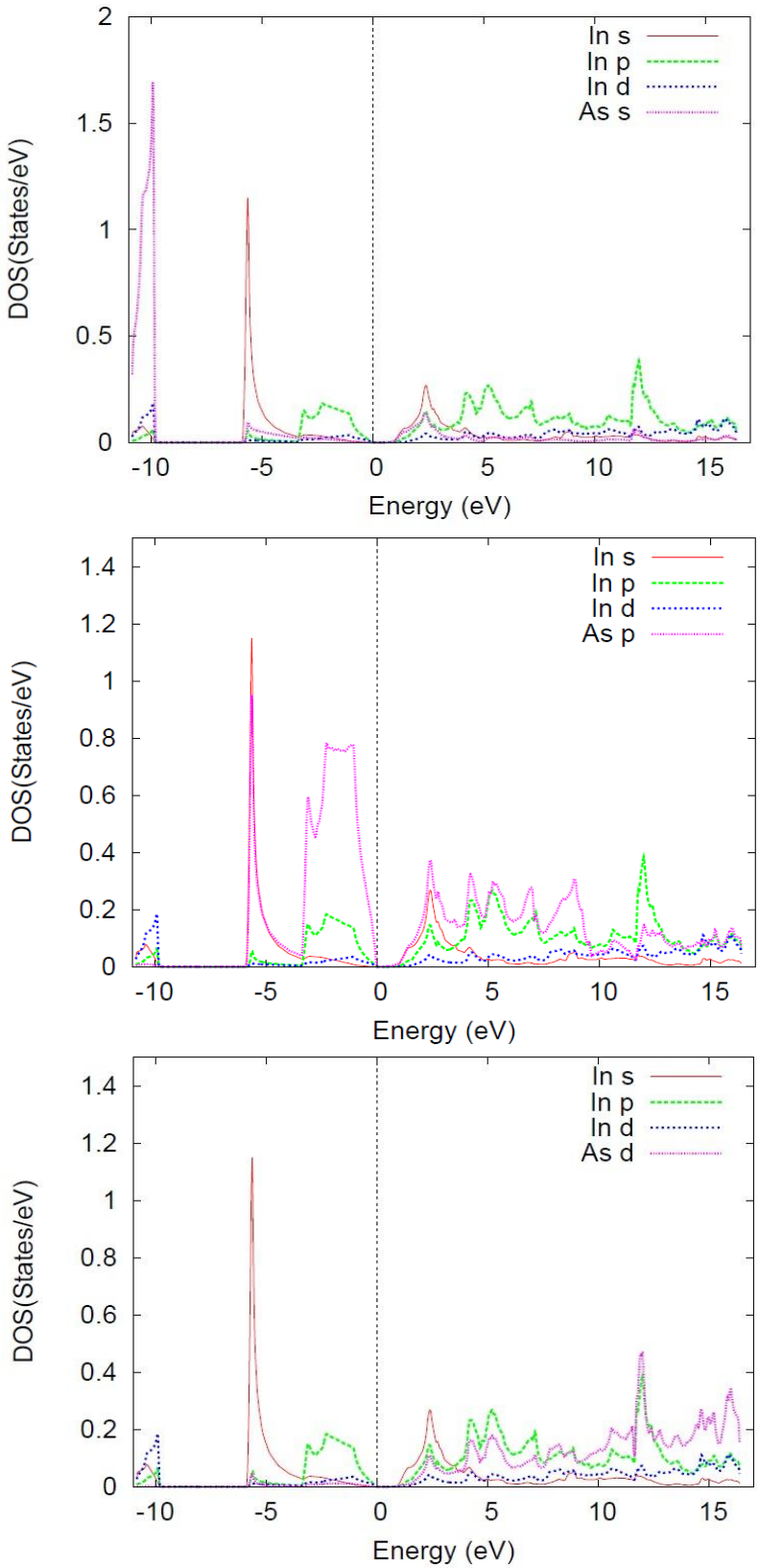

Figure 5.6(c). Partial Density of States for InAs. The vertical dotted lines at E = 0 eV indicates the Fermi energy level.

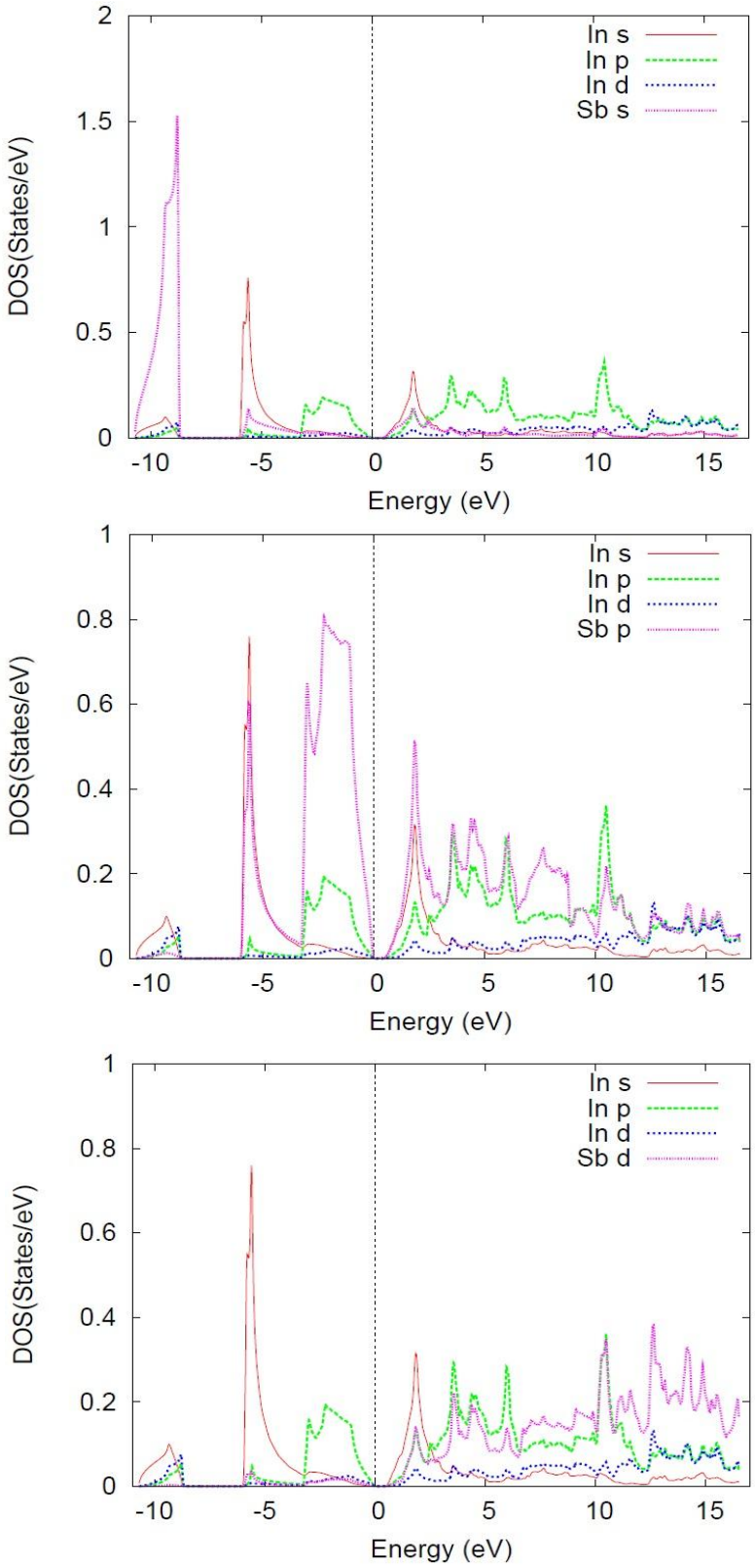

Figure 5.6(d). Partial Density of States for InSb. The vertical dotted lines at E = 0 eV indicates the Fermi energy level.

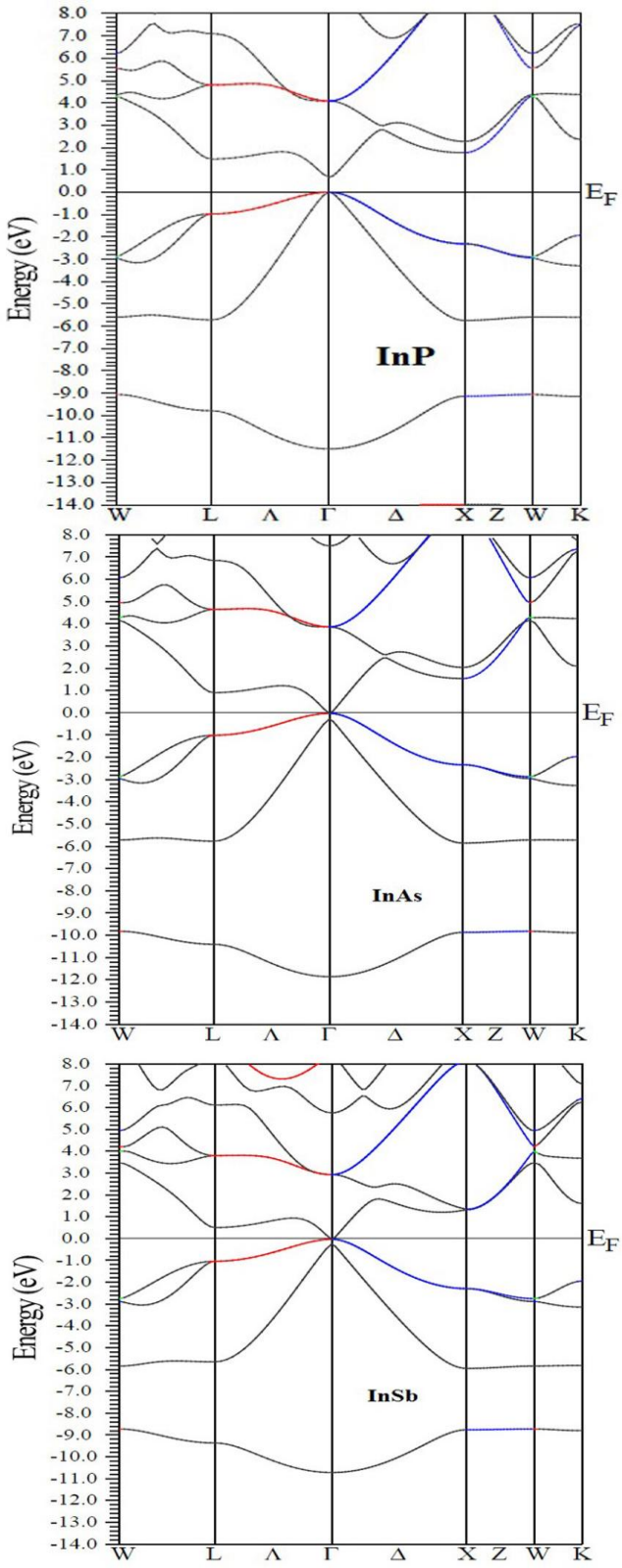

Figure 5.6(e). Band structure for InP, InAs and InSb along the high symmetry directions.

E_F = 0 eV corresponds to the Fermi level.

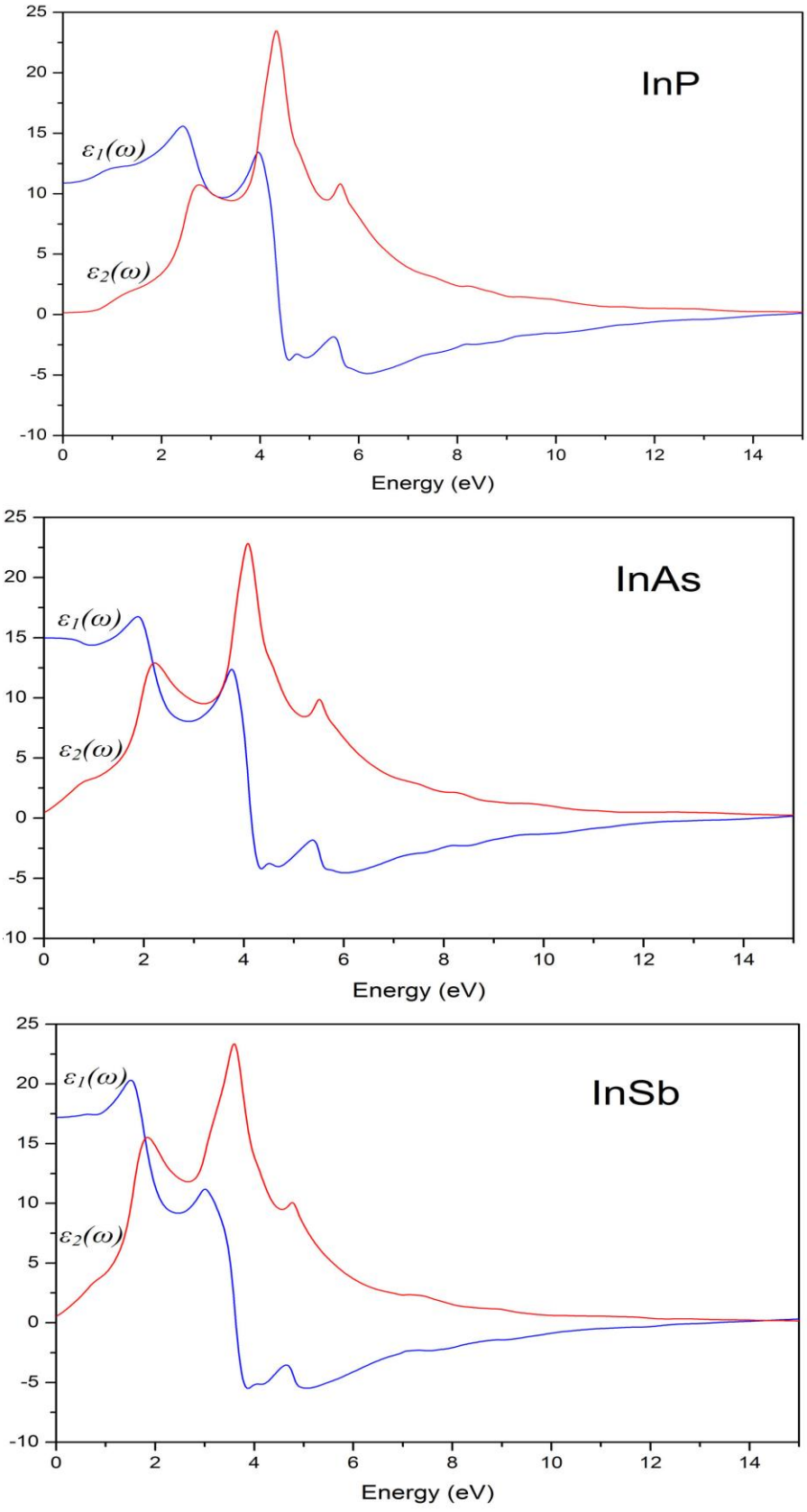

Figure 5.6(f). Real and Imaginary part of dielectric function for InP, InAs and InSb.

CHAPTER 6

CONCLUSION

In this thesis, we have presented the calculations of electromagnetic fields, photocurrent, electronic and linear optical properties of II-VI semiconductors of BeX and ZnX (X = S, Se, Te) as well as III-V semiconductors of AlX, GaX and InX (X = P, As, Sb). The electromagnetic fields in the bulk, surface and vacuum regions of these systems were calculated using the modified form of dielectric model developed by Bagchi and Kar (1978). In all these systems, we have found that in the surface region, the plot of vector potential $\left|\tilde{A}_{\omega}(z)\right|^2$ showed maxima in peak at $\hbar\omega_s = \frac{\hbar\omega_p}{\sqrt{2}}$, where $\hbar\omega_s$ is the surface plasmon energy and $\hbar\omega_p$ is the bulk plasmon energy of compound semiconductors. Interestingly, all compound semiconductors showed a minimum in the value of vector potential where value of incident photon energy ($\hbar\omega$) was equal to $\hbar\omega_p$. With the further increase of incident photon energies, beyond the plasmon energy, the field values increase and attain a small hump, and then decreased towards minimum. Our calculated results showed good agreement with the calculated value (Kumar *et al*. 2013; Yadav and Kumar, 2013; Yadav and Singh, 2010; Kumar, 2013; Reddy *et al.* 2003). From our results, we can also conclude that the vector potential $\tilde{A}_{\omega}(z)$ deduced for the surface region of solid can be used in the calculation of surface photocurrent from compound semiconductors.

We have presented photocurrent calculations by using the Mathieu potential model which is used to describe the lattice potential. We have calculated with the case of strong lattice potential as the semiconductors have band gaps, for which results of photocurrent is plotted against photon energy. Surface photocurrent had been calculated for the localized surface state at z_0 = -2 a.u. and z_0 = -8 a.u. for II-VI semiconductors of BeX and ZnX as well as III-V semiconductors of AlX, GaX and InX. In all the cases, for

the location of the initial state wavefunction at the z_0 = - 2 a.u.(surface-vacuum interface), photocurrents showed maximum value below plasmon energy and suppression at the plasmon energy ($\hbar\omega_p$). Our calculated results were compared with the previous calculated value eV (Kumar *et al*. 2013; Yadav and Kumar, 2013; Yadav and Singh, 2010; Kumar, 2013; Reddy *et al.* 2003) and found to agree qualitatively well. The inclusion of initial state wavefunction into the matrix element appears to produce the qualitative features as observed earlier in the experimentally measured data (Levinson *et al.*, 1979; Bartynski *et al.*, 1985). The main drawback of the model used is that the same initial state wavefunction ψ_i is used to describe both the surface and bulk regions of the solids under study. It was also found that bulk potential has very little effect on surface photocurrent. This fact had been explained by Levinson *et al.* (1979) that it is the rapid variation of the photon field vector in the surface which causes surface photocurrent. Further, the large drop in the value of photocurrent as photon energy approached the plasmon energy is due to the decrease in the value of $\frac{d\,\tilde{A}_\omega}{dz}$. However, it can be shown that one can also make use of Mathieu type of potential in calculations of surface photocurrent from compound semiconductors.

Knowledge of the band structure is required to calculate the optical properties which are governed by the electronic energy states at E_F and away from E_F. The GGA in the FPLAPW method was used for calculations of the electronic band structure, density of states and optical properties from II-VI semiconductors of BeX and ZnX as well as III-V semiconductors of AlX, GaX and InX which crystallize in the Zinc-blende structure.

In Beryllium chalcogenides, an indirect gap of 3.12 eV, 2.64 eV and 1.98 eV for BeS, BeSe and BeTe were found respectively. In Zinc chalcogenides, a direct gap of 2.1

eV for ZnS, 1.5 eV for ZnSe and 1.3 eV for ZnTe were found. In Aluminum pnictides, an indirect energy band gap of 1.58 eV, 1.46 eV, 1.2 eV for AlP, AlAs and AlSb were found respectively. In Gallium pnictides, an indirect energy gap about 1.65 eV for GaP was found. But for GaAs and GaSb compounds, a direct energy gap of about 0.52 and 0.17 eV were found respectively. In Indium pnictides, a direct gap of 0.7 eV for InP, 0.031 eV for InAs, and 0.01 eV for InSb were found. In all the cases, the calculated values were in agreement with experiment (Strehlow and Cook 1973; Huang and Ching 1993; Martienssen and Warlimont, 2005) and previous theoretical work. (Kalpana *et al.,* 1998; Reshak and Auluck, 2007; Rahaman *et al.,* 2009; Al-Douri and Reshak, 2011; Korti-Baghdadli, 2013)

In the linear optical properties of compound semiconductors under studies, the variation of real $\varepsilon_1(\omega)$ and imaginary $\varepsilon_2(\omega)$ parts of the dielectric function with photon energy were plotted. We have compared our results with the experimental data (Aspnes and Studna, 1983; Freeouff, 1973; Kim *et al.,* 1993; Huang and Ching, 1993) and found generally in good agreement in the case of the peak position and peak height. The effect of replacing S by Se and Te in the case of II-VI semiconductors of BeX and ZnX and the effect of replacing P by As and Sb in the case of III-V semiconductors of AlX, GaX and InX on the band structure and optical properties were discussed. We have found that the energy band gaps are underestimated in comparison with the experimental data, which is attributed to our use of GGA. For optical calculation, a dense mesh of *k* points is required for accurate results. We can conclude that FP-LAPW method is very appropriate for the calculation of electronic band structure, density of states and optical properties of the semiconductor compounds. Thus, to study the electronic structures of most of the materials, one usually used the DFT method with GGA and LDA, but they underestimated the band gap of semiconductors. There are some alternative methods to

improve the band gap with respect to the experimental values like the Hybrid functionals (HSE) (Heyd *et al.,* 2005), the DFT+U method (Anisimov *et al.,* 1997), the LDA+DMFT theory (Georges *et al.,* 1996) and the GW (Bechstedt *et al.,* 2009). Recently, Tran and Blaha (2009) proposed a semilocal modified Beck-Johnson potential (mBJ) for the improvement in the results for band gaps. This new orbital independent mBJ potential in which mBJ exchange term is coupled with LDA correlation, could predict the energy bands more accurately so that calculated band gaps of the semiconductor materials could come out in good agreement with the experimental results.

References

Ahmed R., Fazal-e-Aleem, Hashemifar S. J., Rashid H. and Akbarzadeh H. (2009), Physical Properties of III-Antiminodes - a First Principles Study. *Commun. Theor. Phys.* **52**: 527–533

Al-Douri Y. and Reshak A. H. (2011), Calculated optical properties of GaX (X = P, As, Sb) under hydrostatic pressure. *Appl Phys A***104**: 1159-1167

Al-Douri Y., Baaziz H., Charifi Z., Reshak A. H. (2012), Density functional study of optical properties of beryllium chalcogenides compounds in nickel arsenide B8 structure. *Physica* B **407**: 286–296

Ameri M., Rached D., Rabah M., El Haj Hassan F., Khenata R. and Doui-Aici M. (2008), First principles study of structural and electronic properties of $Be_xZn_{1-x}S$ and $Be_xZn_{1-x}Te$ alloys. *Phys. Stat. Sol. (b*) **245** [1]: 106-113

Anisimov V. I., Aryasetiawan F. and Lichtenstein A. I. (1997), First-principles calculations of the electronic structure and spectra of strongly correlated systems: the LDA+ U method. *J. Phys.: Condens. Matter* **9:** 767-808

Appelbaum J.A. (1975), In: *Surf. Phys. of Materials*, (ed.) J.H. Blakely, Vol. I, Academic Press, New York

Aspnes D.E. and Studna A.A. (1983), Dielectric functions and optical parameters of Si, Ge, GaP, GaAs, GaSb, InP, InAs, and InSb from 1.5 to 6.0 eV. *Phys. Rev. B* **27**: 985-1009

Baaziz H., Charifi Z., El Haj Hassan F., Hashemifar S. J. and Akbarzadeh H. (2006), FP-LAPW investigations of $Zn_{1-x}Be_xS$, $Zn_{1-x}Be_xSe$ and $Zn_{1-x}Be_xTe$ ternary alloys. *Phys. Stat. Sol. (b)* **243** [6]: 1296-1305

Bagchi A. and Kar N. (1978), Refraction effects in angle-resolved photoemission from surface states on metals. *Phys. Rev.* B**18**: 5240-5247

Bang C. Y., Lee M. S., Kim T. J., Kim Y. D., Aspnes A. E., Yu Y. M., Sung O B. and Choi Y. D. (2001), Above Bandgap Optical Properties of ZnS and $ZnS_{1-x}T_{ex}$ Alloys Grown by Using Hot-Wall Epitaxy. J. Korean Physical Society **39**:462-465.

Barth U. V. and Hedin L. (1972), A local exchange-correlation potential for the spin polarized case. J. Phys. C: **5**, 1629-1642

Bartynski R.A., Jensen E., Gustafson T. and Plummer E.W. (1985), Angle-resolved photoemission investigation of the electronic structure of Be: Surface states. *Phys. Rev*. **B32**: 1921-1926

Bechstedt F., Fuchs F. and Kresse G. (2009), Ab-initio theory of semiconductor band structures: New developments and progress, *Phys. Status Solidi* (b) **246[8]**: 1877-1892

Bentouaf A., Ouahrani T., Ameri M., Mebsout R., Hachemane D. (2013), Theoretical study of structural, electronic, optical and Thermodynamic properties of AlP, InP and AlAs compounds. *Optoelectronics and Advanced Materials* **7**:659 – 666

Berglund C.N. and Spicer W.E. (1964), Photoemission studies of copper and silver: theory. *Phys. Rev*. **136**: A1030–A1044

Blaha P., Schwarz K., Madsen G. K. H., Kvasnicka D. and Luitz J. (2008), *An Augmented Plane Wave + Local Orbitals Program for Calculating Crystal Properties*, (Revised Edition). Vienna University of Technology: Inst. of Physical and Theoretical Chemistry, Getreidemarkt 9/156, A-1060 2008, Vienna, Austria.

Born M. and Oppenheimer R. (1927), Connecting the quantum theory of molecules. *Ann. Phys. Lpz*. **84**: 457-484.

Bosi M. and Pelosi C. (2007), The Potential of III-V Semiconductors as Terrestrial Photovoltaic Devices. *Prog. Photovolt: Res. Appl*. **15**:51–68

Braun J. (1996), The theory of angle-resolved ultraviolet photoemission and its applications to ordered materials. *Rep. Prog. Phys.* **59**: 1267-1338

Brillouin L. (1953), *Wave Propagation in Periodic Structures*, Dover, New York.

Cardona M. and Ley L. (eds) (1978), *Photoemission in Solids I* (*Topics in Applied Physics* vol.26) (Berlin: Springer)

Caroli C., Lederer-Rozenblatt D., Roulet B., Saint-James D. (1973), Inelastic effects in photoemission: microscopic formulation and qualitative discussion. *Phys. Rev.* B **8**: 4552–4569

Carver T. R. (1971), Mathieu's functions and electrons in a periodic lattice. *Amer. J. Phys*. **39** : 1225–1231

Christensen N.E. and Gorczyca I. (1994), Optical and structural properties of III-V nitrides under pressure. *Phys. Rev.* B **50**: 4397–4415

Chu J. and Sher A. (2008), *Physics and Properties of Narrow Gap Semiconductors,* Springer Science, New York.

Corso A.D., Mauri F. and Rubio A. (1996), Density-functional theory of the nonlinear optical susceptibility: Application to cubic semiconductors. *Phys. Rev., B* **53**: 15638-15642

Damascelli A., Hussain Z., Shen Z.X. (2003), Angle-resolved photoemission studies of the cuprate superconductors. *Rev. Mod. Phys.* **75**: 473–541

Damascelli A. (2004), Probing the Electronic Structure of Complex Systems by ARPES. *Physica Scripta* **T109**: 61–74.

Davison S.G. and Steslicka M. (1992), *Basic Theory of Surface State,* Claredon, Oxford University Press.

Deyirmenjian V.B. and Sipe J. E. (1999), Coherent Control of the Angular Distribution of Electrons Photoemitted from Metal Surfaces. *Phys. Rev. Lett.* **82:** 4942-4945.

Dose V. (1983), Ultraviolet Bremsstrahlung Spectroscopy. *Prog. Surf. Sci*. **13**:225-284

Dressel M. and Gruner G. (2003), *Electrodynamics of Solids - Optical Properties of Electrons in Matter*, Cambridge University Press.

Erdiven U and Ufuktepe Y. (2011). Photonic band structures of ZnX (X = S, Se, Te). *Optoelectronics and Advanced materials* **5:** 900-905.

Erkan Erbarut (2003), Optical response functions of ZnS, ZnSe, ZnTe by the LOM method. *Solid State Commun.* **127[7]:** 515-519.

Feibelman P.J. and Eastman D.E. (1974), Photoemission spectroscopy—correspondence between quantum theory and experimental phenomenology. *Phys. Rev*. B **10**: 4932–4947

Feibelman P.J. (1975), Self-Consistent Calculation of the Surface Photoelectric Effect. *Phys. Rev. Lett*. **34**: 1092-1095; Microscopic calculation of electromagnetic fields in refraction at a jellium-vacuum interface *Phys. Rev.* B**12**: 1319-1336

Feuerbacher B., Fitton B. and Willis R. F. (1978), *Photoemission and the Electronic Properties of Surfaces*, Wiley.

Fleszar A. and Hanke W. (2000), Electronic excitations in beryllium chalcogenides from the *ab initio* GW approach. *Phys. Rev.* B **62:** 2466-2474.

Freeouf J. L. (1973), Far-Ultraviolet Reflectance of II-VI Compounds and Correlation with the Penn—Phillips Gap. *Phys. Rev*. B **7**: 3810-3830

Georges A., Kotliar G., Krauth W. and Rozenberg M. J. (1996), Dynamical mean-field theory of strongly correlated fermion systems and the limit of infinite dimensions, *Rev. Mod. Phys.* **68**: 13-125

Ghahramani E., Moss D.J. and Sipe J. E. (1991), Full-band-structure calculation of first-, second-, and third-harmonic optical response coefficients of ZnSe, ZnTe, and CdTe. *Phys. Rev*. B **43**: 9700-9710

Gonzalez-Diaz M., Rodriguez-Hernandez P. and Munoz A. (1997), Elastic constants and electronic structure of beryllium chalcogenides BeS, BeSe, and BeTe from first-principles calculations. *Phys. Rev.* B **55**: 14043-14046

Gunnarsson O., Schönhammer K., Allen J.W., Karlsson K. and Jepsen O. (2001), Information from photoemission spectral weights and shapes. *J. El. Spec. Rel. Phen*. **117-118**: 1-11.

Gunshor R., Nurmikko A. and Koyabashi M. (1992), II – VI semiconductors come of age. *Physics World* **5**: 46-49

Hacini K., Meradji H., Ghemid S., and El Haj Hassan F. (2012), Theoretical prediction of structural, electronic and optical properties of quaternary alloy $Zn_{1-x}Be_xS_ySe_{1-y}$. *Chin. Phys.* B **21**: 036102-1-7

Hammer B., Hansen L.B. and Norskov J.K. (1999), Improved adsorption energetics within density-functional theory using revised Perdew-Burke-Ernzerhof functional. *Phys. Rev.* B **59** : 7413-7421.

Haneman D. (1987), Surfaces of silicon. *Rep. Prog. Phys.*, **50** : 1045-1084

Hassan F. E. H and Akbarzadeh H. (2006), Ground state properties and structural phase transition of beryllium chalcogenides. *Computational Materials Science* **35**: 423-421.

Hedin L. and Lundqvist B. I. (1971), Explicit local exchange-correlation potentials *J. Phys.* C **4**: 2064-2083

Heyd J., Peralta J. E., Scuseria G. E. and Martin R. L. (2005), Energy band gaps and lattice parameters evaluated with the Heyd-Scuseria-Ernzerhof screened hybrid functional. *J. Chem. Phys.* **123**: 174101-1-8

Hohenberg P. and Kohn W. (1964). Inhomogeneous Electron Gas. *Phys. Rev*. **136**: B864-B871.

Huang M.Z. and Ching W.Y., (1993), Calculation of optical excitations in cubic semiconductors. I. Electronic structure and linear response. *Phys. Rev. B* **47**: 9449 – 9463.

Hüfner S. (2003), *Photoelectron Spectroscopy - Principles and Applications*, third edition, Springer, Berlin

Inglesfield, J. E. (1982). Surface electronic structure. *Rep. Prog. Phys*. **45**: 223-284.

Inglesfield J.E. and Plummer E.W. (1992), *The physics of photoemission, Angle-resolved photoemission*, S.D. Kevan (ed.), Elsevier.

Imad Khan, Iftikhar Ahmad, Zhang D., Rahnamaye Aliabad H.A., Jalali Asadabadi S., (2013), Electronic and optical properties of mixed Be-chalcogenides. *Journal of Physics and Chemistry of Solids* **74**: 181-188

Ishii A. and Aisaka T. (1991), Theoretical analysis of angle-resolved photoemission for simple metals. *Surf. Sci*. **242**: 250-255.

Jackson J. D. (2007), *Classical Electrodynamics*, 3rd Edition, Wiley, New Delhi

Jivani A. R. and Jani A. R. (2012), Prediction of some mechanical and vibrational properties of Ga*X* (*X* = P, As, Sb) semiconductor compounds. *Turk J Phys.* **36**: 215 – 223.

Kalpana G., Pari G., Mookerjee A. and Bhattacharyya K. (1998), *Ab initio* Electronic Band Structure Calculations for Beryllium Chalcogenides. *Int. J. Mod. Phys.* B **12**: 1975-1984

Karazhanov S. Zh., Ravindran P., Kjekshus A., Fjellvåg H. and Svensson B. G. (2007), Electronic structure and optical properties of Zn*X* (*X*=O, S, Se, Te): A density functional study. Phys. Rev B **75**: 155104-1-14.

Khenata R., Bouhemadou A., Hichour M., Baltache H., Rached D., Rerat M. (2006), Elastic and optical properties of BeS, BeSe and BeTe under pressure. *Solid-State Electronics* **50**: 1382–1388

Kiejna A. (1999), Stabilized jellium-simple model for simple metal surfaces, *Prog. Surf. Sci.* **61**: 85-125.

Kim Y.D., Cooper S.L., Klein M.V. (1993), Optical characterization of pure ZnSe films grown on GaAs. *Appl. Phys. Lett.* **62**:2387-2389

Kittel C. (1994), *Introduction to Solid State Physics*, fifth ed., Wiley Eastern, India.

Kohn W. and Sham L. J. (1965), Self-Consistent Equations Including Exchange and Correlation Effects. *Phys. Rev. A* **140**: 1133–1138.

Kohn S.E., Yu P.Y., Petroff Y., Shen Y.R., Tsang Y.W. and Cohen M.L. (1973), Electronic Band Structure and Optical Properties of PbTe, PbSe, and PbS. *Phys. Rev*. B**8**: 1477-1488

Korti-Baghdadli N., Merad A. E., and Benouaz T., (2013), Adjusted Adashi's Model of Exciton Bohr Parameter and New Proposed Models for Optical Properties of III-V Semiconductors. *American Journal of Materials Science and Technology* **3**: 65-73

Krasovskii E. E. and Schattke W. (1995), The extended-LAPW-based $\mathbf{k} \cdot \mathbf{p}$ method for complex band structure calculations. *Solid State Commun.* **93**: 775-779

Kronig R.de L. and Penney W.G. (1931), Quantum Mechanics of Electrons in Crystal Lattices. *Proc. Roy. Soc*. A**130**: 499-513.

Kumar G.S. (2013) Analysis of ionicity using plasmon energy and electro negativity differences of binary tetrahedral semiconductors and ionic compounds. *Res. J. Physical Sci.* **1**:5-11

Kumar V., Shrivastava A.K., Anita Sinha and Vijeta Jha (2013), Dielectric properties of different materials. *Indian Journal of Pure and Applied Physics* **51**:49-54

Landau L.D. and Lifsitz E.M. (1984), *The Electrodynamics of Continuous Media* (Pergamon Press, New York) **86** 293-304.

Langreth D. C. and Perdew John P. (1980), Theory of nonuniform electronic systems. I. Analysis of the gradient approximation and a generalization that works. *Phys. Rev.* B **21**: 5469-5493.

Langreth D. C. and Mehl M. J. (1983), Beyond the local-density approximation in calculations of ground-state electronic properties. *Phys. Rev*. B **28**: 1809-1834.

Laref S. and Laref A. (2012), Thermal properties of BeX (X = S, Se and Te) compounds from ab initio quasi-harmonic method. *Computational Materials Science* **51**: 135–140

Levine J.D. (1968), Ionic, Covalent, and Metallic Surface States of a One-Dimensional Mathieu Potential with Arbitrary Termination. *Phys. Rev*. **171**: 701-712

Levinson H.J., Plummer E.W. and Feibelman P.J. (1979), Effects on Photoemission of the Spatially Varying Photon Field at a Metal Surface. *Phys. Rev. Lett.* **43** : 952-955.

Madsen G.H.K., Blaha P., Schwarz K., Sjostedt E., Nordstrom L. (2001), Efficient linearization of the augmented plane-wave method. *Phys. Rev*. B **64**: 195134-1-9.

Mahan G.D. (1970), Theory of photoemission in simple metals. *Phys. Rev*. B**2:** 4334–4350

Malsawmtluanga A., Lalnunpuia, Chhangte Lawrence Z., Ralte Ricky L. and Pachuau Z. (2014), Application of FP-LAPW Method to study Electronic and Optical Properties of Beryllium Chalcogenides BeX (X= S, Se, Te). *Int. J. P. & App. Phys.* **10** [1]: 37-42.

Malsawmtluanga A., Lalnunpuia, Ralte Ricky L. and Pachuau Z. (2014), Study of Electronic and Optical Properties of Gallium pnictides GaX (X= P, As, Sb). *Ind. J. Sci. Res. & Tech.* **2**[5]:108-111.

Malsawmtluanga A., Lalnunpuia, Chhangte Lawrence Z., Ralte Ricky L. and Pachuau Z. (2014), Theoretical investigation of Electronic and Optical Properties of Zinc-blende structure of Beryllium Sulphide BeS. *Sci. Vis.* **14** [2] : 89-93.

Malsawmtluanga A., Lalnunpuia, Chhangte Lawrence Z., Ralte Ricky L. and Pachuau Z. (2012), Application of FP-LAPW Method to study Electronic and Optical Properties of Zinc Chalcogenides ZnX (X= S, Se, Te). In: P*roceeding of 8th National Conference of Physics Academy of North East (PANE),* Mizoram University, Aizawl, 17th -19th December.

Malsawmtluanga A., Lalnunpuia, Ralte Ricky L. and Pachuau Z. (2014), Study of Electronic and Optical Properties of Aluminium pnictides AlX (X= P, As, Sb). *Sci. Vis.* **14[4]**: 195-199

Makinistian L. and Albanesi E. A. (2007), *Ab initio* calculations of the electronic and optical properties of germanium selenide. *J. Phys.: Cond. Matt.*, **19:** 186211, pp.1-24

Maniv T. and Metiu H. (1980), Electrodynamics at a metal surface with applications to the spectroscopy of adsorbed molecules. I. General theory *Phys. Rev.* B**22**: 4731 - 4738

Martienssen W. and Warlimont H. (2005), *Springer Handbook of Condensed Matter and materials Data*, Spinger Berlin Heidelberg New York.

Mastro M. (2011), *III-V compound semiconductors: Integration with Silicon-Based Microelectronics*, (Eds.) Li T., Mastro M. and Dadgar A., CRC Press, Taylor & Francis Group, Boca Raton

McLachlan N.W. (1951), *Theory and Application of Mathieu Functions*, Oxford University Press, New York.

Moll N., Bockstedte M., Fuchs M., Pehlke E. and Scheffler M. (1995), Application of generalized gradient approximations: The diamond–β-tin phase transition in Si and Ge. *Phys. Rev*. B **52**: 2550-2556.

Mukhopadhyay G. and Lundqvist S. (1978), The electromagnetic field near a metal surface. *Physica Scripta* **17**: 69.

Okoye C. M. I. (2004), Structural, electronic, and optical properties of beryllium monochalcogenides. *Eur. Phys. J.* B **39:** 5–17

Pachuau Z., Zoliana B., Khathing D.T., Patra P.K. and Thapa R.K. (2000), Application of Mathieu potential to photoemission from metals. Phys. *Lett*. A**275**: 459-462.

Pachuau Z., Zoliana B., Patra P.K., Khathing D.T., Thapa R.K. (2002) Application of Mathieu potential to photoemission calculation: the case of a strong potential. *Phys. Letts.*, **A 294**: 52-57

Pachuau Z. (2001), *Theoretical Study of Photoemission from Metals and Semiconductors*, Ph.D. thesis, North Eastern Hill University.

Pendry J.B. (1976), Theory of photoemission. *Surf. Sci*. **57** : 679-705.

Penn D.R. (1972), Photoemission Spectroscopy in the presence of adsorbate-covered surfaces. *Phys. Rev. Lett.* **28[16]**: 1041-1044.

Perdew J. P. and Wang Yue (1986), Accurate and simple density functional for the electronic exchange energy: Generalized gradient approximation. *Phys. Rev*. B **33**: 8800-8802.

Perdew J. P. (1986), Density-functional approximation for the correlation energy of the inhomogeneous electron gas. *Phys. Rev*. B **33**: 8822-8824.

Perdew J. P., Chevary J.A., Vosko S.H., Jackson K.A., Pederson M.R., Singh D.J. and Fiolhais C. (1992), Atoms, molecules, solids, and surfaces: Applications of the

generalized gradient approximation for exchange and correlation. *Phys. Rev.* B **46**: 6671-6687.

Perdew J. P., Burke Kieron, and Ernzerhof Matthias (1996), Generalized Gradient Approximation Made Simple. *Phys. Rev. Lett*. **77[18]**: 3865-3868

Postigo P. A., Armelles G., Utzmeier T., and Briones F. (1998), In *situ* optical spectroscopy of Ga dimers on GaP, GaAs, and GaSb by surface chemical modulation. *Phys. Rev. B* **57**: 1359-1361

Plummer E.W. and Eberhardt W. (1982), Angle-Resolved Photoemission as a Tool for the Study of Surfaces. *Advances in Chemical Phys*. **49**: 533-656.

Rabah M., Al-Douri Y., Sehil M., Rached D. (2003), Pressure effect on electronic band structure of III–V compounds. *Mater. Chem. Phys.* **80**: 34-38

Rahaman M., Ganguly S., Samal P., Harbola M. K., Saha-Dasgupta T., Mookerjee A. (2009), A local-density approximation for the exchange energy functional for excited states: The band-gap problem. *Physica B* **404**: 1137–1142

Rashkeev S.N., Lambrecht W.R.L. (2001), Second Harmonic Generation of I-III-VI_2 Chalcopyrite Semiconductors: Effects of Chemical Substitutions. *Phys. Rev. B* **63**: 165212-165224

Reddy R.R., Nazeer Ahammed Y., Abdul Azeem P., Ramma Gopal K., Sasikala Devi B. and Rao T.V.R. (2003), Dependence of Physical Parameters of Compound Semiconductors on Refractive Index. *Defence Science Journal* **53** [3]: 239-248

Remediakis I.N. and Efthimios Kaxiras, (1999), Band-structure calculations for semiconductors within generalized-density-functional theory. *Phys. Rev. B***59**: 5536-5543

Reshak A.H. (2005), First-principle calculations of the linear and nonlinear optical

response for GaX (X = As, Sb, P). *Eur. Phys. J. B* **47**: 503-508

Reshak A.H. (2006), Electronic, linear and nonlinear optical properties of III-V Indium compounds semiconductors. *J. Chemical Phys.* **125**: 034710-1-8.

Reshak A. H. and Auluck S. (2007), Investigation of the electronic properties, first and second harmonic generation for $A^{XIII}B^{XV}$ zinc-blende semiconductors. *Physica B* **395**:143–150

Reshak A.H. and Auluck S. (2007), Ab initio calculations of the electronic, linear and nonlinear optical properties of zinc chalcogenides. *Physica B* **388**: 34-42

Sapra S., Shanthi N. and Sarma D. D. (2002), Realistic Tight Binding Model for the Electronic Structure of II-VI Semiconductors. *Phys. Rev.* B **66**: 205202-1-8

Schaich W.L. and Ashcroft N.W. (1971), Model calculations in the theory of photoemission. *Phys.Rev*. B **3**: 2452–2465

Schattke W. (1997), Photoemission within and beyond the one-step model. *Prog. Surf. Sci*. **54**: 211-227

Schattke W. and Van Hove M. A. (Eds.) (2003), *Solid-State Photoemission and Related Methods*, Wiley-VCH GmbH & Co.

Singh D. (1991). Ground-state properties of lanthanum: Treatment of extended-core states. *Phys. Rev.* B**43**: 6388-6392

Slater J.C. (1952), A Soluble Problem in Energy Bands. *Phys. Rev*. **87**: 807-835

Slater J.C. and Koster G.F. (1954), Simplified LCAO Method for the Periodic Potential Problem. *Phys. Rev*. **94**: 1498-1524.

Statz H. (1950), *Z. Naturforsch*, **5*A*** : 534

Strasser T., Kipp L., Skibowski M. and Schattke W. (2005), Photoemission study of S adsorption on GaAs (001). *New Journal of Physics*, **7**: 115 pp. 1-14

Strehlow W.H. and Cook E.L. (1973), Compilation of Energy Band Gaps in Elemental and Binary Compound Semiconductors and Insulators. *J. Phys. Chem. Ref. Data* **2** : 163-199 and references therein.

Strocov V. N., Starnberg H. I., Nilsson P. O., Brauer, H. E. and Holleboom L. J. (1997), New Method for Absolute Band Structure Determination by Combining Photoemission with Very-Low-Energy Electron Diffraction: Application to Layered VSe_2. *Phys. Rev. Lett.* **79**: 467-470

Strocov V. N., Claessen R., Nicolay G., Hüfner S., Kimura A., Harasawa A., Shin S., Kakizaki A., Nilsson P. O., Starnberg H. I. and Blaha P. (1998), Absolute Band Mapping by Combined Angle-Dependent Very-Low-Energy Electron Diffraction and Photoemission: Application to Cu. *Phys. Rev. Lett.* **81**: 4943

Stukel D. J. (1970), Energy-Band Structure of BeS, BeSe, and BeTe**.** *Phys. Rev.* B **2**: 1852-1858

Thapa R. K. (1993), *A Theoretical Study of Photon fields near Surfaces with Application to Photoemission*, Ph.D. thesis, North Bengal University.

Thapa R.K. and Kar N. (1995), Photocurrent calculations in Beryllium using a local dielectric model. *Phys. Rev*. B **51**: 17980-17983.

Tran F. and Blaha P. (2009), Accurate band gaps of semiconductors and insulators with a semilocal exchange-correlation potential. *Phys. Rev. Lett.* **102**: 226401-1-4

Tsuchiya T., Ozaki S. and Adachi S. (2003), Modelling the optical constants of cubic ZnS in the 0-20 eV spectral region. J. Phys. : Condens. Matter **15**: 3717-3730.

Von Niessen W. (1991), Application of a Green's Function method to the calculation of photoelectron spectra. *Butll. Soc. Cat. Cien.* **XI**: 227-262

Walter J. P., Cohen M. L., Petroff Y. and Balkanski M. (1970), Calculated and Measured Reflectivity of ZnTe and ZnSe. *Phys. Rev*. B **1**: 2661-2667.

Welker H. (1952), Uber neue Halbleiter-Verbindungen. *Z. Naturforsch*. A **7**: 744-749.

Williams R. H., Srivastava G. P. and Mcgovern I. T. (1980), Photoelectron spectroscopy of solids and their surfaces. *Rep. Prog. Phys*. **43**: 1358-1414.

Yadav D. S. and Kumar C. (2013), Structural properties of binary semiconductors. *Int. J. Phys. Sci.* **8**: 1174-1178

Yadav D.S. and Singh S.P. (2010) Electronic properties of aluminum, gallium and indium pnictides. *Phys. Scr.* **82**: 065705-1-4

Yamaguchi M. (2001), Proceeding of 17th Photovoltaic European conference (WIP-Munich and ETZ-Florence) 2144.

Yamasaki T., Suzuki N. and Motizuki K. (1987), Electronic structure of intercalated transition-metal dichalcogenides: M_xTiS_2 (M=Fe, Cr). *J. Phys. C* **20:** 395-404

Yim W. M., Dismukes J. P., Stofko E. J. and Paff R. J. (1972), Synthesis and some properties of BeTe, BeSe and BeS**.** *J. Phys. Chem. Solids* **33:** 501-505

Zachariasen W. (1926), Simple Oxide. *Z. Phys. Chem.* **119**: 201-213.

Zoliana B., Pachuau Z., Lalthakimi Zadeng, Khathing D.T. and Thapa R.K. (2003), A model photoemission calculations using projection operator method. *Intl. J. Mod. Phys*. B **17**: 2897-2902.

Zupan A., Burke K., Ernzerhof M., and Perdew J.P. (1997), Distributions and averages of electron density parameters: Explaining the effects of gradient corrections, *J. Chem. Phys.* **106**: 10184-10193.

APPENDIX I

CALCULATION OF PHOTOCURRENT BY USING WAVEFUNCTION DEDUCED BY MATHIEU POTENTIAL MODEL FOR THE SURFACE STATE (THE CASE OF STRONG POTENTIAL)

We consider a periodic lattice potential represented by sinusoidal Mathieu potential function $V(z)=V_a \cos\left(\frac{2\pi z}{a}\right)$, where $2q=\frac{V_a}{a}$, and a is the lattice constant as shown in Fig. (3.1) of Chapter 3. The most general form for the initial state wavefunction will be a linear combination of sine and cosine elliptic functions for all the Fermi gap m which is given by

$$\phi(z_0', q)=\lambda_m \, ce_m(z_0', q)-se_m(z_0', q) \quad \ldots \quad (I.1)$$

where λ_m is the hybridization parameter which can be written as

$$\lambda_m=\frac{se_m(z_0', q)-(\xi+\mu)^{-1} se_m'(z_0', q)}{ce_m(z_0', q)-(\xi+\mu)^{-1} ce_m'(z_0', q)} \quad \ldots \quad (I.2)$$

The sine and cosine elliptic functions in the expanded form can be written as

$$se_m(z_0', q)=\sin m z_0'-\frac{q}{4}\left[\frac{\sin(m+2)z_0'}{m+1}-\frac{\sin(m-2)z_0'}{m-1}\right]$$

$$+\frac{q}{3}\left[\frac{\sin(m+4)z_0'}{(m+1)(m+2)}+\frac{\sin(m-4)z_0'}{(m-1)(m-2)}\right]+\ldots\ldots\ldots \quad \ldots \quad (I.3)$$

and $$ce_m(z_0', q)=\cos m z_0'-\frac{q}{4}\left[\frac{\cos(m+2)z_0'}{m+1}-\frac{\cos(m-2)z_0'}{m-1}\right]$$

$$+\frac{q}{3}\left[\frac{\cos(m+2)z_0'}{(m+1)(m+2)}+\frac{\cos(m-4)z_0'}{(m-1)(m-2)}\right]+\ldots\ldots\ldots \quad \ldots \quad (I.4)$$

For finite surface potential (q > 0), surface state existence condition implies that

$$z_0 = \frac{a}{2},\ \xi = \frac{12}{a},\quad \lambda > 0 \quad \text{and} \quad m = 3,5,\ldots\ldots \qquad \ldots \text{(I.5)}$$

We are considering surface state occurring for m = 3 and hence we can write,

$$ce_3(z_0', q) = 0 \quad , \qquad ce_3'(z_0', q) = 3\left(1 + \frac{q}{16} - \frac{q^2}{640}\right)$$

$$se_3(z_0', q) = -1 + \frac{q}{16} - \frac{11}{640}q^2 \quad , \qquad se_3'(z_0', q) = 0 \qquad \ldots \text{(I.6)}$$

The hybridization constant λ_3 now reduces to:

$$\lambda_3 = \frac{(\xi + \mu)\left[1 - \frac{q}{16} + \frac{11}{640}q^2\right]}{3\left(1 + \frac{q}{16} - \frac{q^2}{640}\right)} \qquad \ldots \quad \text{(I.7)}$$

Since Eq. (I.5) is the condition for the surface state existence, with the help of Eqs. (I.6) and (I.7), therefore the final form of initial state wavefunctions corresponding to electronic states in the surface and bulk, and vacuum regions, can be written as

$$\psi_i(z, q) = \begin{cases} \left(\frac{1}{4\pi k_i}\right)^{\frac{1}{2}}\left(1 - \frac{q}{16} + \frac{11}{640}q^2\right)e^{-\mu(z_0' - z)}, & z \le 0 \\ (2\xi)^{\frac{1}{2}}\, e^{-\xi(z - z_0')}, & z \ge 0 \end{cases} \qquad \ldots \quad \text{(I.8)}$$

Photocurrent had been calculated by using the formula,

$$\frac{d\, j(E)}{d\,\Omega} = \frac{2\pi}{\hbar}\sum_f \left|\langle \psi_f \left| \mathrm{H}^{/} \right| \psi_i \rangle\right|^2 \delta(E - E_f)\,\delta(E_f - E_i - \hbar\omega)\, f_o(E - \hbar\omega)\left[1 - f_o(E)\right] \quad \ldots \text{(I.9).}$$

In Eq. (I.9) above, ψ_i is given by Eq. (I.8), and ψ_f and perturbation term $\mathrm{H}^{/}$ in one-dimension is

$$\psi_f(z)=\begin{cases}\left(\frac{1}{2\pi q_f}\right)^{\frac{1}{2}}\frac{2q_f}{q_f+k_f}e^{ik_f z}e^{-\alpha|z|} & z\le 0\\ \left(\frac{1}{2\pi q_f}\right)^{\frac{1}{2}}\left(e^{iq_f z}+\frac{q_f-k_f}{q_f+k_f}\right)e^{-iq_f z} & z\ge 0\end{cases} \quad \ldots \text{(I.10)}$$

$$H' = \frac{e}{mc}\left[\tilde{A}_\omega(z)\frac{d}{dz}+\frac{1}{2}\frac{d\tilde{A}_\omega(z)}{dz}\right] \quad \ldots \text{(I.11)}$$

Matrix element in Eq. (I.9) can be expanded as

$$\mathbf{I}= \int_{-\infty}^{-d}\psi_f^*\,\tilde{A}_\omega\,\psi_i\,dz+\int_{-d}^{0}\psi_f^*\,\tilde{A}_\omega\frac{d}{dz}\psi_i\,dz+\frac{1}{2}\int_{-d}^{0}\psi_f^*\frac{d\tilde{A}_\omega}{dz}\psi_i\,dz+\int_0^\infty\psi_f^*\,\tilde{A}_\omega\varepsilon(\omega)\frac{d}{dz}\psi_i dz$$

$$\ldots \text{(I.12)}$$

$$= I_1 + I_2 + I_3 + I_4 \quad \ldots \text{(I.13)}$$

Using Eqs. (I.8), (I.10) and (I.11), the integrals in Eq.(I.13) can now be expanded as follows:

$$I_1 = \int_{-\infty}^{-d}\psi_f^*\,\tilde{A}_\omega\,\psi_i\,dz$$

$$= \frac{1}{2\pi}\left(\frac{1}{2q_f k_i}\right)\frac{2q_f}{q_f+k_f}A_1(2\mu+\xi)e^{-\frac{\mu\pi}{2}}\left[1-\frac{q}{16}+\frac{11}{640}q^2\right]$$

$$\times\int_{-\infty}^{-d}e^{(a+\mu)z}e^{-ik_f z}dz$$

$$= \frac{1}{\pi(a+\mu)}\left(\frac{1}{2q_f k_i}\right)\frac{q_f}{q_f+k_f}A_1(2\mu+\xi)e^{-\frac{\mu\pi}{2}}\left[1-\frac{q}{16}+\frac{11}{640}q^2\right]$$

$$\times e^{-[\mu z_0+(a+\mu)d]}\int_{-\infty}^{-d}e^{-ik_f z}dz$$

$$= \frac{1}{\pi(a+\mu)}\left(\frac{1}{2q_f k_i}\right)\frac{q_f}{q_f+k_f}A_1(2\mu+\xi)e^{-\frac{\mu\pi}{2}}\left[1-\frac{q}{16}+\frac{11}{640}q^2\right]$$

$$\times e^{-[\mu z_0+(a+\mu)d]}\int_{-\infty}^{-d}\left(\cos k_f z - i\sin k_f z\right)dz \qquad \ldots \quad (I.14)$$

$$I_2 = \int_{-d}^{0}\psi_f^{*}\,\tilde{A}_\omega\,\frac{d\psi_i}{dz}\,dz$$

$$= \frac{1}{2\pi}\left(\frac{1}{2q_f k_i}\right)\frac{2q_f}{q_f+k_f}A_1(2\mu+\xi)e^{-\frac{\mu\pi}{2}}\left[1-\frac{q}{16}+\frac{11}{640}q^2\right]$$

$$\times\varepsilon(\omega)d\int_{-d}^{0}\frac{1}{[1-\varepsilon(\omega)]z+d}e^{(a+\mu)d}e^{-ik_f z}\,dz$$

$$= \frac{1}{\pi}\left(\frac{1}{2q_f k_i}\right)\frac{q_f}{q_f+k_f}A_1(2\mu+\xi)e^{-\frac{\mu\pi}{2}}\left[1-\frac{q}{16}+\frac{11}{640}q^2\right]$$

$$\times\varepsilon(\omega)d\left[e^{-(a+\mu)d}-1\right]\int_{-d}^{0}\frac{1}{[1-\varepsilon(\omega)]z+d}e^{-ik_f z}\,dz$$

$$= \frac{1}{\pi}\left(\frac{1}{2q_f k_i}\right)\frac{q_f}{q_f+k_f}A_1(2\mu+\xi)e^{-\frac{\mu\pi}{2}}\left[1-\frac{q}{16}+\frac{11}{640}q^2\right]$$

$$\times\varepsilon(\omega)d\left[e^{-(a+\mu)d}-1\right]\int_{-d}^{0}\frac{1}{[1-\varepsilon(\omega)]z+d}(\cos k_f z - i\sin k_f z)dz \qquad \ldots \ (I.15)$$

$$I_3 = \frac{1}{2}\int_{-d}^{0}\psi_f^{*}\,\frac{d\,\tilde{A}_\omega}{dz}\psi_i\,dz$$

$$= \frac{1}{2\pi}\left(\frac{1}{2q_f k_i}\right)\frac{q_f}{q_f+k_f}A_1(2\mu+\xi)e^{-\frac{\mu\pi}{2}}\left[1-\frac{q}{16}+\frac{11}{640}q^2\right]$$

$$\times\varepsilon(\omega)d\,e^{-\frac{\mu\pi}{2}}\int_{-d}^{0}e^{az}e^{-ik_f z}\,\frac{d}{dz}\left\{\frac{1}{[1-\varepsilon(\omega)]z+d}e^{\mu z}\right\}dz$$

$$= \frac{1}{2\pi}\left(\frac{1}{2q_f k_i}\right)\frac{q_f}{q_f+k_f}A_1(2\mu+\xi)e^{-\frac{\mu\pi}{2}}\left[1-\frac{q}{16}+\frac{11}{640}q^2\right]$$

$$\times \varepsilon(\omega) d[1-\varepsilon(w)] \int_{-d}^{0} e^{(a+\mu)z} e^{-ik_f z} \frac{1}{\{[1-\varepsilon(\omega)]z+d\}^2} dz$$

$$= \frac{1}{2\pi}\left(\frac{1}{2q_f k_i}\right)\frac{q_f}{q_f+k_f} A_1(2\mu+\xi) e^{-\frac{\mu\pi}{2}}\left[1-\frac{q}{16}+\frac{11}{640}q^2\right]$$

$$\times \varepsilon(\omega) d[1-\varepsilon(\omega)]\left[e^{-(a+\mu)}-1\right]\int_{-d}^{0} \frac{1}{\{[1-\varepsilon(\omega)]z+d\}^2}(\cos k_f z - i\sin k_f z) dz \quad \ldots \quad (I.16)$$

$$I_4 = \int_0^\infty \psi_f^* \tilde{A}_\omega \varepsilon(\omega) \frac{d\psi_i}{dz} dz$$

$$= \frac{1}{2\pi}\left(\frac{1}{2q_f k_i}\right) A_1 \varepsilon(\omega) e^{-\frac{\mu\pi}{2}} \int_0^\infty \left[e^{-iq_f z} + \frac{q_f - k_f}{q_f + k_f} e^{iq_f z}\right]$$

$$\times \frac{d}{dz}[\lambda_3 ce_3(z_0, q) - se_3(z_0, q)] dz$$

$$= \frac{1}{2\pi}\left(\frac{1}{2q_f k_i}\right) A_1 \varepsilon(\omega) e^{-\frac{\mu\pi}{2}} \int_0^\infty \left[e^{-iq_f z} + \frac{q_f - k_f}{q_f + k_f} e^{iq_f z}\right]$$

$$\times e^{-\xi z}(2\xi+3\mu)\left(1-\frac{q}{16}+\frac{11}{640}q^2\right) dz$$

$$= \frac{1}{2\pi}\left(\frac{1}{2q_f k_i}\right) A_1 \varepsilon(\omega) e^{-\frac{\mu\pi}{2}}(2\xi+3\mu)\left(1-\frac{q}{16}+\frac{11}{640}q^2\right)$$

$$\times \int_0^\infty \left[e^{-iq_f z} + \frac{q_f - k_f}{q_f + k_f} e^{iq_f z}\right] e^{\xi z} dz \quad \ldots \quad (I.17)$$

Photocurrent is calculated by evaluating the integrals I_1 , I_2 , I_3 and I_4 by writing FORTRAN programmes, details of which is given in APPENDIX- II.

APPENDIX II

FORTRAN PROGRAMME FOR PHOTOCURRENT CALCULATIONS BY USING MATHIEU POTENTIAL MODEL (THE CASE OF STRONG POTENTIAL)

```
c     _____________________________________________________
c     Name of program : MATH1.FOR (MATHU1.FOR)
c     SURFACE STATE CALCULATIONS, z extends from -d to 0.
c     Written by Dr. R.K. Thapa, Dept. of Physics, MZU
c     Updated by Dr. Z. Pachuau, Last change: 9 Aug 2014 9:21 pm
c     Program to calculate photocurrent by using Mathieu potential model
c     Refer : Phys. Letts. A294 (2002)52-57.
c     _____________________________________________________
c     alamb3 = (xi+mu)*0.295         q <---> aqq
c     alamb3 = 1.275                 mu <---> amu
c     mu=0.5                       zo'<--->xo
c     xi=2.0                       xo --> is the location of the
c     m=3.                               surface state wavefunction.
c     qm=1.
c     q=1,
c     zo'=(pi/a)*zo
c     a=6.
c     _____________________________________________________
      complex a1,ci,t2,t3,eps,cmplx,aqf,ex,ttf,ttx,tty
      common aki,akf,aqf,ci,d,amu,aqq,alpha,xo
      ci=cmplx(0.,1.)
      pi=22./7.
      OPEN (UNIT=1,FILE="ZnTe.in")
      OPEN(UNIT=6,FILE="ZnTe(0).out")
      read (1,*)np,nint
      read(1,*)  ei,theta,d,vz,alpha,amu,aqq,xo,ne
c     read (1,*) ei,theta,d,a,mu,xi,vz,alpha,ne
c     write (np,2) ei,theta,d,a,mu,xi,vz,alpha,ne
      aki=sqrt(2.*ei)
      do 90 ie=1,ne
       read (1,*) w,eps1,eps2
        wev=w*27.2
          akf=sqrt(2.*(ei+w))
          ex=ei+w-vz
         aqf=sqrt(2.*ex)
       ttx=aqf-akf
       tty=aqf+akf
       ttf=ttx/tty
      eps=cmplx(eps1,eps2)
      call refrac (w,wp,theta,eps,a1)
      call term2 (a1,eps,t2,nint)
      call term3 (a1,eps,t3,nint)
c      write (np,3) w,aqf,t2,t3
```

```
      xint=cabs(t2+t3)
      xcur=xint*xint
      cur=(xcur*akf*akf)/w
c       cur=cur/0.157637E-01
c       write (np,3) wev,eps1,eps2,cur
          write (np,3) wev,cur
c  3   format(2x,f8.4,2x,2(f15.6,2x),2x,f20.6,2x)
  3   format(2x,f8.4,10x,f20.6,2x)
c   5    format (2x,'w=',f7.4,2x,'eps=',2(f15.6,1x),'cur='e15.6)
   90   continue
      stop
      end

c     ____________________________________________________________
      subroutine term2 (a1,eps,t2,nint)
      complex eps,a1,t2,r1,ci,f1,q,aqf
      dimension f1(700),f2(700)
      common aki,akf,aqf,ci,d,amu,aqq,alpha,xo
      ci=cmplx(0.,1.)
      q1=(1.-(aqq/16.)+(11./640.)*aqq**2.)
      q=a1*d*eps*q1*amu
      q=q*sqrt(1./(2.*aqf*aki))*(aqf/(aqf+akf))
      ag=-d
      ah=0.
      dd=(ah-ag)/(nint-1)
      do 10 i=1, nint
      x=ag+(i-1)*dd
      amx=amu*(xo-x)
      f1(i)= (cos(akf*x)-ci*sin(akf*x))*exp(-amx)
   10   f1(i)=f1(i)*EXP(-alpha*x)/((1.-eps)*x+d)
      call sint(ag,ah,f1,nint,r1)
      t2=r1*q/3.1416
      return
      end
c     ____________________________________________________________
      subroutine term3 (a1,eps,t3,nint)
      complex eps,a1,t3,r1,ci,f1,cmplx,q,aqf
      dimension f1(700),f2(700)
      common aki,akf,aqf,ci,d,aqq,amu,alpha,xo
      ci=cmplx(0.,1.)
      q1=(1.-(aqq/16.)+(11./640.)*aqq**2.)
      q=a1*d*eps*q1
      q=q*sqrt(1./(2.*aqf*aki))*(aqf/(aqf+akf))
      ag=-d
      ah=0.
      dd=(ah-ag)/(nint-1)
      do 10 i=1,nint
      x=ag+(i-1)*dd
      amx=amu*(xo-x)
      f1(i)=(cos(aqf*x)-ci*sin(aqf*x))*exp(-amx)
```

```
   10   f1(i)=f1(i)*EXP(-alpha*x)/((1.-eps)*x+d)**2.
        call sint(ag,ah,f1,nint,r1)
        t3=r1*q/(2.*3.1416)
        return
        end
c       _____________________________________________________________
c       This subroutine calculates the portion a1 of the field.
c       _____________________________________________________________
        subroutine refrac (w,wp,theta,eps,a1)
        complex a1,cx,csqrt,eps,ci,cmplx,cy
        s2=sin(2.*theta)
        s1=sin(theta)
        c1=cos(theta)
c       b1=1.-eps
c       b1=1./(b1*x+d)
        cy=eps-s1*s1
        cx=csqrt(cy)
        a1=-s2/(cx+eps*c1)
        return
        end
c       _____________________________________________________________
c       This subroutine performs integration of term1 and term2
c       by using SIMPSON'S ONE THIRD RULE
c       _____________________________________________________________
        subroutine sint (a,b,f,n,r)
        complex f,r,s
        dimension f(n)
        h=(b-a)/(n-1)
        s=0.0
        s=s+f(1)+f(n)
        m=n-1
        do 10 i=2,m,2
   10   s=s+4.*f(i)+2.*f(i+1)
        r=h*s/3.
        return
        end
```

Biodata

Name	:	Aldrin Malsawmtluanga
Father's Name	:	R. Lalkhawhluna
Date of Birth	:	04. 01 . 1977
Office Address	:	Mizoram Science Centre Mizoram Council of Science & Technology Govt. of Mizoram
Home Address	:	Tuikual South, A-94/2, Aizawl-796001 Mizoram.
E-mail Address	:	aldmst@rediffmail.com aldmst@gmail.com
Designation	:	Scientific Officer
Year of entry into Service	:	2002
Working Experience	:	13 years
Publications	:	Five(5) papers published and six (6) conference papers (See Research Publications).

Academic Qualifications :

Sl.No.	Examination	Division	% of marks	Year	Board/ University
1	HSLC	First	72.66	1992	MBSE
2	P.U. (Sc)	Second	57.3	1995	NEHU
3.	B.Sc.(Physics)	Second	54.5	1998	NEHU
4	M.Sc.(Physics)	First	66.94	2000	NEHU

RESEARCH PUBLICATIONS

I. Journal Papers

1. **Aldrin Malsawmtluanga**, Lalnunpuia, Lawrence Z. Chhangte, Ricky L. Ralte and Z. Pachuau, (2014), Application of FP-LAPW Method to study Electronic and Optical Properties of Beryllium Chalcogenides BeX (X= S, Se, Te). *International Journal of Pure and Applied Physics* **10** [1]: 37-42.

2. **Aldrin Malsawmtluanga**, Lalnunpuia, Ricky L. Ralte and Z. Pachuau (2014), Study of Electronic and Optical Properties of Gallium pnictides GaX (X= P, As, Sb). *Indian Journal of Scientific Research & Technology* **2**[5]:108-111.

3. **Aldrin Malsawmtluanga**, Lalnunpuia, Lawrence Z. Chhangte, Ricky L. Ralte and Z. Pachuau (2014), Theoretical investigation of Electronic and Optical Properties of Zinc-blende structure of Beryllium Sulphide BeS. *Sci. Vis.* **14** [2] : 89-93.

4. Ricky Ralte, **Aldrin Malsawmtluanga**, Lalrintluanga Sailo, Lalnunpuia and Z. Pachuau (2014), Study of band structure and spin splitting energy in Gallium (GaX, X=P,As,Sb) compounds using GGA and mBJ-GGA method. *International Journal of Innovative Science, Engineering & Technology* **1** [9]: 389-394

5. **Aldrin Malsawmtluanga**, Lalnunpuia, Lawrence Z. Chhangte, Ricky L.Ralte and Z. Pachuau (2012), Application of FP-LAPW Method to study Electronic and Optical Properties of Zinc Chalcogenides ZnX (X= S, Se, Te). In: P*roceeding of 8th National Conference of Physics Academy of North East (PANE),* Mizoram University, Aizawl, 17th -19th December (*In press*).

6. Lalnunpuia, **Aldrin Malsawmtluanga**, Z. Pachuau and R. K. Thapa (2012), Surface state photocurrent calculations in magnetic solids. *Sci. Vis.* **12** [1]: 11-16.

7. **Aldrin Malsawmtluanga**, Lalnunpuia, Ricky L. Ralte and Z. Pachuau (2015), Study of Electronic and Linear Optical Properties of Indium pnictides InX (X= P, As, Sb). *International Journal of Physics and Applications* **7 [1]**: 9-14.

8. **Aldrin Malsawmtluanga**, Lalnunpuia, Ricky L. Ralte and Z. Pachuau(2014), Study Electronic and Optical Properties of Aluminium pnictides AlX (X= P, As, Sb). *Science Vision* **14[4]**: 195-199

II. Conference Papers

1. **Aldrin Malsawmtluanga**, Lalnunpuia, Lawrence Z. Chhangte, Ricky L. Ralte and Z. Pachuau (2014), Application of FP-LAPW Method to study Electronic and Optical Properties of Beryllium Chalcogenides BeX (X= S, Se, Te). *International Conference cum Exhibition on Drugs Discovery and Development from Natural Resources*, RIPANS, Aizawl, 5^{th} – 6^{th} February.
2. Lalnunpuia, **Aldrin Malsawmtluanga**, L. Zonunmawia and Z. Pachuau (2012), Surface state photocurrent calculations in magnetic solids by using relativistic and non-relativistic Kronig-Penney potential model, *8^{th} National Conference of Physics Academy of North East*, Mizoram University, Aizawl, 17^{th} – 19^{th} December.
3. **Aldrin Malsawmtluanga**, Lalnunpuia, Z. Pachuau & R. C. Tiwari (2010), Electromagnetic Fields near the surface of semiconductor materials using a

local dielectric model. *National Conference on Condensed Matter Physics*, NEHU, Shillong, 22nd – 23rd March.

4. Lalnunpuia, **Aldrin Malsawmtluanga**, Z. Pachuau (2010), Photocurrent Calculations from the Surface State of d-block Metals using the Mathieu Potential. *National Conference on Condensed Matter Physics*, NEHU, Shillong, 22nd – 23rd March.
5. **Aldrin Malsawmtluanga**, Lalnunpuia, Z. Pachuau & R. C. Tiwari (2010), Electromagnetic Fields in Semiconductor Alloys near the surface by using a local dielectric model. *National Seminar on Condensed Matter Physics (SCMP-2010)*, Tripura University, Agartala, 16th February.
6. Lalnunpuia, **Aldrin Malsawmtluanga** & Z.Pachuau (2010), Surface State Photocurrent Calculations in Magnetic Solids by using the Mathieu Potential. *National Seminar on Condensed Matter Physics (SCMP-2010)*, Tripura University, Agartala, 16th February.

International Journal of Pure and Applied Physics.
ISSN 0973-1776 Volume 10, Number 1 (2014), pp. 37-42

http://www.ripublication.com

Application of FP-LAPW Method to Study Electronic and Optical Properties of Beryllium Chalcogenides BeX (X= S, Se, Te)

Aldrin Malsawmtluanga[1*], Lalnunpuia[2], Lawrence Z. Chhangte[3], Ricky L.Ralte[1], Z.Pachuau[1]

Department of Physics, Mizoram University, Aizawl 796 004, Mizoram, India
Physics Department, Govt. Champhai College, Champhai 796321, Mizoram, India
Physics Department, Govt. Zirtiri Residential Science College, Aizawl 796 001, Mizoram, India
**Author for CorrespondenceE-mail: aldmst@rediffmail.com, Mob.: 09436351500*

Abstract

We have applied the full-potential linearized augmented plane wave (FP-LAPW) method) within density-functional theory (DFT) to study the theoretical study of electronic and optical properties of BeX (X = S, Se, Te) as implemented in WIEN2k code. Our results are in agreement with previous theoretical and experimental studies on this important semiconductor compounds. For the optical calculations, the dipole approximation is used. The imaginary part of dielectric function is calculated in momentum representation, which requires matrix elements of the momentum *p* between occupied and unoccupied states. The microscopic origin of the main features in the optical spectra is identified and also the factors responsible for most of the optical absorption.

Key words: BeX, FP-LAPW, band structure, optical property, WIEN2k.

PACS Nos.: 71.15.Ap, 71.15.Mb, 71.20.Nr, 78.20.Ci

1. Introduction

There is an intense investigation of wide band gap semiconductors because of their unusual properties and possible applications in various electrical and optical devices. Keeping this in mind the group IV and III–V compounds have been extensively studied theoretically as well as experimentally. Recently, there has been a dedicated

effort to understand the II–VI compounds. In fact, probably as a result of their very high toxic nature only few experimental studies [1] have been performed on these compounds but more theoretical studies of these compounds are available in the literature [2-13]. Theoretical calculation of the optical and electronic properties of BeX (X = Te, Se and S) compounds were performed by Stukel [2] using a first-principle self-consistent orthogonalized-plane wave (OPW). The calculated dielectric functions were not compared with the experimental data because no data were available at that time. A few non-relativistic local density approximation (LDA) calculations of the structural, electronic and optical properties have been performed [3, 4] for beryllium monochalcogenides. Fleszar and Hanke [5] have calculated electronic excitations in BeX using the many-body Green's functions technique (GW) and have given a detailed discussion of LDA versus GW. Hassan and Akbarzadeh [6] have present detail calculation of the band structure using more advanced Engel Vosko's GGA (EV-GGA) formalism. Imad Khan et al. [7] have calculated electronic and optical properties of mixed Be-Chalcogenides with the FP-LAPW method using a recently developed modified Beck and Johnson potential. The structural and electronic properties have also been theoretically investigated using the tight-binding linear muffin-tin orbital method (TB-LMTO) [12].

The aim of this paper is to give a comparative and complementary study of electronic properties to both experimental and other theoretical works by using FP-LAPW method as well as optical studies for BeS, BeSe and BeTe.

2. Calculation Method

We have calculated the optical properties of BeX using the FPLAPW method [14] as implemented in the WIEN2K package [15]. We choose the exchange-correlation potential parameterized by Perdew et al. [16] which is derived by using the generalized gradient approximation (GGA). In the FPLAPW method, a basis set is obtained by dividing the unit cell into non-overlapping atomic spheres (centered on the atomic sites) and an interstitial region. Inside the atomic sphere, a linear combination of radial function times spherical harmonic is used, and in the interstitial region a plane wave expansion is augmented by an atomic like function in every atomic sphere. This method yields accurate energy eigenvalues and wavefunctions, therefore appropriate for calculating the electronic and optical properties of crystalline solids. We have chosen sphere radii of 1.8 Å for Be, 2.1 Å, 2.4 Å and 2.8 Å respectively for S, Se and Te. For our calculation, we used lattice parameters a = 4.8630 Å, 5.1520 Å, and 5.6270 Å for BeS, BeSe, and BeTe respectively [17]. The values of Kmax × RMT = 7.0 (where RMT is the atomic sphere radius and Kmax is the interstitial plane wave cut-off), In the atomic region, the basis set consists of spherical harmonics with angular quantum number l = 10 and a non spherical contribution with l = 4 are kept constant throughout the calculations The self-consistent iterations are considered to be converged when the total energy of the system are stable within 10^{-5} Ry. The semiconducting beryllium chalcogenides crystallized in the zinc-blende structure. The space group is F-43 m. The Be atom is located at the origin and the X atom is located at (1/4, 1/4, 1/4). In a cubic unit cell

only one component of the dielectric function has to be calculated, i.e. ε_{xx}, written as

$$\varepsilon(\omega) = \varepsilon_1(\omega) + i\varepsilon_2(\omega) \quad (1)$$

describes the optical response of the system at all photon energies $E = \hbar\omega$. The imaginary part of the dielectric function $\varepsilon_2(\omega)$ is given by [18]

$$\varepsilon_2(\omega) = \left(\frac{4\pi e^2}{m^2\omega^2}\right)\sum_{ij}\langle i|M|j\rangle^2 f_i\left(1-f_j\right)\times\delta\left(E_F - E_i - \omega\right)d^3k \quad (2)$$

where M is the dipolematrix element, i and j are the initial and final states, respectively, fi is the Fermi distribution function for the i^{th} state. E_i is the energy of electron in the i^{th} states. The real part of the dielectric function $\varepsilon_1(\omega)$ can be extracted from the imaginary part of the dielectric function $\varepsilon_2(\omega)$ by using the Kramers–Kronig relation [19]

$$\varepsilon_1(\omega) = 1 + \frac{2}{\pi}P\int_0^\infty \frac{\omega'\varepsilon_2(\omega')}{(\omega'^2-\omega^2)}d\omega' \quad (3)$$

where P implies the principal value of the integral.

3. Results and discussions

3.1. Electronic properties

The calculated total density of states, the partial density of states and band structures for Beryllium chalcogenides are shown in figures 1, 2 and 3. The band structure calculated for BeS, BeSe and BeTe are rather similar. The valence band maximum (VBM) occurs at the Γ point and conduction band minimum (CBM) at the X point resulting in an indirect gap in agreement with experiment and previous theoretical work [1–13]. The lowest-lying band shown in the graph arises mainly from the chalcogen valence *s* states and the upper valence bands arises from the chalcogen valence *p* states with the top occurring at the Γ point. The conduction band arises mainly from the 2*s*-Be states with the minimum energy occurring at X-points.

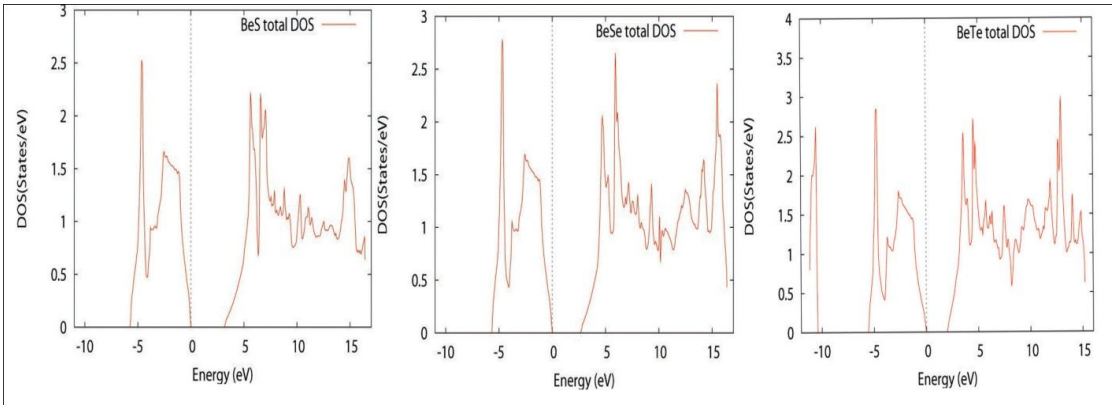

Fig. 1. Total Density of States for BeS, BeSe and BeTe

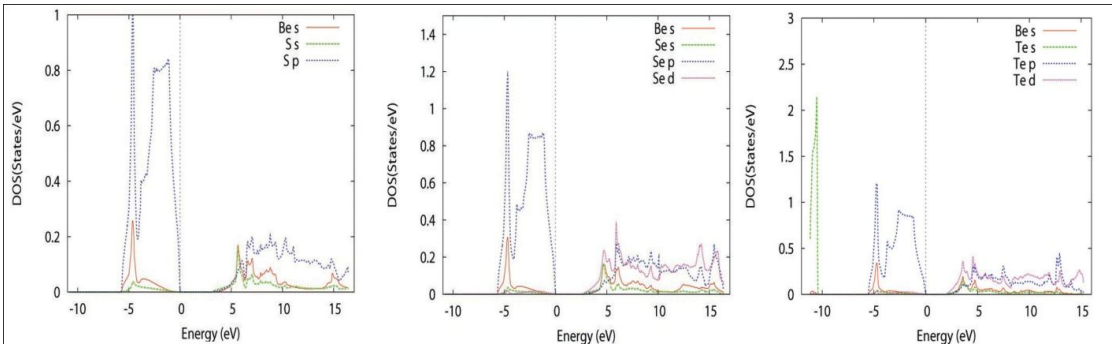

Figure 2. Partial Density of States for BeS, BeSe and BeTe

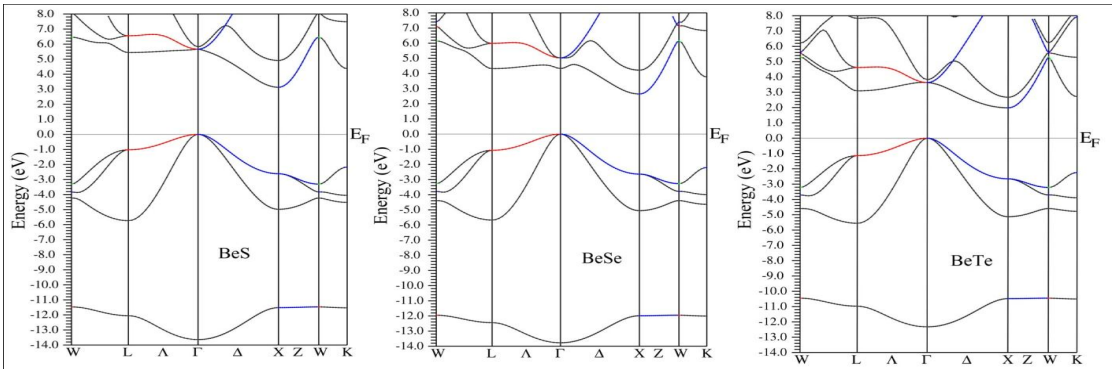

Figure 3. Band structure for BeS, BeSe and BeTe

Table 1: Our calculated energy band gap values and the experimental and theoretical band gap (all values are in eV)

System study	Expt. Band gap	Theoretical Band gap				Present work GGA
		OPW	TB-LMTO	EV	GGA	
BeS	>5.5[a]	4.17[b]	3.78[c]	4.23[d], 4.26[f], 4.241[g], 4.247[h]	3.12[d], 4.20[e], 3.14[f], 3.141[g], 3.148[h], 2.911[i]	3.12
BeSe	4-4.5[a]	3.61[b]	3.12[c]	3.61[d], 3.64[f], 3.655[g], 3.634[h]	2.66[d], 3.55[e], 2.67[f], 2.682[g], 2.672[h],	2.64
BeTe	2.7[a]	2.94[b]	2.17[c]	2.79[d], 2.81[f], 2.921[g]	1.98[d], 2.60[e], 2.03[f], 2.070[g],1.879[i]	1.98

[a]Ref. [1], [b]Ref. [2], [c]Ref. [12], [d]Ref. [6], [e]Ref. [7], [f]Ref. [8], [g]Ref. [9], [h]Ref. [10], [i]Ref. [11],

The band gap of semiconductor BeX in the tetragonal phase as calculated by using the FP-LAPW method and using GGA approximation was found to be 3.12 eV, 2.64 eV and 1.98 eV for BeS, BeSe & BeTe respectively. The important features of the band structure for each compound are given in Table 1. It is clearly seen that the band gap obtained by GGA are lower than the corresponding experimental values and

results obtained from OPW and EV-GGA and not far from the results obtained by the TB-LMTO methods with the same exchange correlation approximation. This underestimation of the band gap is mainly due to the fact that the simple forms of GGA are not sufficiently flexible to accurately reproduce both exchange correlation energy and its charge derivative.

3.2. Optical properties

The determination of the optical properties of a compound in the spectral range above its band gap plays an important role in the understanding of the nature of that material and also gives a clear picture of its applications in optoelectronic devices. The detailed variation of real, $\varepsilon_1(\omega)$ and imaginary $\varepsilon_2(\omega)$ parts of the dielectric function for BeX with photon energy are shown in Figure (4). The $\varepsilon_1(\omega)$ spectra appears at the same energy as a peak in the corresponding $\varepsilon_2(\omega)$ spectra. Metallic reflectance characteristics are exhibited in the range of $\varepsilon_1(\omega) < 0$. We have found that the three compounds have the same structure that is attributed to the fact that the band structures of these compounds are similar with minor differences causing insignificant changes in the structures of $\varepsilon_2(\omega)$. The decrease in the energy band gap moving from S to Se to Te causes to shift the whole structure $\varepsilon_2(\omega)$ to lower energies by around 1.0 eV, resulting in the edge of optical absorption (fundamental absorption edge) for $\varepsilon_2(\omega)$, which is located at 5.6, 4.45 and 3.6 eV. These edges of optical absorption give the threshold for direct optical transitions between the highest valence and the lowest conduction band along the symmetry lines Γ.

The peak of the imaginary part of the dielectric function is related to the electron excitation. It is clear from the figure that $\varepsilon_2(\omega)$ shows single peak at 6.95 eV, 6.22 eV, 5.07 eV for BeS, BeSe and BeTe respectively. The peaks are primarily due to transitions between valence bands and conduction bands above the Fermi energy along the symmetry lines Γ-X direction. Moving from S to Se, the insignificant hump on the right shoulder of the main peak of BeS at 7.42 eV clearly appears in the 6.98 eV at the $\varepsilon_2(\omega)$ structures of BeSe; this hump disappears again when we move from Se to Te. We compare our calculated $\varepsilon_2(\omega)$ with the previous theoretical calculations [4, 9, 13] and agreement is found.

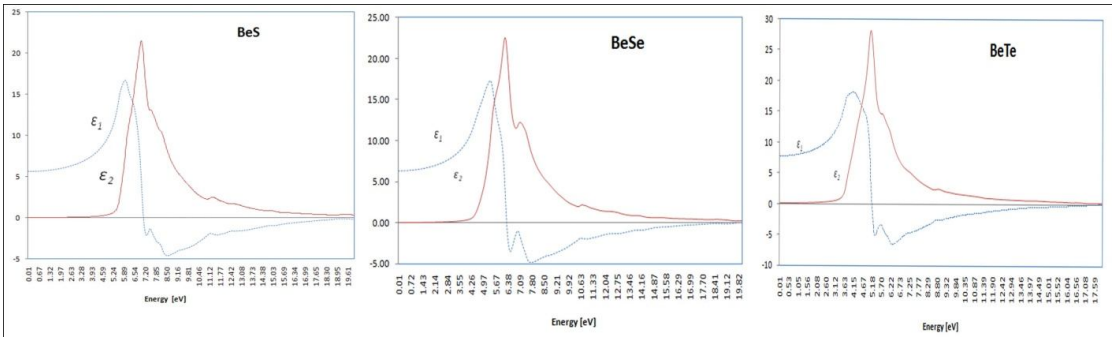

Figure 4. Real and Imaginary part of dielectric function for BeS, BeSe and BeTe

4. Conclusions

This paper has reported calculations of the energy bands, density of states and optical properties of BeX using generalized gradient approximation (GGA) within the FP-LAPW method. Our results for band structure and DOS show that these compounds have similar structures and the energy gap decreases when S replaced by Se and Te. All the structures in the imaginary part of the dielectric function $\varepsilon_2(\omega)$ are shifted towards lower energies when S is replaced by Se and Te. We compare our calculated $\varepsilon_2(\omega)$ with the previous theoretical calculations [4, 9, 13] and agreement is found. We also identified the microscopic origin of the main features in the optical spectra and found that transitions between highest lying valence band (HVB) and lowest lying conduction band (LCB) are responsible for most of the optical absorption in BeX. It is an established fact that indirect band gap materials are bad emitters of light because phonons are involved in the de- excitation of electron and hence the absorbed photon energy is trapped. Due to this disadvantage, BeX are ineffective for optoelectronic industry. In order to use these compounds in the green, blue and ultra violet (UV) optical devices the indirect band gaps of these materials must have to be transformed into direct ones through band gap engineering (i.e. doping, creating, applying external pressure or current etc).

References:

[1] Yim W M et al 1972 J. Phys. Chem. Solids 33 501
[2] Stukel D J 1970 Phys. Rev. B 2 1852
[3] Di´az Gonz´alez M et al 1997 Phys. Rev. B 55 14043–6
[4] Okoye C M I 2004 Eur. Phys. J. B 39 5–17
[5] Fleszar A and Hanke W 2000 Phys. Rev. B 62 2466
[6] Haj Hassan, F.E. and Akbarzadeh, H. 2006 Computational Materials Science 35 428
[7] Imad Khan et al 2013 Journal of Physics and Chemistry of Solids 74 182
[8] Baaziz, H. et al. 2006 Phys. Stat. Sol. (b) 243, No. 6, 1299
[9] Al-Douri,Y. et al. 2012 Physica B 407 289
[10] Hacini K et al 2012 Chin. Phys. B Vol. 21, No. 3, 036102
[11] Ameri, M. et al. 2008 Phys. Stat. Sol. (b) 245, No. 1, 108
[12] Kalpana, G. et al 1998 Int. J. Mod. Phys. B 12 1975
[13] Khenata R et al. 2006 Solid-State Electronics 50 1382–1388
[14] Singh, D.J., (1994) Planewaves Pseudopotentials and the LAPW Method (Boston, MA: Kluwer–Academic)
[15] Blaha P et al (2001) Computer code WIEN2k Vienna University of Technology which was published by P Blaha updated Unix/Linux version of the original copyrighted WIEN code Schwartz K et al (1990) Comput. Phys. Commun. 59: 339
[16] Perdew J P et al 1996 Phys. Rev. Lett. 77 3865
[17] Martienssen, W and H. Warlimont, H (2005) Springer Handbook of Condensed Matter and materials Data (Spinger Berlin Heidelberg New York)
[18] Kumar, S., Maurya, T.K. and Auluck, S. (2008). J. Phys.: Condens. Matter 20:075205
[19] Wooten, F. 1972 Optical Properties of Solids (New York:Academic)

Science Vision 14(4), 195-199

Original Research

2014
October-December
ISSN (print) 0975-6175
ISSN (online) 2229-6026

Study of electronic and optical properties of aluminium pnictides (AlX, X = P, As, Sb)

Aldrin Malsawmtluanga*, Lalnunpuia, Ricky L. Ralte and Z. Pachuau

Department of Physics, Mizoram University, Aizawl 796 004, Mizoram, India

Received 30 October 2014 | Revised 24 November 2014 | Accepted 5 December 2014

Abstract

A comparative study of theoretical and experimental electronic properties and linear optical dielectric function of zinc blende structure of aluminium pnictides is presented by applying the full-potential linearized augmented plane wave (FP-LAPW) method within density-functional theory (DFT) as implemented in WIEN2k code. Results are presented for the band structures, for the density of states, and for the real and imaginary parts of the linear dielectric functions for photon energies up to 10 eV. The results are compared with other existing calculations and experimental data and agreement was found.

Key words: AlX; FP-LAPW; band structure; optical properties; WIEN2k.
PACS Nos.: 71.15.Ap, 71.15.Mb, 71.20.Nr, 78.20.Ci

Introduction

Recently, III–V zinc blende semiconductors compounds occupy a privileged position in the domain of materials science. These compounds semiconductors are favorite hosts for photonic and optoelectronic devices. These semiconductors have higher electron mobility and have wider band gaps than silicon. In the past two decades, remarkable progress has been made toward accurate calculations of the total energy, using density functional theory in the local density approximation[1] and more recently in the generalized gradient approximation[2]. In the present work we use the full potential linear augmented plane wave (FP-LAPW) method which has proven to be one of the most accurate methods[3] for the computation of the electronic structure of solids within density functional theory (DFT). Hence the effect of the full potential on the linear optical properties can be ascertained.

Although there have been numerous calculations of the electronic and optical properties of AlX (X=P, As, Sb) using different methods, to our knowledge there is only one report had been used the full potential calculation[4] to calculate the electronic structures. Our calculations will highlight the effect of replacing P by As and As by Sb on the electronic and optical properties of

Corresponding author: Malsawmtluanga
Phone: +91-9436351500
E-mail: aldmst@rediffmail.com

the investigated compounds.

The aim of this paper is to give a comparative and complementary study of electronic and optical properties to both experimental and other theoretical works by using FP-LAPW method for AlX.

METHOD

The calculation of optical properties of AlX was based on the FPLAPW method[5] as implemented in the WIEN2K package[6]. We choose the exchange-correlation potential parameterized by Perdew *et al.,*[2] which is derived by using the generalized gradient approximation (GGA). In the FPLAPW method, a basis set is obtained by dividing the unit cell into non-overlapping atomic spheres (centered on the atomic sites) and an interstitial region. Inside the atomic sphere, a linear combination of radial function times spherical harmonic is used, and in the interstitial region a plane wave expansion is augmented by an atomic like function in every atomic sphere. This method yields accurate energy eigenvalues and wavefunctions, therefore appropriate for calculating the electronic and optical properties of crystalline solids. We have chosen sphere radii of 2.1 Å for Al, 2.3 Å for P, 2.5 Å for As and 2.8 Å for Sb. For our calculation, we used lattice parameters a = 5.4635 Å, 5.66139 Å, and 6.09593 Å for AlP, AlAs and AlSb respectively[7]. The values of Kmax × RMT = 7.0 (where RMT is the atomic sphere radius and Kmax is the interstitial plane wave cut-off), In the atomic region, the basis set consists of spherical harmonics with angular quantum number l = 10 and a non spherical contribution with l = 4 are kept constant throughout the calculations The self-consistent iterations are considered to be converged when the total energy of the system are stable within 10^{-5} Ry. The compound AlX crystallized in the zinc-blende structure. The space group is F-43 m. The Al atom is located at the origin and the X atoms are located at (1/4, 1/4, 1/4).

The dielectric function of a solid is usually describes in terms of a complex parameter as $\varepsilon(\omega) = \varepsilon_1(\omega) + i\varepsilon_2(\omega)$,in which the imaginary or the absorptive part of the dielectric function, $\varepsilon_2(\omega)$ can be obtained directly from the band structure calculation[8]. While the real part $\varepsilon_1(\omega)$ can be obtained from the imaginary part $\varepsilon_2(\omega)$ by using the Kramers-Kronig dispersion relation.[9]

RESULTS AND DISCUSSION

Band structure and density of states

The calculated total density of states, the partial density of states and band structures for aluminum pnictides are shown in Figures 1, 2 and 3. The band structure and TDOS can be divided into three main groups/structures. From the partial DOS we are able to identify the angular momentum character of the various structures. The lowest energy group has mainly X-s states. The second group is mainly Al-s and X-p states. The third group is mainly from p state of Al and X. From the partial DOS, we note a strong hybridization between Al-s and X-p states below and above E_F. The valence band maximum (VBM) is located around Γ and the conduction band minimum (CBM) is located around X resulting in an indirect energy bad gap of 1.58 eV,

Table 1. Indirect energy band gap values and the experimental and theoretical band gap (all values are in eV).

System study	Expt. band gap	Theoretical band gap			Our calculated band-gaps GGA
		TB	LDA	GGA	
AlP	2.50[a]	2.45[b]	2.17[a], 1.49[c]	1.638[d]	1.58
AlAs	2.3[a]	2.153[b]	1.37[a], 1.39[c]	1.494[d]	1.46
AlSb	1.87[a]	1.615[b]	1.23[a], 1.17[c]	1.214[e]	1.20

[a]Ref. 11; [b]Ref. 10; [c]Ref. 12; [d]Ref. 13; [e]Ref. 14.

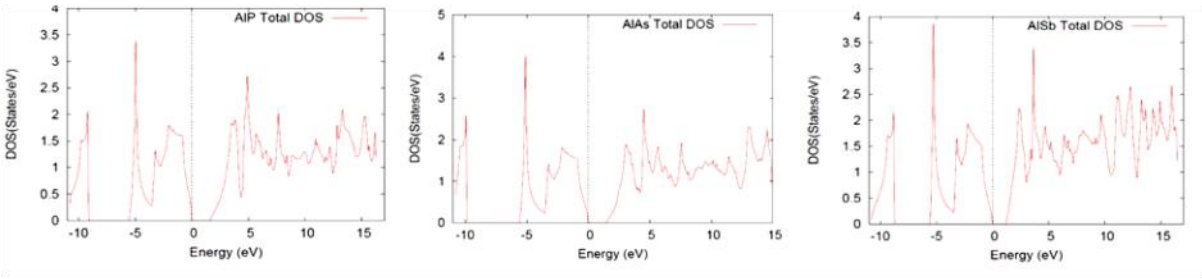

Figure 1. Total density of states for AlP, AlAs and AlSb.

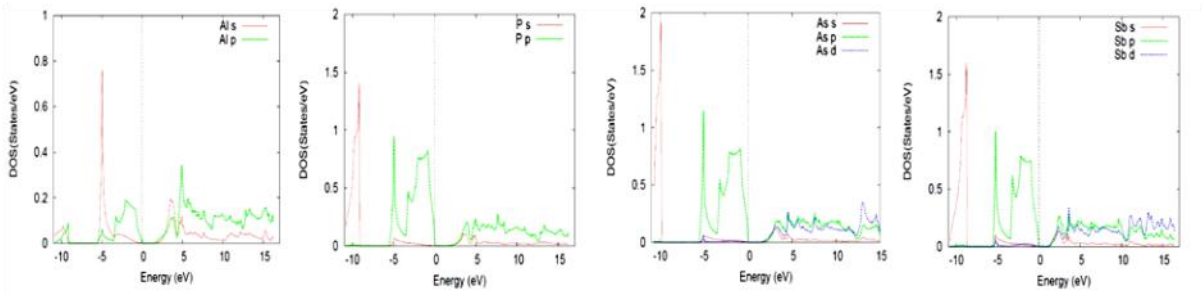

Figure 2. Partial density of states for AlP, AlAs and AlSb.

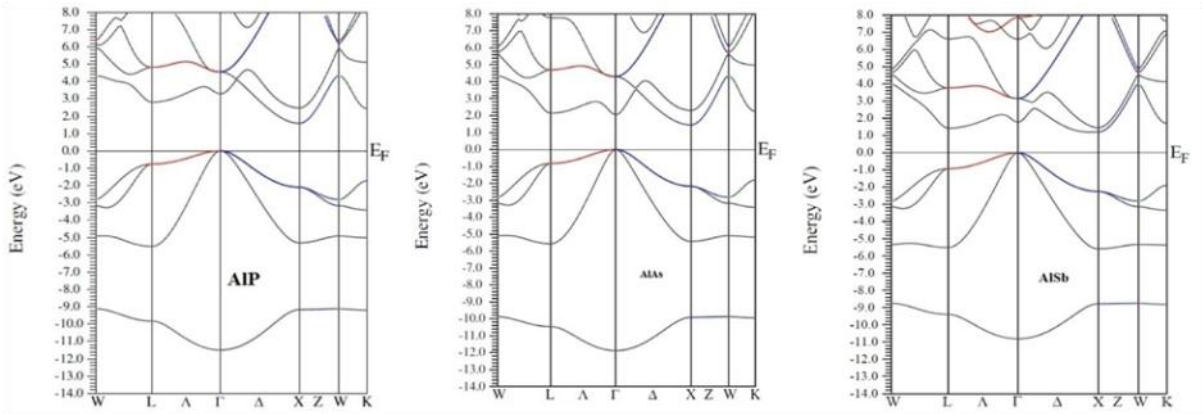

Figure 3. Band structure for AlP, AlAs and AlSb.

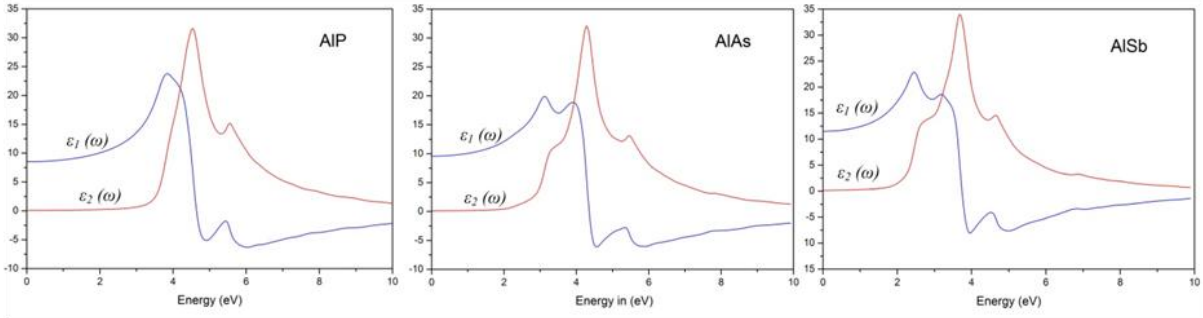

Figure 4. Real and imaginary part of dielectric function for AlP, AlAs and AlSb.

1.46 eV, 1.2 eV for AlP, AlAs and AlSb respectively. A comparison of the experimental and theoretical band gaps are given in Table I. It is clearly seen that the band gap obtained by GGA are lower than the corresponding experimental values and results obtained from tight binding method (TB)[10]. Our results are in a good agreement with the other theoretical work with the same exchange correlation approximation of LDA[11,12] and GGA[13,14].We note that the energy gap decreases when P replaced by As and As by Sb in agreement with the previous theoretical calculations and experimental data.

Linear optical properties

The detailed variation of real, $\varepsilon_1(\omega)$ and imaginary $\varepsilon_2(\omega)$ parts of the dielectric function for AlX with photon energy are shown in Figure 4. Since the investigated compounds have cubic symmetry, we need to calculate only one dielectric tensor component to completely characterize the linear optical properties. This component is $\varepsilon_2(\omega)$ the imaginary part of the frequency dependent dielectric function. We note that $\varepsilon_2(\omega)$ shows a large peak located at 4.5 eV for AlP, 4.3 eV for AlAs, and 3.7 eV for AlSb. All the structures in $\varepsilon_2(\omega)$ are shifted towards the lower energies when P is replaced by As and As by Sb. This is attributed to the increases in the band width of the conduction bands when we move from P to As to Sb. We note that the peak heights are increases when we move from P to As to Sb. We compare our calculated $\varepsilon_2(\omega)$ with the most recent calculations of Huang and Ching[11]. Previous calculations[11] underestimate the magnitude of $\varepsilon_2(\omega)$ in the low energy regime. This could be due to an inaccurate representation of the wave functions.

CONCLUSION

The calculations of band structure, DOS and linear optical response for AlP, AlAs, and AlSb compounds using FP-LAPW method based on the DFT in GGA are presented in this work. Our results for band structure and DOS, show that these compounds have similar structures and the energy gap decreases when P is replaced by As and As by Sb. This is attributed to the fact that the bandwidth of the conduction bands increases on going from P to As to Sb. All the structures in the imaginary part of the dielectric function $\varepsilon_2(\omega)$ are shifted towards lower energies when P is replaced by As and As by Sb. We compare our calculated $\varepsilon_2(\omega)$ with the previous theoretical calculations and found good agreement. We also identified the microscopic origin of the main features in the optical spectra and found that transitions between highest lying valence band (HVB) and lowest lying conduction band (LCB) are responsible for most of the optical absorption in AlX. It is an established fact that indirect band gap materials are bad emitters of light because phonons are involved in the de-excitation of electron and hence the absorbed photon energy is trapped. Due to this disadvantage, AlX are ineffective for optoelectronic industry. In order to use these compounds in the green, blue and ultra violet (UV) optical devices the indirect band gaps of these materials must have to be transformed into direct ones through band gap engineering (i.e. doping, creating, applying external pressure or current etc.).

REFERENCES

1. Kohn W & Sham LJ (1965). Self-consistent equations including exchange and correlation effects. *Phys Rev*, A**140,** 1133–1138.
2. Perdew JP, Burke K & Ernzerhof M (1996). Generalized gradient approximation made simple. *Phys Rev Lett,* **77,** 3865–3868.
3. Schwarz K (2003). DFT calculations of solids with LAPW and WIEN2k. *J Solid State Chem*, **176,** 319–328.
4. Khanin DV & Kulkova SE (2005). Electronic properties of III – V semiconductors. *Russian Phys J*, **48,** 70–77.
5. Singh DJ (1994). *Planewaves, Pseudopotentials and the LAPW Method.* Kluwer Academic Publishers, Boston, Dordrecht, London.
6. Blaha P, Schwarz K, Madsen GKH, Kvasnicka D & Luitz J (2008). *An Augmented Plane Wave + Local Orbitals Program for Calculating Crystal Properties*, (Revised Edition). Vienna University of Technology: Inst. of Physical and Theoretical Chemistry,

Getreidemarkt 9/156, A-1060 2008, Vienna, Austria.

7. Martienssen W & Warlimont H (2005). *Springer Handbook of Condensed Matter and materials Data*. Spinger Berlin, Heidelberg, New York, pp. 610.
8. Kittel C (1994). *Introduction to Solid State Physics*, 5th ed. Wiley Eastern, India, pp. 324.
9. Wooten F (1972). *Optical Properties of Solids*. Academic Press, New York, pp. 173–179.
10. Korti-Baghdadli N, Merad AE & Benouaz T (2013). Adjusted Adashi's Model Of Exciton Bohr Parameter And New Proposed Models For Optical Properties Of III-V semiconductors. *Amer J Mater Sci Technol*, **3,** 65–73.
11. Huang MZ & Ching WY (1993). Calculation of optical excitations in cubic semiconductors. I. Electronic structure and linear response. *Phys Rev*, *B* **47,** 9449–9463.
12. Reshak AH & Auluck S (2007). Investigation of the electronic properties, first and second harmonic generation for $A^{XIII}B^{XV}$ zinc-blende semiconductors. *Physica B: Condensed Matter*, **395**, 143–150.
13. Bentouaf A, Ouahrani T, Ameri M, Mebsout R, Hachemane D (2013). Theoretical study of structural, electronic, optical and thermodynamic properties of AlP, InP and AlAs compounds. *Optoelectron Adv Mater*, **7**, 659–666.
14. Ahmed R, Fazal-e-Aleem, Hashemifar SJ, Rashid H & Akbarzadeh H (2009). Physical properties of III-antiminodes - a first principles study. *Commun Theor Phys*, **52**, 527–533.

Ind. J. Sci. Res. and Tech. 2014 2(5):108-111/Malsawmtluanga et al ISSN:-2321-9262 (Online)
Online Available at: http://www.indjsrt.com
Research Article

STUDY OF ELECTRONIC AND OPTICAL PROPERTIES GALLIUM PNICTIDES (GaX, X = P, As, Sb)

***Aldrin Malsawmtluanga, Lalnunpuia, Ricky L. Ralte, Z. Pachuau**
Department of Physics, Mizoram University, Aizawl 796 004, Mizoram, India
** Author for correspondence*

ABSTRACT
We presented a theoretical study of electronic properties and linear optical dielectric function of zinc blende structure of Gallium pnictides by using the full-potential linearized augmented plane wave (FP-LAPW) method within density-functional theory (DFT). In this approach, the generalized gradient approximation (GGA) was used for the exchange-correlation potential calculation. Results are presented for the band structures, for the density of states, and for the real and imaginary parts of the linear dielectric functions for photon energies up to 8 eV. Detailed comparisons are made with published experimental and theoretical data and show generally good agreement.

Key words: Band structure, FP-LAPW, GaX, Optical properties and WIEN2k
PACS Nos. : 71.15.Ap, 71.15.Mb, 71.20.Nr, 78.20.Ci

INTRODUCTION

The group III-V semiconductors are having great technological importance. They are becoming of increasing importance in many emerging optoelectronic and electronic device applications. Among these applications are light emitting diodes, photovoltaic cells, photo detectors, lasers, modulators, integrated circuits, filters etc (Jivani & Jani, 2012).

There have been many electronic band structure calculations for III–V semiconductors. These include the empirical pseudopotential method (EPM) (Al-Douri & Aourag, 2002; Al-Douri et al., 2003), the tight binding (TB) (Rabah et al., 2003; Reshak, 2005), full potential method (Reshak, 2005; Bouhemadouet al., 2009) and the pseudopotential total energy approach (Froyen & Cohen, 1983). In the present work, we have reported the FP-LAPW calculations of the band structures in GaX (X = P, As and Sb) to study the electronic and optical properties. The exchange and correlation potential has been calculated using the generalized gradient approximation (GGA) (Perdew et al., 1996) for the total energy calculations.

In semiconductor GaX (X=P, As, Sb), there is a large variation in the energy gaps, suggesting that the energy band gap depends on the method of the band structure calculation[4,5,9,10]. In this work, we describe detailed calculations of the band structure, density of states and linear optical properties for the semiconductor GaX (X=P, As, Sb,) compound with zinc-blende structure. Our calculations will highlight the effect of replacing P by As and As by Sb on the electronic and optical properties in GaX compounds. The aim of this paper is to give a comparative and complementary study of electronic and optical properties to both experimental and other theoretical works by using FP-LAPW method.

METHODOLOGY

The electronic configurations of elements in Gallium pnictides are Ga : [Ar] $3d^{10}\,4s^2\,4p^1$; P : [Ne] $3s^2\,3p^3$; As : [Ar] $3d^{10}\,4s^2\,4p^3$ and Sb : [Kr] $4d^{10}\,5s^2\,5p^3$. We have chosen sphere radii of 2.2 Å for Ga, 2.1 Å, 2.3 Å and 2.7 Å respectively for P, As and Sb. The calculations reported here were performed using the FPLAPW method[11] as implemented in the WIEN2K package[12]. We choose the exchange-correlation potential parameterized by Perdew et al., (1996) which is derived by using the generalized gradient approximation (GGA). In the FPLAPW method, a basis set is obtained by dividing the unit cell into non-overlapping atomic spheres (centered on the atomic sites) and an interstitial region. Inside the atomic sphere, a linear combination of radial function time's spherical harmonic is used, and in the interstitial region a plane wave expansion is augmented by an atomic like function in every atomic sphere. This method yields accurate energy eigenvalues and wave functions, therefore appropriate for calculating the electronic and optical properties of crystalline solids.

The Gallium pnictides crystallize in the zinc-blende structure at ambient pressure and temperature with lattice parameter 5.4506 Å for GaP, 5.65359 Å for GaAs and 6.09593 Å for GaSb[13]. The space group is F-43 m. The Ga atom is located at the origin and the X atom is located at (1/4, 1/4, 1/4).The values of $K_{max} \times R_{MT} = 7.0$ (where R_{MT} is the atomic sphere radius and K_{max} is the interstitial plane wave cut-off), In the atomic region, the basis set consists of spherical harmonics with angular quantum number $l = 10$ and a non spherical contribution with $l = 4$ are kept constant throughout the calculations. The self-consistent iterations are considered to be converged when the total

energy of the system are stable within 10^{-5} Ry. A mesh point of 5000 k-points were used to obtain 111 special *k*-points in the irreducible wedge of the Brillouin zone for GaP, GaAs, and GaSb. Both the muffin-tin radius and number of *k*-points were varied to ensure total energy convergence.

The dielectric function of a solid is usually describes in terms of a complex parameter as $\varepsilon(\omega) = \varepsilon_1(\omega) + i\varepsilon_2(\omega)$, in which the imaginary or the absorptive part of the dielectric function, $\varepsilon_2(\omega)$ can be obtained directly from the band structure calculation. While the real part $\varepsilon_1(\omega)$ can be obtained from the imaginary part $\varepsilon_2(\omega)$ by using the Kramers-Kronig dispersion relation (Wooten, 1972).

RESULTS AND DISCUSSION

Band Structure and Density of States

The calculated total density of states, the partial density of states and band structures for Gallium pnictides are shown in figs. 1, 2 and 3.The band structure, partial and total DOS can be divided into three main groups. From fig. 2 i.e. the partial DOS, the angular momentum character of the various structures can be identifying. The lowest energy group has mainly X-s states. The second group between –7 eV to E_F is composed of Ga-sp and X-p states. The last group from 1.65 for GaP, 0.52 eV for GaAs, and 0.17 eV for GaSb and above has contributions from Ga-spd and X-p states. The valence band maximum (VBM) is located at Γ for all the three compounds. In GaP compound the conduction band minimum (CBM) is located at X resulting in indirect energy gap of about 1.65 eV. While in GaAs and GaSb compounds the CBM located at Γ resulting in a direct energy gap of about 0.52 and 0.17 eV respectively. The location of the VBM and CBM is agreed with experiment (Postigo et al., 1998; Strehlow & Cook, 1973) and previous theoretical work (Reshak, 2005; Al-Douri & Reshak, 2011; Rahaman et al., 2009); Postigo et al., 1998 and Korti-Baghdadli et al., 2013). The trends in the band structures in moving from P to As to Sb can be summarized as follows: The first group in GaAs is shifted towards lower energies by around 0.5 eV in comparison with GaP, while in GaSb it is shifted towards higher energies by around 0.5 eV. The bandwidth of the second group is increased. The bandwidth of the conduction band slightly increases by around 0.5 eV towards Fermi energy (EF) on going from P to As to Sb which causes to reduce the energy gap near Γ.

Table 1: Our calculated direct energy band gap values and the experimental and theoretical band gap

Compo-unds	a (A°)	Expt. Band gap (eV)	Theoretical Band gap (eV)			Our Calculated Band-gaps (eV)
			TB	LDA	GGA	
GaP	5.4506[a]	2.2[b], 2.26[c], 2.38[d], 2.22[e]	2.272[f]	1.22[d], 1.45[g], 1.62[h]	2.0[i]	1.65
GaAs	5.6536[a]	1.8[b], 1.43[c], 1.52[d],1.42[e]	1.419[f]	1.04[d], 0.4[g], 0.37[h]	0.49[i]	0.52
GaSb	6.0959[a]	1.2[b], 0.78[c], 0.81[d], 0.725[e]	0.725[f]	0.8[d], 0.2[g], 0.07[h]	0.4[i]	0.17

[a]Ref. [13], [b]Ref. [15], [c]Ref. [16], [d]Ref. [17], [e]Ref. [18], [f]Ref. [19], [g]Ref. [5], [h]Ref. [10], [i]Ref. [9],

The important features of the band structure for each compound are given in Table 1. It is clearly seen that the band gaps obtained by GGA are lower than the corresponding experimental values. This underestimation of the band gap is mainly due to the fact that the simple forms of GGA are not sufficiently flexible to accurately reproduce both ex-change correlation energy and its charge derivative. Whereas our results are in a good agreement with theoretical results obtained from GGA and LDA except TB method with the same exchange correlation approximation. We note that the reduction in the energy gap in agreement with the experimental data. GaAs and GaSb exhibit an overall reduction of the gap over the entire Brillouin zone.

Optical properties

The optical properties of solids can be described in terms of the optical dielectric function. The detailed variation of real, $\varepsilon_1(\omega)$ and imaginary $\varepsilon_2(\omega)$ parts of the dielectric function for GaX with photon energy are shown in Fig. 4. The $\varepsilon_1(\omega)$ spectra appears at the same energy as a peak in the corresponding $\varepsilon_2(\omega)$ spectra. Metallic reflectance characteristics are exhibited in the range of $\varepsilon_1(\omega) < 0$. Since the investigated compounds have cubic symmetry, we need to calculate only one dielectric tensor component to completely characterize the linear optical properties. This component is $\varepsilon_2(\omega)$ the imaginary part of the frequency dependent dielectric function.

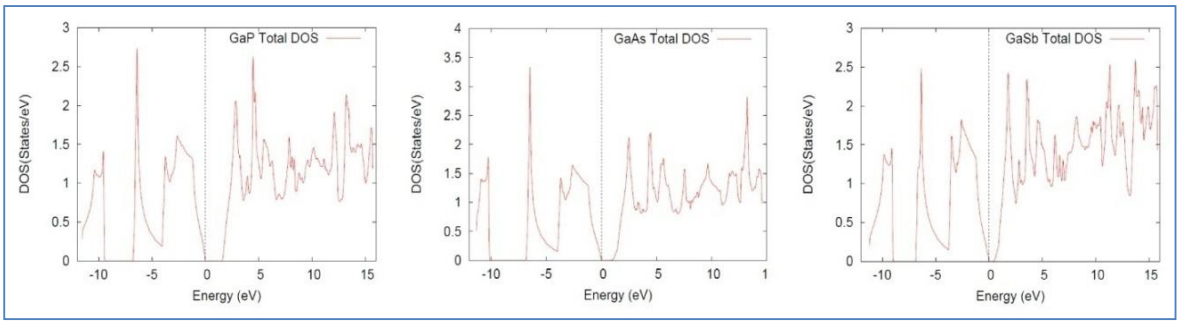

Figure 1: Total Density of States for GaP, GaAs and GaSb

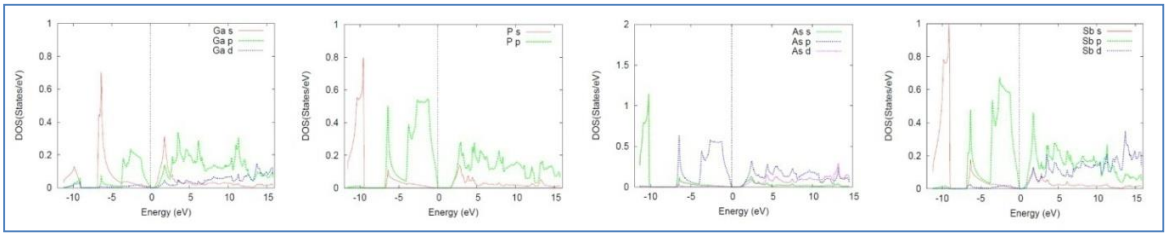

Figure 2: Partial Density of States for GaP, GaAs and GaSb

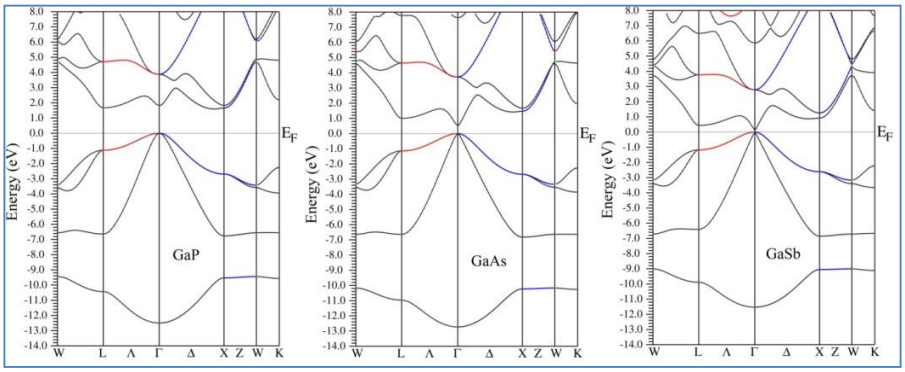

Figure 3: Band structure for GaP, GaAs and GaSb

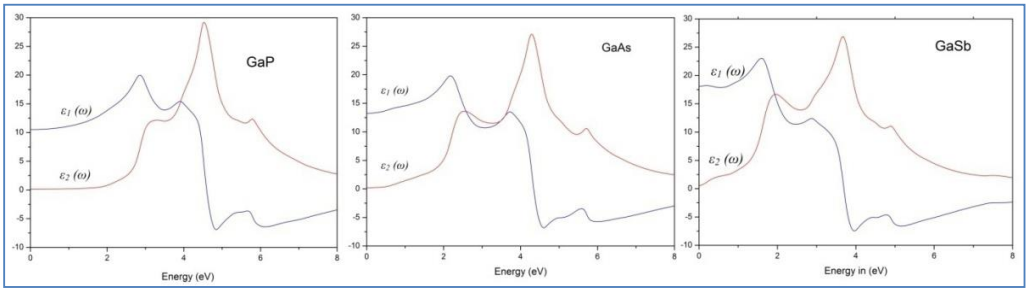

Figure 4: Real and Imaginary part of dielectric function for GaP, GaAs and GaSb

Our analysis of the $\varepsilon_2(\omega)$ curves show that the first critical points of the dielectric function occurs at 1.65 eV, 0.52 eV and 0.17 eV for GaP, GaAs and GaSb respectively. These critical points are followed by small structure located at 3.03 eV in GaP, 2.4 eV in GaAs and 1.84 eV in GaSb). The main peaks in the spectra are situated at 4.48 eV, 4.23 eV and 3.61 eV respectively. The main peaks are followed by small hump situated at 5.70 eV, 5.59 eV and 4.83 eV respectively. The peak of the imaginary part of the dielectric function is related to the electron excitation.

We have found that the three compounds have the same structure that is attributed to the fact that the band structures of these compounds are similar with minor differences causing insignificant changes in the structures of $\varepsilon_2(\omega)$. All

the structures in $\varepsilon_2(\omega)$ are shifted towards the lower energies with reduces in the peak heights when P is replaced by As and As by Sb, in agreement with the experimental data (Aspnes & Studna, 1983). This is attributed to the reduction in the band gaps. We compare our calculated $\varepsilon_2(\omega)$ with the experimental data (Aspnes & Studna, 1983). This comparison shows very good agreement in the matter of the peaks position and peaks height.

CONCLUSION

This paper has reported calculations of the energy bands structure, density of states and linear optical properties of GaX (X=P, As, Sb) compounds using generalized gradient approximation (GGA) within the FP-LAPW method. Our result for band structure and DOS shows that these compounds are semiconductors with energy gaps of 1.65, 0.52, 0.17 eV. We note that the energy gap reduces when P replaced by As and As by Sb in agreement with the experimental data and pervious theoretical calculations. We compare our calculated linear optical properties with the experimental data (Aspnes & Studna, 1983). This comparison shows very good agreement in the matter of the peaks position and peaks height.

REFERENCES

Aspnes DE & Studna AA (1983). Dielectric functions and optical parameters of Si, Ge, GaP, GaAs, GaSb, InP, InAs, and InSb from 1.5 to 6.0 eV. *Physical Review B,* **27** 985-1009.

Al-Douri Y & Aourag H (2002). The effect of pressure on the ionicity of In–V compounds. *Physica B,* **324** 173-178.

Al-Douri Y, Mecabih S, Benosman N & Aourag H (2003). Pressure effect on electronic and positron charge densities of $Zn_{0.5}Cd_{0.5}Se$. *Physica B,* **325** 362-371.

Al-Douri Y & Reshak AH (2011). Calculated optical properties of GaX (X = P, As, Sb) under hydrostatic pressure. *Applied Physics A,* **104** 1159-1167.

Blaha P, Schwarz K, Madsen GKH, Kvasnicka D & Luitz J (2001). WIEN2k, An Augmented Plane Wave Plus Local Orbitals Program for Calculating Crystal Properties, Vienna University of Technology, Austria.

Bouhemadou A, Khenata R, Kharoubi M, Seddik T, Reshak AH & Al-Douri Y (2009). FP-APW + lo calculations of the elastic properties in zinc-blende III-P compounds under pressure effects. *Computational Materials Science,* **45** 474-479.

Froyen S & Cohen MR (1983). Structural properties of III-V zinc-blende semiconductors under pressure. *Physical Review B,* **28** 3258-3265.

Huang MZ & Ching WY (1993). Calculation of optical excitations in cubic semiconductors. I. Electronic structure and linear response. *Physical Review B,* **47** 9449-9463.

Jivani AR & Jani AR (2012). Prediction of some mechanical and vibrational properties of Ga*X* (*X* = P, As, Sb) semiconductor compounds. *Turkish Journal of Physics,* **36** 215-223.

Kittel C (1994). Introduction to Solid State Physics. fifth edition Wiley Eastern, India 210.

Korti-Baghdadli N, Merad AE & Benouaz T (2013). *American Journal of Materials Science and Technology,* **3** 65-73.

Martienssen W & Warlimont H (2005). *Springer Handbook of Condensed Matter and materials Data* (Spinger Berlin Heidelberg New York) 621.

Perdew JP, Burke K & Ernzerhof M (1996). Generalized Gradient Approximation Made Simple. *Physical Review Letters,* **77** 3865-3868.

Postigo PA, Armelles G, Utzmeier T & Briones F (1998). In situ optical spectroscopy of Ga dimers on GaP, GaAs, and GaSb by surface chemical modulation. *Physical Review B,* **57** 1359-1361.

Rabah M, Al-Douri Y, Sehil M & Rached D (2003). Pressure effect on electronic band structure of III–V compounds. *Materials Chemistry and Physics,* **80** 34-38.

Rahaman M, Ganguly S, Samal P, Harbola MK, Saha-Dasgupta T & Mookerjee A (2009). A local-density approximation for the exchange energy functional for excited states: The band-gap problem. *Physica B,* **404** 1137-1142.

Reshak AH (2005). First-principle calculations of the linear and nonlinear optical response for GaX (X = As, Sb, P). *The European Physical Journal B,* **47** 503-508.

Singh DJ (1994). Planewaves, Pseudopotentials and the LAPW Method. Kluwer Academic Publishers, Boston, Dordrecht, London.

Strehlow WH & Cook EL (1973). Compilation of Energy Band Gaps in Elemental and Binary Compound Semiconductors and Insulators. *Journal of Physical and Chemical Reference Data - Scitation,* **2**(1) 163-199.

Wooten F (1972). Optical Properties of Solids. Academic Press, New York 173-179.

www.sciencevision.org

Original Research

Sci Vis Vol 14 Issue No 2
April-June 2014
ISSN (print) 0975-6175
ISSN (online) 2229-6026

Theoretical investigation of electronic and optical properties of zinc blende structure of beryllium sulphide, BeS

Aldrin Malsawmtluanga[1*], Lalnunpuia[2], Lawrence Z. Chhangte[3], Ricky L. Ralte[1] and Z. Pachuau[1]

[1] *Department of Physics, Mizoram University, Aizawl 796 004, India*
[2] *Physics Department, Govt. Champhai College, Champhai 796321, India*
[3] *Physics Department, Govt. Zirtiri Residential Science College, Aizawl 796 001, India*

Received 2 May 2014 | Revised 24 May 2014 | Accepted 30 May 2014

Abstract

A theoretical study of electronic and optical properties of zinc blende structure of BeS is presented by applying the full-potential linearized augmented plane wave (FP-LAPW) method within density-functional theory (DFT) as implemented in WIEN2k code. Our results are in agreement with previous theoretical and experimental studies on this important semiconductor compound. For the optical calculations, the dipole approximation is used. The imaginary part of dielectric function is calculated in momentum representation, which requires matrix elements of the momentum p between occupied and unoccupied states. The microscopic origin of the main features in the optical spectra is identified and also the factors responsible for most of the optical absorption.

Key words: BeS; FP-LAPW; band structure; optical property; WIEN2k.
PACS Nos.: 71.15.Ap, 71.15.Mb, 71.20.Nr, 78.20.Ci

Introduction

The II–VI semiconductors compounds have been extensively studied in recent years because of their scientific and technology interests. They are used in the fabrication of light-emitting devices that are employed in optical processing, detection systems for environmental pollution and color-displaying modules. In particular, the beryllium chalcogenides BeS, BeSe and BeTe are the II–VI compounds that crystallize in the four-fold coordinated zinc blende (B3) structure at low pressure. In fact, probably as a result of their very high toxic nature only few experimental studies[1] have been performed on these compounds but more theoretical studies of these compounds are available in the literature.[2-13] Theoretical calculation of the optical and electronic properties of BeX (X = Te, Se and S) compounds were performed by Stukel[2] using a first-principle self-consistent orthogonalized-

Corresponding author: Malsawmtluanga
Phone: +91-9436351500
E-mail: aldmst@rediffmail.com

plane wave (OPW). The calculated dielectric functions were not compared with the experimental data because no data were available at that time. A few non-relativistic local density approximation (LDA) calculations of the structural, electronic and optical properties have been performed for beryllium monochalcogenides.[3,4] Fleszar and Hanke[5] have calculated electronic excitations in BeX using the many-body Green's functions technique (GW) and have given a detailed discussion of LDA versus GW. Hassan and Akbarzadeh[6] have present detail calculation of the band structure using more advanced Engel Vosko's GGA (EV-GGA) formalism. Imad Khan *et al.*[7] have calculated electronic and optical properties of mixed Be-chalcogenides with the FP-LAPW method using a recently developed modified Beck and Johnson potential. The structural and electronic properties have also been theoretically investigated using the tight-binding linear muffin-tin orbital method (TB-LMTO).[12]

The aim of this paper is to give a comparative and complementary study of electronic properties to both experimental and other theoretical works by using FP-LAPW method as well as optical studies for BeS.

METHOD

We calculated the optical properties of BeS using the FPLAPW method[14] as implemented in the WIEN2K package.[15] We choose the exchange-correlation potential parameterized by Perdew *et al*.[16] which is derived by using the generalized gradient approximation (GGA). In the FPLAPW method, a basis set is obtained by dividing the unit cell into non-overlapping atomic spheres (centered on the atomic sites) and an interstitial region. Inside the atomic sphere, a linear combination of radial function times spherical harmonic is used, and in the interstitial region a plane wave expansion is augmented by an atomic like function in every atomic sphere. This method yields accurate energy eigenvalues and wavefunctions, therefore appropriate for calculating the electronic and optical properties of crystalline solids. We have chosen sphere radii of 1.8 Å for Be and 2.8 Å for S. For our calculation, we used lattice parameters a = 4.8630 Å for BeS.[17] The values of Kmax × RMT = 7.0 (where RMT is the atomic sphere radius and Kmax is the interstitial plane wave cut-off), In the atomic region, the basis set consists of spherical harmonics with angular quantum number l = 10 and a non spherical contribution with l = 4 are kept constant throughout the calculations The self-consistent iterations are considered to be converged when the total energy of the system are stable within 10^{-5} Ry. The semiconducting beryllium sulphide crystallized in the zinc blende structure. The space group is F-43 m. The Be atom is located at the origin and the S atom is located at (1/4, 1/4, 1/4). In a cubic unit cell only one component of the dielectric function has to be calculated, i.e. ε_{xx}, written as

$$\varepsilon(\omega) = \varepsilon_1(\omega) + i\varepsilon_2(\omega) \quad (1)$$

describes the optical response of the system at all photon energies $E = h\omega$. The imaginary part of the dielectric function $\varepsilon_2(\omega)$ is given by[18]

$$\varepsilon_2(\omega) = \left(\frac{4\pi e^2}{m^2\omega^2}\right)\sum_{ij}\langle i|M|j\rangle^2 f_i(1-f_j)\times\delta(E_F - E_i - \omega)d^3k \quad (2)$$

where M is the dipolematrix element, i and j are the initial and final states, respectively, fi is the Fermi distribution function for the i^{th} state. E_i is the energy of electron in the i^{th} states. The real part of the dielectric function $\varepsilon_1(\omega)$ can be extracted from the imaginary part of the dielectric function $\varepsilon_2(\omega)$ by using the Kramers–Kronig relation[19]

$$\varepsilon_1(\omega) = 1 + \frac{2}{\pi}P\int_0^\infty \frac{\omega'\varepsilon_2(\omega')}{(\omega'^2 - \omega^2)}d\omega' \quad (3)$$

where P implies the principal value of the integral.

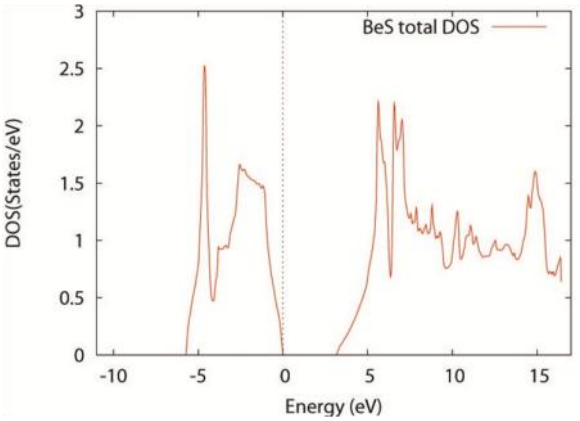

Figure 1. Total density of states for ZB BeS.

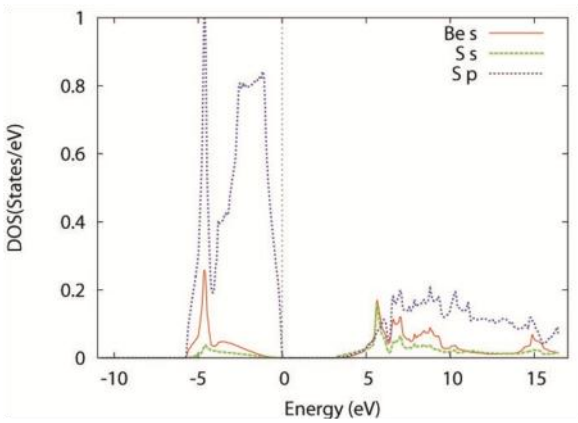

Figure 2. Partial density of states for ZB BeS.

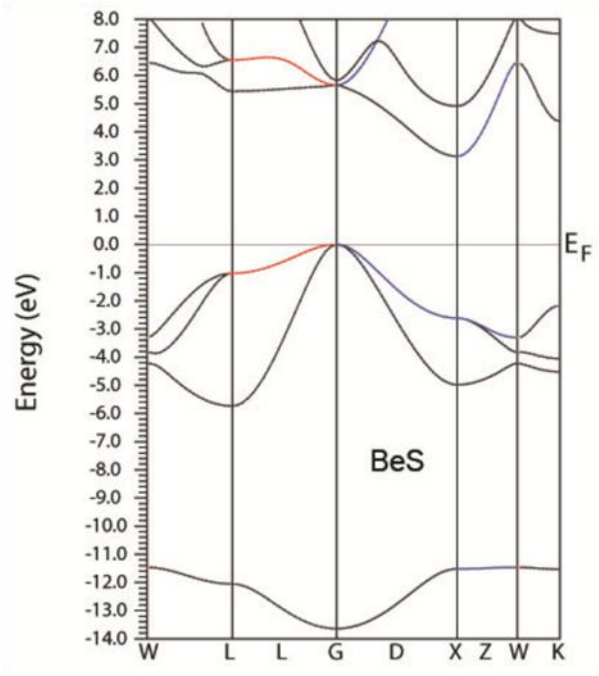

Figure 3. Band structure for BeS.

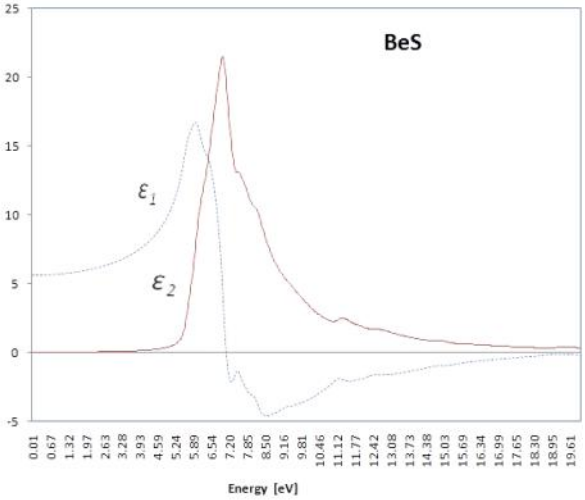

Figure 4. Real and imaginary part of dielectric function for BeS.

Table 1. Our calculated energy band gap values and the experimental and theoretical band gap (all values are in eV).

System study	Expt. Band gap	Theoretical Band gap				Present work GGA
		OPW	TB-LMTO	EV	GGA	
BeS	>5.5[a]	4.17[b]	3.78[c]	4.23[d], 4.26[f], 4.241[g], 4.247[h]	3.12[d], 4.20[e], 3.14[f], 3.141[g], 3.148[h], 2.911[i]	3.12

[a]Ref. 1, [b]Ref. 2, [c]Ref. 12, [d]Ref. 6, [e]Ref. 7, [f]Ref. 8, [g]Ref. 9, [h]Ref. 10, [i]Ref. 11.

Results and Discussions

Electronic properties

For zinc blende structured of BeS, the calculated total density of states, the partial density of states and band structures are illustrated in Figures 1, 2 and 3. The valence band maximum (VBM) occurs at the **Γ** point and con-duction band minimum (CBM) at the **X** point resulting in an indirect gap in agreement with experiment and previous theoretical work.[1-13] The lowest-lying band shown in the graph arises mainly from the chalcogen valence *s* states and the upper valence bands arises from the chalcogen valence *p* states with the top occurring at the **Γ** point. The conduction band arises mainly from the 2*s*-Be states with the minimum energy occurring at X-points.

The band gap of semiconductor BeS in the tetragonal phase as calculated by using the FP-LAPW method and using GGA approximation was found to be 3.12 eV. The important features of the band structure are given in Table 1. It is clearly seen that the band gap obtained by GGA are lower than the corresponding experimental values and results obtained from OPW and EV-GGA and not far from the results obtained by the TB-LMTO methods with the same exchange correlation approximation. This underestimation of the band gap is mainly due to the fact that the simple forms of GGA are not sufficiently flexible to accurately reproduce both exchange correlation energy and its charge derivative.

Optical properties

The determination of the optical properties of a compound in the spectral range above its band gap plays an important role in the understanding of the nature of that material and also gives a clear picture of its applications in optoelectronic devices. The detailed variation of real, $\varepsilon_1(\omega)$ and imaginary $\varepsilon_2(\omega)$ parts of the dielectric function for BeS with photon energy are shown in Figure 4. The $\varepsilon_1(\omega)$ spectra appears at the same energy as a peak in the corresponding $\varepsilon_2(\omega)$ spectra. Metallic reflectance characteristics are exhibited in the range of $\varepsilon_1(\omega) < 0$. The peak of the imaginary part of the dielectric function is related to the electron excitation. It is clear from the figure that $\varepsilon_2(\omega)$ shows single peak at 6.95 eV for BeS. The peaks are primarily due to transitions between valence bands and conduction bands above the Fermi energy along the symmetry lines Γ-X direction. We compare our calculated $\varepsilon_2(\omega)$ with the previous theoretical calculations[4,9,13] and agreement is found.

Conclusions

We present the electronic and optical properties of Zinc blende structure of BeS using generalized gradient approximation (GGA) within the FP-LAPW method. We found that the ZB structured BeS has indirect gap which is induced by the (**Γ** - X) transition with its value being 3.12 eV. We compare our calculated $\varepsilon_2(\omega)$ with the previous theoretical calculations[4,9,13] and agreement is found. The band calculations are com-

parable very well to available measurements. In addition, we revealed behaviours of TDOS and PDOS of the ZB BeS. The obtained optical parameters suggest that the strong absorption spectrum appears mostly in the ultra-violet region, and the optical absorption decreases with photon energy in the high energy range.

REFERENCES

1. Yim WM, Dismukes JP, Stofko EJ & Paff RJ (1972). Synthesis and some properties of BeTe, BeSe and BeS**.** *J Phys Chem Solids*, **33,** 501–505.
2. Stukel DJ (1970). Energy-band structure of BeS, BeSe, and BeTe**.** *Phys Rev* B, **2,** 1852.
3. Gonzalez-Diaz M, Rodriguez-Hernandez P & Munoz A (1997). Elastic constants and electronic structure of beryllium chalcogenides BeS, BeSe, and BeTe from first-principles calculations. *Phys Rev* B, **55,** 14043.
4. Okoye CMI (2004). Structural, electronic, and optical properties of beryllium monochalcogenides. *Eur Phys J* B, **39,** 5–17.
5. Fleszar A & Hanke W (2000). Electronic excitations in beryllium chalcogenides from the *ab initio* GW approach. *Phys Rev* B, **62,** 2466.
6. El Haj Hassan F & Akbarzadeh H (2006). Ground state properties and structural phase transition of beryllium chalcogenides. *Comput Materials Sci*, **35,** 423–421.
7. Khan I, Ahmad I, Zhang D, Rahnamaye Aliabad HA & Jalali Asadabadi S (2013). Electronic and optical properties of mixed Be-chalcogenides. *J Phys Chem Solids*, **74,** 181 –188.
8. Baaziz H, Charifi Z, El Haj Hassan F, Hashemifar SJ & Akbarzadeh H (2006). FP-LAPW investigations of $Zn_{1-x}Be_xS$, $Zn_{1-x}Be_xSe$ and $Zn_{1-x}Be_xTe$ ternary alloys. *Phys Stat Sol (b)*, **243**, 1296–1305.
9. Al-Douri Y, Baaziz H, Charifi Z & Reshak AH (2012). Density functional study of optical properties of beryllium chalcogenides compounds in nickel arsenide B8 structure. *Physica* B, **407**, 286–296.
10. Hacini K, Meradji H, Ghemid S & El Haj Hassan F (2012). Theoretical prediction of structural, electronic and optical properties of quaternary alloy $Zn_{1-x}Be_xS_ySe_{1-y}$. *Chin Phys* B, **21**, 036102.
11. Ameri M, Rached D, Rabah M, El Haj Hassan F, Khenata R & Doui-Aici M (2008). First principles study of structural and electronic properties of $Be_xZn_{1-x}S$ and $Be_xZn_{1-x}Te$ alloys. *Phys Stat Sol (b)*, **245**, 106–113.
12. Kalpana G, Pari G, Mookerjee A & Bhattacharyya AK (1998). *Ab initio* electronic band structure calculations for beryllium chalcogenides. *Int J Mod Phys* B, **12**, 1975.
13. Khenata R, Bouhemadou A, Hichour M, Baltache H, Rached D & Rerat M (2006). Elastic and optical properties of BeS, BeSe and BeTe under pressure. *Solid-State Electron*, **50,** 1382–1388.
14. Singh DJ (1994). *Planewaves, Pseudopotentials and the LAPW Method.* Kluwer Academic Publishers, Boston, Dordrecht, London.
15. Blaha P, Schwarz K, Madsen GKH, Kvasnicka D & Luitz J (2001). WIEN2k, An Augmented Plane Wave Plus Local Orbitals Program for Calculating Crystal Properties, Vienna University of Technology, Austria. *Computer code WIEN2k* which was updated Unix/Linux version of the original copyrighted WIEN code. [Blaha KP, Schwarz K, Sorantin P & Trickey SB (1990). *Comput Phys Commun*, **59,** 339–415]
16. Perdew JP, Burke K & Ernzerhof M (1996). Generalized gradient approximation made simple. *Phys Rev Lett*, **77**, 3865–3868.
17. Martienssen W & Warlimont H (2005). *Springer Handbook of Condensed Matter and materials Data.* (Spinger Berlin Heidelberg New York), pp. 652.
18. Kumar S, Maurya TK & Auluck S (2008). Electronic and optical properties of ordered $Be_xZn_{1-x}Se$ alloys by the FPLAPW method. *J Phys Condens Matter*, **20**, 075205.
19. Wooten F (1972). *Optical Properties of Solids*. Academic Press, New York, pp. 173–179.

International Journal of Physics and Applications.
ISSN 0974-3103 Volume 7, Number 1 (2015), pp. 9-14

http://www.irphouse.com

Study Of Electronic And Linear Optical Properties Of Indium Pnictides (InX, X = P, As, Sb)

Aldrin Malsawmtluanga*, Lalnunpuia, Ricky L. Ralte, Z. Pachuau

Department of Physics, Mizoram University, Aizawl 796 004, Mizoram, India
** Author for correspondence*
E-mail: aldmst@rediffmail.com, Mob.: 09436351500

ABSTRACT

A comparative study of theoretical and experimental electronic properties and linear optical dielectric function of zinc blende structure of Indium pnictides is presented by using the full-potential linearized augmented plane wave (FP-LAPW) method within the DFT formalism. In this approach, the generalized gradient approximation (GGA) was used for the exchange-correlation potential calculation. Results are presented for the band structures, for the density of states, and for the real and imaginary parts of the linear dielectric functions for photon energies up to 15 eV. Detailed comparisons are made with published experimental and theoretical data and generally showed good agreement.

Key words: Band structure, FP-LAPW, InX, Optical properties, WIEN2k.

PACS Nos. : 71.15.Ap, 71.15.Mb, 71.20.Nr, 78.20.Ci

INTRODUCTION

In the last century considerable advances have been realized in the research and applications of semiconductors. It is well known that semiconductor technology has a great impact on our society. The III-V semiconductors are extensively used in the high-tech photonic and optoelectronic devices because of their wide range of band gaps. Narrow band gaps semiconductors Indium Pnictides InX (X=P, As, Sb) compounds have attracted much attention for their potential as new device materials [1].

There have been many electronic band structure calculations for III–V semiconductors. These include the empirical pseudopotential method (EPM)[2], the tight binding (TB)[3], full potential method[4], and the pseudopotential total energy

approach[5]. In the present work, we have reported the FP-LAPW calculations of the band structure, density of states and linear optical properties for the semiconductors InX (X=P, As, Sb,) compounds with zinc-blende structure. The exchange and correlation potential has been calculated using the generalized gradient approximation (GGA)[6] for the total energy calculations.

CALCULATION METHOD

The electronic configurations of elements in Indium pnictides are In: [Kr] $4d^{10}\,5s^2\,5p^1$; P: [Ne] $3s^2\,3p^3$; As: [Ar] $3d^{10}\,4s^2\,4p^3$ and Sb: [Kr] $4d^{10}\,5s^2\,5p^3$. We have chosen sphere radii of 2.3 Å for In, 2.1 Å, 2.5 Å and 2.8 Å respectively for P, As and Sb. The calculations reported here were performed using the FPLAPW method [7] as implemented in the WIEN2K package [8]. We choose the exchange-correlation potential parameterized by Perdew et al.[6] which is derived by using the generalized gradient approximation (GGA). In the FPLAPW method, a basis set is obtained by dividing the unit cell into non-overlapping atomic spheres (centered on the atomic sites) and an interstitial region. Inside the atomic sphere, a linear combination of radial function times spherical harmonic is used, and in the interstitial region a plane wave expansion is augmented by an atomic like function in every atomic sphere. This method yields accurate energy eigenvalues and wavefunctions, therefore appropriate for calculating the electronic and optical properties of crystalline solids.

The Indium pnictides crystallize in the zinc-blende structure at ambient pressure and temperature with lattice parameter 5.8687 Å for InP, 6.0583 Å for InAs and 6.47937 Å for InSb[9]. The space group is F-43 m. The In atom is located at the origin and the X atom is located at (1/4, 1/4, 1/4).The values of $K_{max} \times R_{MT} = 7.0$ (where R_{MT} is the atomic sphere radius and K_{max} is the interstitial plane wave cut-off), In the atomic region, the basis set consists of spherical harmonics with angular quantum number $l = 10$ and a non spherical contribution with $l = 4$ are kept constant throughout the calculations. The self-consistent iterations are considered to be converged when the total energy of the system are stable within 10^{-5} Ry. A mesh point of 5000 k-points were used to obtain 111 special *k*-points in the irreducible wedge of the Brillouin zone for InP, InAs, InSb. Both the muffin-tin radius and number of *k*-points were varied to ensure total energy convergence.

The dielectric function of a solid is usually describes in terms of a complex parameter as $\varepsilon(\omega) = \varepsilon_1(\omega) + i\varepsilon_2(\omega)$, in which the imaginary or the absorptive part of the dielectric function, $\varepsilon_2(\omega)$ can be obtained directly from the band structure calculation. While the real part $\varepsilon_1(\omega)$ can be obtained from the imaginary part $\varepsilon_2(\omega)$ by using the Kramers-Kronig dispersion relation[10].

RESULTS AND DISCUSSION

BAND STRUCTURE AND DENSITY OF STATES

Figures 1, 2 and 3 shows the calculated total density of states, the partial density of states and band structures for Indium pnictides InX (X=P, As, Sb). The band structure, partial and total DOS can be divided into three main groups. The lowest

energy group has mainly pnictide s states. The second group between –7 eV to E_F is composed of In-sp and pnictide p states. The last group from 0.7 for InP, 0.031 eV for InAs, and 0.01 eV for InSb and above has contributions from In-spd and pnictide pd states. The valence band maximum (VBM) is located at Γ for all the three compounds. The valence band maximum (VBM) and the conduction band minimum (CBM) are located at Γ resulting in a direct gap in agreement with experiment and previous theoretical work [11]. The conduction bands shift towards Fermi energy (E_F) when moving from P to As to Sb.

A comparison of the experimental and theoretical band gaps are given in Table-I. It is clearly seen that the band gap obtained by GGA are lower than the corresponding experimental values and results obtained from Tight Binding method [12]. We note that DOS does show a lager energy gaps than the band structures. This is attributed to the fact that the DOS near the conduction band minimum is very small because of the small effective mass. Following Yamasaki *et al.* [13], we can define degree of hybridization by the ratio of In-d states and pnictide p states within the muffin tin sphere. Based on this we can say that the hybridization between In-d and pnictide p states is very weak.

Optical properties

The detailed variation of real, $\varepsilon_1(\omega)$ and imaginary $\varepsilon_2(\omega)$ parts of the dielectric function for InX with photon energy are shown in Figure 4. We note that $\varepsilon_2(\omega)$ shows a large peak located at 4.3 eV for InP, 4.0 eV for InAs, and 3.5 eV for InSb in between two small peaks. All the structures in $\varepsilon_2(\omega)$ are shifted towards the lower energies when P is replaced by As and As by Sb, in agreement with the experimental data [14]. This is attributed to the reduction in the band gaps. We compare our calculated $\varepsilon_2(\omega)$ with the experimental data [14] and shows very good agreement in the matter of the peaks position and peaks height.

CONCLUSIONS

This paper has reported calculations of the energy bands structure, density of states and linear optical properties of InX (X=P, As, Sb) compounds using generalized gradient approximation (GGA) within the FP-LAPW method. Our result for band structure and DOS shows that these compounds are semiconductors with energy gaps of 0.7, 0.031, 0.01 eV. We note that the energy gap reduces when P replaced by As and As by Sb in agreement with the experimental data and pervious theoretical calculations. We compare our calculated linear optical properties with the experimental data [14]. This comparison shows very good agreement in the matter of the peaks position and peaks height.

Table 1: Our calculated direct energy band gap values and the experimental and theoretical band gap (all values are in eV)

Com-pounds	Expt. Band gap	Theoretical Band gap			Present work GGA
		TB	LDA	GGA	
InP	1.39[a], 1.35[b], 1.351[c]	1.34[d]	1.39[a], 1.804[e], 0.71[f], 0.7[g],	0.85[g]	0.7
InAs	0.42[a], 0.35[b], 0.356[c]	0.35[d]	0.55[a], 0.259[e], 0.03[f], 0.24[g],	0.31[g]	0.031
InSb	0.24[a], 0.18[b], 0.17[c]	0.17[d]	0.24[a], 0.00[e], 0.01[f], 0.14[g],	0.18[g]	0.01

[a]Ref. [11], [b]Ref. [15], [c]Ref. [16], [d]Ref. [12], [e]Ref. [17], [f]Ref. [18], [g]Ref. [19]

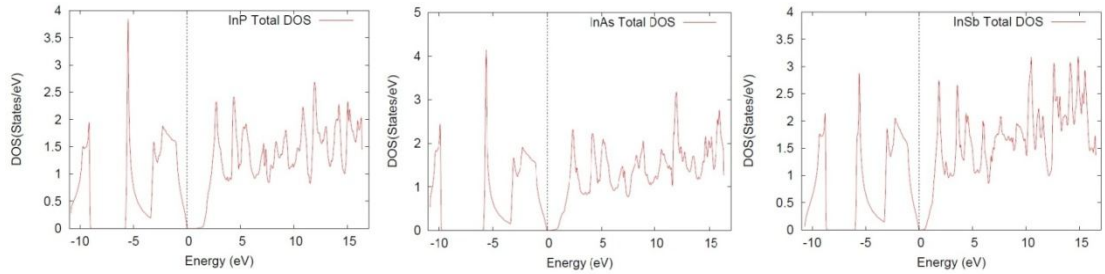

Figure 1: Total Density of States for InP, InAs and InSb

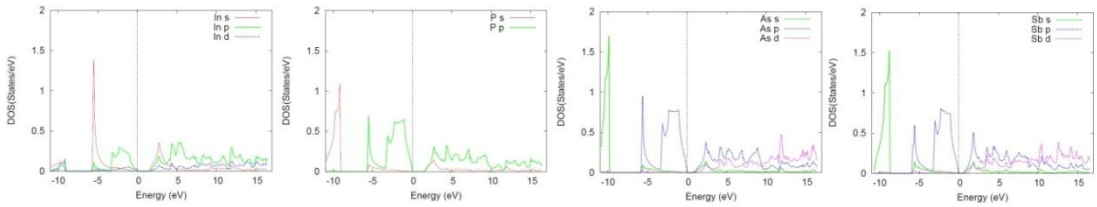

Figure 2: Partial Density of States for InP, InAs and InSb

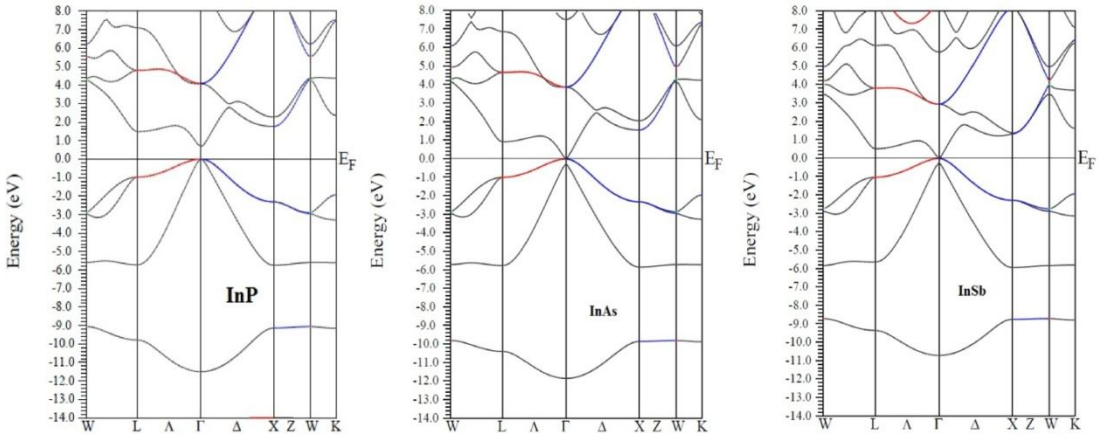

Figure 3: Band structure for InP, InAs and InSb

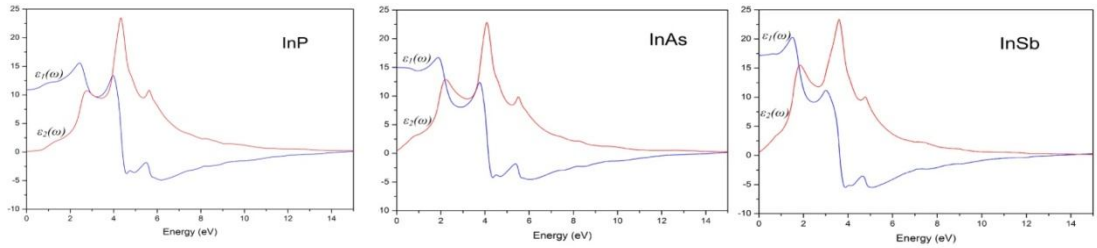

Figure 4: Real and Imaginary part of dielectric function for InP, InAs and InSb

REFERENCES

[1] Prasher, R., Dass, D. and Vaid, R., (2013). Study of novel channel materials using III-V compounds with various gate dielectrics. *International Journal on Organic Electronics (IJOE)* **2**, 11-18

[2] Al-Douri, Y., Mecabih, S., Benosman, N., Aourag, H., (2003). Pressure effect on electronic and positron charge densities of $Zn_{0.5}Cd_{0.5}Se$. Physica B **325**, 362-271

[3] Rabah, M., Al-Douri, Y., Sehil, M., Rached, D., (2003). Pressure effect on electronic band structure of III–V compounds. Mater. Chem. Phys. **80**, 34-38

[4] Bouhemadou, A., Khenata, R., Kharoubi, M., Seddik, T., Reshak, A. H., Al-Douri, Y., (2009). FP-APW + lo calculations of the elastic properties in zinc-blende III-P compounds under pressure effects. Comput. Mater. Sci. **45**, 474-479

[5] Froyen, S., Cohen, M. L., (1983). Structural properties of III-V zinc-blende semiconductors under pressure. Phys. Rev. B **28**, 3258-3265

[6] Perdew, J. P., Burke, K., Ernzerhof, M., (1996). Generalized Gradient Approximation Made Simple. *Phys. Rev. Lett.* **77**:3865-3868

[7] Singh, D. J., (1994). Planewaves, Pseudopotentials and the LAPW Method. Kluwer Academic Publishers, Boston, Dordrecht, London.

[8] Blaha, P., Schwarz, K., Madsen, G. K. H., Kvasnicka, D. and Luitz, J. (2008). *An Augmented Plane Wave + Local Orbitals Program for Calculating Crystal Properties*, (Revised Edition). Vienna University of Technology: Inst. of Physical and Theoretical Chemistry, Getreidemarkt 9/156, A-1060 2008, Vienna, Austria.

[9] Martienssen, W. and Warlimont, H. (2005). *Springer Handbook of Condensed Matter and materials Data* (Spinger Berlin Heidelberg New York). pp. 638

[10] Wooten, F., (1972). *Optical Properties of Solids*. Academic Press, New York, pp. 173–179.

[11] Huang, M.Z. and Ching, W.Y., (1993). Calculation of optical excitations in cubic semiconductors. I. Electronic structure and linear response. *Phys. Rev. B* **47**: 9449 – 9463.

[12] Korti-Baghdadli, N., Merad, A. E., and Benouaz, T., (2013). Adjusted Adashi's Model of Exciton Bohr Parameter and New Proposed Models for Optical Properties of III-V Semiconductors. *American Journal of Materials*

Science and Technology **3**: 65-73

[13] Yamasaki, T., Suzuki, N. and Motizuki, K. (1987). Electronic structure of intercalated transition-metal dichalcogenides: M_xTiS_2 (M=Fe, Cr). *J. Phys. C* **20,**395

[14] Aspnes, D.E. and Studna, A.A., (1983). Dielectric functions and optical parameters of Si, Ge, GaP, GaAs, GaSb, InP, InAs, and InSb from 1.5 to 6.0 eV. Phys. Rev. B **27**, 985-1009

[15] Kittel, C., (1994). Introduction to Solid State Physics, fifth ed., Wiley Eastern, India. pp. 210.

[16] Strehlow, W.H. and Cook, E.L., (1973). Compilation of Energy Band Gaps in Elemental and Binary Compound Semiconductors and Insulators. *J. Phys. Chem. Ref. Data, Vol. 2, No.1,* 177-178 and references therein.

[17] Remediakis, I.N. and Efthimios Kaxiras, (1999). Band-structure calculations for semiconductors within generalized-density-functional theory. *Phys. Rev. B***59**, 5536-5543

[18] Rahaman, M., Ganguly, S., Samal, P., Harbola, M. K., Saha-Dasgupta,T., Mookerjee, A., (2009). A local-density approximation for the exchange energy functional for excited states: The band-gap problem. *Physica B: Condensed Matter* **404**, 1137–1142

[19] Reshak, A. H., (2006). Electronic, linear and nonlinear optical properties of III-V Indium compounds semiconductors. *J. Chemical Phys.* **125**, 034710